VICTORIA UNIVERSITY OF WELLINGTON

DOCTORAL THESIS

Deglacial climate and ice sheet evolution of the Ross Embayment, Antarctica

---

Author:
Daniel P. Lowry

Supervisors:
Dr. Nicholas R. Golledge
Dr. Nancy A.N. Bertler

A thesis submitted in fulfillment of the requirements
for the degree of Doctor of Philosophy
Geology

in the

Antarctic Research Centre
School of Geography, Earth and Environmental Science

September 30, 2019

Declaration of Authorship

I, Daniel P. Lowry, declare that this thesis titled, "Deglacial climate and ice sheet evolution of the Ross Embayment, Antarctica" and the work presented in it are my own. I confirm that:

- This work was done wholly or mainly while in candidature for a research degree at this University.
- Where any part of this thesis has previously been submitted for a degree or any other qualification at this University or any other institution, this has been clearly stated.
- Where I have consulted the published work of others, this is always clearly attributed.
- Where I have quoted from the work of others, the source is always given. With the exception of such quotations, this thesis is entirely my own work.
- I have acknowledged all main sources of help.
- Where the thesis is based on work done by myself jointly with others, I have made clear exactly what was done by others and what I have contributed myself.

Signed: 

Date: September 30, 2019

VICTORIA UNIVERSITY OF WELLINGTON

Deglacial climate and ice sheet evolution of the Ross Embayment, Antarctica

by Daniel P. Lowry

Abstract

Reconstructing past grounding-line evolution can help inform future sea level projections by constraining marine ice sheet sensitivities to changes in climate. The Ross Embayment, the largest sector of Antarctica, experienced substantial grounding-line retreat since the Last Glacial Maximum. However, different interpretations for the timing and spatial pattern of deglacial grounding-line retreat in this region persist, suggesting either very high or low sensitivity to external forcings. Complicating matters is the sparse paleoclimate record, which is limited spatially and temporally. In this thesis, I address these issues by analysing the output of two transient climate simulations in relation to Antarctic ice core and marine sediment records, and performing and analysing the largest ensemble to date of regional ice sheet model simulations of the last deglaciation in the Ross Sea. The climate models and paleoclimate proxy records exhibit key differences in the timing, magnitude and duration of millennial-scale climate change events through the deglacial period. Using this diverse set of deglacial climate trajectories as ocean and atmosphere forcings, the ice sheet model ensemble produces a wide range of ice sheet responses, supporting the view that external forcings are the main drivers of past grounding-line retreat in the region. The simulations demonstrate that atmospheric conditions early in the deglacial period can enhance or diminish ice sheet sensitivity to rising ocean temperatures, thereby controlling the initial timing and spatial pattern of grounding-line retreat. Through the Holocene, grounding-line position is more sensitive to sub-shelf melt rates as the ocean cavity below the ice shelf expands. Model parameters that control the physical properties of the bed, deformation of the continental shelf, and rheological properties of the ice strongly influence the sensitivity of ice sheets to external forcing. Basin-wide differences in these forcings, driven by oceanic and atmospheric circulation, and spatial heterogeneity of bed properties likely contribute to the asynchronous pattern of retreat in the eastern and western parts of the embayment, as indicated by marine and terrestrial proxy records.

Acknowledgements

This thesis would not be possible without the help of many people. I am very grateful to have had two amazing supervisors, Nick Golledge and Nancy Bertler, who not only helped guide me through this thesis, but also made sure that I had ample opportunities to collaborate with others and grow as a scientist. Both have been incredible mentors and friends and they inspire me every day with their positivity, work ethic, and accomplishments.

Discussions with Laurie Menviel, Rich Jones and Rob McKay were critical for the development of ideas and writing of this thesis, and I gratefully acknowledge their input. I also thank Constantine Khroulev and Andy Aschwanden for their constructive advice regarding the Parallel Ice Sheet Model. The computing support of Aleks Beliaev and Kevin Buckley were crucial for the success of this research. I also thank the the teams behind the TraCE-21ka and LOVECLIM DGns experiments for producing and sharing climate model output as well as the Antarctic ice core and marine proxy communities for the use of their data.

Funding for this PhD was provided by the Royal Society Te Aparangi Marsden Fund through Victoria University of Wellington (15-VUW-131), the New Zealand Antarctic Research Institute (NZARI2014-11), and the Antarctica New Zealand doctoral scholarship program. I thank Rebecca McLeod and the Antarctica New Zealand Scholarship team for supporting this work. I am also indebted to Craig Stevens and Mike Brewer of NIWA for the opportunity to assist them as part of New Zealand's Ross Ice Shelf Programme. Knowledge gained from that experience has forever shaped my perspective of Antarctic ice shelves, and I thank everyone at the hot water drill site for their insights and putting up with me for multiple weeks.

I was very fortunate to work in the Antarctic Research Centre with other amazing scientists, staff and fellow PhD students. I have never worked in such a collaborative department and everyone's passion for Antarctica was contagious. I am grateful for Michelle and Dao for their administrative assistance. I appreciate Abhi, Jamey, Katelyn, Lauren, Laurine and Lukas for helping me work through various technical problems and interpret my results, and Georgia, Hannah, Arran, Marjo, Kostas, Bryant, Chet, Dani and many others for making the 5th floor a fun place to be.

I am also grateful for my family and friends back in the United States and in New Zealand, who may not understand exactly what I am doing, but have supported me regardless. I'm especially thankful to my parents, Bryan,

Megan, and Mark. I also thank Lehyla, Matt, Margaret, Luke, Lauren, Brendon, and Amanda. Lastly, I am also very fortunate to have had some amazing educators over the years that first instilled in me an interest in Earth systems and helped prepare me for undertaking a PhD, including Dorothy Ponisciak, Mark Bertness, Jan Tullis, Warren Prell, Jim Russell, Jessica Whiteside, Chris Poulsen, and Allison Steiner. I thank Carrie Morrill for first introducing me to numerical modelling and inspiring me to seek a career in scientific research. I also thank Tim Springfield, Ron Warhurst, Pat Devine, and Greg Bielecki for teaching me the meaning of resiliency, which came in handy over these past three years.

Contents

Declaration of Authorship **iii**

Abstract **v**

Acknowledgements **vii**

1 Introduction **1**
1.1 Context and Rationale 2
1.1.1 Interpretations of deglacial ice sheet evolution 2
1.1.2 Limitations in paleorecords 5
1.1.3 Research Questions 7
1.2 Theoretical framework and methods overview 9
1.2.1 Description of transient climate models 9
1.2.2 Antarctic ice sheet modelling 10
1.2.3 Regional ice sheet model set up 11
1.2.4 Paleoclimate and geological proxy records 13
1.3 Thesis Chapter Outline 15

2 Deglacial Antarctic climate evolution **17**
2.1 Abstract 17
2.2 Introduction 18
2.3 Materials and Methods 20
2.3.1 Transient climate model simulations 20
2.3.2 Spatial and Temporal Analysis 22
2.3.3 Proxy Records 24
2.4 Results 27
2.4.1 Surface temperatures 27
2.4.2 Surface mass balance 29
2.4.3 Accumulation-temperature scaling and rates of change 33
2.4.4 Ocean temperatures 35
2.4.5 Sea Ice 40
2.4.6 Southern Ocean-Antarctic climate connections 42

2.5 Discussion . . . 49
2.5.1 Regional patterns of deglacial climate evolution . . . 49
2.5.2 Regional patterns of deglacial ocean evolution . . . 51
2.5.3 Transient climate modeling limitations . . . 54
2.6 Summary and Conclusions . . . 56
2.7 Supplementary Information . . . 57
2.7.1 TraCE-21ka Sensitivity Experiments . . . 57
2.7.2 Surface albedo over the Southern Ocean . . . 59

3 Ice sheet response to deglacial climate forcing 61
3.1 Abstract . . . 61
3.2 Introduction . . . 62
3.3 Results . . . 67
3.3.1 Sensitivity of grounding-line retreat to climate forcing 67
3.3.2 Comparison of model simulations to the geologic record 73
3.4 Discussion . . . 77
3.5 Conclusions . . . 81
3.6 Materials and Methods . . . 82
3.6.1 Regional ice sheet model set up and initialization . . . 82
3.6.2 Sub-shelf melt rate/back pressure forcing sensitivity experiments . . . 83
3.6.3 Climate forcing details . . . 85
3.6.4 Deglacial climate forcing experiments . . . 86
3.7 Supplementary Information . . . 87

4 Roosevelt Island Climate Evolution ice core record 95
4.1 Abstract . . . 95
4.2 Introduction . . . 96
4.3 Geological Setting . . . 97
4.3.1 Site glaciology . . . 97
4.3.2 Site climatology . . . 99
4.4 Materials and Methods . . . 101
4.4.1 Ice core stable isotope record . . . 101
4.4.2 Climate Model Analysis . . . 101
4.4.3 Ice sheet model simulations and analysis . . . 102
4.5 Results . . . 104
4.5.1 RICE δD record . . . 104
4.5.2 Temporal climate evolution in climate simulations . . . 104
4.5.3 Factors influencing western Ross Embayment climate . 109

4.5.4 Effect of atmosphere forcing on ice sheet retreat 112
4.5.5 Effect of precipitation forcing on ice sheet retreat 118
4.6 Discussion 123
4.6.1 Interpretation of the RICE δD reconstruction 123
4.6.2 Climate sensitivity of ice sheet retreat 126
4.7 Summary and Conclusions 129

5 Effects of basal properties, the solid Earth, and ice rheology 131
5.1 Abstract 131
5.2 Introduction 132
5.3 Materials and Methods 133
5.4 Results 135
5.4.1 Effect of external forcing on ice sheet retreat 135
5.4.2 Influence of the stress balance on ice sheet retreat . . . 137
5.4.3 Influence of basal resistance on ice sheet retreat 140
5.4.4 Influence of the solid Earth on ice sheet retreat 143
5.4.5 Spatiotemporal uncertainty 146
5.4.6 Comparison to EAIS and WRS proxy records 148
5.4.7 Comparison to WAIS deglacial reconstructions 151
5.5 Discussion 156
5.6 Conclusions 160

6 Research Chapter Synthesis and Discussion 163
6.1 Research Chapter Synthesis 163
6.1.1 Deglacial evolution of Antarctic climate and the Southern Ocean 163
6.1.2 Role of climate forcing on ice sheet retreat in the Ross Embayment 165
6.1.3 Modulators of ice sheet sensitivity to climate forcing . 168
6.2 Discussion 171
6.2.1 Future of the Ross Embayment 171
6.2.2 Intermodel comparisons and priorities for Antarctic Ice Sheet modelling 176

7 Summary and Conclusions 183

Bibliography 187

List of Figures

1.1 Deglacial timeslices of Antarctic ice sheet surface elevation from the ICE-6G dataset. 4
1.2 Two hypotheses for deglacial grounding-line retreat in the Ross Sea. 5
1.3 Post-initialization modelled ice thickness. 12
1.4 Modelled surface ice velocity of the Ross Embayment regional domain. 13
1.5 Proxy record locations of Antarctic ice core and Southern Ocean marine sediment records. 14

2.1 Antarctic climate regions and proxy record locations. 23
2.2 Deglacial surface temperature change in transient climate model simulations. 28
2.3 Deglacial precipitation change in transient climate model simulations. 32
2.4 Centennial-scale rates of surface temperature and relative accumulation change in proxy records and climate model simulations. 34
2.5 Accumulation-temperature scaling relationships in transient climate model simulations and ice core records. 36
2.6 Deglacial sea surface temperature change in transient climate model simulations. 38
2.7 Time series of regional circum-Antarctic ocean temperature anomalies. 39
2.8 Deglacial time slices of longitudinal cross-sections of temperature anomalies of the Southern Ocean. 41
2.9 Modelled deglacial austral winter sea ice extent changes compared to LGM sea ice reconstructions. 42
2.10 Time series of modelled regional sea ice concentration and thickness changes. 43
2.11 Spatial correlations between surface air temperature, surface albedo and sea ice concentration. 45

2.12 Spatial correlations between Southern Ocean SST and precipitation at ice core locations in the LOVECLIM DGns simulation. 46
2.13 Spatial correlations between Southern Ocean SST and precipitation at ice core locations in the TraCE-21ka simulation. . . . 47
2.14 Deglacial time slices of geopotential height anomalies in transient climate model simulations. 48
2.15 Deglacial surface temperature changes in TraCE-21ka sensitivity experiments. 58
2.16 Spatial correlations between surface air temperature, snow depth over sea ice, and sea ice surface melt in TraCE-21ka and LOVECLIM DGns. 59

3.1 Climate forcings and modelled grounded ice volume. 68
3.2 Modelled grounding-line retreat scenarios in response to deglacial climate forcing. 71
3.3 Modelled ice surface velocity and ice shelf formation. 72
3.4 Uncertainty of modelled ice thickness due to climate forcing. . 74
3.5 Ice sheet model comparison to deglacial surface-exposure chronologies. 76
3.6 Sea level forcing effect on ice sheet-ice shelf evolution. 87
3.7 Time slices of the high mantle viscosity/ocean forcing simulation. 88
3.8 Ross Sea ocean temperature change in response to freshwater forcing. 90
3.9 LGM results of the sub-shelf melt rate-back pressure forcing sensitivity experiments. 91
3.10 Present-day results of the sub-shelf melt rate-back pressure forcing sensitivity experiments. 92
3.11 Deglacial time slices of the moderate ocean/atmosphere forcing simulation 93

4.1 Overview map of Roosevelt Island, eastern West Antarctica. . 98
4.2 Spatial correlation of Southern Ocean sea ice concentration and RICE snow accumulation and δD. 100
4.3 Decadally averaged stable isotope records of ice core sites in the Ross Sea region. 105
4.4 Deglacial time series of surface temperature and precipitation of the of the eastern Ross Embayment and Ross Sea sea ice concentration and SST in LOVECLIM DGns and TraCE-21ka. 107

4.5 Modelled surface temperature and precipitation changes during the Antarctic Cold Reversal. 108
4.6 Spatial correlations between modelled Southern Ocean SST and precipitation over the western Ross Embayment. 110
4.7 Spatial correlations between modelled Southern Ocean sea ice coverage and precipitation over the western Ross Embayment. 111
4.8 Modelled wind stress and sea ice concentration for the LGM and early Holocene. 113
4.9 Ice core-derived atmosphere forcings of the ice sheet model simulations and simulated ice volume changes. 115
4.10 Deglacial grounding-line retreat scenarios with ice core-derived atmosphere forcings. 116
4.11 Ocean forcing effect on ice sheet retreat with RICE-derived atmosphere forcing. 117
4.12 WAIS Divide-derived precipitation forcing and simulated ice sheet volume. 119
4.13 Deglacial grounding-line retreat scenarios with different precipitation and ocean forcings. 121
4.14 Differences in ice sheet evolution due to precipitation forcing. 122

5.1 Deglacial grounding-line retreat scenarios in response to external forcings. 136
5.2 Experiments varying the enhancement factor of the shallow ice approximation. 138
5.3 Experiments varying the enhancement factor of the shallow shelf approximation. 139
5.4 Experiments varying the basal resistance parameter, q. 141
5.5 Experiments varying the minimum till friction angle, ϕ_{min}. . . 142
5.6 Experiments varying the mantle viscosity term. 144
5.7 Time slices of ice sheet evolution in the simulation with no bed deformation. 145
5.8 Uncertainty of modelled ice thickness due to model parameters and climate forcing. 147
5.9 Comparison of ice sheet simulations to Transantarctic surface-exposure chronologies. 149
5.10 Modelled grounding-line changes in the Western Ross Sea. . . 152
5.11 Modelled ice surface elevation at West Antarctic ice core sites. 154
5.12 Modelled changes in grounding-line position along the Siple Coast during the Holocene. 155

6.1 Projected ocean temperature anomalies at 400 m depth of the Ross Sea of three CMIP5 models for the RCP4.5 and RCP8.5 scenarios. 173
6.2 Projected continental surface temperature anomalies of three CMIP5 models for the RCP4.5 and RCP8.5 scenarios for the Ross sector of Antarctica. 174
6.3 Projected continental precipitation anomalies of three CMIP5 models for the RCP4.5 and RCP8.5 scenarios for the Ross sector of Antarctica. 175
6.4 Sea level equivalent mass changes of initMIP-Antarctica models. 177
6.5 Mean and standard deviation of modelled ice thickness and velocity of initMIP Antarctica models in response to surface mass balance anomaly forcing. 179
6.6 Mean and standard deviation of modelled ice thickness and velocity of initMIP Antarctica models in response to basal mass balance anomaly forcing. 180
6.7 Evolution of ice shelf area of control and basal mass balance anomaly experiments of initMIP Antarctica. 180

List of Tables

2.1 Climate model details and specifications. 21
2.2 Antarctic and Southern Ocean proxy record details. 26
2.3 Comparison of modelled and reconstructed temperature and accumulation of Antarctic ice core sites and sea surface temperature at marine sediment record sites. 30

3.1 Atmosphere-ocean forcing combinations applied to the ice sheet model. 66
3.2 Sub-shelf mass flux-sea ice back pressure sensitivity experimental setup. 89
3.3 Ice sheet model parameters used in the deglacial climate-forcing experiments. 90

Chapter 1

Introduction

As consequences of increasing emissions of greenhouse gases, global atmospheric and oceanic temperatures are predicted to increase (Rogelj, Meinshausen, and Knutti, 2012; Bopp et al., 2013; Raftery et al., 2017), and global and regional sea levels are predicted to rise (Slangen et al., 2014; Kopp et al., 2014; Horton et al., 2014), partly due to mass loss from the Greenland and Antarctic Ice Sheets (Vizcaíno et al., 2014; Golledge et al., 2015; DeConto and Pollard, 2016; Golledge et al., 2019; Calov et al., 2018). The Fifth Assessment Report of the Intergovernmental Panel on Climate Change (IPCC-AR5) has projected global sea level to rise by as much as 98 cm by the year 2100 under the high emissions scenario (Church et al., 2013). A main factor in future sea level rise is the instability of the West Antarctic Ice Sheet (WAIS) given that the reverse slope bathymetry of the continental shelf creates an ice sheet configuration prone to runaway retreat (Mercer, 1978; Schoof, 2007; Joughin, Smith, and Medley, 2014). Over longer timescales, the potential sea level contribution of the East Antarctic Ice Sheet (EAIS) to climate warming is also concerning (Golledge et al., 2015).

The stability of the ice sheet grounding line, which is the transition between the grounded ice sheet and floating ice shelf, is a key control on marine ice sheet dynamics (Schoof, 2007). Rapid grounding-line retreat of ice grounded below sea level, referred to as marine ice sheet instability, has recently been observed along parts of the WAIS grounding line in response to warming oceanic conditions and sub-ice shelf melting (Pritchard et al., 2012; Favier et al., 2014; Seroussi et al., 2017). However, large uncertainties remain in terms of the Antarctic Ice Sheet response to future climate warming scenarios in numerical ice sheet models, with substantial differences in ice sheet sensitivity to atmosphere and ocean forcing related to model parameterizations and initialization procedures (Golledge et al., 2015; DeConto and Pollard, 2016; Golledge et al., 2019; Edwards et al., 2019; Seroussi et al., 2019). Understanding past grounding-line evolution can help inform future

sea level projections by constraining marine ice sheet sensitivities to changes in climatic conditions.

In this thesis, I assess ice sheet sensitivity to past changes in climate in the largest catchment of Antarctica, the Ross Embayment. Since the Last Glacial Maximum (LGM; ∼20-18 ka), the grounding line in the Ross Embayment has retreated by more than 1000 km (Bentley et al., 2014; Anderson et al., 2014b), but the specific influences of environmental forcings in this deglacial retreat remain hotly contested (Conway et al., 1999; Yokoyama et al., 2016; Kingslake et al., 2018; Goehring et al., 2019). Contributing to this debate is the limited number of paleoclimate and geological constraints, which together offer an incomplete picture of the deglacial climate and ice sheet evolution in this region. To address this issue, I analyse the output of two deglacial climate model simulations and an ensemble of regional ice sheet model simulations. The context and rationale for this topic and approach, the methodological framework, and an outline of the thesis chapters are described in the subsequent sections of this Introduction.

1.1 Context and Rationale

1.1.1 Interpretations of deglacial ice sheet evolution

During the LGM, global sea level was approximately 130 m lower than the modern sea level (Lambeck et al., 2014). Although much of this change in global sea level can be attributed to the ice sheets of North America (Simms et al., 2019), the Antarctic Ice Sheet was undoubtedly larger in terms of ice volume and extent during this period of cooler global climate (Mackintosh et al., 2011; Whitehouse et al., 2012; Golledge et al., 2013). Estimations of the LGM Antarctic ice sheet configuration suggest that the Antarctic contribution to this sea level lowering ranged from 6.7 m to 17.7 m sea level equivalent (Golledge et al., 2012; Argus and Peltier, 2010; Simms et al., 2019), implying a significant change in both Antarctic ice thickness and extent through the deglacial period (18 to 0 ka). From this maximal configuration, continental-scale reconstructions of the Antarctic Ice Sheet through the deglacial period indicate a retreat that was asynchronous in both timing and extent (Bentley et al., 2014). The Ross Embayment, currently the largest catchment of Antarctica, exhibited some of the largest changes in ice thickness and surface elevation according to glacial isostatic adjustment (GIA) modelling (Argus

et al., 2014), with a substantial reduction occurring between 15 and 5 ka (Fig 1.1).

From its LGM position, extending nearly to the continental shelf edge, the grounding line in the Ross Embayment has retreated over 1000 km to its modern position along the Siple Coast and the Transantarctic Mountains (Anderson et al., 2014a). However, disagreements on the timing, spatial pattern and controls of grounding-line retreat continue to persist. The traditional view is the "swinging gate" model of retreat (Fig 1.2a), first proposed by Conway et al. (1999), in which the grounding-line retreat only occurred in the late Holocene, in the absence of external forcings, such as climate and sea level forcing. This interpretation, which envisaged more pronounced retreat on the western side of the embayment relative to the east, is based on radiocarbon ages of postglacial shells from sediment cores in the western Ross Sea Embayment north of Ross Island, the McMurdo Ice Shelf, and raised marine deposits along the South Coast (Conway et al., 1999).

Through time, however, interpretations have evolved with additional radiocarbon ages and multibeam bathymetry data from the Ross Sea (McKay et al., 2016; Halberstadt et al., 2016; Lee et al., 2017; Bart et al., 2018), and terrestrial ice thinning records from the Transantarctic Mountains (Jones et al., 2015; Spector et al., 2017; Anderson et al., 2017; Goehring et al., 2019). More complex modes of retreat have been offered in the literature, including the "saloon door" model discussed in McKay et al., (2016) and Lee et al., (2017)(Fig 1.2b), and the marine-based model proposed in Halberstadt et al., (2016). These models suggest that a combination of marine forcing and physiographic controls resulted in an earlier retreat than that proposed by Conway et al. (1999), with a landward migration from the central embayment. More recently, King-slake et al. (2018) argued that the grounding line retreated substantially earlier and more extensively than previously estimated, which would suggest considerably higher sensitivity to environmental forcing in the early deglacial period. In this scenario, the grounding line retreated beyond its modern position along the Siple Coast of WAIS and re-advanced during the Holocene due to isostatic rebound.

In addition to the debate of the timing and pattern of grounding line retreat, little consensus exists with regard to the drivers of ice sheet retreat in the Ross Embayment. While the traditional "swinging gate" model attributes the entirety of ice sheet retreat to internal forcings, sea level forcing and a combination of ocean and atmosphere forcing have both recently been argued as the primary controls (Goehring et al., 2019; Yokoyama et al., 2016).

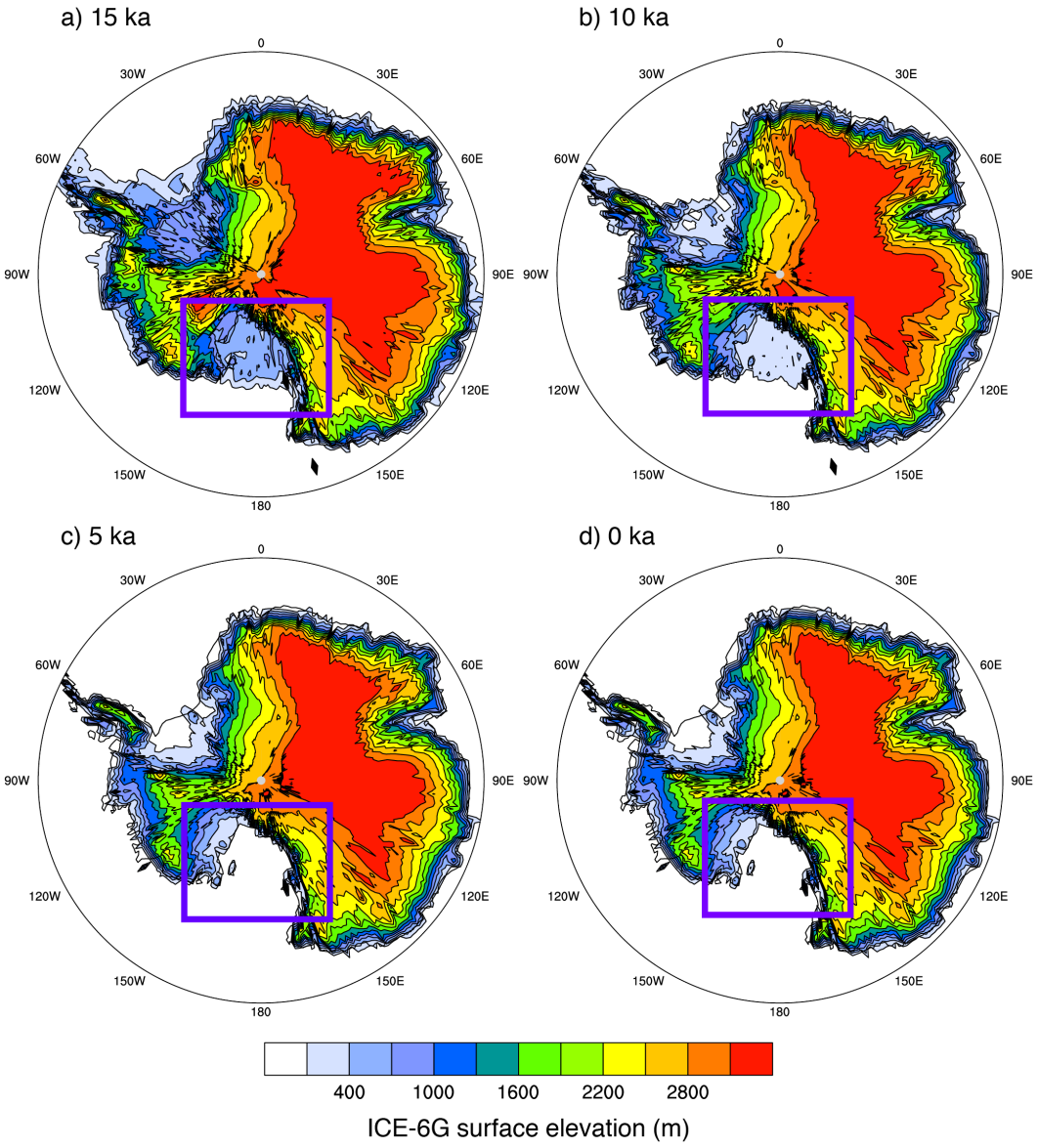

FIGURE 1.1: Deglacial timeslices of Antarctic ice sheet surface elevation from the ICE-6G dataset (Argus et al., 2014): (a) 15 ka, (b) 10 ka, (c) 5 ka, and (d) 0 ka. The purple box indicates the location of the Ross Embayment.

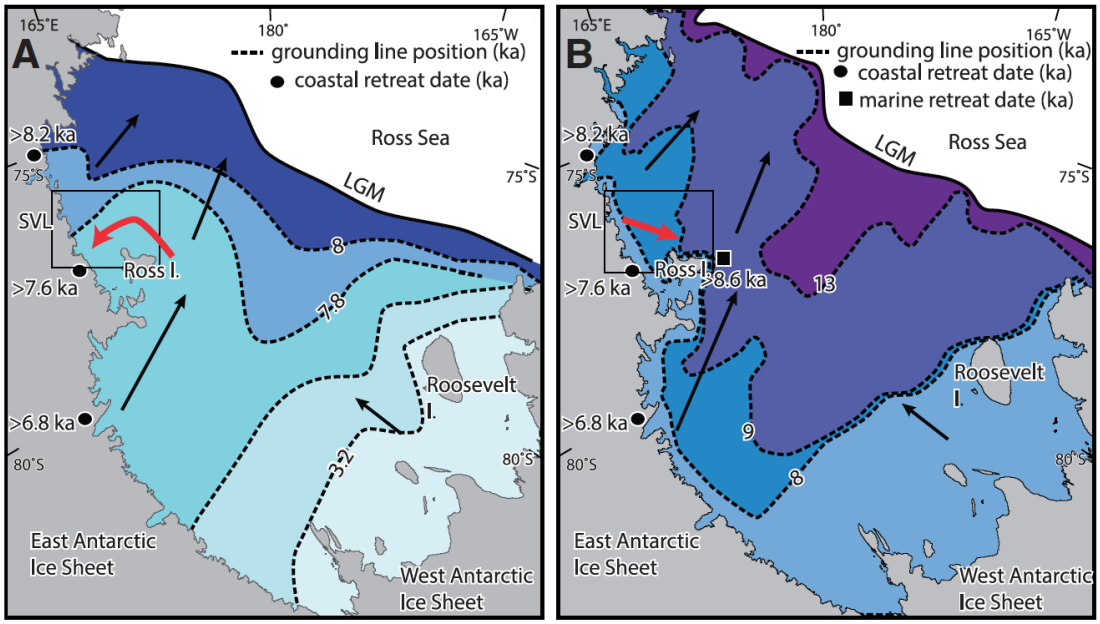

FIGURE 1.2: Two hypotheses for Ross Sea retreat adapted from Lee et al. (2017). (a) The "swinging-gate" grounding-line retreat pattern proposed by Conway et al. (1999); (b) The "saloon-door" retreat pattern proposed by McKay et al. (2016). The red arrow indicates ice flow direction of South Victoria Land required for each scenario.

Differences in seafloor bathymetry and substrate type may explain the asynchronous retreat of the eastern, western and central troughs of the Ross Sea (Halberstadt et al., 2016; Simkins, Anderson, and Greenwood, 2016). However, the specific roles of ocean and atmosphere forcings as drivers of ice sheet changes remain poorly understood through this time interval. During the deglacial period, Antarctic climate and the Southern Ocean experienced significant millennial-scale changes, including the last glacial termination, Heinrich event 1, the Antarctic Cold Reversal (ACR), and the Meltwater Pulse 1a and 1b (MWP-1A,B) events (Menviel et al., 2011; Pedro et al., 2016; Bereiter et al., 2018). Determining ice sheet responses to these events, in which oceanic and atmospheric temperatures changed considerably, will offer useful constraints for predicting future ice sheet responses to climate warming.

1.1.2 Limitations in paleorecords

Much of the current understanding of the ice sheet retreat history in the Ross Embayment is based on geological reconstructions in the form of cosmogenic nuclide surface-exposure records of marginal sites. These surface-exposure records, which are mainly derived from EAIS outlet glaciers of

the Transantarctic Mountains, indicate the timing of ice thinning, with dates along an altitudinal transect corresponding to exposure of glacial erratic clasts (Jones et al., 2015). These site-specific records are useful for understanding local glacier evolution, but large compilations are required for an improved interpretation of the broader-scale ice sheet evolution. Some complications include shielding by snow cover, post-depositional disturbance by periglacial processes, and recycling of rock from older deposits (Spector et al., 2017). Age uncertainty also exists in these chronologies, as the technique is highly dependent on knowledge of nuclide production rates, which are poorly constrained (Borchers et al., 2016), and the surface elevation, which can be impacted by glacial isostatic adjustment (Jones et al., 2019). As a result, this field is rapidly evolving as techniques improve, and Jones et al. (2019) estimate that ages may be up to 2.5 ka older than previously thought.

In addition to terrestrial ice thinning, interpretations of past grounding-line retreat have mainly relied on marine radiocarbon ages of postglacial shells and interpretations of multi-beam bathymetry data. The main complication is the difficulty in obtaining reliable ages due to the poor preservation of $CaCO_3$ in the corrosive bottom waters of the Southern Ocean as well as subglacial reworking and bioturbation of marine sediment (Andrews et al., 1999). As a result, few reliable estimates for the minimum age constraints of open ocean conditions exist in the Ross Sea (McKay et al., 2016; Bart et al., 2018), offering an incomplete view of grounding-line retreat. This can be supplemented by multi-beam bathymetry data (Lee et al., 2017; Greenwood et al., 2018), which through the identification of subglacial landforms, can indicate changes in paleo-ice flow and grounding-line position. However, these data only provide an interpretation of the sequence of grounding line migration rather than any age controls.

To the assess the role of deglacial climate forcing, in the form of changes in atmosphere and ocean temperatures, as a driver of ice sheet retreat in the Ross Embayment, it is important to have an accurate understanding of the regional climate evolution. However, the sites of Antarctic ice cores used for paleoclimate reconstructions are often located at high altitudes on the East Antarctic Plateau (Veres et al., 2013), far from the fringes of the ice sheet where grounding-line retreat initiates. Coastal ice cores, obtained from high accumulation and low elevation sites, are more useful, but they often have higher uncertainties. In particular, sea ice variability can influence isotopic concentrations in precipitated snow over coastal areas through the increased contribution of enriched water vapour and higher moisture transport (Noone

and Simmonds, 2004; Thomas and Bracegirdle, 2009; Küttel et al., 2012; Holloway et al., 2016). Isotopic signals are influenced by moisture source regions (Uemura et al., 2012) and the seasonality of precipitation (Erb et al., 2018), both of which can change through time.

Reconstruction of ocean temperatures at the depths of ice sheet grounding-lines is even more complex considering the previously described preservation issues (Andrews et al., 1999). Southern Ocean sea surface temperature (SST) reconstructions are based on alkenone- and Mg/Ca-SST relationships at latitudes far from ice sheet and closer to the polar Antarctic front (Calvo et al., 2007; Caniupán et al., 2011; Anderson et al., 2014b). However, these SST reconstructions also require cautious interpretations due to their relatively low temporal resolution, which can have millennial-scale gaps (Kaiser, Lamy, and Hebbeln, 2005), uncertainties in their age scales (Anderson et al., 2009), as well as their potential for seasonal biases (Leduc et al., 2010). The alkenone-derived SSTs in particular can be biased in regions of high seasonality in accordance with the seasonal cycles of marine archaea (Prahl et al., 2010). Comparisons between SSTs derived from different proxies, such as Mg/Ca, can also be challenging because they may be recording different seasonal signals (Leduc et al., 2010). All of these limitations complicate the understanding of deglacial ice-ocean relationships.

1.1.3 Research Questions

The goal of this thesis is to offer an improved understanding of ice sheet sensitivity to changes in climate, in the form of atmosphere and ocean forcing, in the Ross Embayment. As previously described, the Ross Embayment is a useful region for this task because it experienced substantial grounding-line retreat during the deglacial period, but little consensus exists for the relative roles of ocean and atmosphere forcing. This is related to the many limitations and uncertainties in the geologic and paleoclimate proxy records of Antarctica and the Southern Ocean. The specific research questions that I seek to address in this thesis are as follows:

1. How did Antarctic climate and the Southern Ocean evolve through the deglacial period?

Paleoclimate proxy records in the form of Antarctic ice cores and Southern Ocean sediment cores offer an incomplete picture of past Antarctic climate changes due to uncertainties and temporal gaps. Multiple records taken together can achieve greater insight with regard to regional and global climate

dynamics, however, each record acts as its own unique point in space. Climate models can aid in the interpretation by demonstrating the physics of the climate system under a given set of boundary and initial conditions. In this respect, transient climate simulations, with continuously varying boundary conditions, are especially useful as a comparison to proxy records and can address the many gaps in the data. In this thesis, I analyse output from two transient climate simulations of the last deglaciation: TraCE21ka (Liu et al., 2009; He, 2011; He et al., 2013), and LOVECLIM DGns (Menviel et al., 2011). These model simulations are described in greater detail in the subsequent section. I focus on climate model output related to Antarctica ice sheet mass balance in different regions, and in particular, the Ross Embayment.

2. How sensitive is the ice sheet to deglacial changes in atmospheric and oceanic conditions?

The timing and spatial pattern of grounding-line retreat in the Ross Embayment is uncertain, and the extent to which ocean and atmosphere forcing contributed to ice sheet retreat in this region is a hot topic of debate, with relevance to predicting future ice sheet changes. The geological record offers few age controls to constrain the grounding-line migration over the deglacial period. Additionally, the precise magnitudes and timing of climate changes are difficult to determine on a regional scale given the sparse spatial and temporal coverage and large uncertainties of available paleoclimate proxy records. To investigate this, I perform regional ice sheet simulations using a wide range of atmosphere and ocean forcings derived from the transient climate model simulations, Antarctic ice core records, and marine sediment records. Differences between the simulations are used to decipher the sensitivity of the ice sheet to atmosphere and ocean forcing. Comparisons of the simulations to the geologic record are in turn used to inform which deglacial climate forcings are the most reasonable for the Ross Embayment.

3. What is the influence of sub-ice sheet topography, the solid Earth and ice rheology on ice sheet sensitivity to climate forcing?

Ice sheet models have been demonstrated to be highly sensitive to the physical representation of the bed, the evolution and deformation of the continental shelf, and model parameters related to the ice flow laws (Martin et al., 2011; Matsuoka et al., 2015; Kingslake et al., 2018; Colleoni et al., 2018). However, the degree to which these factors impact ice sheet sensitivity to climate forcing is uncertain. In this thesis, I explore the effect of physical model

parameters that control basal properties, the solid Earth response to an evolving ice sheet, and ice flow and rheology on the response to deglacial climate forcing in regional ice sheet model simulations. The results of this analysis can help prioritize the geological constraints required for accurate projections of the future Antarctic response to anthropogenic climate warming.

1.2 Theoretical framework and methods overview

In this thesis, I analyse the output of two transient climate model simulations of the last deglaciation and perform and analyse an ensemble of regional ice sheet model simulations to assess ice sheet sensitivity to climate forcing in the Ross Embayment. The following sub-sections offer brief descriptions of each aspect of the methodology.

1.2.1 Description of transient climate models

Climate model simulations can help address the data gaps in the proxy record, however, relatively few transient climate model simulations exist given the computational demands and uncertainties of evolving external and internal forcings. In this study, I evaluate the output of two publicly available transient climate simulations of the last deglaciation, one using a fully coupled general circulation model (GCM; Liu et al., 2009) and one using an Earth system model of intermediate complexity (Menviel et al., 2011).

TraCE-21ka is a transient climate simulation of the last 22,000 years using the Community Climate System Model version 3 (CCSM3), a synchronously coupled GCM with atmosphere, ocean, land surface and sea ice components and a dynamic global vegetation module (Collins et al., 2006; Liu et al., 2009; He, 2011). The transient forcings included evolving orbital forcing following Milankovich theory (Genthon et al., 1987), greenhouse gas concentrations (CO_2, CH_4, N_2O; Joos and Spahni, 2008), ice sheet and paleogeography changes based on the ICE-5G reconstruction (Peltier, 2004), and prescribed meltwater fluxes into the Atlantic, North Atlantic and Southern Oceans (see He, 2011).

LOVECLIM DGns is a transient simulation of the glacial termination to mid-Holocene (18-6.2 ka) using the intermediate complexity LOVECLIM model version 1.1 (Driesschaert et al., 2007; Goosse et al., 2007). This climate model consists of a quasi-geostrophic atmosphere model, an ocean general circulation model, a dynamic/thermodynamic sea ice model, an ocean carbon cycle

model and a terrestrial vegetation model (Menviel et al., 2011). The transient forcings included time-varying solar insolation (Berger, 1978), Northern Hemisphere ice sheet topography updated every 100 years (Peltier, 1994), and atmospheric CO_2 determined from the EPICA Dome C ice core (Monnin et al., 2001), with CH_4 and N_2O fixed at LGM levels, and prescribed meltwater fluxes into the Atlantic, North Atlantic and Southern Oceans (see Menviel et al., 2011).

The climate model simulations differ in a number of key ways. TraCE-21ka has a higher atmospheric model resolution than DGns (3.75° with 26 vertical levels versus 5.75° with 3 vertical levels), though the resolutions of the ocean model components are similar. TraCE-21ka also has an evolving Antarctic Ice Sheet configuration, whereas the configuration remains fixed in DGns. Lastly, considering limitations in paleo-constraints, the models differ in terms of the timing, location, and amount of prescribed meltwater forcings. These differences, and their consequences, are described in greater detail in Chapter 2 of this thesis.

1.2.2 Antarctic ice sheet modelling

Three-dimensional thermo-mechanical modelling of the Antarctic Ice Sheet has improved tremendously over the past decades (Pattyn et al., 2017). The earliest iterations of continental-scale models were run at relatively coarse resolution (∼40 km), and were mainly applied to investigate long-term change on the order of glacial-interglacial cycles, with the assumption of a primarily diffusive response to surface mass balance change (Huybrechts, 1990). These early models consisted of two flow regimes, i.e., grounded ice flow and ice shelf flow, with a transition at the ice sheet grounding line. However, growing recognition of the importance of ice streams in Antarctica led to the development of a third flow regime in ice sheet models in order to represent ice stream zones with faster ice flow (Ritz, Rommelaere, and Dumas, 2001). In terms of the primary processes that weaken ice shelves, such as calving fluxes and basal melt (Depoorter et al., 2013), a number of parameterizations have been developed for sub-shelf melt (Beckmann and Goosse, 2003; Winkelmann et al., 2011), calving (Albrecht et al., 2011; Levermann et al., 2012), and hydrofracturing and ice cliff failure (Pollard, DeConto, and Alley, 2015). Lastly, improved understanding of ice sheet grounding line dynamics (Schoof, 2007), led to advancement of grounding line representation by imposing a new mass-flux condition (Pollard and DeConto, 2009).

In this thesis, I perform regional ice sheet model simulations using the Parallel Ice Sheet Model (PISM; Bueler and Brown, 2009; Martin et al., 2011). PISM is an improvement on previous thermo-mechanical ice sheet models in that it employs a hybrid approximation of the Stokes stress balance to better capture the wide range of ice sheet velocities (i.e., grounded ice, ice shelf, and ice stream flow regimes) in a more computationally efficient manner. In this hybrid stress balance scheme, velocities are calculated by the superposition of the shallow ice approximation (SIA), which dominates in grounded regions, and the shallow shelf approximation (SSA), which dominates in ice shelves and ice streams and serves as a basal sliding velocity of grounded regions (Winkelmann et al., 2011). This scheme effectively avoids discontinuities at the onset of sliding by using the SSA as a sliding law for grounded regions, and is thus advantageous for modeling marine ice sheets. To account for anisotropy and other uncertainties related to variations in viscosity and basal resistance, enhancement factors of the SIA and SSA can be applied (E_{SIA} and E_{SSA}, respectively). The grounding line scheme uses a sub-grid interpolation of basal driving stress to improve grounding-line reversibility, with similar performance to higher-order models (Feldmann et al., 2014), and is thus suitable for investigation of ice sheet responses to climate forcing.

PISM has previously been applied to understand the response of the Antarctic Ice Sheet to deglacial climate forcing in Golledge et al. (2014). This thesis is an advancement of this earlier work in that the model simulations here are performed for a regional sector of the ice sheet, allowing for higher spatial resolution (10 km versus 15 km), and a wider range of ocean and atmosphere forcings is considered. Additionally, I more specifically explore the effects of model parameters related to the sub-glacial topography and flow regimes on the climate sensitivity of the ice sheet. As a result, this thesis offers the largest model ensemble of ice sheet simulations of the Ross Sea sector of Antarctica for the last deglaciation. The ice sheet model simulations are described in greater detail in Chapters 3, 4 and 5.

1.2.3 Regional ice sheet model set up

In this thesis, I consider a regional ice sheet domain of the Ross Embayment. In order to set up the regional domain, I first used the ALBMAP version 1 dataset of Le Brocq, Payne, and Vieli (2010), which includes ice thickness and bedrock topography at a full continental-scale. The ice sheet model was initialized following the procedure of Martin et al. (2011). This

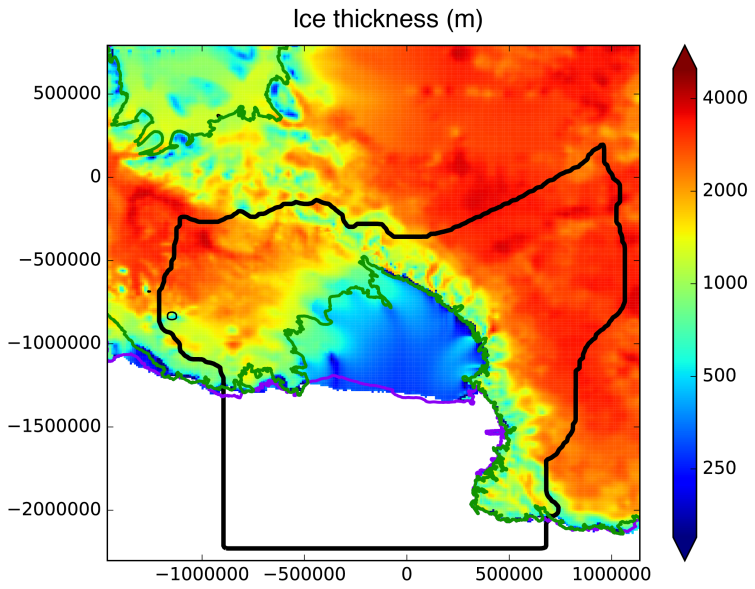

FIGURE 1.3: Post-initialization modelled ice thickness (m). The black line indicates the ice drainage basins that evolve, while the surrounding ice remains fixed as a time-independent boundary condition. The green line shows the observed modern grounding-line position and the purple line shows the observed modern calving line position.

procedure consists of an initial smoothing run (100-yr), in which the ice sheet evolves by internal deformation to remove any steep gradients and inconsistencies of the ice thickness input data, followed by a 200-kyr thermal evolution run, in which the temperature field evolves, but the ice geometry remains fixed. Lastly, I performed a 100-kyr evolutionary run with constant climate forcing. Following this full-continent model spin-up, the regional domain is determined based on the ice sheet thickness and surface elevation. The ice shelf and ice drainage basins of the grounded ice are allowed to dynamically evolve, and a larger area around the drainage basins is maintained at a constant thickness as a time-independent boundary condition of the model (Fig 1.3). This approach allows for higher computational efficiency due to the smaller domain size, while simultaneously allowing for the grounding-line position to change through time.

The regional model is tuned according to present-day (PD) conditions of the grounding line position, ice shelf extent, ice thickness, and ice surface velocity (Fig 1.4), in order to determine model parameter values, including the calving thickness threshold and rate in the calving parameterization scheme, enhancement factors of the SIA and SSA equations, the effective pressure on the till, the till friction angle, and the sliding exponent

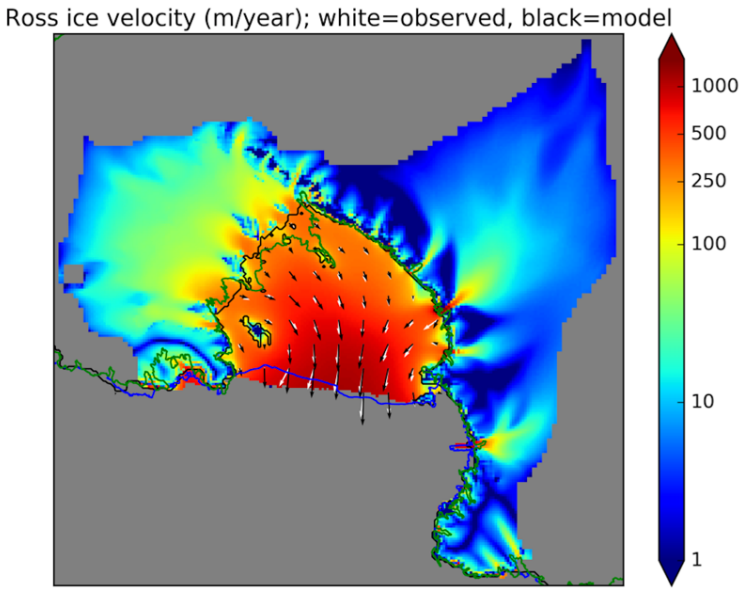

FIGURE 1.4: Surface ice velocity (m/yr) of the 10 km PD simulation. The black (white) vectors show modelled (observed) ice shelf surface velocity. The black line represents the modelled grounding line position, and the green and blue lines represent the observed grounding and calving line positions.

parameter. This PD simulation was performed using a paleoclimate forcing using the EPICA Dome C (EDC) temperature record (Parrenin et al., 2007) with paleo-precipitation determined based on the Clausius-Clapeyron relationship to temperature as anomalies to a modern climatology (precipitation-temperature scaling of 7.0%/°C). For the first 100 ka of the regional simulation, the ice shelf extent is fixed, and for the remainder of the run (15-0 ka), the calving scheme is incorporated. Starting from this regional PD configuration, we perform an initial climate forcing simulation from 131 ka (last interglacial) to 35 ka (early glacial) at 10 km resolution. This 35 ka configuration serves as the initial condition for the deglacial experiments, which are described in Chapters 3, 4 and 5.

1.2.4 Paleoclimate and geological proxy records

To assess model performance, I rely on a number of paleoclimate and geological proxy records. In terms of climate model performance, I compare the model output to Antarctic ice core records of temperature and accumulation and marine sediment reconstructions of SST of the Southern Ocean (Fig 1.5a). Specifically, I use the temperature reconstructions of the Vostok (V; Petit et al., 1999), Dome Fuji (DF; Uemura et al, 2012), and James Ross Island

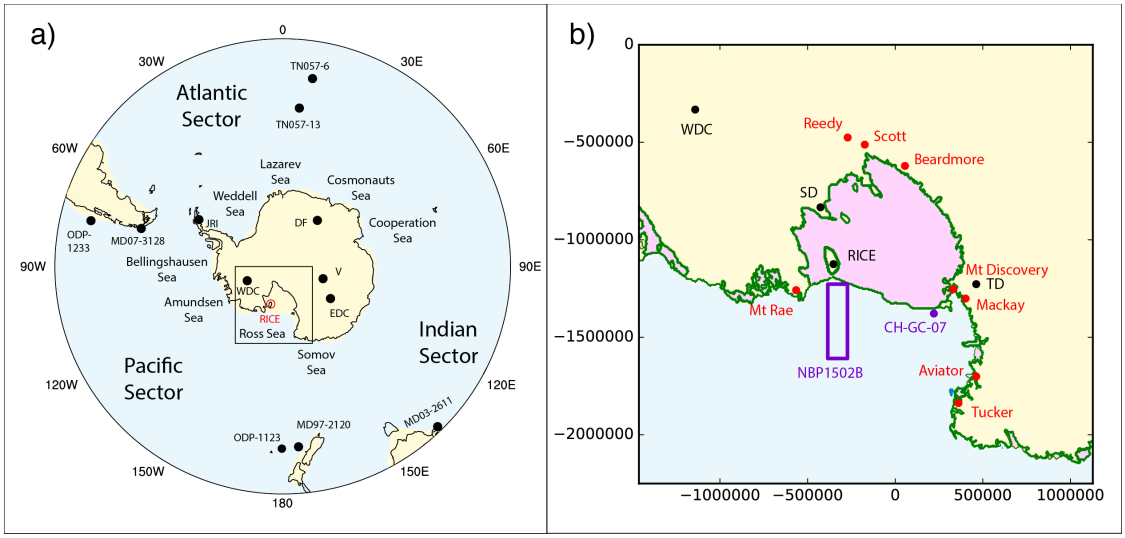

FIGURE 1.5: (a) Proxy record locations of Antarctic ice core and marine sediment records that are compared to the climate model simulations. The black box outlines the Ross Embayment, shown in panel b. (b) Marine radiocarbon sites (purple), surface-exposure chronology sites (red) and ice core sites (black) used for ice sheet model assessment. Modern observed floating ice shelf is shown in pink and outlined in green (Le Broq et al., 2010).

ice cores (JRI; Mulvaney et al., 2012), and the temperature and accumulation reconstructions of the EPICA Dome C (EDC; Parennin et al., 2007) and West Antarctic Ice Sheet Divide ice cores (WDC; Fudge et al., 2016). For the purposes of the Ross Embayment, I also use the water stable isotope record (deuterium, δD) of the Roosevelt Island Climate Evolution (RICE) ice core (Bertler et al., 2018), obtained from an ice dome in the eastern Ross Sea. However, temperature and accumulation records are not currently available for this site.

In addition to the ice cores, I use SST reconstructions from the Southern Ocean. These include the alkenone-derived SST reconstructions from Core MD03-2611 off the coast of South Australia (Calvo et al., 2007), Core TN057-6 in the South Atlantic (Anderson et al., 2014b), and Core MD07-3128 (Caniupán et al., 2011) and the Ocean Drilling Program (ODP) Core 1233 off the coast of Southern Chile (Kaiser, Lamy, and Hebbeln, 2005), the Mg/Ca-derived SST reconstruction of Core MD97-2120 from Chatham Rise (Pahnke et al., 2003), and the diatom-derived seasonal SST reconstruction of Core TN057-13 from the East Atlantic Polar Front (Anderson et al., 2009). Additional details of these records are provided in Chapter 2.

For the ice sheet model, I consider the marine radiocarbon ages of McKay et al. (2016) and Bart et al. (2018), i.e., from core CH-GC-07 and expedition NBP1502B, respectively (Fig 1.5b). I compare modelled ice thinning rates to

the surface-exposure records of Mt Rae (Stone et al., 2003), Reedy Glacier (Todd et al., 2010), Scott and Beardmore Glaciers (Spector et al., 2017), Mt Discovery (Anderson et al., 2017), Mackay Glacier (Jones et al., 2015), and Aviator and Tucker Glaciers (Goehring et al., 2019). Lastly, the simulations are analyzed in the context of the ice core records within the regional model domain, namely, the WDC and RICE ice cores, as well as the Siple Dome (Brook et al., 2005) and Taylor Dome (Steig et al., 2000; Baggenstos et al., 2018) ice cores (SD and TD, respectively).

1.3 Thesis Chapter Outline

In this thesis, I seek to better the understanding of the climate evolution in the Ross Embayment over the last deglaciation and the roles of ocean and atmosphere forcing in driving ice sheet retreat. The subsequent Chapters are organized as follows:

In Chapter 2, I conduct a spatial and temporal analysis of two transient climate model simulations of the last deglaciation in the context of the broader-scale Antarctic and Southern Ocean paleoclimate and paleoceanographic records to identify the main strengths and limitations of the models and the regional differences.

In Chapter 3, I perform regional ice sheet simulations using a wide range of ocean and atmosphere forcings derived from the climate models and paleoclimate proxy records discussed in Chapter 2. The intent is to identify the individual roles of ocean and atmosphere forcing as drivers of ice sheet retreat in the Ross Embayment.

In Chapter 4, I apply both the climate model simulations and the ice sheet model ensemble to interpret the δD record of the RICE ice core. Additional model experiments are also performed with RICE-derived climate forcing.

In Chapter 5, I perform an additional set of ice sheet simulations, all with the same climate forcing, but with different model parameters related to the basal properties, the solid Earth and ice rheology. These experiments highlight the effect of individual model parameters on the ice sheet response to climate forcing.

Chapter 6 offers a synthesis of Chapters 2 through 5 as well as a discussion of the main priorities in the field of Antarctic ice sheet modelling and the future of the Ross Embayment. In Chapter 7, I summarise the main findings of the thesis.

Chapter 2

Deglacial evolution of Antarctic climate and Southern Ocean conditions

This Chapter has been adapted from:

Lowry, D. P., Golledge, N. R., Menviel, L., Bertler, N. A. (2019). Deglacial evolution of regional Antarctic climate and Southern Ocean conditions in transient climate simulations. Climate of the Past, 15(1), 189-215.

Author contributions: D.L., N.G. and N.B. conceived the concept for this analysis. D.L. performed the analysis and wrote the manuscript. All authors contributed to the editing and refining of the text.

2.1 Abstract

Constraining Antarctica's climate evolution since the end of the Last Glacial Maximum (∼18 ka) remains a key challenge, but is important for accurately projecting future changes in Antarctic ice sheet mass balance. Here we perform spatial and temporal analysis of two transient deglacial climate simulations, one using a fully coupled GCM (TraCE-21ka) and one using an intermediate complexity model (LOVECLIM DGns), to determine regional differences in deglacial climate evolution and identify the main strengths and limitations of the models in terms of climate variables that impact ice sheet mass balance. The greatest continental surface warming is observed over the continental margins in both models, with strong correlations between surface albedo, sea ice coverage and surface air temperature along the coasts, as well as regions with the greatest decrease in ice surface elevation in TraCE-21ka. Accumulation-temperature scaling relationships are fairly linear and

constant in the continental interior, but exhibit higher variability in the early to mid-Holocene over coastal regions. Circum-Antarctic coastal ocean temperatures at grounding line depths are highly sensitive to the meltwater forcings prescribed in each simulation, which are applied in different ways due to limited paleo-constraints. Meltwater forcing associated with the Meltwater Pulse 1A (MWP-1A) event results in sub-surface warming that is most pronounced in the Amundsen and Bellingshausen Sea sector in both models. Although modelled centennial-scale rates of temperature and accumulation change are reasonable, clear model-proxy mismatches are observed with regard to the timing and duration of the Antarctic Cold Reversal (ACR) and Younger Dryas/early Holocene warming, which may suggest model bias in large-scale ocean circulation, biases in temperature reconstructions from proxy records, or that the MWP-1A and 1B events are inadequately represented in these simulations. The incorporation of dynamic ice sheet models in future transient climate simulations could aid in improving meltwater forcing representation, and thus model-proxy agreement, through this time interval.

2.2 Introduction

Ice sheet model simulations of both past and future climates often rely on paleoclimate forcings derived from a combination of proxy data and climate model simulations (Pollard and DeConto, 2009; Golledge et al., 2014; Gregoire et al., 2016; Bakker et al., 2017). As such, the long memory of ice sheets with respect to past climatic conditions means that a model spin-up with an accurate deglacial climate forcing is important for any future Antarctic ice sheet model simulations. However, paleoclimate proxy data generally have sparse spatial coverage and relatively large uncertainties. Regional differences also persist in many of the Antarctic ice core records due to local climate effects (Pedro et al., 2011; Veres et al., 2013), complicating their use as climate forcings for an entire ice sheet. In addition to the ice core record, the marine proxy record is limited in aiding ice sheet modellers due to the corrosive nature of Southern Ocean bottom waters, which inhibits the preservation of microfossils that can be dated to provide age controls or geochemically analysed to provide a proxy for ocean temperature (McKay et al., 2016). Although climate forcings derived from compilations of multiple records and global datasets can help alleviate some of these issues, the regional differences between proxy archives may actually be consequential to ice sheet

mass changes (Golledge et al., 2017). For example, the Antarctic ice sheet retreat during the last deglaciation likely occurred asynchronously (Bentley et al., 2014), suggesting that different sectors of the ice sheet responded either to different forcings, or in different ways to uniform forcings.

Climate model simulations can help address the data gaps in the proxy record, however, they are often assessed in terms of skill during climate states of relative stability, such as the Last Glacial Maximum (LGM), the mid-Holocene or the Last Millennium (Braconnot et al., 2012; Schmidt et al., 2012; Hargreaves et al., 2013; Sueyoshi et al., 2013), rather than over long-term periods of dramatic climate change. In fact, for the last deglaciation, only one series of transient climate simulations using a fully coupled atmosphere-ocean general circulation model (GCM) has been performed (Liu et al., 2009; He, 2011; He et al., 2013), and it may miss important synoptic-scale processes related to the surface mass balance of West Antarctica (Fudge et al., 2016). It also shows some discrepancies related to the timing and magnitude of the Antarctic Cold Reversal (ACR; He (2011)). Given that the task of simulating global climate with a variety of evolving internal and external forcings is computationally demanding, the use of intermediate complexity models is especially appealing, and such models have been successfully applied to better understand past climate changes (Menviel et al., 2011; Goosse et al., 2012; Menviel et al., 2014). However, the coarser resolution and relatively simpler parameterization schemes of the atmospheric models may introduce further challenges with regard to simulating the climatic processes that affect ice sheet mass balance.

In this study, we evaluate the output of two transient deglacial climate simulations, one using a fully coupled GCM (Liu et al., 2009) and one using an Earth system model of intermediate complexity (Menviel et al., 2011). Given that the mass balance of the West and East Antarctic ice sheets is largely controlled by the accumulation of snow on the surface minus the ice that is lost through sublimation, iceberg calving, sub-ice shelf melt and thermal erosion of marine-based grounded ice, we focus on the aspects of climate that are most relevant to these processes, including surface temperature, surface mass balance, ocean temperatures to grounding line depths and sea ice. This analysis is performed in the context of the Antarctic ice core and Southern Ocean marine sediment records. The main goals of this study are to (1) determine the regional differences in the deglacial climate evolution of Antarctica and the Southern Ocean as recorded in the models and proxy records, and (2) identify the main strengths and biases of the models

in capturing the rates and magnitudes of climatic changes that impact ice sheet mass balance. We focus our analysis on the period from the last glacial termination (18 ka)(Denton et al., 2010) to the mid-Holocene (6.5 ka).

2.3 Materials and Methods

2.3.1 Transient climate model simulations

In this study, we consider two transient deglacial climate simulations, namely, the TraCE-21ka and LOVECLIM DGns deglacial experiments (Table 2.1). TraCE-21ka is a transient climate simulation of the last 22,000 years using the Community Climate System Model version 3 (CCSM3), a synchronously coupled GCM with atmosphere, ocean, land surface and sea ice components and a dynamic global vegetation module (Collins et al., 2006; Liu et al., 2009; He, 2011). The transient forcings included evolving orbital forcing (Genthon et al., 1987), greenhouse gas concentrations (CO_2, CH_4, N_2O; Joos and Spahni (2008)), ice sheet and paleogeography changes based on the ICE-5G reconstruction Peltier, 2004, and prescribed meltwater fluxes into the Atlantic, North Atlantic and Southern Oceans (see He (2011)).

The LOVECLIM DGns experiment was performed with the intermediate complexity LOVECLIM model version 1.1 (Driesschaert et al., 2007; Goosse et al., 2007), which includes a quasi-geostrophic atmosphere model, an ocean general circulation model, a dynamic/thermodynamic sea ice model as well as ocean carbon cycle and terrestrial vegetation components (Menviel et al., 2011). The horizontal resolution of the atmosphere component is coarser than that of TraCE-21ka (spectral resolution of T21 compared to T31), with 3 levels in the atmosphere, but those of the ocean and sea ice components are similar (Table 2.1). The transient forcings included time-varying solar insolation (Berger, 1978), Northern Hemisphere ice sheet topography updated every 100 years Peltier, 1994, and atmospheric CO_2 determined from the EPICA Dome C ice core (Monnin et al., 2001), with CH_4 and N_2O fixed at LGM levels. Freshwater pulses were applied to the North Atlantic and Southern Ocean based on $^{231}Pa/^{230}Th$ data of the North Atlantic (McManus et al., 2004) and Greenland temperature reconstructions (Alley, 2000). Two transient simulations were performed; one with freshwater input in the Southern Ocean at the time of the ACR, and one without; we consider the former (see Menviel et al. (2011)). We also note that the ice sheet topography over Antarctica was

Model simulation	Atmosphere component	Land component	Ocean component	Sea ice component
TraCE-21ka	Community Atmospheric Model 3 (CAM3) (Collins et al., 2006) 3.75° horizontal resolution 26 hybrid coordinate vertical resolution	Community Land Model-Dynamic Global Vegetation Module (CLM-DGVM) (Levis et al., 2004) 3.75° horizontal resolution	Parallel Ocean Program (POP) (Collins et al., 2006) vertical z coordinate with 25 levels 3.6° longitudinal resolution and variable latitudinal resolution, with finer resolution near the Equator ($\sim 0.9°$)	Community Sea Ice Model (CSIM) (Collins et al., 2006) thermodynamic–dynamic model that includes sub-grid ice thickness distribution 3.6° longitudinal and variable latitudinal resolution, with finer resolution near the Equator ($\sim 0.9°$)
LOVECLIM DG_{ns}	ECBilt (Opsteegh et al., 1998) 5.6° horizontal resolution quasi-geostrophic T21 spectral, three levels	VECODE (Brovkin et al., 1997) dynamic vegetation module 5.6° horizontal resolution	CLIO (Campin and Goosse, 1999) primitive equations, z coordinate, 3° horizontal resolution with 20 vertical levels LOCH (Mouchet and Francois, 1996) three-dimensional ocean carbon cycle model	thermodynamic–dynamic sea ice model coupled to CLIO

TABLE 2.1: Model details and specifications.

unchanged in this simulation. Additional model details of TraCE-21ka and LOVECLIM are presented in Table 2.1.

In terms of the transient forcings, one of the most uncertain aspects concerns the timing, magnitude and location of meltwater fluxes, which are handled in the two simulations in different ways. In both models, the freshwater is applied over large areas of the ocean surface in order to capture millennial-scale discharge events that occurred during the deglacial period, but the amounts and locations vary due to limited paleo-constraints. In the early part of the study period (18-14.5 ka), a prescribed freshwater flux into the North Atlantic in TraCE-21ka is increased to $\sim$0.17 Sv, at which point it is held constant until 14.67 ka. DGns likewise has a prescribed freshwater flux into the North Atlantic during this time interval, however the flux ceases earlier than in TraCE-21ka (0.2 Sv from 18-17.4 ka; 0.25 Sv from 17.4 to 15.6 ka). Meltwater Pulse 1A (MWP-1A) is also represented differently: in TraCE-21ka, very high, short-lived freshwater fluxes into the Ross and Weddell Seas occur between 14.35 and 13.85, peaking at $\sim$14.1 ka (0.33 Sv each), with lower freshwater forcing applied to the Mackenzie River and Gulf of Mexico regions (reaching 0.11 Sv each). In contrast, in DGns a higher freshwater flux is

applied in the North Atlantic as compared to those in the Ross and Weddell Seas (0.2-0.25 Sv vs. 0.15 Sv, linearly decreasing to 0 Sv, respectively), and the meltwater forcing occurs over a longer duration than in TraCE-21ka (14.4 to 13.0 ka). For the Younger Dryas, an Arctic Ocean meltwater forcing is applied from 13-12.2 ka in DGns (0.25 Sv), whereas in TraCE-21ka, a lower meltwater forcing is applied in the mid-latitude St. Lawrence River region from 12.9 to 11.7 ka (0.17 Sv). In the Holocene, TraCE-21ka has a large meltwater forcing of 5 Sv in the Hudson Strait region at 8.47 ka for half a year to represent the 8.2 ka event, but no such forcing is applied in DGns. Additional details on the prescribed meltwater forcings in the DGns and TraCE-21ka experiments can be found in Menviel et al. (2011) and He (2011), respectively.

2.3.2 Spatial and Temporal Analysis

Considering differences observed between Antarctic ice core records from East and West Antarctica and between coastal and interior regions, we focus our analysis on the following four continental regions (see Fig 1): the interior of the East Antarctic ice sheet (EAIS interior; 83°S-75°S, 30°W-16°E), coastal East Antarctica (coastal EAIS; 75°S-68°S, 15°W-165°E), West Antarctica (WAIS; 83°S-72°S, 165°E-30°W), and the Antarctic Peninsula (AP; 72°S-64°S, 64°W-59°W). We assess the magnitudes and rates of continental surface temperature and accumulation changes in the climate simulations from the start of the glacial termination (18 ka)(Denton et al., 2010) to the mid-Holocene (6.5 ka), a period of time covered by both climate model simulations.

Here, we define accumulation as precipitation minus surface evaporation/sublimation (P – E). Accumulation from the ERA-Interim Analysis defined as precipitation minus sublimation has been shown to closely match airborne radar observations over the Thwaites Glacier in West Antarctica (Medley et al., 2013), however, we note that the contribution of wind-transported snow may also be locally significant in some areas, particularly in coastal areas dominated by katabatic winds (Palm et al., 2017). As such, we emphasize caution in interpreting accumulation changes in the climate models in areas of strong wind speed, but in terms of overall ice sheet mass balance, wind-transported snow is generally considered to be a relatively minor component (Palm et al., 2017). We also ignore the surface runoff term given that it is dependent on snow thickness thresholds that are set in the climate models,

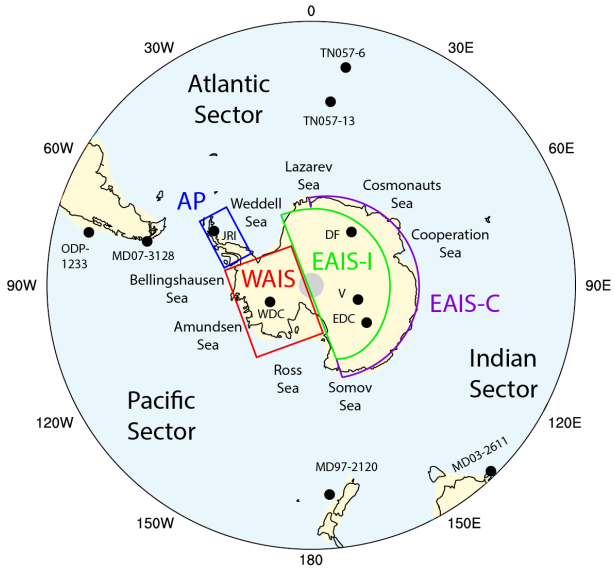

FIGURE 2.1: Polar-stereographic view of Antarctica and the Southern Ocean (maximum Latitude of 35°S). The colors indicate the land and ocean mask of the TraCE-21ka simulation (yellow and light blue, respectively). The continental regions, namely, the Antarctic Peninsula (AP), the West Antarctic Ice Sheet (WAIS), the East Antarctic Ice Sheet interior (EAIS-I), and the East Antarctic Ice Sheet coastal region (EAIS-C) are outlined in the colored boxes (blue, red, green, and purple, respectively). The locations of the Antarctic ice core and marine sediment records used in this analysis are indicated by the black dots.

hence over long timescales, it balances P-E over Antarctica. For each continental region, we determine the scaling relationships between temperature and accumulation in both climate model simulations and compare these relationships to those recorded in the ice core records.

In addition to continental surface temperature and accumulation, we examine the coastal seas around Antarctica to depths corresponding to modern-day grounding lines (0-800 m), including the Ross Sea (70°S-62°S, 168°E-160°W), the Amundsen and Bellingshausen Seas (68°S-62°S, 135°W-60°W), the Weddell Sea (70°S-62°S, 60°W-30°W), the coastal region from Lazarev Sea to Cosmonauts Seas (67°S-62°S, 15°W-50°E), and the coastal region from Cooperation Sea to Somov Sea (67°S-62°S, 55°E-165°E), as well as the surface of the entire Southern Ocean. We identify changes in the surface ocean temperatures near the continental shelf as well as sea ice thickness, concentration and extent. Since the TraCE-21ka ocean and sea ice outputs are available at the decadal scale, we focus this analysis on decadal- to centennial-scale changes.

2.3.3 Proxy Records

To assess climate model performance, we rely on publicly available proxy records of Antarctic climate and the Southern Ocean conditions with reconstructions that are directly comparable to the climate model output (Table 2.2; Fig 2.1). Specifically, we use the temperature reconstructions of the Vostok (V) (Lorius et al., 1985; Petit et al., 1999), Dome Fuji (DF) (Uemura et al., 2012), and James Ross Island (JRI) ice cores (Mulvaney et al., 2012), and the temperature and accumulation reconstructions of the EPICA Dome C (EDC)(Jouzel et al., 2007; Parrenin et al., 2007; Stenni et al., 2010) and West Antarctic Ice Sheet Divide ice cores (WDC)(Fudge et al., 2013; Cuffey et al., 2016; Fudge et al., 2016). Only ice core records with temperature and/or accumulation reconstructions that overlapped with the period covered in both models (18-6.5 ka) were used in this analysis. The exception is James Ross Island, which does not extend back to 18 ka, hence only the period of 14.2 to 6.5 ka is considered for this site.

The temperature reconstructions are commonly calculated as anomalies to modern temperatures based on deuterium (δD), deuterium excess (d) and oxygen isotope measurements (δ^{18}O) using site-specific temperature-dependence relationships that assume the modern-day calibration holds over the entire record (Jouzel et al., 1997; Mulvaney et al., 2012). However, there is inherent uncertainty in this approach as the isotopic signals can be influenced by

changes in moisture source regions (Uemera et al., 2012), sea ice content (Holloway et al., 2016), and the seasonality of precipitation (Erb et al., 2018). In East Antarctic ice cores, for example, temperature reconstructions have been estimated to have an uncertainty range of -10% to +30% (Jouzel et al., 2003), or +/-2 °C for glacial-interglacial temperature change (Stenni et al., 2010). Recent improvements to this traditional method have been successfully applied to the WDC ice core, however, with the use of additional borehole temperature and nitrogen isotope data, yielding a temperature reconstruction with relatively lower uncertainty (+/-1.8 °C or 16%; Cuffey et al. (2016)). The accumulation reconstructions are more difficult to obtain, but can be estimated from the depth-age relationship by correcting the annual-layer thicknesses for flow-induced thinning using an ice flow model (Parrenin et al., 2007; Fudge et al., 2016). Sources of uncertainty in accumulation reconstructions include both the timescale and the amount of thinning, which can be quantified using a firn densification model (Fudge et al., 2016). Uncertainties of accumulation reconstructions for the deglacial period are estimated to range from ∼15-25% (Frieler et al., 2015; Fudge et al., 2016).

In addition to Antarctic ice core records, we use marine sediment records from the Southern Ocean (Table 2.2; Fig 2.1). The records include alkenone-derived SST reconstructions from Core MD03-2611 off the coast of South Australia (Calvo et al., 2007), Core TN057-6 in the South Atlantic (Anderson et al., 2014b), and Core MD07-3128 (Caniupán et al., 2011) and the Ocean Drilling Program (ODP) Core 1233 off the coast of Southern Chile (Kaiser, Lamy, and Hebbeln, 2005), the Mg/Ca-derived SST reconstruction of Core MD97-2120 from Chatham Rise (Pahnke et al., 2003), and the diatom-derived seasonal SST reconstruction of Core TN057-13 from the East Atlantic Polar Front (Anderson et al., 2009). These SST reconstructions require cautious interpretations as they record temperatures at the depth at which the foraminifera and diatoms live, and therefore may not offer straightforward reconstructions of SST. Other limitations to comparing these records to the model SST output include their relatively low temporal resolution, which can have millennial-scale gaps, uncertainties in their age scales, as well as the potential for seasonal biases. The alkenone-derived SSTs in particular can be biased to lower or higher values than the annual mean in regions of high seasonality in accordance with the seasonal cycles of marine archaea (Prahl et al., 2010). Existing calibrations have the tendency to overestimate SSTs at high latitudes, and even with recent improvements, uncertainties of alkenone-derived SSTs

Record name	Type	Measurement	Method	Location	Reference
Vostok (V)	Ice core	Temperature anomaly	δD temperature calibration ($9.0‰\,°C^{-1}$)	East Antarctica; 78.5° S, 107° E	Lorius et al. (1995), Petit et al. (1999)
Dome Fuji (DF)	Ice core	Temperature anomaly	d temperature calibration ($7.7‰\,°C^{-1}$)	East Antarctica; 77° S, 39° E	Uemura et al. (2012)
James Ross Island (JRI)	Ice core	Temperature anomaly	δD temperature calibration ($6.7 \pm 1.3‰\,°C^{-1}$)	Antarctic Peninsula; 64° S, 58° W	Mulvaney et al. (2012)
EPICA Dome C (EDC)	Ice core	Temperature anomaly; accumulation	δD temperature calibration ($7.6‰\,°C^{-1}$); ice flow model	East Antarctica; 75° S, 124° E	Jouzel et al. (2007), Parrenin et al. (2007), Stenni et al. (2010)
WAIS Divide (WDC)	Ice core	Surface temperature; accumulation	Water stable isotope record, borehole temperatures, and nitrogen isotopes ($7.9‰\,°C^{-1}$); ice flow model	West Antarctica; 79.5° S, 112° W	WAIS Divide Project Members (2013), Cuffey et al. (2016), Fudge et al. (2016)
Core MD03-2611	Marine sediment core	SST	Alkenone derived	Murray Canyons area; 36° S, 136° E	Calvo et al. (2007)
ODP site 1233 core	Marine sediment core	SST	Alkenone derived	South Chile; 41° S, 74° W	Kaiser et al. (2005)
Core MD97-2120	Marine sediment core	SST	Mg/Ca derived	Chatham Rise; 45° S, 175° E	Pahnke et al. (2003)
Core TN057-6	Marine sediment core	SST	Alkenone derived	East Atlantic; 43° S, 9° E	Anderson et al. (2014)
Core MD07-3128	Marine sediment core	SST	Alkenone derived	Magellan Strait; 53° S, 75° W	Caniupán et al. (2011)
Core TN057-13	Marine sediment core	Seasonal SST (February)	Diatom derived	East Atlantic Polar Front; 52° S, 5° E	Anderson et al. (2009)

TABLE 2.2: Antarctic and Southern Ocean proxy record details.

in the Southern Ocean over the Quaternary period are estimated to generally be >5°C (Tierney and Tingley, 2018). Comparisons between SSTs derived from different proxies, such as Mg/Ca, can also be challenging because they may be recording different seasonal signals (Leduc et al., 2010). Given that the true uncertainties of these marine records are difficult to quantify, we suggest caution with respect to their direct comparison to the climate model output.

2.4 Results

2.4.1 Surface temperatures

The DGns and TraCE-21ka deglacial simulations both show fairly uniform temperature increases over the continent and Southern Ocean of >6°C (Fig 2.2a,b). The exception is the continental interior in the DGns simulation, which exhibits more modest temperature increases, particularly closer to the pole. In contrast, the TraCE-21ka simulation experiences the greatest warming over the pole and much of WAIS (>12°C). This difference is primarily driven by the change in ice sheet topography in TraCE-21ka; the decrease in surface elevation can explain most of the temperature increase, as indicated by a sensitivity simulation in which only the ice sheet topography is changed while all other boundary conditions remain the same (Supplementary Information). If the same topographic changes were applied to the DGns simulation, ∼2.5-6.5°C of the difference in temperature change between the two models in the continental interior could be accounted for, considering a glacial lapse rate of 0.54°C/100m calculated in DGns over the continent. Both models simulate large temperature increases along the coasts over the Ross, Amundsen, Bellingshausen and Weddell Seas, as well as along parts of the East Antarctic coast (>10°C). DGns displays a larger temperature increase over the Antarctic Peninsula and Weddell Sea (10-13°C), whereas TraCE21ka shows a larger temperature increase at Prydz Bay and the Ross Sea (∼12°C).

In comparison to the temperature change estimated in the ice core records over the analysed period (6.5 – 18 ka), DGns displays lower mean annual temperature changes at each site except for JRI (Fig 2.2a), whereas TraCE-21ka displays higher temperature changes at each site (Fig 2.2b). However, with the exception of V in DGns, the range of seasonal temperature change of both models (i.e., the change in austral summer and winter temperatures) is within the uncertainty of the temperature reconstructions at each site (Table 2.3). For the first 4 kyr of the simulation, DGns has a warm bias in the EAIS interior in terms of the mean annual temperature anomaly close to the pole due to its use of a modern Antarctic ice sheet configuration and model edge effects (Fig 2.2c). In contrast, TraCE-21ka has a cold bias for the full extent of the analyzed time period for WAIS and until ∼9 kyr in the EAIS interior (Fig 2.2c,e). Compared to the WDC ice core, TraCE-21ka underestimates the surface temperature change until a substantial increase occurs at 11.3 ka due to an abrupt decrease in the ice surface elevation. This occurs at a time of stable temperature in the ice core record (Fig 2.2e). Both models show cold

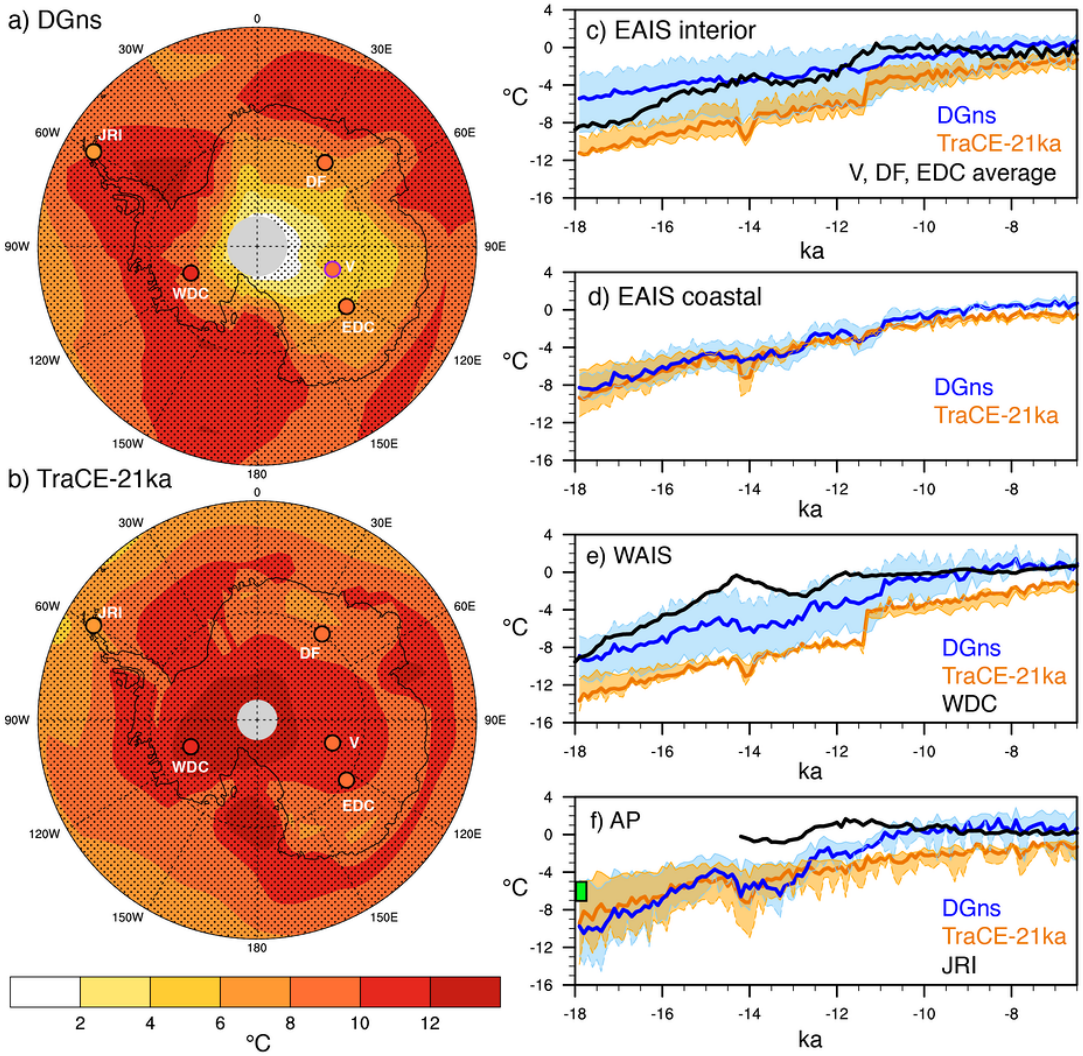

FIGURE 2.2: Surface temperature change (°C) as simulated in (a) DGns and (b) TraCE-21ka for the period of 18 to 6.5 ka (maximum Latitude of 60°S). Dotted lines indicate latitude (intervals of 15°) %and longitude (intervals of 30°). Ice core locations of the JRI, WDC, DF, V, and EDC sites are marked by filled circles, with the fill color corresponding to the change estimated in the ice core record, black outlines indicating a match in warming between the ice core and model simulation (i.e., the ice core temperature change from 18 to 6.5 ka is within the range of seasonal temperature changes of the climate model), and green (purple) outlines indicating an overestimation (underestimation) in warming by the models. For these model-proxy comparisons, we use site-specific model averages of land surface grid cells: JRI (63-65°S, 59-62°W), WDC (77-82°S, 115-109°W), DF (75-79°S, 36-42°E), V (77-82°S, 104-110°E), EDC (73-77°S, 121-127°E). Stippling indicates a difference between decadal output of 18.0-17.5 ka and 7.0-6.5 ka that is significant at the 95% confidence level. (c-e) 100-yr average surface temperature time series (°C) of four regions (EAIS interior: 83-75°S, 30°W-165°E; coastal EAIS: 75-68°S, 15°W-165°E; WAIS: 83-72°S, 165°E-30°W; AP: 72-64°S, 64-59°W) relative to PI of both model simulations and ice core temperature reconstructions of sites located therein (DGns in blue, TraCE-21ka in orange, ice cores in black). The colored shading indicates the seasonal range calculated from the 100-yr average austral summer and winter temperature anomalies. For EAIS, the ice core reconstruction is an average of the DF, V and EDC sites. The green box in (f) indicates the LGM temperature anomaly estimated for JRI (6.01+/-1.0°C; Mulvaney et al., 2012).

biases for the AP, but DGns converges with the JRI reconstruction in the early Holocene. Overall, the temperature anomalies are more similar between the model simulations and ice cores in the Holocene than earlier in the deglacial period.

In each region, the main discrepancy of the models with the Antarctic ice core temperature records is the timing and magnitude of the ACR. The TraCE-21ka simulation displays a sharp ACR following a large pulse of freshwater into the Southern Ocean and the Gulf of Mexico, with a decrease in surface temperature of $\sim$2.5°C in continental Antarctica, and a minimum occurring at approximately 14 ka. The duration of the event is short-lived, lasting less than 500 years, as AMOC strength decreases back to its pre-meltwater forcing level (He, 2011). The ACR duration is longer in the DGns simulation ($\sim$1-1.5 kyr), initiating at approximately the same time as in the TraCE21ka simulation, but the magnitude of the surface temperature change is lower, especially over the EAIS interior region (Fig 2.1c). In contrast to the simulations, the EAIS ice core records show a later initiation of the ACR, beginning at about 14 ka, rather than peaking at this time. The WDC ice core exhibits a similar initiation timing to the climate model simulations, but shows a more gradual decrease and subsequent increase in temperature (Fig 2.1e). The overall surface temperature change of the ACR is moderate in the ice core records as compared to the low (high) temperature change in DGns (TraCE21ka), and the event lasts for approximately 2 kyr, depending on the site. The JRI ice core shows the subtlest expression of the ACR, with the WDC, EDC and V ice cores displaying more pronounced signals. Both climate simulations show larger temperature changes associated with the ACR over the AP, which may be due to the strong influence of sea ice changes on surface temperature.

2.4.2 Surface mass balance

Precipitation increases in every grid cell over the continent and Southern Ocean in the TraCE-21ka simulation over the period from 18 to 6.5 ka, and these changes are significant at the 95% confidence level (Fig 2.3a). The greatest increases occur over WAIS, coastal EAIS, and most of the Southern Ocean (>8 cm/yr). The AP, EAIS interior, and the Roosevelt Island region show modest increases (<4 cm/yr). The DGns simulation shows a similar precipitation increase over the Southern Ocean (>8 cm/yr), however, precipitation decreases of 1-6 cm/yr occur over the South Pole and the coastal EAIS

Record	Proxy estimation (6.5–18 ka)	DG_{ns} seasonal range (6.5–18 ka)	TraCE-21ka seasonal range (6.5–18 ka)
V	8.04 °C (7.24–10.45 °C)	*2.75–6.25 °C*, 6.60–11.21 cm yr^{-1}	9.02–10.40 °C, 0.99–1.42 cm yr^{-1}
EDC	8.18 °C (6.18–10.18 °C), 1.42 cm yr^{-1} (1.14–1.70 cm yr^{-1})	**3.25–9.87 °C**, 3.25–17.60 cm yr^{-1}	8.99–10.12 °C, 1.68–4.16 cm yr^{-1}
DF	8.70 °C (7.83–11.31 °C)	3.70–8.23 °C, 0.85–7.72 cm yr^{-1}	**8.33–10.69 °C**, 3.58–4.09 cm yr^{-1}
WDC	10.20 °C (8.4–12.0 °C), 11.8 cm yr^{-1} (8.85–14.8 cm yr^{-1})	**8.40–11.68 °C**, *−5.00–8.11 cm yr^{-1}*	10.34–15.28 °C, **11.37–19.91 cm yr^{-1}**
JRI	6.26 (5.26–7.26 °C)	6.99–11.84 °C, 10.07–21.25 cm yr^{-1}	**3.74–8.75 °C**, 4.04–5.25 cm yr^{-1}
MD03-2611	7.77 °C	1.51–1.90 °C	2.26–3.05 °C
ODP-1233	3.44 °C	2.90–4.02 °C	2.32–3.06 °C
MD97-2120	3.40 °C	3.09–4.58 °C	1.64–2.52 °C
TN057-6	5.69 °C	2.89–3.95 °C	2.03–2.44 °C
MD07-3128	5.66 °C	4.68–5.08 °C	2.28–2.83 °C
TN057-13	0.14 °C	2.97–3.49 °C	1.29–2.17 °C

TABLE 2.3: Change from 18 to 6.5 ka at Antarctic ice core sites (surface temperature, °C; accumulation, cm/yr) and marine sediment core sites (SST, °C) estimated in the proxy records and simulated in DGns and TraCE-21ka for austral summer (December to February) and austral winter (June to August). Proxy records were linearly interpolated to 100 year averages. Bold font indicates a match between the seasonal range of change in the models and the proxy estimation at Antarctic ice core sites. Italicized font indicates that the seasonal range of change in the model does not overlap with the uncertainty range of the ice core record. We use uncertainties of +30% to -10% for V and DF temperature (Jouzel et al. 2003), +/- 2°C for EDC temperature (Stenni et al., 2010), +/-1.8°C for WDC temperature (Cuffey et al., 2016), and +/-1.0°C for JRI temperature (Mulvaney et al., 2012). For accumulation, we assume uncertainties of +/-25% (Fudge et al., 2016).

(Fig 2.3b). In the coastal region, where the decrease is larger, this is related to the coarse model resolution, which cannot adequately reproduce the steep slopes of East Antarctica and thus underestimates snow deposition in this region (Goosse et al., 2012). Changes in atmospheric circulation lead to the slightly reduced precipitation over the South Pole. Also, in contrast to TraCE-21ka, DGns precipitation over the AP increases by >12 cm/yr, and increases by 4-10 cm/yr over the EAIS interior.

Modelled P-E anomalies relative to the preindustrial era (PI) are quite distinct in each region and differ to the accumulation reconstructions of the ice core records (Fig 2.3c-f). In general, the E term is substantially lower than the P term, hence E has a negligible effect on the surface mass budget. At 18 ka, both models generally show negative mean annual P-E anomalies relative to PI. The exception is the coastal EAIS region in the DGns simulation, which shows higher relative mean annual P-E and a negative trend through time (Fig 2.3d). The models show the highest P-E variability over the AP, and show a pronounced decrease in mean annual P-E associated with the ACR (Fig 2.3f). In this region, TraCE-21ka remains near PI P-E levels, whereas DGns shows a more substantial increase through time.

The overall accumulation change reconstructed at the WDC site for the analyzed period is similar to that of TraCE-21ka (Fig 2.3b,e), though the model has a negative P-E bias until the large ice sheet configuration change (decrease in surface elevation) that occurs at 11.3 ka. In contrast, DGns underestimates the overall accumulation change at this site (Fig 2.3a,e). Accumulation recorded in the EDC ice core is relatively stable. In fact, Cavitte et al. (2018) highlights the stability of accumulation patterns at Dome C over the last glacial cycle, and the greatest change in the centennial-averaged record of annual average accumulation is only 2.17 cm/yr. TraCE-21ka shows a negative P-E anomaly relative to PI through this time interval, however, it exhibits a similar magnitude of change and variability in the deglacial period to the EDC accumulation record over the broader EAIS interior region (Fig 2.3c). In contrast to TraCE-21ka, the DGns simulation overestimates the magnitude and variability of P-E in the EAIS interior.

Another discrepancy between the two model simulations is the larger difference between austral summer and winter accumulation anomalies in DGns as compared to TraCE-21ka (color shading in Fig 2.3c-f). While this is true in each region, the most extreme case is the EAIS coastal region, in which the austral summer accumulation anomaly relative to PI is as high

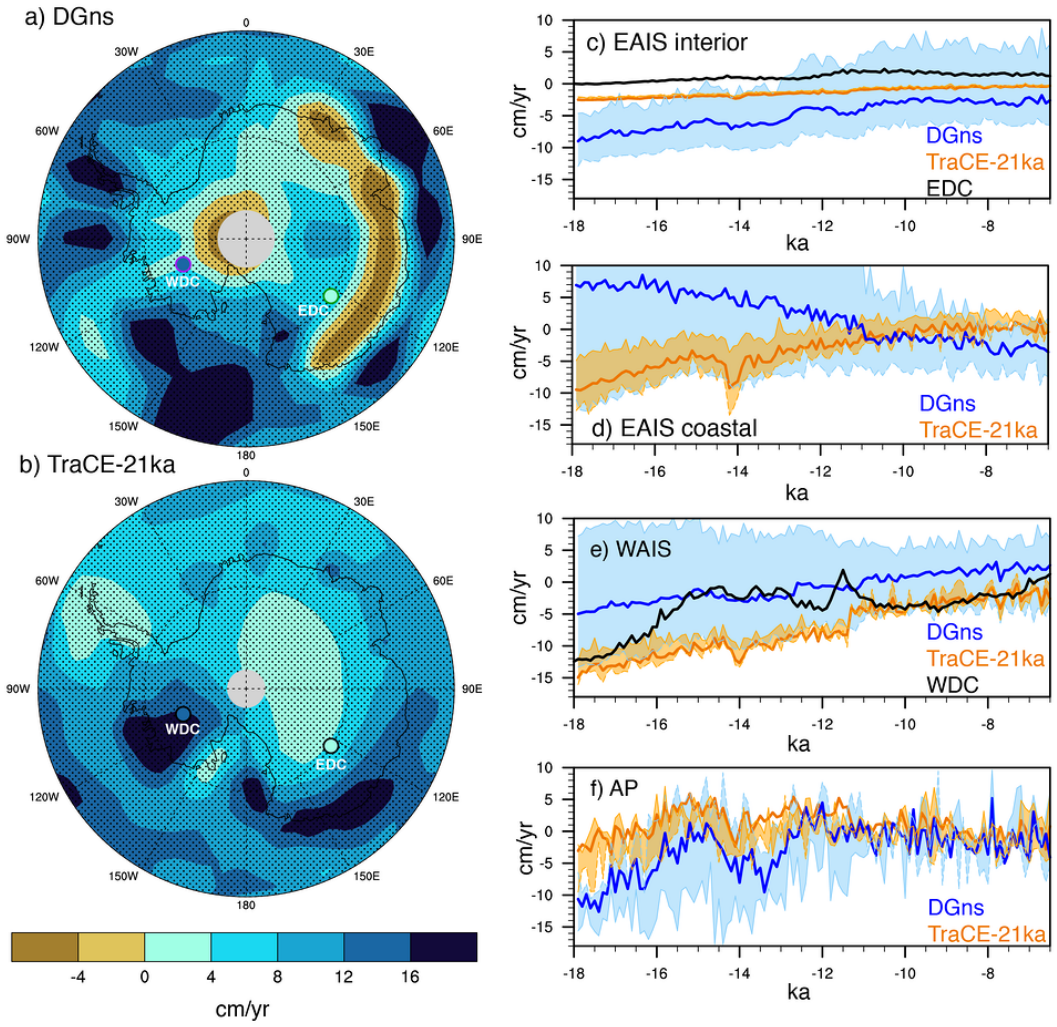

FIGURE 2.3: Precipitation change (cm/yr) as simulated in (a) DGns and (b) TraCE-21ka for the period of 18 to 6.5 ka (maximum Latitude of 60°S). Dotted lines indicate latitude (intervals of 15°) and longitude (intervals of 30°). Ice core locations of WDC and EDC are marked by filled circles, with the fill color corresponding to the change estimated in the ice core record, black outlines indicating a match in warming between the ice core and model simulation (i.e., the ice core temperature change from 18 to 6.5 ka is within the range of seasonal temperature changes of the climate model), and green (purple) outlines indicating an overestimation (underestimation) in warming by the models. For these model-proxy comparisons, we use site-specific model averages of land surface grid cells: WDC (77-82°S, 115-109°W), EDC (73-77°S, 121-127°E). Stippling indicates a difference between decadal output of 18.0-17.5 ka and 7.0-6.5 ka that is significant at the 95% confidence level. (c-f) 100-yr average accumulation time series (cm/yr) of four regions (EAIS interior: 83-75°S, 30°W-165°E; coastal EAIS: 75-68°S, 15°W-165°E; WAIS: 83-72°S, 165°E-30°W; AP: 72-64°S, 64-59°W) relative to PI of both model simulations (P-E) and ice core accumulation reconstructions of sites located therein (DGns in blue, TraCE-21ka in orange, ice cores in black). The colored shading indicates the seasonal range calculated from the 100-yr average austral summer and winter temperature anomalies.

40.8 cm/yr at the start of the simulation, whereas the austral winter accumulation anomaly is -12.65 cm/yr. Through time, austral summer (winter) accumulation decreases (increases) in this region, thereby reducing the seasonal anomaly range in the Holocene relative to the early deglacial period.

2.4.3 Accumulation-temperature scaling and rates of change

Centennial-scale rates of surface temperature and accumulation changes in the ice core records are well-matched by the climate model simulations, although the timing of the largest changes are generally offset (Fig 2.4a-d). This is particularly true for surface temperature, with the ice core records showing warming (cooling) not exceeding 0.4°C (-0.2°C)/100 yrs and the climate models showing a slightly larger range (-0.5 to 0.6°/100 years in the case of TraCE-21ka). The greatest discrepancies between the ice cores and the models are the timing and magnitude of cooling and warming associated with the ACR and an artificial warming spike in TraCE-21ka associated with the change in ice surface topography at 11.3 ka (Fig 2.4a-d). The DGns simulation also shows a high warming rate following the ACR in each region, however, this is not due to any change in ice surface elevation. The models show similar variability in the precipitation changes (% relative to PI)/100yrs to those of the ice core accumulation records (Fig 2.3e-h). Of note is the increase and subsequent decrease in the accumulation rate that occurs following the ACR, which is present in both the WDC and EDC records, which slightly exceed the climate model precipitation rate variability (Fig 2.4e,g). As expected, the models both show substantially higher variability in the rate of precipitation change along the coasts.

In terms of the relationship between temperature and accumulation, Frieler et al. (2015)demonstrated that in 5 East Antarctic ice core records of the deglacial period, a consistent positive linear scaling relationship exists, with an average of $\sim$6.0% $^{\circ}C^{-1}$, in accordance with that expected of the Clausius Clapeyron relationship. The TraCE-21ka simulation captures these relationships at these individual sites relatively well, generally falling within the range of uncertainty in the ice core record. Here, we show that the DGns simulation using the intermediate complexity model can likewise reproduce this positive scaling relationship in the EAIS interior, however, the model fails in the coastal region of the EAIS (Fig 2.5a,b). This is explained by the model resolution issue mentioned previously, which is enhanced through time as the

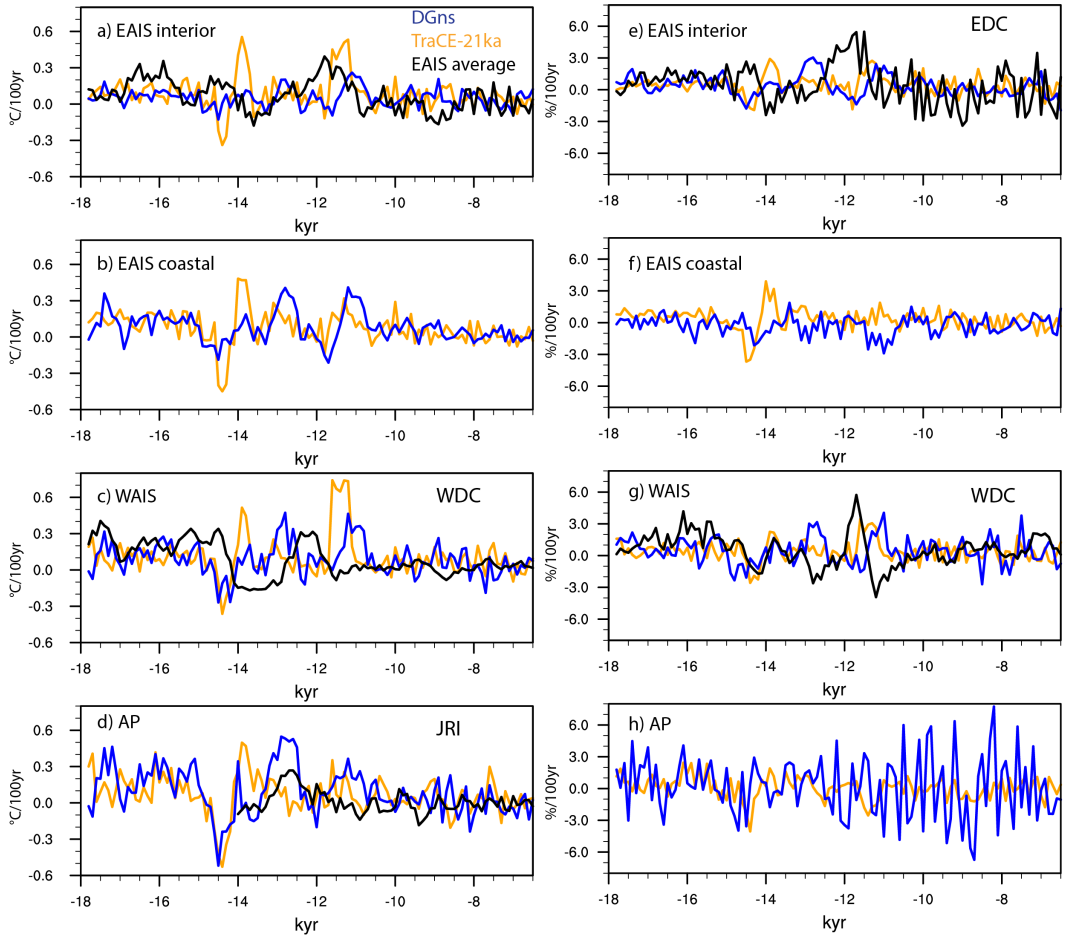

FIGURE 2.4: Centennial-scale rates of (a-d) surface temperature change (°C) and (e-h) relative accumulation change (%; DGns in blue, TraCE-21ka in orange, ice cores in black).

moisture gradient between the EAIS interior and the Southern Ocean is reduced.

In contrast to the EAIS ice cores, Fudge et al. (2016) highlighted the variability of the accumulation-temperature scaling relationship at the WDC site, noting three distinct periods in the 31-kyr record: an initial positive relationship from 31-15 ka (5.7% $°C^{-1}$), a weak negative relationship from 15-8 ka (-2.2% $°C^{-1}$), and a strong positive relationship from 8-0 ka (17.0% $°C^{-1}$). This suggests that the WDC site experiences synoptic-scale variability in precipitation not present at the EAIS ice core locations, and also not reproduced by the TraCE-21ka simulation. The DGns simulation shows higher variability in accumulation as West Antarctic temperatures approach near-PI levels in the mid-Holocene (Fig 2.5c). We have no accumulation record for the JRI site to compare with the models. However, both simulations exhibit similar

behavior in the AP region, with a shift in the scaling relationship with warming temperatures (Fig 2.5d). TraCE-21ka shifts to a slight negative relationship, while DGns begins to show a weaker relationship with high variability, suggesting that the AP region is also impacted by dynamical changes in the model simulations that counters the thermodynamic temperature scaling. In the case of TraCE-21ka, this circulation change reduces the amount of precipitation over this region.

We also examine the ratio of the 500 yr precipitation change to the 500 yr temperature change to explore how this relationship temporally evolves in the climate models (Fig 2.5e-h). Since some of the Antarctic ice core accumulation reconstructions are not fully independent from the temperature reconstructions (Veres et al., 2013; Frieler et al., 2015), analysis of the relationship cannot be performed for the ice cores except at multi-millennial timescales (Fudge et al., 2016), hence only the climate models are considered here. Figure 2.5e-h shows that the models remain nearly constant at the average scaling relationship, however, high variability occurs in the mid-Holocene in TraCE-21ka in the coastal regions (yellow bars), and to a lesser extent in DGns, suggesting a greater influence of synoptic-scale processes in precipitation at this time. The onset of high variability in accumulation-temperature scaling occurs earlier in DGns over the AP than over the coastal EAIS, but it occurs synchronously over the two regions at $\sim$9.5 ka in TraCE-21ka (Fig 2.5h,f). The WAIS and EAIS regions exhibit comparatively less variability in the scaling relationship (Fig 2.5e,g), but the relationship is not constant in time for either region.

2.4.4 Ocean temperatures

Both models simulate higher SSTs throughout the Southern Ocean in 6.5 ka relative to 18 ka, with the largest increase occurring $\sim$50°S (Fig 2.6a,b). SSTs generally increase by more over this the deglacial period in DGns than in TraCE-21ka, particularly in the Indian Ocean sector, southwest of New Zealand, and to the east of southern South America, where SST increases of >5°C between 18 and 6.5 ka are observed in DGns. The models show reasonable agreement with the SST change for the same period estimated in the marine proxy record, with differences of <1.0°C at four of the six sites (Fig 2.6a-h). The mismatches occur at site MD03-2611 (south Australia) and site TN057-13 (East Atlantic), where the models underestimate and overestimate the SST change, respectively.

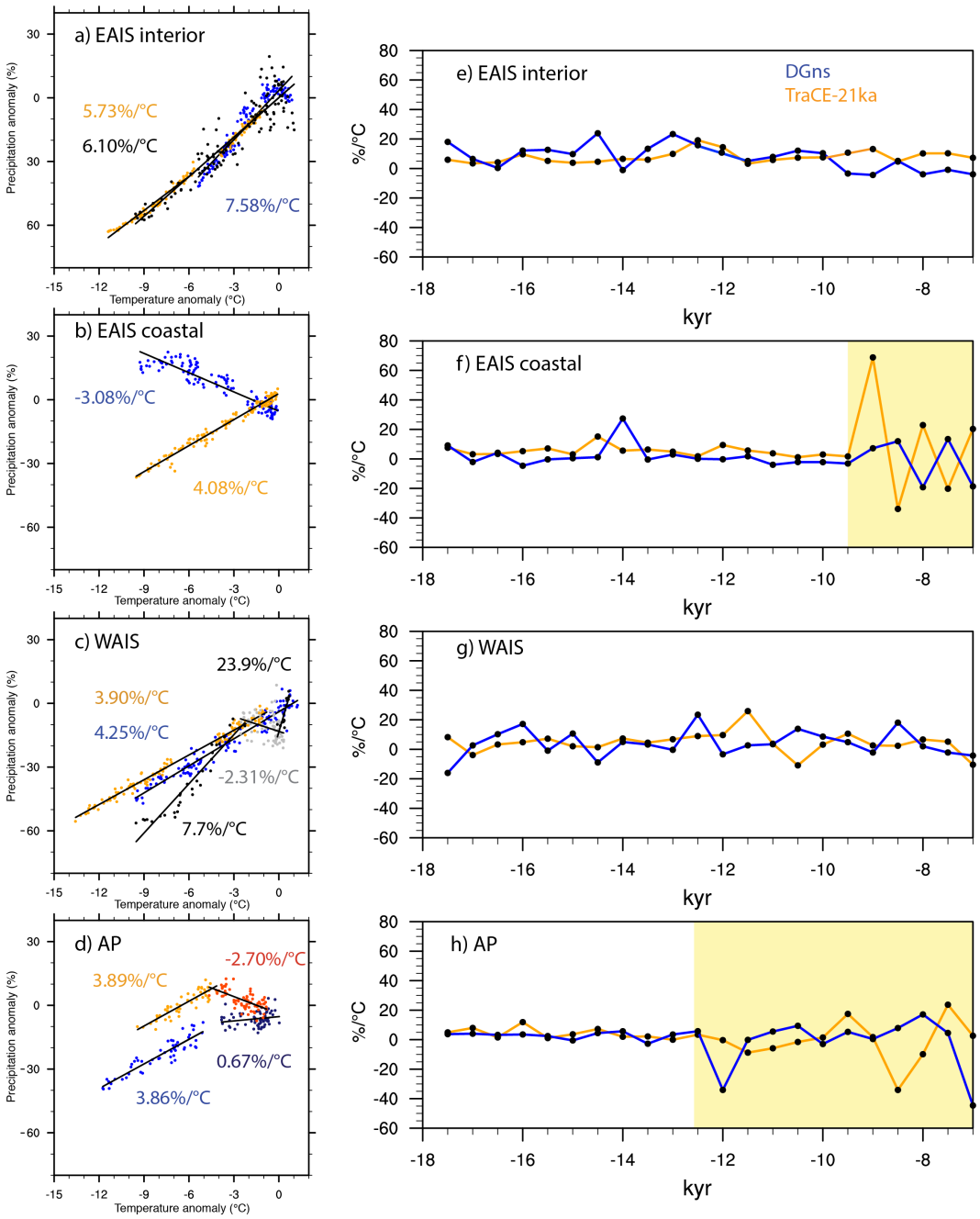

FIGURE 2.5: (a-d) Scaling relationships of accumulation (% relative to PI) and temperature (°C relative to PI) in each region. Black and grey dots refer to the proxy record, blue and purple dots refer to the DGns simulation, and orange and red dots refer to the TraCE21ka simulation. (e-h) The ratio of the change in precipitation (%) to the change in temperature (°C) per 500 years. The yellow bars in panel f and h indicate a shift to higher variability in accumulation-temperature scaling in the AP and EAIS coastal regions.

In terms of the absolute SSTs, the austral summer SSTs of the model generally show better agreement with the SSTs reconstructed from marine sediments (high end of color shading in Fig 2.6c-h). DGns exhibits higher austral SSTs than TraCE-21ka at five out of the six sites, and thus more closely matches the reconstructed SSTs. The main exception occurs in the Holocene at site TN057-13, in which the austral summer SST of the proxy record declines and converges with the TraCE-21ka austral summer SSTs. Temporally, the SST records show the largest SST increases in the early deglacial (Fig 2.6c,d,f,h) and in the early Holocene (Fig 2.6c-h), however, the models show relatively lower increases over these time periods.

At latitudes higher than 62°S, SSTs in both the TraCE-21ka and DGns simulations exhibit modest warming, with similar increases in the Ross, Amundsen and Bellingshausen Seas (Fig 2.7b-e). The DGns simulation shows greater sea surface warming in the Weddell Sea and the East Antarctic coastal seas (0.3-0.6°C). In the subsurface, TraCE-21ka initially shows much cooler temperatures during the LGM relative to PI. As a result, temperatures at 400 m depth increase by 2.1-2.7°C between 18 and 6.5 ka. In comparison, the DGns simulation, which is much closer to its PI temperature at 18 ka, shows relatively modest warming during the simulation period.

Meltwater input in the Southern Ocean at the time of MWP-1A decreases AABW formation and enhances the incursion of Circumpolar Deep Water on the Antarctic shelf in climate model simulations (Menviel et al., 2010), thus leading to a sub-surface warming along the Antarctic coasts. Following the different meltwater forcings used in the two models (see Methods), this subsurface warming occurs earlier and for a shorter duration in the TraCE-21ka than in DGns, with an offset of 1.2 kyr in the Weddell Sea (Fig 2.7c). SSTs show the opposite response in both models to this meltwater forcing. With the exception of MWP-1A, the greatest amount of sub-surface warming in TraCE-21ka occurs between 11.5 and 9.5 ka (Fig 2.7a-e). DGns shows also shows pronounced warming during this time interval along the East Antarctic coast (Fig 2.7d,e), but relatively modest temperature changes along the West Antarctic coast.

Considering the zonal perspective (64°S latitudinal band), the models display some similarities in the deglacial evolution of ocean temperatures to the depths of modern-day grounding lines (Fig 2.8). In response to the forcing of MWP-1A, warmer ocean temperatures relative to PI are simulated in both models in the eastern Ross Sea to the Bellingshausen Sea, though at different depths (Fig 2.8c,i). In TraCE-21ka the warming is more pronounced and

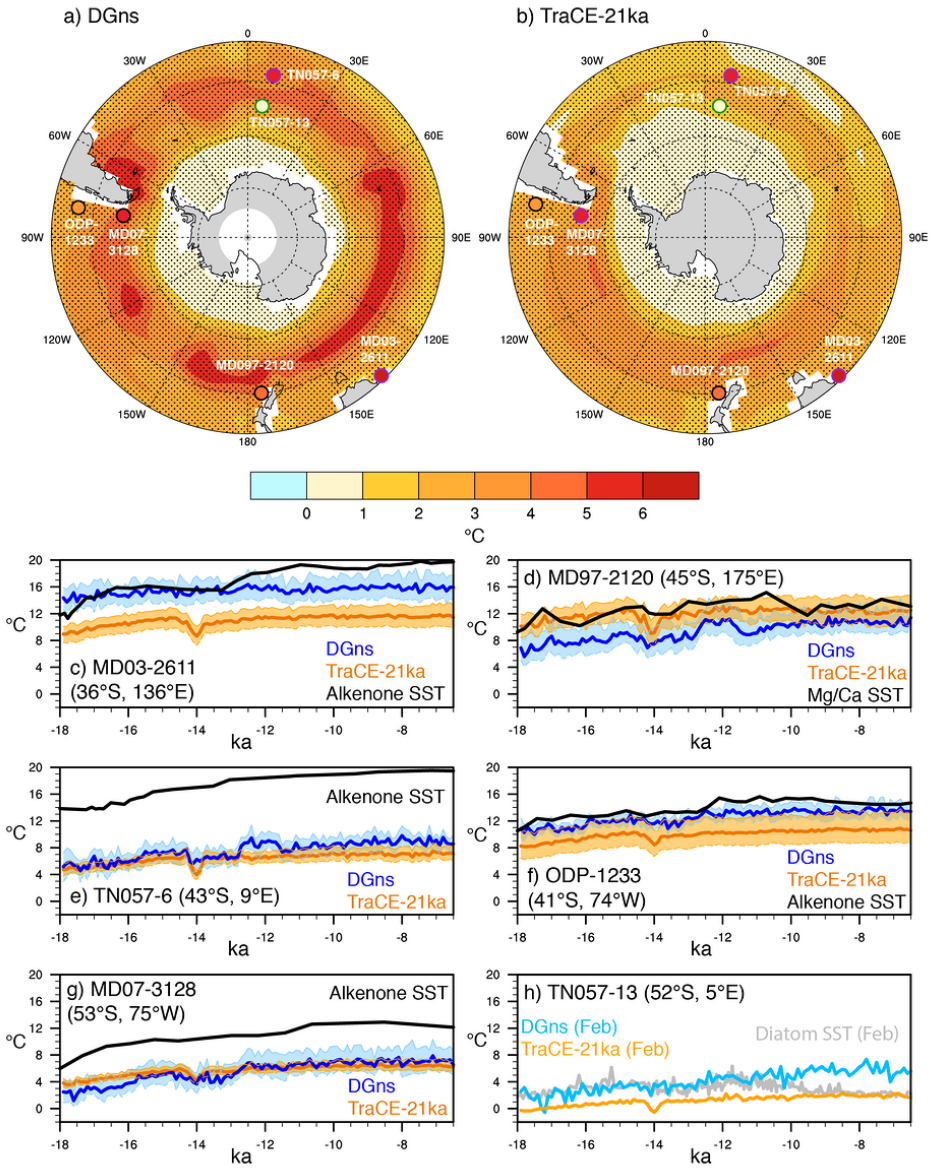

FIGURE 2.6: Sea surface temperature (SST) change (°C) as simulated in (a) DGns and (b) TraCE-21ka for the period of 18 to 6.5 ka (maximum Latitude of 35°S). Dotted lines indicate latitude (intervals of 15°) and longitude (intervals of 30°). Marine sediment locations are marked by open circles, with black outlines indicating a match in warming between the ice core and model simulation (i.e., the estimated proxy SST change from 18 to 6.5 ka is within the range of seasonal SST changes of the climate model), and green (purple) outlines indicating an overestimation (underestimation) in warming by the models. Stippling indicates a difference between decadal output of 18.0-17.5 ka and 7.0-6.5 ka that is significant at the 95% confidence level. (c-h) Time series of 100-yr average mean annual SST from the models and SST proxy reconstructions (°C) at each individual marine sediment core site. The color shading represents the seasonal range calculated from the 100-yr average austral summer and winter temperature anomalies. In panel h, only a seasonal (February) proxy reconstruction is available; therefore, we only show modelled February SSTs from the climate models for this site.

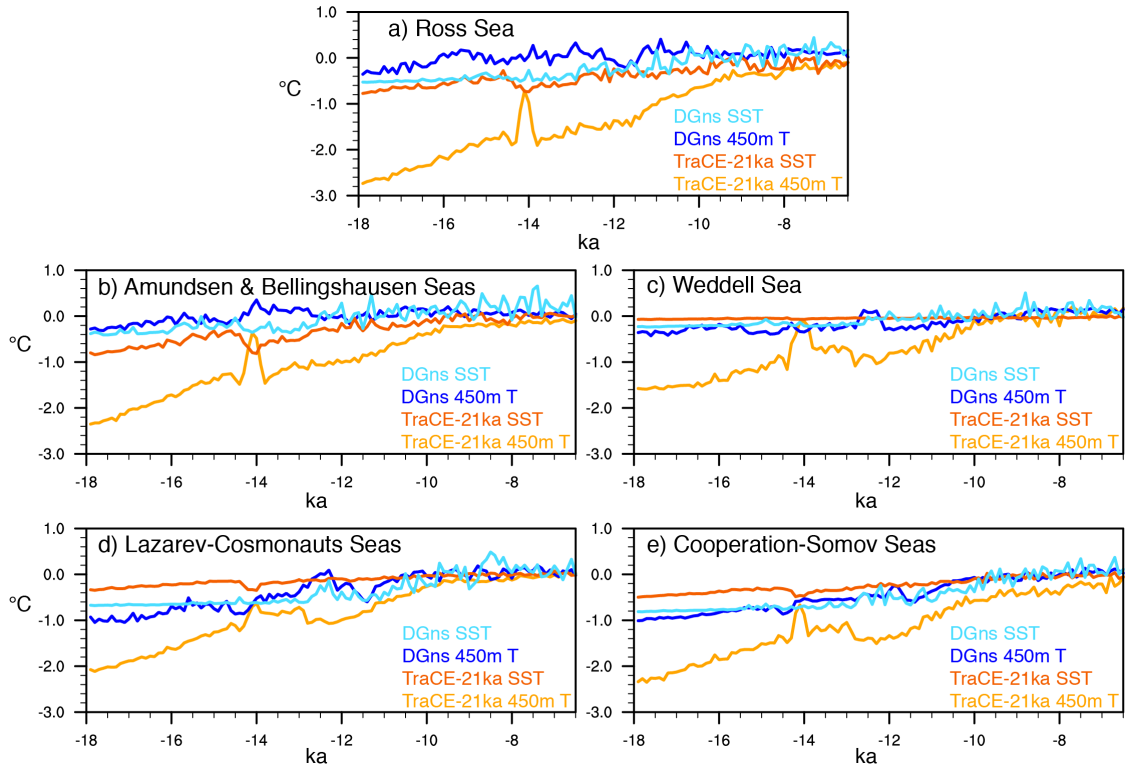

FIGURE 2.7: Time series of 100-yr mean annual average SST and 450 m depth ocean temperature anomalies relative to the Preindustrial era (°C) of the coastal seas around Antarctica, namely, (a) the Ross Sea (70S—62°S, 168°E—160°W), (b) the Amundsen and Bellingshausen Seas (68—62°S, 60—135°°W), (c) the Weddell Sea (70—62°S, 30—60°W), (d) the coastal region from Lazarev Sea to Cosmonauts Seas (67—62°S, 15°W—50°E), and (e) the coastal region from Cooperation Sea to Somov Sea (67—62°S, 55—165°E).

shallower (∼100-200 m), with temperatures remaining higher than PI into the Holocene (Fig 8a-f). In DGns, the warmer-than-PI temperatures occur at deeper depths, in the layer between 250 and 800 m (Fig. 2.8g-l). By 8 ka, much of the surface ocean exhibits temperatures similar to PI temperatures (Fig 2.8l). In contrast, TraCE-21ka shows slightly cooler temperatures, with the exception of the Amundsen and Bellingshausen sector at ∼150 m depth, where temperatures remain higher than PI (Fig 2.8f).

2.4.5 Sea Ice

Both deglacial simulations show a substantial decrease in sea ice extent, thickness, and coverage in each sector between 18 and 6.5 ka, interrupted only by an increase in sea ice during the ACR (Fig 2.9,2.10). In comparison to the austral winter LGM sea ice extent and concentration reconstructions (Gersonde et al., 2005), DGns austral winter sea ice extent (15% coverage) at 18 ka is consistent with the proxy-estimated LGM austral winter sea ice extent in the Indian and Pacific Ocean sectors, but DGns may overestimate sea ice extent in the eastern Atlantic sector (Fig 2.9a). TraCE-21ka is also consistent with the proxy record in the Indian and Pacific sectors, but overestimates the austral winter sea ice extent in the western Atlantic sector (Fig 2.9b). It should be noted that present-day simulations using the same GCM yield more extensive sea ice cover than observed (Yeager et al., 2006).

The models are consistent in terms of the behavior and absolute values of sea ice thickness and coverage (%) in each sector (Fig 2.10). The exceptions are the Weddell Sea and along the EAIS coast, in which TraCE-21ka produces sea ice that is approximately double in thickness. In contrast, thicker ice is observed in DGns along the WAIS coast in the Ross, Amundsen and Bellingshausen Sea sectors. DGns also exhibits higher centennial-scale variability in sea ice thickness, particularly in the Ross Sea sector. Mean 100 yr-average sea ice coverage (%) decreases in the TraCE-21ka simulation by 22, 23, 25 and 9% in the Ross Sea, the Amundsen and Bellingshausen Seas, along the EAIS coast, and the Weddell Sea, respectively, through this interval (Fig 2.10e-h). The DGns simulation shows similar sea ice coverage decreases of 24, 21, 30, and 12% in these coastal regions, respectively.

Similar to the behavior observed with ocean temperatures, TraCE-21ka displays a shorter, but higher magnitude response to Southern Ocean meltwater forcing associated with MWP-1A. The TraCE-21ka austral winter sea ice extent at 14 ka reaches lower latitudes than at 18 ka in the Atlantic sector

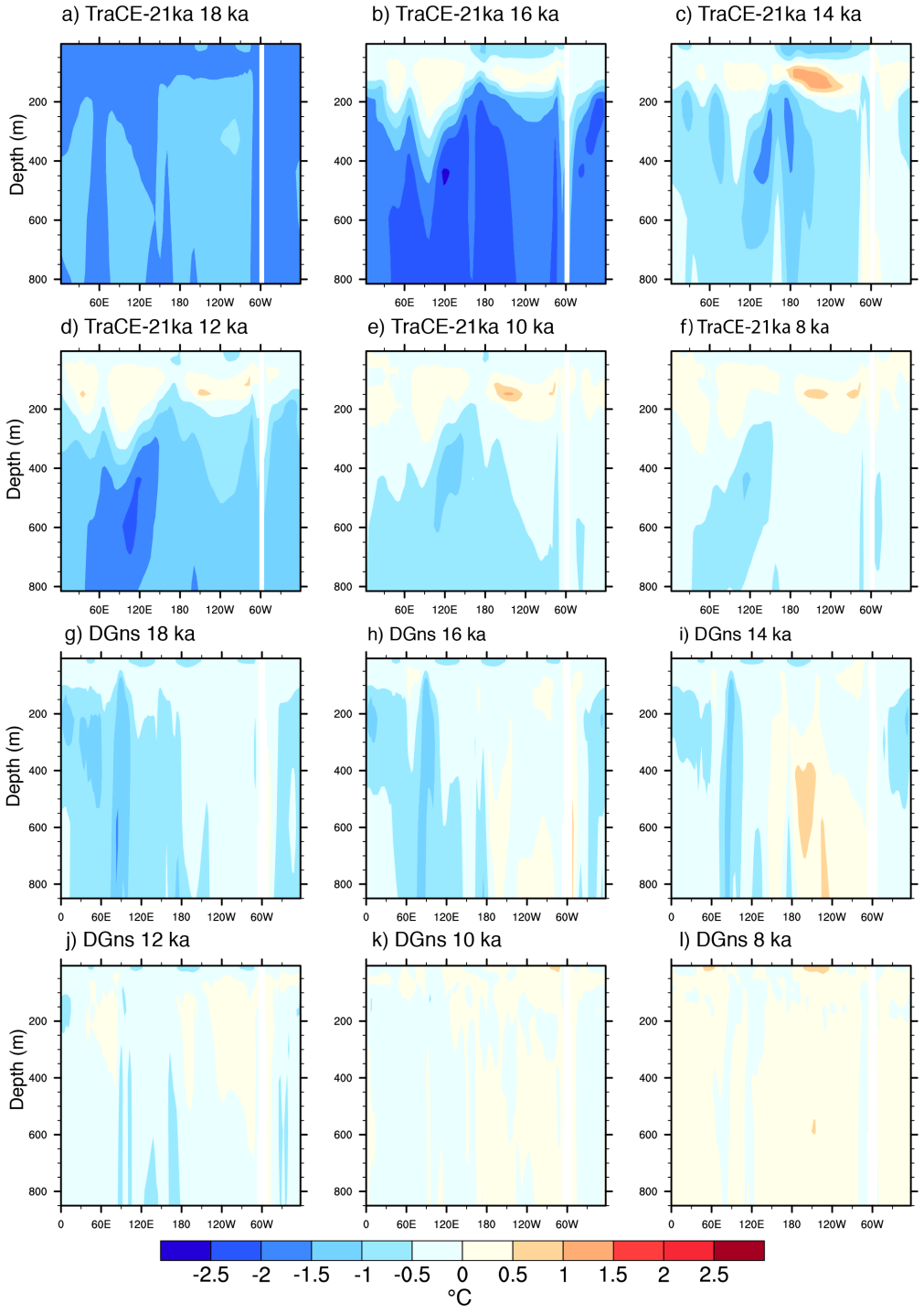

FIGURE 2.8: 2-ka time slices of longitudinal cross-sections of 100 yr-averaged ocean temperature anomalies relative to PI at 64°S the surface to 800 m depth: (a-f) TraCE-21ka 18ka to 8 ka; (g-l) DGns 18ka to 8ka.

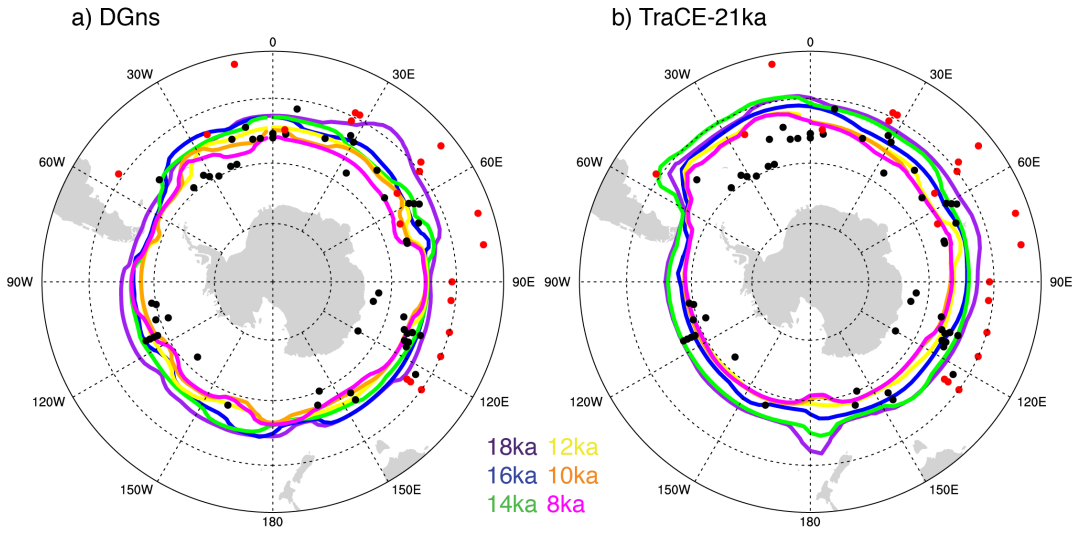

FIGURE 2.9: Modelled austral winter sea ice extent (15% coverage contour) per 2-ka for (a) DGns and (b) TraCE-21ka from 18-8 ka (maximum Latitude of 35°S). Dotted lines indicate latitude (intervals of 15°) and longitude (intervals of 30°). The circles refer to marine sediment core sites with black circles corresponding to sites that indicate the presence of winter LGM sea ice, whereas the red circles represent sites that indicate no presence of winter LGM sea ice (adapted from Gersonde et al., 2005).

(Fig 2.9b), and each coastal zone exhibits a short-lived increase in coverage and thickness (Fig 2.10). In contrast, DGns maintains relatively higher sea ice thickness and coverage following the meltwater forcing for a longer duration (∼1-1.5 ka), but with higher variability (Fig 2.10). Another difference is the increase in sea ice coverage in the EAIS coastal sector in DGns in the early Holocene (∼12-11 ka), which is not observed in TraCE-21ka. DGns also shows increases in sea ice coverage in the Ross, Amundsen and Bellingshausen sectors at this time, though with higher variability.

2.4.6 Southern Ocean-Antarctic climate connections

As described in section 3.1, the regions displaying the greatest increases in continental surface temperature that are not associated with changing ice sheet topography occur along the continental margins (Fig 2.2a,b). While many factors, including the changes in greenhouse gas content, orbital forcing and meridional heat transport, contribute to these surface air temperature changes, albedo-driven radiative changes associated with changes in sea ice coverage may also influence this enhanced warming observed in coastal areas. Surface albedo between 60-70°S over the Southern Ocean decreases by

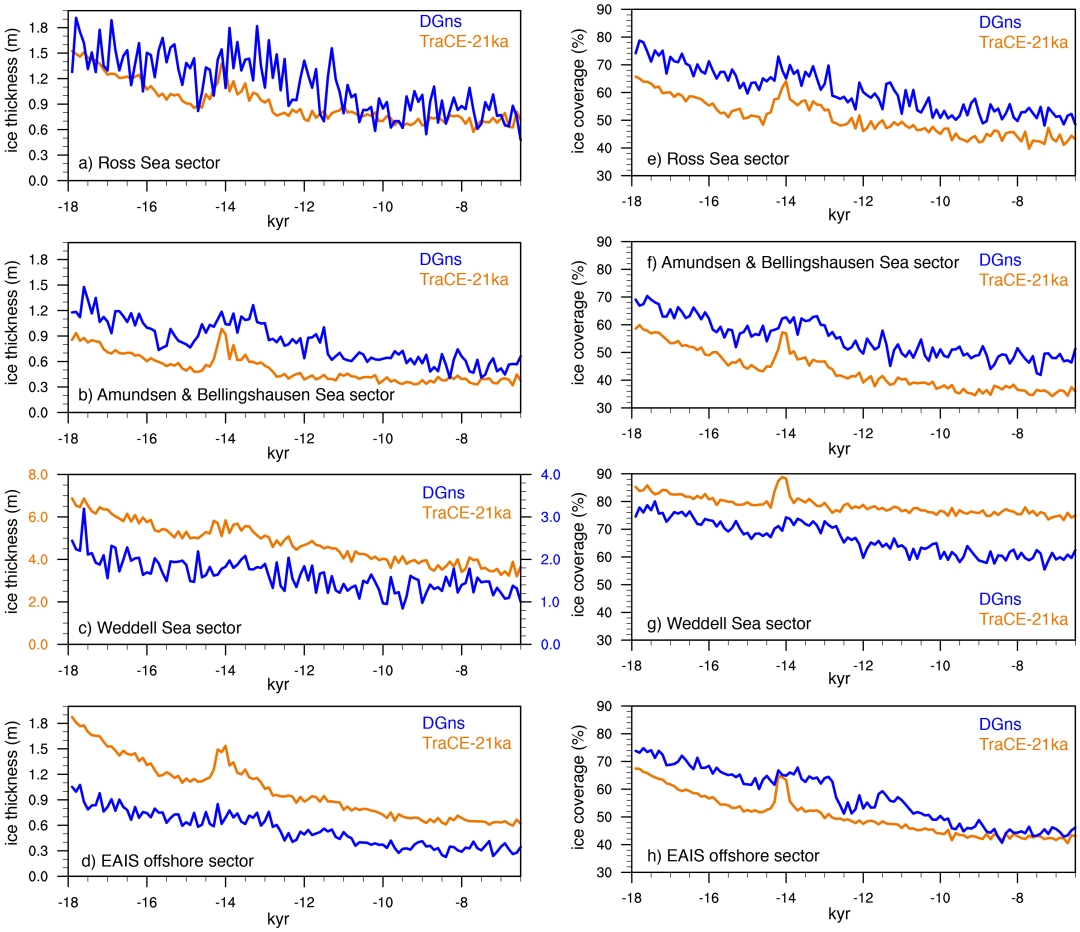

FIGURE 2.10: Time series of 100-yr mean annual average (a-d) sea ice thickness (m) and (e-h) coverage (%) in the Southern Ocean, namely, the Ross Sea sector (70—50°S, 168°E—160°W), the Amundsen and Bellingshausen Sea sector (68—50°S, 60—135°W), the Weddell Sea sector (70—50°S, 30—60°W), and the offshore EAIS sector from Lazarev Sea to Somov Sea (67—50°S, 15°W—165°E). Please note the difference in scale in panel c.

0.18 and 0.15 in DGns and TraCE-21ka, respectively. South of 60°S, TraCE-21ka shows larger decreases in surface albedo over the Ross, Amundsen and Bellingshausen Seas, whereas DGns shows larger decreases over the Weddell Sea and along the eastern Antarctic coast. However, these sector differences are relatively small between the two models at these latitudes (<0.05).

Strong negative correlations exist in both models between surface air temperature, surface albedo and sea ice coverage in both models over the Southern Ocean (Fig 2.11). In both cases, the correlations between surface air temperature and sea ice coverage are weakest in the Weddell Sea, where the decrease in sea ice coverage is relatively lower. TraCE-21ka also shows a small area of positive correlation adjacent to the Antarctic Peninsula (i.e., warmer surface temperatures associated with higher sea ice coverage, and vice versa). In addition to sea ice coverage, the surface albedo parameterization of both models accounts for the state of the sea ice surface, i.e., freezing or melting, snow coverage (Briegleb et al., 2004; Goosse et al., 2010). The TraCE-21ka simulation also accounts for the snow depth and snow age. Snow depth and surface melt also exhibit strong correlations to the surface air temperature over the Weddell Sea in TraCE-21ka, which may account for the difference in correlation with surface air temperature between surface albedo and sea ice coverage (Supplementary Information).

In addition to linkages with continental temperatures, Southern Ocean conditions exert a strong influence on Antarctic accumulation patterns (Delaygue et al., 2000; Stenni et al., 2010). Figures 2.12 and 2.13 show the Pearson linear cross-correlation coefficients (r) of modelled decadal SST and precipitation for 4 ice core locations in each continental region (i.e., WDC, EDC, JRI, and Law Dome (LD)) for DGns and TraCE-21ka, respectively. SSTs generally show strong spatial correlations to continental accumulation in both models in the early deglacial period (18-12 ka), however, these relationships weaken or become more negative in the early to mid-Holocene (12-6.5 ka). The difference in millennial-scale variability between the two periods, which is higher in the early deglacial period, with Heinrich Stadial 1, the ACR, and Younger Dryas, likely contributes to this shift in correlation strength.

The SST-continental precipitation correlations are higher for TraCE-21ka than DGns at every site except JRI, where the difference between the early deglacial period and early to mid-Holocene is starkest as the correlations transition from positive to slightly negative (Fig 2.13g,h). The models both exhibit high positive correlations between SSTs in the Indian and Pacific sectors with EDC precipitation in the early deglacial period (18-12 ka). Both

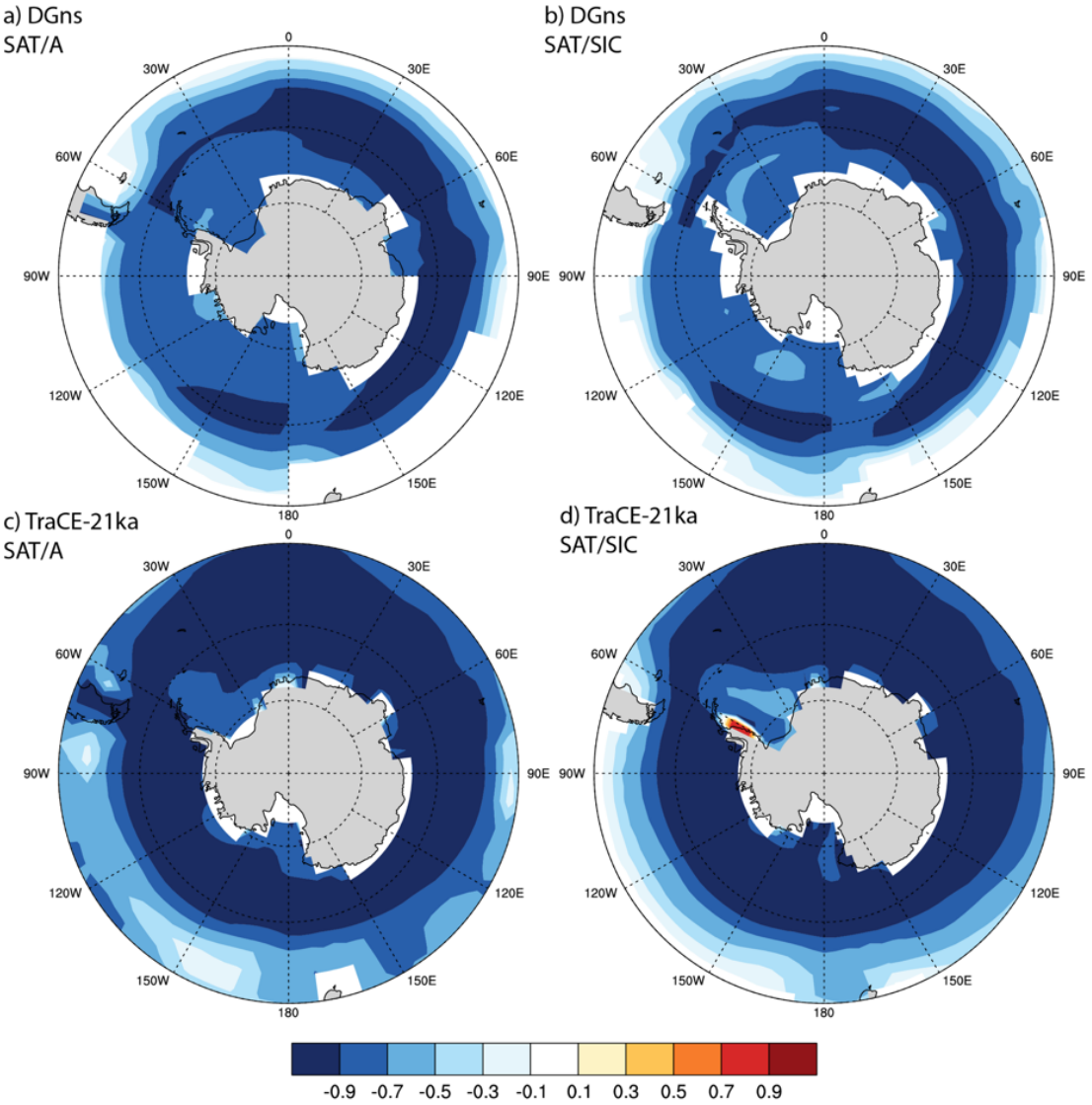

FIGURE 2.11: Spatial Pearson linear cross-correlation coefficients (r) between decadal surface air temperature (SAT, °C), surface albedo (A), and sea ice coverage (SIC, %) for (a-b) DGns and (c-d) TraCE-21ka (maximum Latitude of 45°S). Dotted lines indicate latitude (intervals of 15°) and longitude (intervals of 30°). DGns SAT was regridded to the same grid as DGns SIC using bilinear interpolation in panel b.

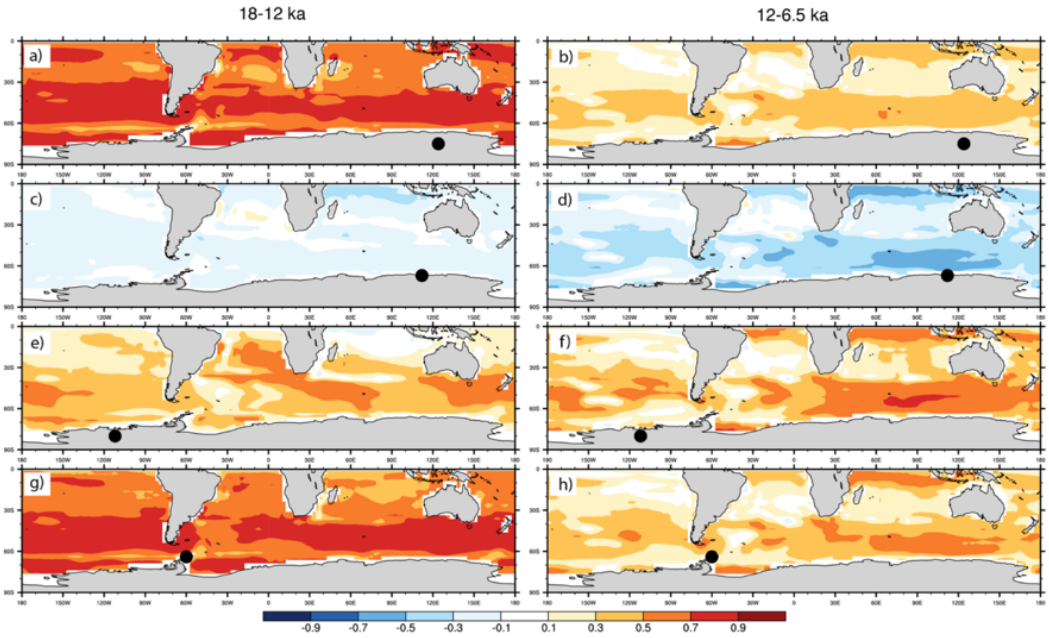

FIGURE 2.12: Spatial Pearson linear cross-correlation coefficients (r) between decadal SST and precipitation of the DGns simulation for (left) 18-12 ka and (right) 12-6.5 ka at the (a,b) EDC (73-77°S, 121-127°E), (c,d) LD (65-70°S, 110-116°E), (e,f) WDC (77-82°S, 115-109°W), and (g,h) JRI (63-65°S, 59-62°W) ice core locations, respectively.

models also show high positive correlations between WDC precipitation and SSTs in the Pacific sector in the early deglacial period, but these correlations weaken in the Holocene, particularly in the DGns simulation (Fig 2.12c). Less model consistency exists at the coastal sites, most notably at LD (Fig 2.12c,d, 2.10c,d), which is likely related to the above-mentioned resolution limitation of DGns along the EAIS coast.

To better understand the transitions in the accumulation relationships to continental temperatures and SSTs in the early Holocene, we consider changes in 500hPa geopotential height anomalies over the Southern Ocean and their relation to changes in atmospheric circulation. More specifically, the Amundsen Sea Low, which is the largest influence on meridional circulation in the region, acts as a major control on the temperature and precipitation in West Antarctica (Raphael et al., 2016). Modeling studies and ice core analyses have suggested that atmospheric teleconnections driven by tropical SST anomalies in the Pacific trigger a quasi-stationary wave response that reduces pressure over the Amundsen Sea. However, they offer conflicting accounts of teleconnection strength during glacial conditions (Timmermann et al., 2010; Jones et al., 2018). At 18 ka, the models display negative 500hPa geopotential height anomalies over much of the Southern Ocean (Fig 2.14), in

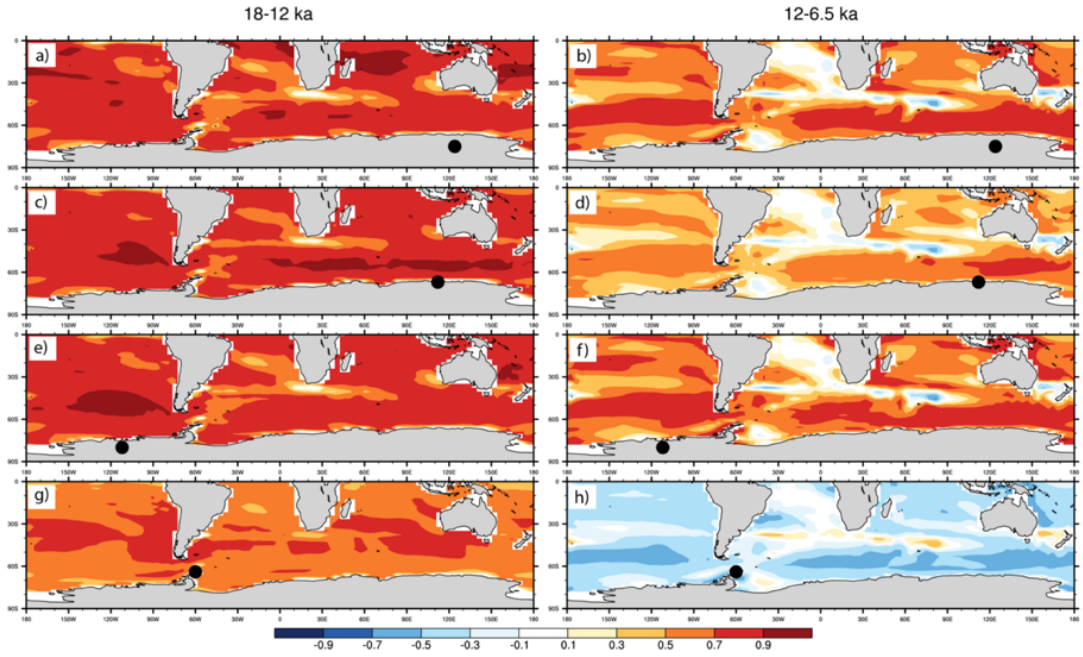

FIGURE 2.13: Spatial Pearson linear cross-correlation coefficients (r) between decadal SST and precipitation of the TraCE-21ka simulation for (left) 18-12 ka and (right) 12-6.5 ka at the (a,b) EDC (73-77°S, 121-127°E), (c,d) LD (65-70°S, 110-116°E), (e,f) WDC (77-82°S, 115-109°W), and (g,h) JRI (63-65°S, 59-62°W) ice core locations, respectively.

contrast to the LGM simulation of Jones et al., (2018), which shows positive anomalies over the Amundsen Sea associated with a more El Niño-like state due to the orographic effects of the North American ice sheet.

The 500 hPa geopotential height anomalies are more extreme in the TraCE-21ka than in DGns, particularly with regard to the positive anomalies observed over the ice sheet, which is primarily driven by the ice sheet topographic changes. Strong negative anomalies over the Amundsen Sea are observed in both models during the ACR (Fig 2.14c,j). A deepened Amundsen Sea Low is generally associated with enhanced northerly flow across the AP, allowing for intrusions of marine air masses over WAIS (Hosking et al., 2013). Through time, the simulated geopotential height increases over the Southern Ocean to near-PI levels, reaching a state of reduced variance over the Amundsen Sea in the early Holocene, consistent with the timing of reduced accumulation-temperature scaling over the AP in both model simulations (Fig 2.5d).

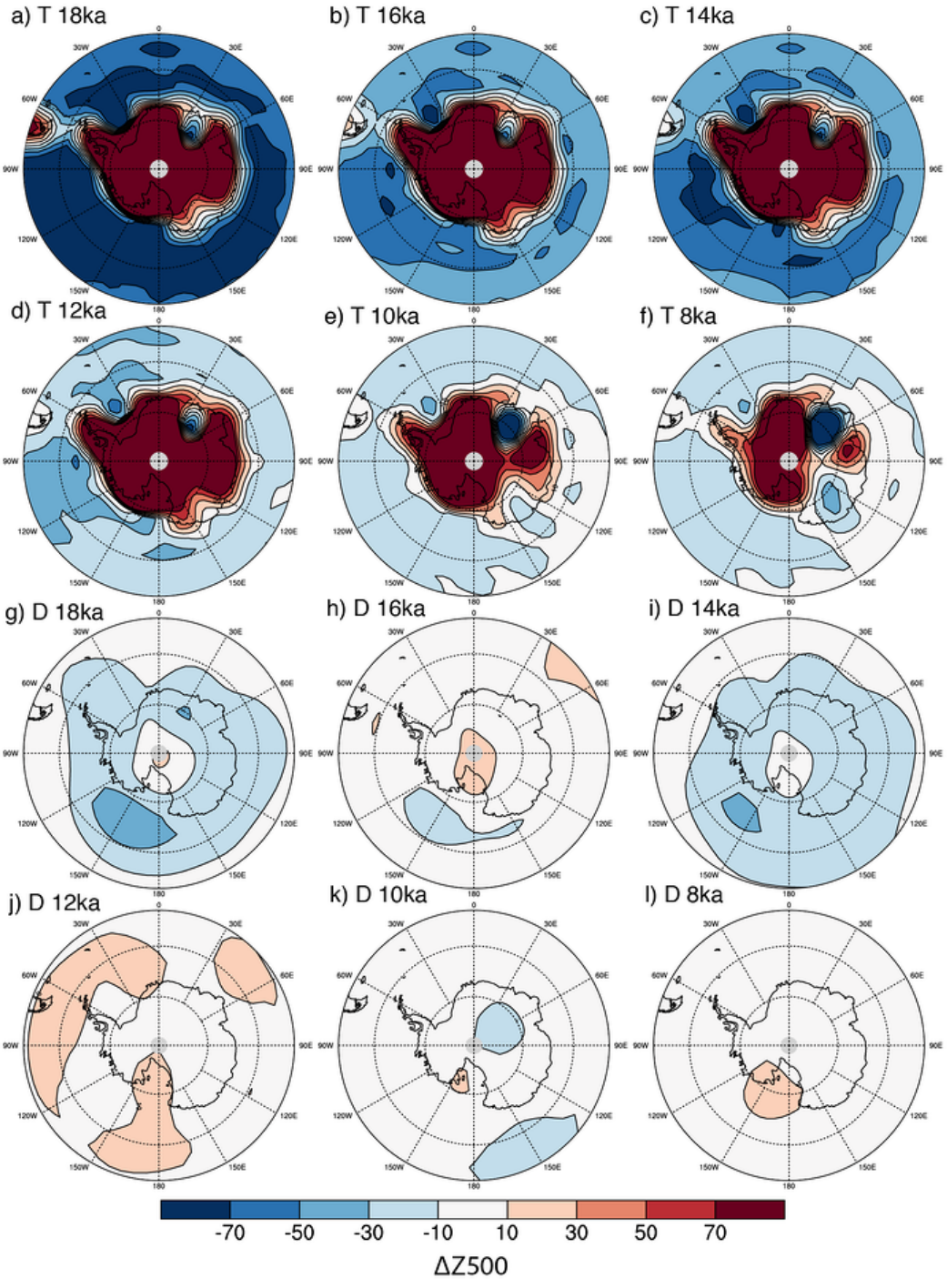

FIGURE 2.14: Geopotential height anomalies (m) at 500hPa relative to PI for the (a-f) TraCE-21ka and (g-l) DGns deglacial experiments (maximum Latitude of 50°S). Dotted lines indicate latitude (intervals of 15°) and longitude (intervals of 30°).

2.5 Discussion

2.5.1 Regional patterns of deglacial climate evolution

The deglacial model simulations and Antarctic ice core records demonstrate clear regional differences between East and West Antarctica as well as between coastal regions and the continental interior in terms of deglacial warming, driven primarily by oceanic influences. In comparison to the East Antarctic ice cores, the WDC isotope record indicates that the glacial termination of the more heavily marine-influenced WAIS initiated ∼2 kyr earlier than EAIS, with warming that reached near-mid Holocene levels by 15 ka, coincident with a decline in circum-Antarctic sea ice (Fudge et al., 2013; Cuffey et al., 2016). Although the climate models underestimate the rate of warming between 18-15 ka over WDC, they do show greater warming rates for the WAIS, AP, and coastal EAIS regions, also occurring synchronously with the greatest declines in coastal sea ice, as compared to the less-marine influenced EAIS interior. The ice cores and models constrain centennial-scale warming rates to within 0.6°C, with the most rapid warming occurring at the end of the ACR, excluding the abrupt ice mask-induced warming in TraCE-21ka.

In terms of the spatial pattern of temperature change from the termination to the mid-Holocene, the greatest continental warming occurs over sea ice-adjacent land and areas of lowered ice surface elevation, highlighting the strong effects of albedo and orography on regional temperatures in Antarctica. The sea ice-albedo effect may be overestimated in the models over the AP, as demonstrated by the JRI temperature reconstruction; however, Mulvaney et al. (2012) do note the strong sensitivity of AP temperature to ice shelf-related changes, with rapid warming events in the early Holocene and over the past 100 years (1.56 ± 0.42°C). Additional temperature and methane sulphonic acid reconstructions of coastal Antarctic ice cores could further elucidate the regional sensitivities to localized ice shelf and sea ice changes and identify possible thresholds.

In comparison to surface temperature, the regional evolution of accumulation and its relationship to surface temperature and conditions in the Southern Ocean through the deglacial period remain less clear. The two climate simulations show substantial differences with regard to the overall magnitude of accumulation changes in each region. In both the ice core records and

the models, accumulation over the ice sheet generally shows higher variability in coastal regions, as expected, with the EAIS interior displaying consistent temperature-accumulation scaling relationships at various sites, as previously demonstrated by Frieler et al. (2015). A primary limitation of the intermediate complexity LOVECLIM model is the inadequate resolution for the steep elevation gradient of the coastal EAIS (Goosse et al., 2012), which leads to a precipitation bias in the region in the DGns simulation. This effect worsens through time due to the reduced moisture gradient between the Southern Ocean and the EAIS interior, as P-E increases over the EAIS interior, presumably from thermodynamic scaling with temperature.

The climate models show limited variability in accumulation-temperature scaling over WAIS, in contrast to the WDC record (Fudge et al., 2016); however, the AP exhibits a marked shift in the early to mid-Holocene, which may be due to changes in atmospheric circulation. This climatic shift in the early to mid-Holocene coincides with the reduced variance and weakening of the Amundsen Sea Low, which achieves near-present day conditions in both models by $\sim$12 ka. The weakened Amundsen Sea Low appears to reduce the accumulation-temperature scaling over the AP in both models, and in the case of TraCE-21ka, a slight negative scaling relationship is observed. Although this is not observed over the greater WAIS region, it should be noted that the timing is roughly consistent with the slight negative scaling period observed in the WDC record (15-8 ka).

It may be expected that the retreat of sea ice and increased area of open ocean may introduce additional moisture sources, thereby enhancing precipitation relative to temperature. In fact, coastal ice core records of the Holocene, including Taylor Dome, Law Dome, Siple Dome, have exhibited decoupling between accumulation and temperature that has been attributed to moist-air cyclonic activity and changes in sea ice conditions (Monnin et al., 2001). Although the climate simulations do not exhibit a substantial increase in the scaling relationship with reduced sea ice coverage, much higher temporal variability is observed over coastal EAIS in the mid-Holocene. Likewise, the reduced correlations between Antarctic precipitation at the inland ice core locations and SSTs in the Holocene may demonstrate that this effect is not limited to the coasts in these climate simulations.

The linkages between sea ice coverage, atmospheric dynamics and continental accumulation may also have important implications for future projections of the more heavily marine-influenced WAIS climate, as GCMs used in the Coupled Model Intercomparison Project 5 (CMIP5) tend to project

higher accumulation-temperature scaling in the future due to reduced sea ice coverage (Palerme et al., 2017). This effect may also be quite regionally dependent, as no statistically significant increase has been observed over the Thwaites glacier over the past three decades (Medley et al., 2013). The results here also highlight that dynamical processes cannot be discounted in Antarctic accumulation projections. Additional moisture budget analysis is warranted to better constrain the effects of circulation changes and cyclonic-driven precipitation on Antarctic accumulation in transient climate simulations, particularly in relation to tropical and mid-latitude teleconnections with the Amundsen Sea Low.

2.5.2 Regional patterns of deglacial ocean evolution

Given the lack of Southern Ocean proxy records and the large uncertainties of those that do exist, the current understanding of the deglacial evolution of Southern Ocean conditions remains limited. The available SST records from this region that cover the deglacial period generally show two key phases of rapid warming, that is, at the start of the deglaciation ($\sim$18-14.5 ka) and following the ACR into the early Holocene ($\sim$12.5-10 ka; Calvo et al., 2007). However, differences between the records can be observed, even between marine records located in close proximity, but at different latitudes; for example, cores ODP-1233 and MD07-3128 off the coast of southern Chile display differences in the timing of SST warming (Caniupán et al., 2011). Also different among the records is the presence and duration of Holocene cooling, with an early and long-term cooling trend observed in TN057-13 (Anderson et al., 2009), but no such trend observed in TN057-6 (Anderson et al., 2014b). Both records are from the East Atlantic, but on opposite sides of the modern Antarctic Polar Front. The SSTs are also based on different proxies, hence the divergent behaviour may be driven by out-of-phase trends of seasonal insolation during the Holocene (Leduc et al., 2010).

Using SST reconstructions to constrain the model results is challenging considering the spatial and temporal gaps in the records, uncertainties in the age scales, and the potential for proxy-related biases. The proxies may also be recording temperatures at depths other than the surface in accordance with the depth at which the diatoms and foraminfera occurred. The modelled austral summer SSTs generally show better agreement with reconstructed SSTs rather than the modelled annual mean SSTs averaged over 100 yr. We focus on decadal- to centennial-scale changes because the TraCE-21ka ocean

output are available as decadal averages, however, we do note that the modelled annual variability of SST in DGns is higher, with average austral summer SST ranges of 4.25°C in the early deglacial (18-17 ka) and 3.27°C in the middle Holocene (7.5-6.5 ka) at the 6 proxy record sites. It is therefore expected that the modelled SSTs do have greater overlap with the proxy reconstructions on an annual-scale, and are likely within the large range of proxy uncertainty (e.g., Tierney and Tingley, 2018). In terms of the temporal evolution, the models do not reproduce a decreasing trend in the mid-Holocene at any of the analysed sites. While this may in part be driven by biases in particular records, since not every SST reconstruction displays this trend, it has also been posited that this Holocene model-data discrepancy is the result of model bias in the sensitivity to decreasing obliquity, with the positive albedo feedback with snow, ice, and vegetation too weakly represented (Liu et al., 2014). Lastly, given that the locations of the marine proxy records are in close proximity to modern ocean frontal systems, it should be noted that shifts in these systems through the deglacial period may account for some differences between the reconstructed and simulated ocean temperatures.

In addition to these challenges, there are a few known model biases with regard to the simulation of modern ocean circulation in both models that should be considered. Although the ocean component of LOVECLIM, which is used for the DGns simulation, generally shows strong agreement with observations of Southern Ocean overturning circulation, it produces shallower convection in the North Atlantic (Driesschaert et al., 2007), which may have implications for ocean circulation over these millennial timescales. The CCSM3 model, which is used for TraCE-21ka, overestimates modern sea ice extent and thickness in both hemispheres, likely resulting from stronger-than-realistic wind forcing (Yeager et al., 2006). This also influences both ocean temperatures and salinities in the Ross and Weddell Seas, leading to AABW that is denser than observed (Danabasoglu et al., 2012). From a paleoclimate perspective, CCSM3 is an outlier in terms of sea ice and southern westerlies strength among climate models in the Paleoclimate Modelling Intercomparison Project 2 (PMIP2) for the LGM (Rojas et al., 2009). It should be noted that more recent versions of these models have improved on these issues, with CCSM4 showing better agreement to the LGM sea ice proxy data of Gersonde et al. (2005) in the Southern Ocean (Brady et al., 2013). Therefore, it is expected that if this transient experiment was performed using an updated version, better model-proxy agreement with regard to sea ice would be observed.

Mesoscale eddies are ubiquitous in the Southern Ocean and the eddy-driven circulation counteracts the Eulerian component driven by Ekman transport. Coarse resolution climate models are not able to resolve mesoscale eddies and instead use the Gent and McWilliams parametrization (Gent and Mcwilliams, 1990; Gent et al., 1995). While previous studies suggested that, due to their coarse resolution, the climate models used here could have a stronger-than-realistic sensitivity to wind forcing (Farneti and Delworth, 2010), more recent studies suggested that the Antarctic Circumpolar Current and Southern Ocean overturning response to wind and freshwater forcing in coarse and high-resolution models was in general agreement (Downes and Hogg, 2013; Menviel, Spence, and England, 2015; Menviel et al., 2018). Nevertheless, a more detailed analysis of the relationship between wind changes and Southern Ocean circulation is required to further explore this possibility. In particular, reconstructions of westerly wind strength and position (e.g., Kohfeld et al. (2013)) paired with reconstructions of Southern Ocean circulation (e.g., Rae et al. (2018)) could offer useful constraints for future paleoclimate simulations.

One of the larger unknowns of the last deglaciation that is of great consequence to Antarctic ice sheet retreat history is the temporal evolution of coastal ocean temperature changes at grounding line depths. This is particularly important for WAIS, as the reverse slope bathymetry of the continental shelf creates a configuration prone to retreat, a process that may be currently impacting some regions (Pritchard et al., 2012; Favier et al., 2014). Although the seafloor geometry likely acted as a first order control on ice sheet retreat of grounded ice in some locations (Bentley et al., 2014; Halberstadt et al., 2016), changes in ocean temperature and warm water intrusions underneath ice shelves can dictate the timing of the retreat. The proxy record provides few constraints on coastal sub-surface ocean temperature changes, but the deglacial climate model simulations analysed here do offer some insights. Both models show differences between ocean temperature evolution in the sub-surface as compared to the surface, suggesting that SST reconstructions may not be useful for understanding past ocean forcing of the Antarctic ice sheet. This difference is more pronounced in TraCE-21ka, which shows substantially cooler glacial ocean temperature anomalies in the sub-surface as compared to the surface close to the continent.

Despite differences in the prescribed meltwater forcings associated with MWP-1A, both TraCE-21ka and DGns show pronounced sub-surface warming following this event. The input of meltwater in the Ross and Weddell

Seas at the time of MWP-1A decreases AABW formation and enhances the incursion of Circumpolar Deep Water on the Antarctic shelf (Menviel et al., 2011). The warming is most evident in the Amundsen and Bellingshausen Sea sector in both models. Ice sheet model simulations using various climate forcings, including DGns output, have suggested that the initial retreat of WAIS occurred in the AP region and outer Weddell Sea, which is consistent with this location of sub-surface ocean warming (Golledge et al., 2014). The meltwater forcing resulting from this retreat may have resulted in a positive feedback between sea ice, AABW production, and thermal erosion at the ice sheet grounding line.

2.5.3 Transient climate modeling limitations

The main limitations of these experiments involve the poor paleo-constraints with regard to certain boundary conditions. Both transient simulations display discrepancies with the paleo-records across the ACR and early Holocene. In the case of TraCE-21ka, the ACR is more abrupt and of a larger magnitude than in the ice core temperature and SST reconstructions, which is related to how the MWP-1A meltwater forcing is applied between 14.35 and 13.85 ka (see Methods).

He (2011) performed a sensitivity experiment with CCSM3, in which the prescribed meltwater discharge in both hemispheres associated with MWP-1A was excluded, that improves on the ACR model-proxy agreement. The meltwater discharge applied to the North Atlantic prior to the ACR (17-14.67 ka) suppresses the upper cell of the AMOC. When this freshwater forcing is terminated at 14.67 ka, AMOC recovers. Without the inclusion of MWP-1A meltwater discharge during the Bølling-Allerød interstadial, Antarctic surface temperatures can remain cooler for a longer duration due to the bipolar seesaw response to the rapid increase in AMOC strength, which leads to a warming in the Northern Hemisphere. Pedro et al. (2016) note that the cooling in this ACR simulation induced by the AMOC strengthening at the end of Heinrich Stadial 1 is further amplified by the expansion of Southern Hemisphere sea ice. However, the ACR simulation is also limited in that it does not capture Older Dryas cooling over the Northern Hemisphere (He, 2011), and the improved ACR representation without freshwater forcing is difficult to reconcile with sea level records that indicate the pronounced meltwater discharge of MWP-1A (Deschamps et al., 2012).

In comparison to TraCE-21ka, the DGns experiment better matches the duration of the ACR, but shows more modest temperature changes, particularly over the EAIS interior region. Prescribed Southern Hemisphere meltwater helps induce the ACR in DGns by reducing AABW formation, thereby decreasing the southward oceanic heat transport (Menviel et al., 2011). The longer duration and lower magnitude of meltwater forcing applied to the Ross and Weddell Seas to represent MWP-1A in DGns likely drives these differences with TraCE-21ka, which shows a shorter and more pronounced ACR. The shutdown of the AMOC at $\sim$13 ka associated with the Younger Dryas and AABW strengthening lead to a significant warming at high southern latitudes in the DGns experiment. However, this warming does not continue into the early Holocene (11.5-10 ka) as indicated by the Southern Ocean SST proxy records. TraCE-21ka similarly does not reproduce the warming through this interval.

Bereiter et al. (2018) suggest that this model-proxy mismatch during the early Holocene is not uncommon among GCMs and intermediate complexity models, and may indicate that the current generation of climate models may underestimate ocean heat uptake or that the understanding of the boundary conditions used for ACR/Younger Dryas climate simulations may be flawed. More specifically, given that the precise timing, magnitudes and locations of MWP-1A and MWP1B remain a subject of debate (Bard, Hamelin, and Delanghe-Sabatier, 2010; Deschamps et al., 2012; Gregoire et al., 2016), yet the prescribed meltwater forcings have significant effects on the climate evolutions in these transient simulations (He, 2011; Menviel et al., 2011), accurate model representation through this interval may remain limited until these meltwater discharge events are better constrained.

Additional transient climate simulations of the deglaciation using different GCMs and intermediate complexity models are required to more clearly determine which of these differences and similarities are model dependent. Considering the significance but high uncertainty of the prescribed meltwater forcings in these simulations, the incorporation of coupling between GCMs and dynamic ice sheet models is a necessary step to ensure that climatically relevant ice-ocean interactions and feedbacks, such as sub-ice shelf melting and ice berg calving, are adequately reproduced in future transient climate simulations. Marine sediment and coastal ice core reconstructions that can be used to evaluate these climate model performances in terms of coastal ocean circulation and sea ice would also be particularly helpful in better understanding Antarctic climate evolution and ice sheet retreat history

during the deglaciation.

2.6 Summary and Conclusions

Based on spatial and temporal analysis of two transient climate simulations of the last deglaciation, one using a fully coupled GCM (TraCE-21ka) and one using an intermediate complexity model (LOVECLIM DGns), we explore the regional aspects of Antarctica's deglacial climate evolution. We also assess climate model performances with regard to model output most relevant to ice sheet model simulations, including surface temperature, surface mass balance, coastal ocean temperatures, and sea ice. The main findings of this study are as follows:

The greatest continental surface temperature warming from the glacial termination (18 ka) to the mid-Holocene (6.5 ka) occurs along coastal margins and, in the case of TraCE-21ka, regions with the greatest decrease in ice surface elevation, suggesting the importance of sea ice-albedo feedbacks and ice sheet dynamics in Antarctica's deglacial evolution. The centennial-scale rates of temperature change are reasonable as compared to the proxy record.

Strong discrepancies in modelled accumulation (P-E) are observed in the two climate simulations, particularly along the EAIS coast, which are related to the coarser resolution of the atmosphere component of DGns compared to TraCE-21ka. TraCE-21ka successfully captures the magnitude of accumulation change estimated for WDC and is within proxy uncertainty of EDC, whereas DGns underestimates the accumulation change at WDC and overestimates the change at EDC. Accumulation-temperature scaling relationships are also not spatially or temporally uniform, with the coastal EAIS and AP showing higher variability in the relationship in the early to mid-Holocene.

The models show some substantial differences with regard to coastal SSTs and sub-surface ocean temperatures. The TraCE-21ka simulation exhibits considerably cooler glacial Southern Ocean temperature anomalies, and as a result, experiences a greater degree of warming to the mid-Holocene. Both models show sub-surface warming in response to Southern Ocean meltwater forcing of MWP-1A that is most pronounced between the Amundsen and Bellingshausen Sea sector, though this warming occurs at different depths.

Both models reasonably capture glacial sea ice extent estimated in the proxy record, but may overestimate austral winter sea ice extent in parts of the Atlantic sector. The models are relatively consistent in terms of changes

in sea ice coverage and thickness along the Antarctic coast. The exception is the Weddell Sea, in which TraCE-21ka shows considerably thicker sea ice.

Correlations between Southern Ocean SSTs and Antarctic accumulation weaken in the Holocene, coinciding with the reduction of sea ice coverage and increased variability in accumulation-temperature scaling over the coastal regions. A weakened and more stable Amundsen Sea Low appears to decrease accumulation-temperature scaling over the AP. A more detailed moisture budget analysis with an emphasis on tropical teleconnections to the Amundsen Sea Low is required to better understand this climatic shift.

The greatest model-proxy mismatch occurs with the temperature and accumulation changes associated with the ACR and the SST changes associated with the early Holocene ocean warming event, in which the models do not adequately capture the precise magnitude and duration of change. These mismatches may result from model bias in large-scale ocean circulation, biases in the proxy records, or poorly constrained boundary conditions during these time periods. In particular, deglacial climate evolution is highly sensitive to the timing, magnitude and location of prescribed meltwater forcing during this time interval.

Given the relatively limited number of transient climate simulations of the deglaciation, it remains challenging to assess model skill and identify model-dependent biases in capturing the transient aspects of climate, including the factors that impact climate-forced ice sheet model simulations. As such, the community would be well served by additional transient climate simulations using different climate models, the incorporation of dynamic ice sheet models in climate simulations, and high-resolution proxy records that can aid in climate model assessment.

2.7 Supplementary Information

2.7.1 TraCE-21ka Sensitivity Experiments

To attribute the causes of surface temperature changes in the TraCE-21ka experiment, we analyze three additional transient sensitivity experiments of each individual forcing using the CCSM3 model (He et al., 2013): TraCE-ORB, with only transient orbital forcing, and all other forcings and boundary conditions remaining at the TraCE state of 22 ka; TraCE-GHG, with only transient greenhouse gas forcing, and all other forcings and boundary conditions

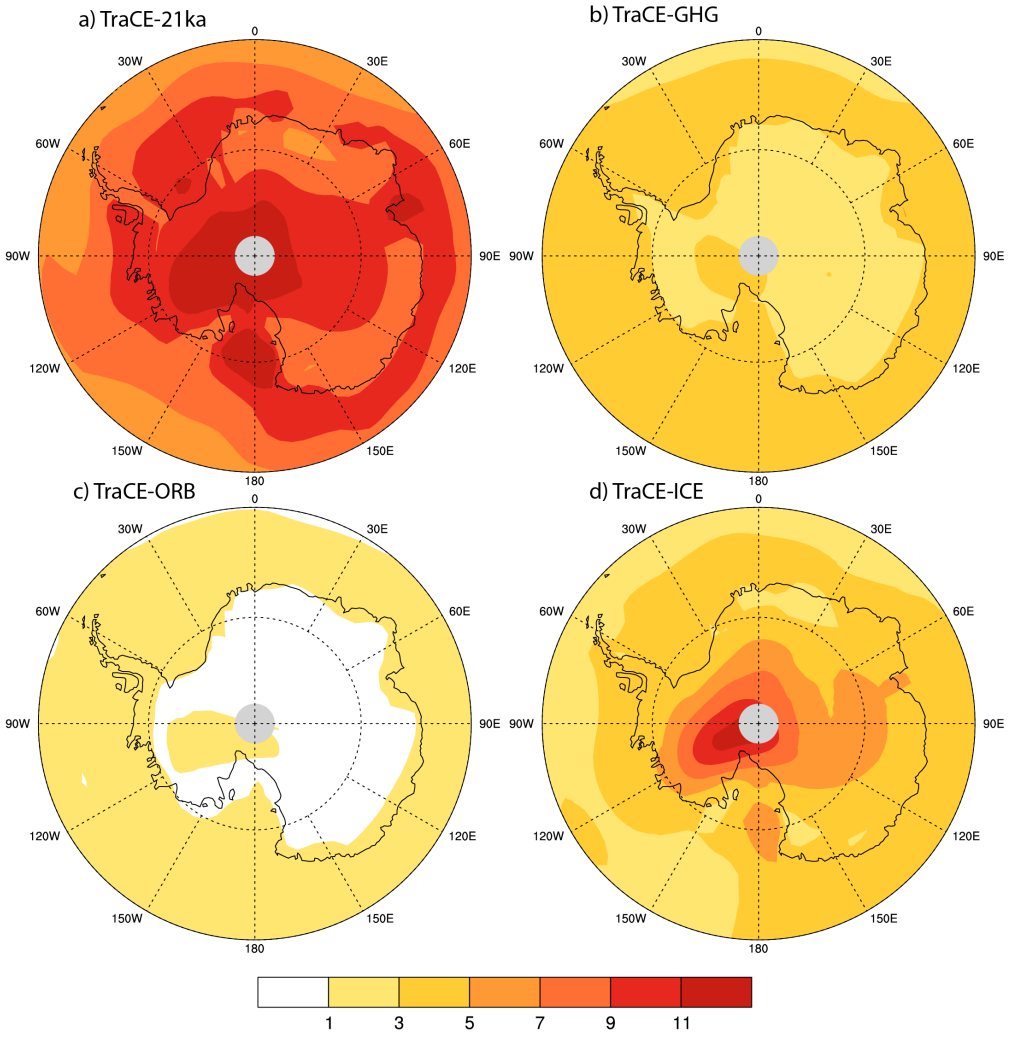

FIGURE 2.15: Surface temperature warming (°C) from 18 kyr to 6.5 kyr in (a) TraCE-21ka and three transient sensitivity experiments.

remaining at the TraCE state of 22 ka; TraCE-ICE, with only changing continental ice sheets, and all other forcings and boundary conditions remaining at the TraCE state of 19 ka. TraCE-GHG and TraCE-ORB show the strongest warming occurring over the Southern Ocean, the continental margins, and interior West Antarctica, but the continental surface warming in these experiments is relatively minor compared to that in TraCE-ICE. The TraCE-ICE experiment demonstrates that the majority of the surface warming that occurs in West Antarctica and over the Antarctic Plateau can be explained by the decrease in ice surface elevation rather than changes in radiative forcing.

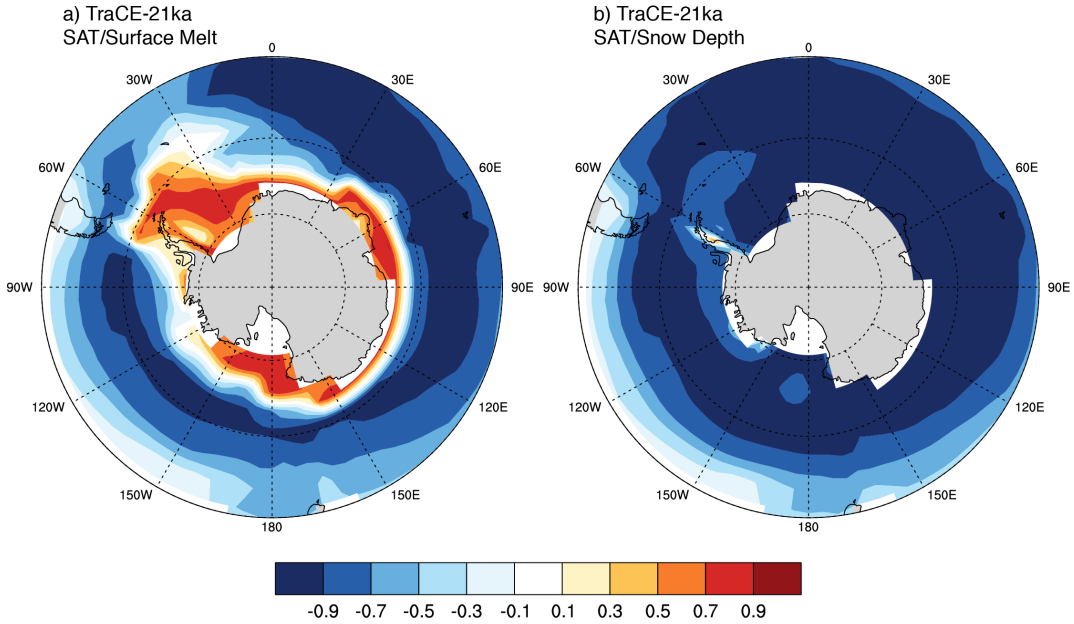

FIGURE 2.16: Spatial Pearson linear cross-correlation coefficients (r) between decadal surface air temperature (SAT, °C) and (a) sea ice surface melt (cm day^{-}1), and (b) sea ice snow depth (m) for TraCE-21ka. Sea ice surface melt and snow depth output were re-gridded to the same grid resolution of SAT using bilinear interpolation.

2.7.2 Surface albedo over the Southern Ocean

Although the sea ice concentration is the strongest control of surface albedo over the Southern Ocean in the climate model simulations, it is not the only contributing factor. In addition to sea ice concentration, the surface albedo parameterization of both models accounts for the state of the sea ice surface (i.e., freezing or melting, snow coverage; Briegleb et al., 2004; Goosse et al., 2010). The TraCE-21ka simulation also depends on the snow depth and snow age. We observe strong correlations between surface air temperature and sea ice surface melt and snow depth over the Southern Ocean in TraCE-21ka (Fig. 2.16). These outputs are unavailable for the DGns simulation.

Chapter 3

Ice sheet response to deglacial climate forcing in the Ross Embayment

This Chapter has been adapted from:

Lowry, D. P., Golledge, N. R., Bertler, N. A., Jones, R. S., McKay, R. (2019). Deglacial grounding-line retreat in the Ross Embayment, Antarctica, controlled by ocean and atmosphere forcing. Sciences Advances, 5(8), eaav8754.

Author contributions: D.L., N.G. and N.B. devised the regional ice-sheet model experiments. D.L. performed the model experiments and analysis and wrote the manuscript. All authors contributed to the editing and refining of the text.

3.1 Abstract

Modern observations appear to link warming oceanic conditions with Antarctic ice sheet grounding-line retreat. Yet interpretations of past ice sheet retreat over the last deglaciation in the Ross Embayment, Antarctica's largest catchment, differ considerably, and imply either extremely high or very low sensitivity to environmental forcing. To investigate this, we perform regional ice sheet simulations using a wide range of atmosphere and ocean forcings. Constrained by marine and terrestrial geological data, these models predict earliest retreat in the central embayment and rapid terrestrial ice sheet thinning during the early Holocene. We find that atmospheric conditions early in the deglacial can enhance or diminish ice sheet sensitivity to rising ocean temperatures, thereby controlling the initial timing and spatial pattern of

grounding-line retreat. Through the Holocene, however, grounding-line position is much more sensitive to sub-shelf melt rates, implicating ocean thermal forcing as the key driver of past ice sheet retreat.

3.2 Introduction

Concerns about the stability of the West Antarctic Ice Sheet (WAIS) have existed for decades and continue to be a topic of discussion today as oceanic and atmospheric warming pose a serious threat to the floating ice shelves that currently buttress the grounded ice (Mercer, 1978; Joughin, Alley, and Holland, 2012; Trusel et al., 2015). As the largest ice shelf in Antarctica, the Ross Ice Shelf (RIS) plays an integral role in buttressing both the West and East Antarctic Ice Sheets, and thus has strong potential to control future sea level rise. Future projections from Antarctic ice sheet models suggest that reduced buttressing resulting from RIS thinning promotes grounding-line retreat into the deep basin of West Antarctica, thereby increasing the Antarctic contribution to global sea levels (Golledge et al., 2015; DeConto and Pollard, 2016). In the past, the grounding-line in the Ross Embayment has shown substantial retreat of more than 1000 km from its Last Glacial Maximum (LGM) position, extending nearly to the continental shelf edge, to its present location (Anderson et al., 2014a; Bentley et al., 2014). However, the sensitivity of the ice sheet system to environmental forcings remains poorly constrained in this region. As a result, conflicting hypotheses have been proposed for both the timing and pathway of grounding-line migration during the deglaciation, indicating either weak or strong sensitivity to early deglacial increases in air and ocean temperatures (Conway et al., 1999; Kingslake et al., 2018).

The traditional view of Ross Embayment grounding-line retreat is the "swinging gate" model (Conway et al., 1999), in which the LGM grounding line only started to retreat during the Holocene, thousands of years after atmospheric and oceanic temperatures, as well as global mean sea level, began to rise. This interpretation envisaged the most pronounced retreat occurring on the western side of the basin, synchronous with changes in the central embayment, and thus chronologies obtained from the Transantarctic Mountain front are reliable indicators of broader scale retreat in the Ross Sea. More recently, it has been posited that the grounding line retreated substantially earlier and more extensively than previously estimated (Kingslake et al., 2018), which would suggest considerably higher sensitivity to early deglacial environmental forcing. In this scenario, the grounding line retreated beyond

its modern position along Siple Coast and re-advanced during the Holocene. Others have also argued for more moderate and dynamic models of retreat, with a combination of oceanic and bathymetric controls driving a landward grounding-line migration from the central embayment (Golledge et al., 2014; Halberstadt et al., 2016; McKay et al., 2016; Lee et al., 2017; Bart et al., 2018). This apparent conflict remains difficult to reconcile as few age constraints exist, and most are biased towards the western margin of the Ross Sea.

In terms of the drivers of retreat, differences in the seafloor bathymetry and substrate conditions likely resulted in asynchronous retreat behavior in the eastern, central and western troughs of the Ross Sea (Halberstadt et al., 2016; Greenwood et al., 2018). Although the specific role of climate remains relatively less understood, it has been noted that the ice shelf may be highly sensitive to warm atmospheric conditions and the incursion of warm ocean currents onto the continental shelf (Yokoyama et al., 2016). Between the LGM and the early Holocene, Antarctic climate and Southern Ocean conditions experienced significant millennial-scale changes that likely affected Antarctic ice sheet mass balance, including the last glacial termination, Heinrich event 1, the Antarctic Cold Reversal (ACR), and the potential influences of the Meltwater Pulse 1a and 1b (MWP-1A,B) events (Golledge et al., 2014; Weber et al., 2014). However, it remains challenging to assess the effects of such climate changes on grounding-line retreat in the Ross Sea given the lack of age control from the central embayment (Anderson et al., 2014a), and because smaller-scale sub-catchments, from where age control data may exist, can behave independently of regional grounding-line retreat (Greenwood et al., 2018).

Additionally, the precise magnitudes and timing of climate changes are difficult to determine on a regional scale given the sparse spatial and temporal coverage and large uncertainties of available paleoclimate proxy records. In particular, changes in sub-surface ocean temperatures in the Ross Sea remain poorly constrained due to the poor preservation of carbonate in Southern Ocean sediments (Andrews et al., 1999). Ice sheet modelers are tasked with selecting between climate forcings that are imperfect due to these limitations of available proxy records, which may not be representative of the area of interest, and transient climate model simulations, of which there are relatively few, and which may also have regional biases (Lowry et al., 2019). To resolve this issue, here we perform regional ice sheet model simulations using a wide range of climate forcings derived from various Antarctic ice core

and marine sediment records and from two transient climate model simulations to investigate the sensitivity of the grounding-line position to changes in atmosphere and ocean conditions, and better constrain both the timing and spatial pattern of grounding-line retreat and ice shelf formation in the Ross embayment. Comparisons of the simulations to the geologic record are in turn used to inform which deglacial climate forcings are the most reasonable for the Ross Embayment.

The regional ice sheet simulations are performed at 10km resolution using the Parallel Ice Sheet Model (PISM), a sophisticated ice sheet model which allows for realistic ice streams that exhibit the full range of observed ice stream velocities (Bueler and Brown, 2009; Martin et al., 2011). As a result, it is one of the few ice sheet models capable of multi-millennia simulations of ice sheets containing freely-evolving ice streams. We consider a domain of the Ross Embayment in which the ice shelf and ice drainage basins of the grounded ice are allowed to dynamically evolve, and a larger area around the drainage basins is maintained at a constant thickness as a time-independent boundary condition of the model. This approach allows for higher computational efficiency due to the smaller domain size, while simultaneously allowing for the grounding-line position to change through time. Details of the regional model set up and initialization procedure are described in the Materials and Methods section.

For the deglacial simulations, which are run from 35 to 0 ka, we apply combinations of the output of two transient climate model simulations, namely, LOVECLIM (Menviel et al., 2011) and TraCE-21ka (Liu et al., 2009), the temperature reconstructions of the EPICA Dome C (EDC) ice core from East Antarctica (75°S, 123°E)(Parrenin et al., 2007) and the WAIS Divide (WDC) ice core from West Antarctica (∼79°S, 112°W)(Cuffey et al., 2016), global and Southern Ocean benthic ocean temperature proxy reconstructions (GOT and SOT, respectively)(Lisiecki and Raymo, 2005; Elderfield et al., 2012), and model-proxy averages (MPA) as climate forcings, for a total of 36 deglacial climate forcing experiments (Table 3.1). The climate model simulations were performed with evolving boundary conditions to reproduce global climate of the last deglaciation (Liu et al., 2009; Menviel et al., 2011). The ice core temperature reconstructions are determined from isotopic measurements and also cover the full deglacial period. The GOT reconstruction is based on a compilation of 57 deep ocean records (Lisiecki and Raymo, 2005), whereas the SOT reconstruction is more specific to the Southern Ocean, derived from a marine sediment core from offshore New Zealand (Elderfield et al., 2012).

The MPA atmosphere and ocean forcings are simple averages of each temperature proxy reconstruction and temperature output of both climate models. Additional details of the climate forcings are provided in the Materials and Methods section.

The climate forcings employed in the ice sheet model simulations include both atmospheric and ocean components. For the atmosphere forcings, we uniformly apply surface air temperature (SAT) and paleo-precipitation based on the Clausius-Clapeyron relationship to temperature (7%/°C) as anomalies to a modern climatology (Lenaerts et al., 2012). We also apply a heuristic time-varying back pressure (calving resistance) offset, intended to mimic the resistive effects of iceberg mélange or dense sea ice that are not specifically modelled (see Materials and Methods). Air temperature affects calving by influencing ice hardness, the presence of surface meltwater on ice shelves, the growth of sea ice and the binding of iceberg clasts, hence this back pressure forcing is an attempt to modulate calving based on atmospheric controls in a similar, though more simplistic, fashion to previous ice sheet modeling studies (DeConto and Pollard, 2016; Robel, 2017; Pollard, DeConto, and Alley, 2019). The back pressure offset is applied as a scalar fraction that is included in the stress boundary condition of the ice shelf. The ocean forcing is in the form of scalar sub-shelf mass flux (melt rate) offset. The offset is a positive or negative basal mass flux (ice loss or gain, respectively) within the mass continuity equation and is applied uniformly to base of the ice shelf, as in Golledge et al. (2014). The sub-shelf melt rate and back pressure offsets are determined using scaling relationships between reconstructed LGM and present-day (PD) ocean temperature and SAT, and applied uniformly as anomalies to present-day (PD) conditions (see Materials and Methods). Lastly, we apply the same sea level forcing in each model run, which is based on statistical analysis of the global sea level proxy record (Clark et al., 2009; Stanford et al., 2011; Deschamps et al., 2012). In addition to the main model ensemble runs, we perform an experiment using a higher mantle viscosity and a more aggressive ocean thermal forcing based on the WDC record, as in Kingslake et al. (2018) (see Materials and Methods).

	LOVECLIM-1 SAT (FULL DOMAIN) "WARM ATMOSPHERE"	*WAIS DIVIDE (WDC) SAT*	*MODEL-PROXY AVERAGE (MPA) SAT "MODERATE ATMOSPHERE"*	*EPICA DOME C (EDC) SAT*	*LOVECLIM-2 SAT2 (COASTAL REGION ONLY)*	*TRACE-21KA SAT "COOL ATMOSPHERE"*
LOVECLIM 400M OCEAN T "WARM OCEAN"	LOVECLIM SAT, LOVECLIM 400m T **"Warm Scenario"**	WDC SAT, LOVECLIM 400m T	MPA SAT, LOVECLIM 400m T	EDC SAT, LOVECLIM 400m T	LOVECLIM SAT2, LOVECLIM 400m T	TraCE SAT, LOVECLIM 400m T
TRACE-21KA 400M OCEAN T	LOVECLIM SAT, TraCE 400m T	WDC SAT, TraCE 400m T	MPA SAT, TraCE 400m T	EDC SAT, TraCE 400m T	LOVECLIM SAT2, TraCE 400m T	TraCE SAT, TraCE 400m T
MODEL-PROXY AVERAGE (MPA) OCEAN T "MODERATE OCEAN"	LOVECLIM SAT, MPA OT	WDC SAT, MPA OT	MPA SAT, MPA OT **"Moderate Scenario"**	EDC SAT, MPA OT	LOVECLIM SAT2, MPA OT	TraCE SAT, MPA OT
SOUTHERN OCEAN BENTHIC OCEAN T (SOT) RECONSTRUCTION (20)	LOVECLIM SAT, SOT	WDC SAT, SOT	MPA SAT, SOT	EDC SAT, SOT	LOVECLIM SAT2, SOT	TraCE SAT, SOT
GLOBAL BENTHIC OCEAN T (GOT) RECONSTRUCTION (19)	LOVECLIM SAT, G OT	WDC SAT, G OT	MPA SAT, G OT	EDC SAT, G OT	LOVECLIM SAT2, G OT	TraCE SAT, GOT
TRACE-21KA SST "COOL OCEAN"	LOVECLIM SAT, TraCE SST	WDC SAT, TraCE SST	MPA SAT, TraCE SST	EDC SAT, TraCE SST	LOVECLIM SAT2, TraCE SST	TraCE SAT, TraCE SST **"Cool Scenario"**

TABLE 3.1: Atmosphere-ocean forcing combinations applied to the ice sheet model. The top row and the leftmost column respectively refer to the 6 atmosphere forcings and the 6 ocean forcings applied to the ice sheet model. In total, 36 simulations of the ensemble are performed, with each table entry referring to an individual simulation. The atmosphere forcing is applied in the form of surface air temperature (SAT), precipitation (7.0%/°C), and sea ice resistance anomalies to a regional climatology from the TraCE-21ka and LOVECLIM transient climate simulations, the EPICA Dome C and WAIS Divide ice core records, and a model-proxy average of each atmosphere forcing. The ocean forcing is applied in the form of sub-shelf mass flux (melt rate) offsets based on the climate model simulations, two benthic ocean temperature (OT) reconstructions, and a model-proxy average (LOVECLIM 400m T and two benthic OT reconstructions). We define three scenarios, namely, warm, moderate, and cool, based on LGM SAT anomalies and timing and amount of early deglacial ocean warming (Fig 3.1-3.2).

3.3 Results

3.3.1 Sensitivity of grounding-line retreat to climate forcing

The differences between the climate forcings allow us to assess the sensitivity of grounding-line retreat to changes in atmosphere and ocean conditions. The surface temperature and precipitation forcings have a wide range of LGM and early deglacial anomalies (e.g., LGM anomalies of -7 to -13°C and -49 to -91% relative to PD, respectively), and differ substantially in terms of the timing and magnitude of the ACR, but are all relatively similar throughout the Holocene (i.e. differences <2°C and 14% from 11.7 ka to 0 ka, respectively; Fig 3.1a). The sub-shelf melt rate and back pressure forcings vary most during the MWP-1A and ACR events, respectively (Fig 3.1b,c), but are all scaled to the same LGM anomaly (see Materials and Methods), and are likewise similar throughout the Holocene. The sub-shelf melt rate forcings are based on the modeled and reconstructed sub-surface ocean temperatures. The models and proxy reconstructions suggest that MWP-1A generally has a sub-surface warming effect, however, the degree and duration of this warming varies considerably among the forcings. We also consider the case of ocean cooling through the ACR (dark blue line in Fig 3.1b), using the near-surface temperature of TraCE-21ka. The back pressure forcings are similarly applied as a scalar offset based on the SAT anomalies, hence the forcings decrease from the LGM, a period of higher sea ice concentration, to PD (no offset). All simulations are performed with the same sea level forcing (Fig 3.1d).

The decline of grounded ice volume initiates between 15.5 and 13.2 ka in the model simulations (Fig 3.1e). The model spread of grounded ice volume is largest through this interval of initial retreat and into the early Holocene as the ice shelf begins to form ($\sim$10-8 ka). Simulations forced with the relatively warmest ocean thermal forcing (i.e., LOVECLIM) show enhanced grounded ice volume decline $\sim$14.5-13.8 ka, roughly synchronous with the timing of MWP-1A (red lines in Fig 3.1e). In contrast, simulations with the relatively coolest ocean thermal forcing (i.e., TraCE-21ka SST) display a rapid decrease in grounded ice volume $\sim$11.2-10.5 ka, roughly synchronous with the timing of MWP-1B (blue lines in Fig 3.1e). Simulations forced with ocean thermal forcing derived from the proxy record and the MPA generally exhibit more gradual decreases in grounded ice volume through this interval of increasing sea level (gray lines in Fig 3.1e).

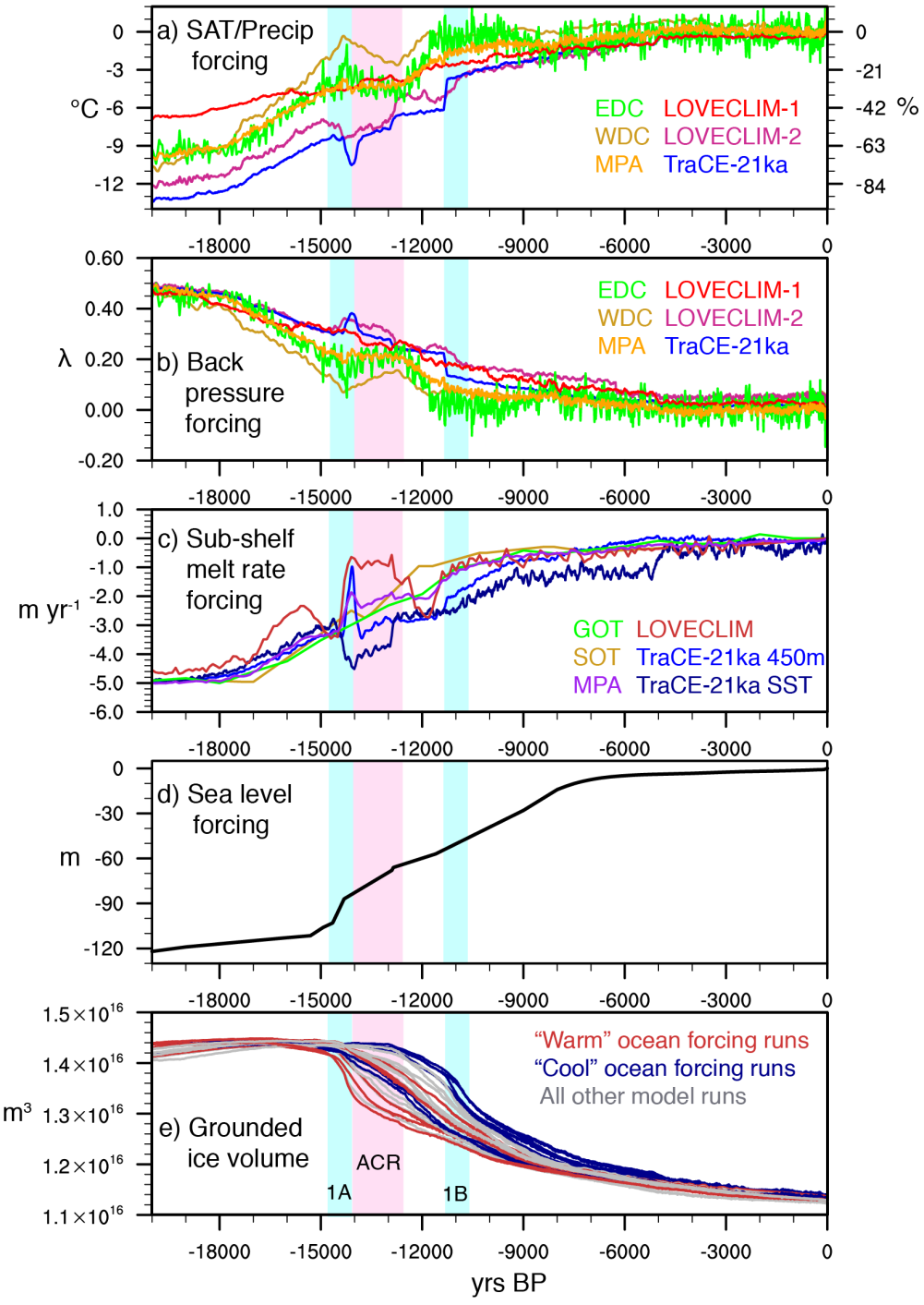

FIGURE 3.1: Climate forcings and modelled grounded ice volume. Time series of the atmosphere forcings of (a) SAT and precipitation anomalies (°C relative to PD; % relative to PD) and (b) back pressure fraction offsets (see Methods), (c) ocean thermal forcings of sub-shelf melt rate offsets (m yr^{-1} relative to PD), (d) sea level forcing (m) and (e) modelled grounded ice volume (m^3). In panel a, all timeseries correspond to both y axes because we use a temperature-precipitation scaling relationship for the precipitation forcing (7% $°C^{-1}$). The blue bars in the panels correspond to the approximate timing of MWP-1A,B and the pink bar corresponds to the ACR. In panel e, the 6 simulations forced with the TraCE-21ka SST (LOVECLIM) sub-shelf melt rate forcing in panel c are shown in dark blue (dark red). All other 24 simulations in the main model ensemble are shown in gray.

The atmosphere forcings (i.e., surface temperature, precipitation, and back pressure) exert a strong modulating effect on the sensitivity to the sub-shelf melt rate offset. In particular, simulations forced with cooler LGM SAT anomalies (e.g., TraCE-21ka SAT forcing) have higher ice hardness, lower temperatures at the bed and decelerated ice flow, which makes the ice sheet more resistant to the increase in ocean thermal forcing from MWP-1A and in the early Holocene, thereby causing a later retreat. The opposite is true for simulations forced with warmer LGM SAT anomalies (e.g., LOVECLIM-1), which are more responsive to ocean thermal forcing, and thus exhibit an earlier retreat. Similarly, steeper gradients of decreasing back pressure in the early deglacial period (e.g., WDC back pressure forcing) allows for higher surface ice flux, also inducing an earlier retreat. Simulations forced with relatively cooler (warmer) atmosphere forcings paired with stronger (weaker) ocean thermal forcing behave more similarly to those forced by moderate ocean thermal forcings (Fig 3.1d). The sea level forcing also contributes to the decline in grounded ice, however, in the absence of climate forcing, it is unable to drive ice sheet retreat (Supplementary Information, Fig 3.6).

In terms of the spatial pattern of grounding-line retreat, we consider individual scenarios: warm (LOVECLIM-1 atmosphere/LOVECLIM ocean), moderate (MPA atmosphere/MPA ocean), and cool (TraCE-21ka atmosphere / TraCE-21ka SST ocean) scenarios (Fig 3.2a-c). These scenarios are defined based on LGM SAT anomalies and timing and amount of early deglacial ocean warming. The model bathymetry is based on the bedmap2 dataset (34), though the bed is smoothed to improve computational efficiency using the bed roughness parameterization of Schoof (2003) (Fig 3.2d). In all three scenarios the earliest retreat occurs in the central Ross Sea, and retreat pathways arising from the different forcings are generally consistent in this area. Some spatial variations exist in the eastern and western basins, with the cooler scenario displaying a delayed retreat in these basins relative to the central Ross Sea. The retreat behavior closely resembles the "saloon-door" and marine-based models of retreat proposed in McKay et al. (2016), Halberstadt et al. (2016), and Lee et al. (2017), in which the grounding-line retreat initiated in the central embayment, with landward migration toward the modern EAIS outlet glaciers. However, the warm scenario initially does exhibit earlier retreat in the eastern and western embayment. Each scenario shows ice remaining grounded on Pennel Bank and Crary Bank into the Holocene ($\sim$11.7 to 0 ka). The moderate scenario displays the most gradual retreat,

whereas the warm (cool) scenario experiences periods of rapid retreat ∼15-13 ka (∼12-10 ka). Once the grounding line has retreated beyond Ross Island, each scenario shows a similar retreat pattern, with a steady progression along the Transantarctic Mountains toward the Siple Coast.

The timing of ice shelf formation varies considerably among the simulations and is related to the climate forcing, with an overall model spread of ∼2 kyr. However, the model simulations are consistent in terms of the process of ice shelf formation. As the grounding line retreats toward the Drygalski Trough in the western Ross Sea, the ice becomes ungrounded and ice flow from South Victoria Land accelerates (Fig 3.3a). The formation of the main ice shelf initiates as the grounding line retreats toward the Byrd ice stream (Fig 3.3b). When the faster flowing ice stream is no longer inhibited by thick grounded ice, its velocity increases, and floating ice shelf begins to expand over an area of deeper topography. Grounding-line migration continues to propagate southwest-ward along the Transantarctic Mountains and eastward towards the Siple Coast.

As the modeled ice shelf area reaches near-modern levels (11-7 ka), the ocean thermal forcing dominates in terms of the model spread, with small differences in the sub-shelf melt rate resulting in large variations in ice shelf area (Fig 3.3c). With the development of the ocean cavity underneath the ice shelf, the sub-shelf melt rate forcing acts on a larger area and becomes the main driver of grounding-line retreat. This effect increases throughout the Holocene, even as the differences between the ocean thermal forcings decrease (Fig 3.1c). The differences in ice shelf area between model simulations are primarily observed along the grounding line of the Siple Coast and the calving line rather than the grounding line along the Transantarctic Mountains.

Based on the ensemble of climate-forcing simulations, we can explore how the sensitivity to climate-forcing selection evolves both temporally and spatially by assessing model agreement in parameters such as ice thickness (Fig 3.4). For example, if a given model grid cell is covered by thick grounded ice in some climate-forcing simulations at a specific time step, but is covered by thinner floating ice shelf or open ocean in other simulations at the same time step, the standard deviation of ice thickness in the ensemble as a whole will be higher at this point in time and space, indicating higher sensitivity to the climate-forcing selection. During the ACR (∼14 ka; yellow line in Fig 3.4), a large area of model disagreement (high standard deviation of ice thickness), covering the western Ross Sea and Ross Island region, is observed, driven by

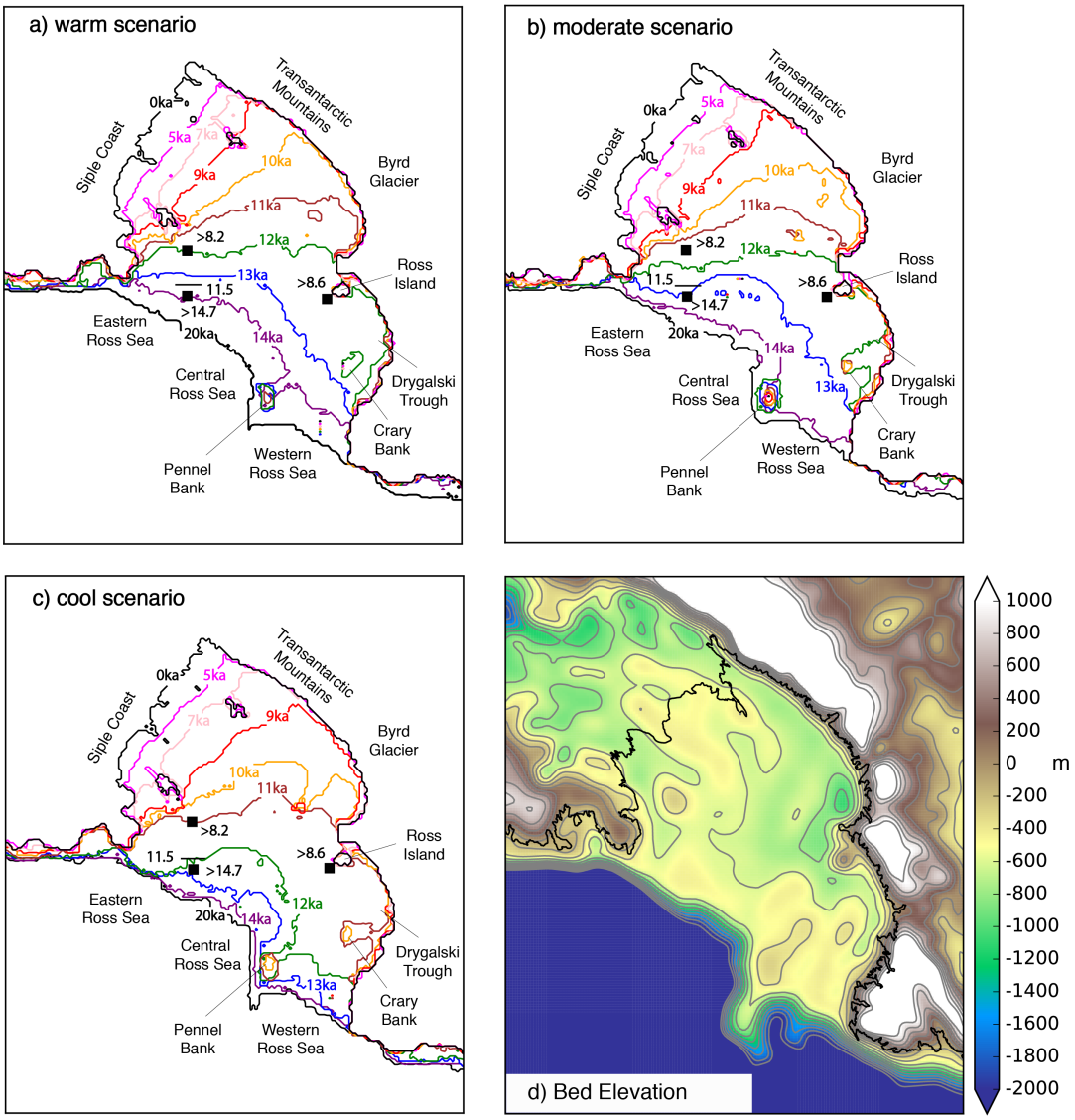

FIGURE 3.2: Grounding-line retreat scenarios. (a) Warm (LOVECLIM SAT/LOVECLIM 400m OT), (b) moderate (MPA SAT/MPA OT), (c) cool (TraCE-21ka SAT/TraCE-21ka SST) grounding-line retreat scenarios. The black squares indicate marine sediment core locations with minimum age constraints of grounding-line migration from radiocarbon dating. The thin black line marks the grounding-line position in the eastern Ross Sea estimated by Bart et al. (2018). (d) Smoothed bed elevation (m a.s.l.) used in the model simulations based on bedmap2 (Fretwell et al., 2013). The gray lines show elevation contours of 200 m. The black line indicates the modern grounding line position.

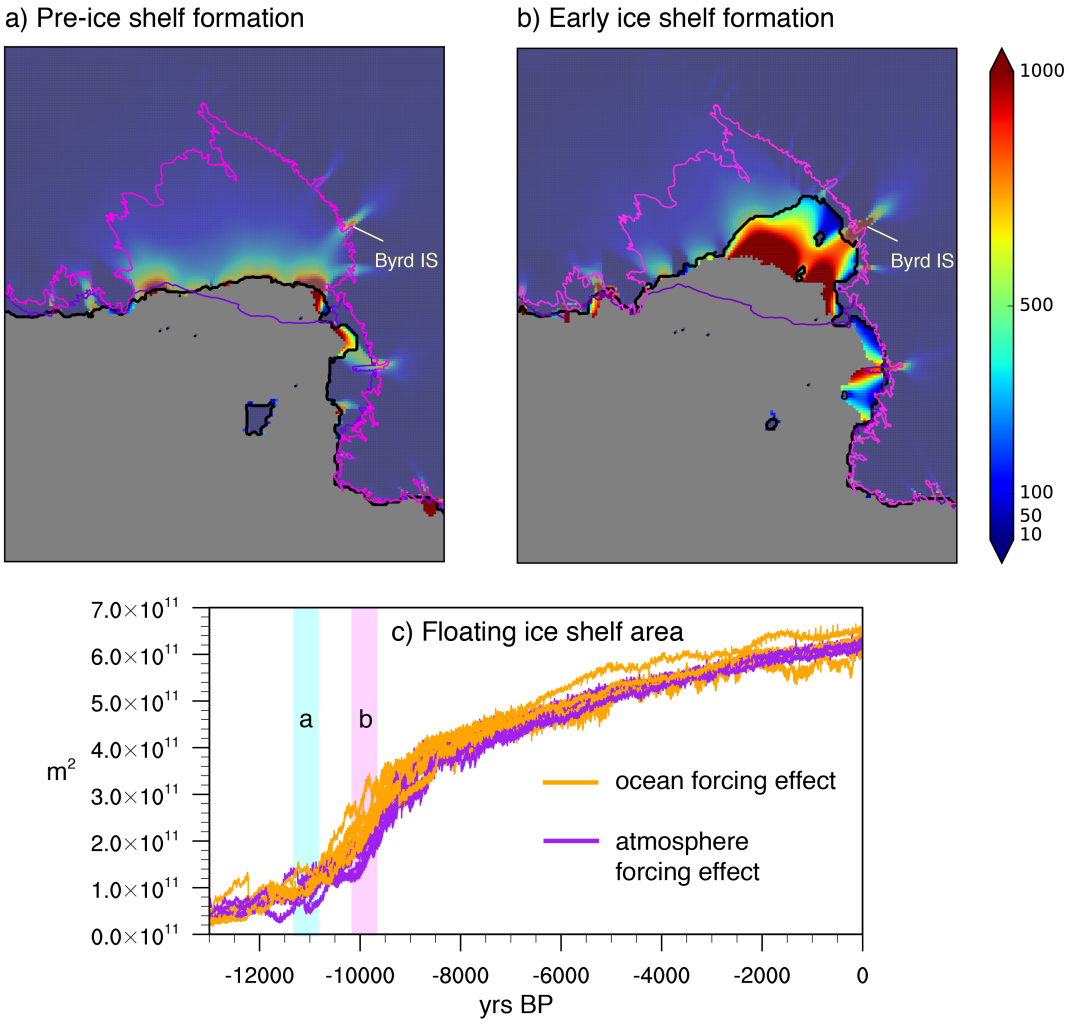

FIGURE 3.3: Ice shelf formation. (a-b) Ice surface velocity (m yr^{-1}) before and after ice shelf formation of the moderate scenario (panel b in Fig 3.2). The modeled grounding-line position is shown in black. For context, the modern grounding (calving) line position is shown in pink (purple). (c) Floating ice shelf area (m^2) of simulations forced with the model-proxy average atmosphere forcing and different ocean forcings (orange lines) and simulations forced with the model-proxy ocean forcing and different atmosphere forcings (purple lines). The timing of panels a and b are indicated by the blue and pink bars in panel c, respectively.

the variation in the timing and spatial pattern of the initial retreat.

The area of highest standard deviation migrates southward through the early Holocene on the western side of the embayment, towards the Transantarctic Mountains. The standard deviations reach peak values ∼12 ka (red line in Fig 3.4), and then decrease through time. As the climate forcings converge in the Holocene, the simulations show higher agreement (i.e., lower standard deviations of ice thickness), and the overall area of high uncertainty (top 30% standard deviation) decreases and becomes concentrated along the grounding and calving lines.

3.3.2 Comparison of model simulations to the geologic record

Few geological constraints exist for the timing of grounding-line retreat in the Ross Sea given the poor preservation of carbonate for radiocarbon dating and large uncertainties in dating of glacimarine sediments (Andrews et al., 1999). However, in the eastern Ross Sea, marine sedimentary facies succession and foraminifera-based radiocarbon chronology show initial grounding-line retreat by as early as 14.7 ka, but the grounding line stabilized on the outer continental shelf until ∼11.5 ka (Bart et al., 2018). In Fig 3.2, the warm scenario is the closest to capturing this early initial retreat in this area, but the cool scenario better matches the grounding-line stagnation and rapid early Holocene retreat.

In the western Ross Sea, radiocarbon chronologies suggest open ocean conditions at Coulman High by 8.6 ka (McKay et al., 2016). This region in the western Ross Sea exhibits the highest sensitivity in the domain to climate forcing, as demonstrated in Fig 4. However, none of the model ensemble simulations conflict with these minimum age constraints in the western Ross Sea (Fig 3.2), with the grounding line reaching Coulman High by as early as 12 ka. The simulations forced with relatively cooler atmosphere/ocean forcings display the most similar timing to these estimated minimum ages (e.g., ∼11 ka).

Ice thinning histories derived from cosmogenic nuclide surface-exposure records of marginal sites in the Ross embayment generally show enhanced thinning rates in the early-to-mid Holocene, although the precise timing differs among individual glaciers over a large time range of ∼14-3 ka (Stone et al., 2003; Todd et al., 2010; Jones et al., 2015; Anderson et al., 2017; Spector et al., 2017; Goehring et al., 2019). Comparisons between ice sheet model simulations and surface-exposure records are difficult due to limitations in model

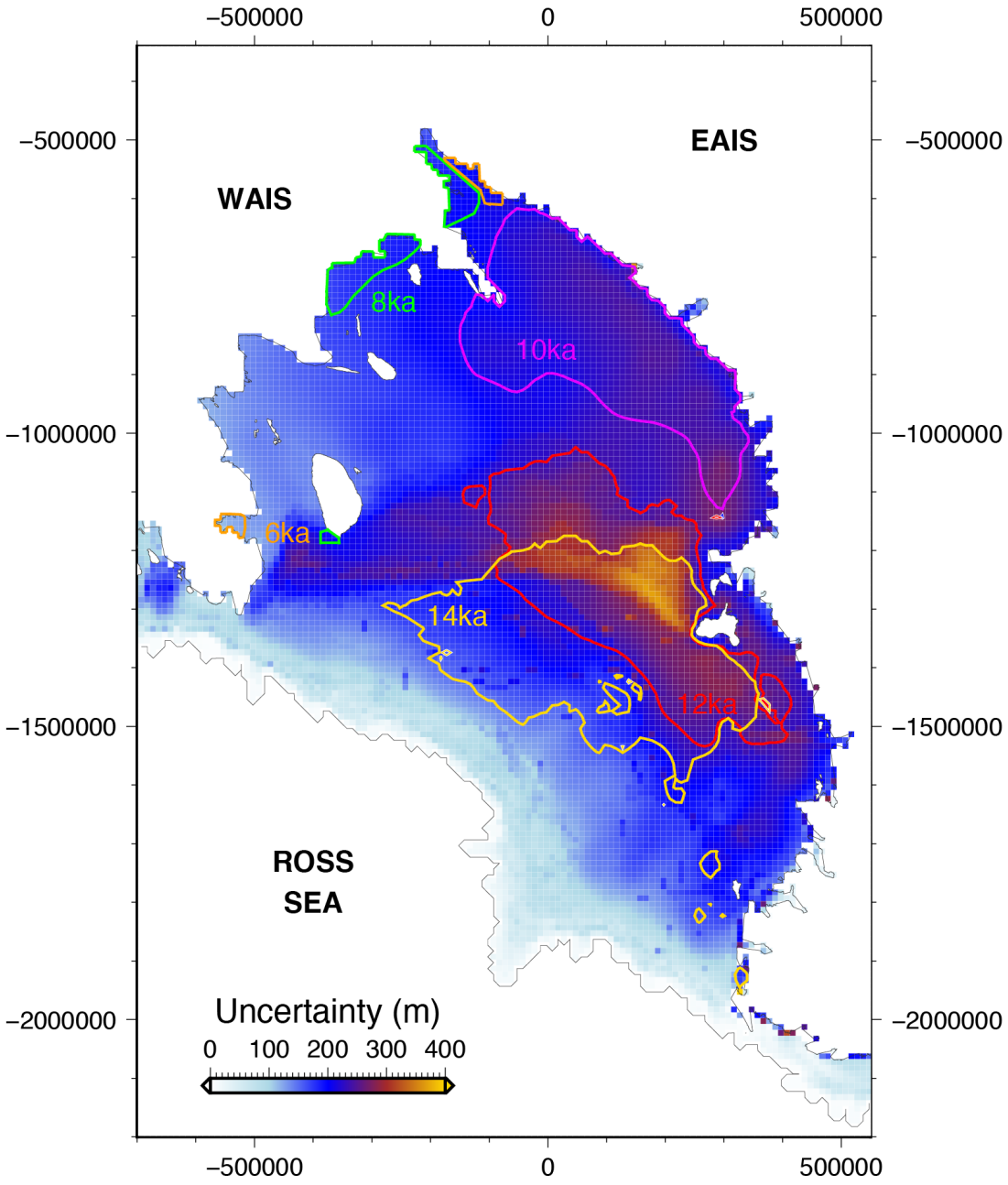

FIGURE 3.4: Uncertainty due to climate forcing. Standard deviation of modeled ice thickness (m) in the Ross embayment of the 36 climate-forced deglacial simulations (Table 3.1). The grid color indicates the time-averaged uncertainty of a given grid cell through the interval of 18-4 ka. The colored lines outline the areas that include the top 30% standard deviation in ice thickness at a given time slice in 2-ka intervals from 14-6 ka.

resolution, which may not be sufficient for resolving smaller-scale features. With this caveat in mind, we compare ice thickness changes of the model ensemble in three regions from which cosmogenic nuclide surface-exposure records exist: the Northern Victoria Land (NVL) region, the McMurdo region, the Southern Transantarctic Mountain (STAM) region and the northern Marie Byrd Land (MBL) region (Fig 3.5). We use regional averages since individual model grid cells, which cannot resolve individual glaciers, may not be fully representative of the regional-scale ice sheet evolution.

Even within these regions, surface-exposure ages of individual glaciers record differences in the timing of ice thinning of >1 ka. This is especially pronounced in the STAM region, where ice thinning of Beardmore Glacier precedes that of Scott glacier by ∼5 ka, and Reedy Glacier, based primarily on dated drift limits, shows relatively less overall thinning (Fig 3.5c). The timing of ice thinning in the model ensemble runs generally occurs between that estimated by the Beardmore and Scott glaciers (i.e., ∼13-10 ka), with simulations forced by relatively warmer (cooler) ocean/atmosphere forcings showing stronger agreement with Beardmore (Scott) Glacier.

In the NVL and McMurdo regions, the majority of simulations exhibit precipitation-driven ice thickening in the early deglacial period (20-14.5 ka). Regional ice thinning occurs ∼14-10 ka, with a substantial model spread, indicating that these regions are highly sensitive to the climate forcing selection (Fig 3.5a,b). A similar timing of ice thinning is observed for the MBL region (i.e., ∼14-10 ka), though the rate of thinning is higher (Fig 3.5d). Assessment of model performance is difficult in these regions given the lack of ice thickness estimations through the key time interval of 14-10 ka. The model ensemble shows similar ice thickness anomalies in the early deglacial period to those estimated at Tucker Glacier, Mackay Glacier, Mt Rae and Mt Discovery. The simulations forced with relatively cooler atmosphere/ocean forcings are also generally consistent with Aviator Glacier and Mt Discovery in the early Holocene.

However, model-proxy mismatches of ice thickness do occur, as no simulation captures the increase and subsequent decrease in ice thinning estimated in the McMurdo region in the mid-Holocene (∼8-6 ka), nor the decrease at Mt Rae in the late Holocene (∼4-2 ka). The NVL glaciers also record a more gradual ice thinning in the early to mid-Holocene than indicated by the model simulations. As explained above, some of this mismatch may be related to glaciers recording local signals instead of the broader regional signals. For example, the recorded rapid thinning of Mackay glacier is likely the

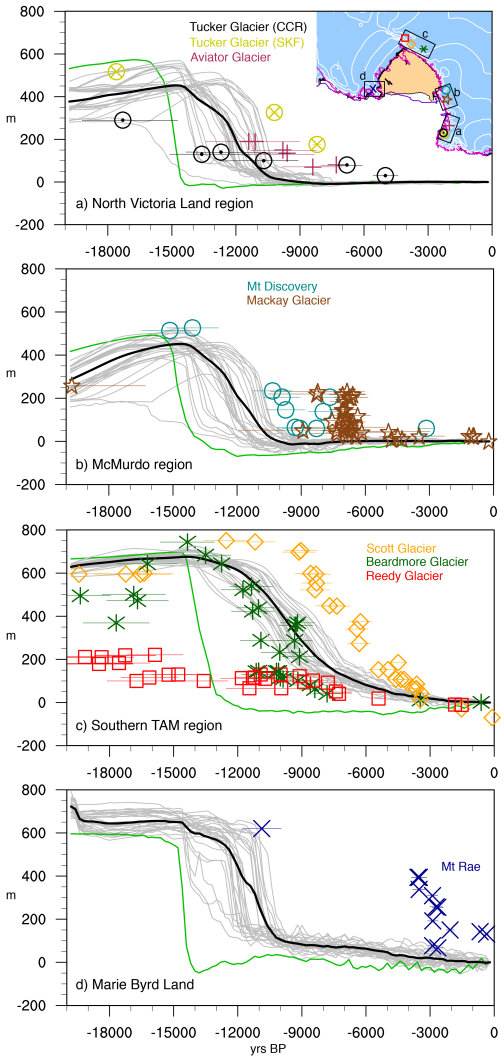

FIGURE 3.5: Model-data comparison. Regional ice thickness anomalies relative to PD of the model simulations for the (a) NVL, (b) McMurdo, (c) STAM, and (d) MBL regions vs. ice thickness anomalies of cosmogenic nuclide surface-exposure records of glaciers within each region. Individual model simulations are shown in gray and the ensemble average is shown in black. Data for Tucker and Aviator Glacier were obtained from Goehring et al. (2019). Data for Mt Discovery and Mackay Glacier were obtained from Anderson et al. (2017) and Jones et al. (2015), respectively. The STAM glacier data were obtained from Spector et al. (2017) and Todd et al. (2010), and those of Mt Rae were obtained from Stone et al. (2003). All surface-exposure ages were recalculated following recent improvements to global production rate (Borchers et al., 2016). Age uncertainties of the records are indicated by the horizontal bars. The inset in panel (a) shows the region locations (black box outline) and the glacier locations overlaid on the ensemble average of the final modeled RIS configuration (yellow shows floating ice, blue shows grounded ice, thick black line shows modeled grounding-line position, white contours show surface elevation in 500m intervals, pink line shows observed modern grounding-line position, and purple line shows observed modern calving line position). In the panels, the green line indicates the early retreat/Holocene re-advance scenario (see Materials and Methods).

result of local retreat into an over-deepened basin rather than reflective of a broader regional deglaciation at this time (Jones et al., 2015). A model resolution of 10km is unlikely to resolve such changes from local topography, and may partly explain why the exact timing of recorded ice thinning at these sites lags the simulated regional-scale changes. In addition, the application of uniform precipitation and ocean forcing does not account for changes in atmospheric and oceanic circulation, which may be significant at the sub-catchment scale, thereby contributing to the model-data mismatch.

Least consistent with the surface-exposure ages and marine radiocarbon dates of the Ross Sea is the simulation using higher mantle viscosity and the WDC record as a sub-shelf melt rate forcing (green line in Fig 3.5a-d), paired with an average atmosphere forcing. In this simulation, which reproduces the early retreat and Holocene isostatic rebound-driven re-advance proposed in Kingslake et al. (2018), the ice sheet is highly sensitive to the sub-shelf ocean forcing, reaching a near-modern sub-shelf melt rate by $\sim$15 ka (see WDC forcing in Fig 3.1a). At this point, precipitous ice thinning occurs in all three regions, considerably earlier than estimated by any of the surface-exposure chronologies.

3.4 Discussion

The deglacial simulations demonstrate that the ocean forcing is the primary control on the timing of grounding-line retreat in the Ross embayment, an effect that is strongly modulated by the atmosphere forcing prior to ice shelf formation and the development of the ocean cavity. The greatest variation in the timing and spatial pattern of retreat, that is, the greatest sensitivity to the climate forcing selection, occurs during the period between the initial decline in grounded ice volume and the early formation of the ice shelf (i.e., $\sim$14-8 ka). The retreat pathways of the climate forcing experiments are relatively consistent, suggesting that the seafloor bathymetry acts as a primary spatial control on the modeled grounding-line migration. In each simulation, the earliest retreat occurs in the central basin relative to the eastern and western basins, in agreement with the "saloon-door" model of retreat, most recently suggested in Lee et al. (2017). The spatial variations that do exist are driven by differences in the relative timing of retreat in each basin, which is influenced by the ocean and atmosphere forcings, implicating these external forcings as secondary controls.

The retreat pathway observed in the simulations is in agreement with the asynchronous and dynamic behavior suggested in Halberstadt et al. (2016), Lee et al. (2017) and Greenwood et al. (2018) based on multibeam bathymetry data of the Ross Sea, however, the model is limited in capturing some smaller-scale features. The simplified ocean forcing applied in these simulations likely contributes to this data-model mismatch, as it neglects the effects of ocean circulation, eddies, turbulence and focusing of Circumpolar Deep Water, and changes in continental shelf water mass formation processes, all of which is consequential considering the importance of these processes to basal melt rates (Rintoul, 2018). Although the climate models account for such circulation changes, we use an average temperature anomaly of the entire Ross Sea to apply the ocean thermal forcing to the domain (see Materials and Methods), thus differences in sub-surface warming and cooling between the eastern and western Ross Sea are not represented. This could explain why the majority of simulations display a later grounding-line retreat than indicated in the Whales Deep basin in the eastern Ross Sea (Bart et al., 2018). In terms of the atmosphere forcings, the temperature-precipitation scaling relationship may not be appropriate over the full domain given the influence of atmosphere dynamics and synoptic-scale processes in millennial-scale changes in snow accumulation over West Antarctica (Fudge et al., 2016). This inhibits comparisons to specific glaciers, as changes in accumulation that are not captured by the precipitation forcings may be relevant for glacier mass balance changes.

Additionally, given the abundance of ice rises in the western Ross Sea, which can act as pinning points that stabilize the grounding line (Halberstadt et al., 2016; Simkins, Anderson, and Greenwood, 2016), it is conceivable that local grounding-line retreat occurred later than modeled in this region due to model resolution limitations, which result in a smoother than realistic seafloor bathymetry. It has recently been suggested that ice flow switching that occurred as the ice sheet retreated may have resulted in a Holocene re-advance in the western Ross Sea (Greenwood et al., 2018). Although the simulations show enhanced flow and direction changes from South Victoria Land, this does not reproduce the Holocene ice sheet advance. These discrepancies between the simulations and observations are likely driven by resolution limitations and differences in seafloor substrates that are not adequately represented in the model, but are important for till deformation and ice flow velocities. Despite these potential local biases, these simulations effectively demonstrate the climate sensitivity of grounding line retreat on the broader

regional scale. Grounding-line retreat displays the highest sensitivity to the climate forcing selection in the western Ross Sea, both spatially and temporally; therefore, establishing reliable age constraints in this region remains a high priority. From a modeling perspective, the roles of model resolution and spatial heterogeneity in substrate type and ocean and precipitation forcing require further exploration in order to understand and improve upon model-data discrepancies.

While most records from the Ross embayment suggest the most significant terrestrial ice thickness changes occurring in the early to late Holocene, Kingslake et al. (2018) recently proposed an early deglacial retreat scenario based on the presence of finite radiocarbon ages measured in the organic carbon from subglacial sediments. In this scenario, the grounding line retreated beyond the modern-day position along Siple Coast in the early Holocene and re-advanced to its current position due to isostatic rebound. In model simulations also using PISM, they simulate the furthest retreat in the Ross sector at 9.7 ka. Using a higher mantle viscosity term and higher early deglacial sub-shelf melt rates, we are able to reproduce a similar timing of ice sheet retreat and re-advance as well as minimum grounding-line extent (9.8 ka) within our regional domain (Fig 3.7). However, we demonstrate here that this simulation is difficult to reconcile with the existing paleo-records because in this scenario the modeled TAM/MBL ice thinning and open ocean conditions in the Ross Sea occur substantially earlier than the empirical data suggest. While this does not eliminate the possibility of ice sheet retreat and re-advance driven by isostatic uplift, the timing of retreat likely occurred later than suggested by Kingslake et al. (2018), suggesting a less sensitive response to climate forcing. We also demonstrate here that the deglacial simulations exhibit high sensitivity to small changes in sub-shelf melt rates along the Siple Coast during the Holocene. Therefore, an additional mechanism of Siple Coast retreat/re-advance that should also be considered is that incursions of warm (cool) ocean water into the RIS cavity in the mid-to-late Holocene could contribute to more extensive retreat (advance). The effects of both mechanisms should be further explored with regard to the grounding line position along the Siple Coast.

Geologic evidence and Antarctic ice sheet modeling indicate that the Ross embayment was not a substantial contributor to MWP-1A (Golledge et al., 2014), despite the continent as a whole most likely having made a multi-meter contribution to this event (Stuhne and Peltier, 2015). However, recent radiocarbon dates suggest that initial grounding-line retreat in the eastern

Ross Sea may have occurred by as early as 14.7 ka (Bart et al., 2018). Differences in sub-surface ocean warming associated with a large meltwater flux from the Antarctic Peninsula and the mid-to-outer Weddell Sea may explain how the grounding line retreated in Whales Deep Basin, with no coincident retreat observed in the western Ross Sea. In fact, Golledge et al. (2014) demonstrate that Southern Ocean freshwater forcing in LOVECLIM results in sub-surface ocean warming in the eastern and central Ross Sea and cooling in the western Ross Sea. TraCE-21ka likewise displays enhanced sub-surface ocean warming in the eastern and central Ross Sea relative to the western Ross Sea resulting from MWP-1A freshwater forcing (Supplmentary Information, Fig 3.8). It is therefore possible that in terms of the initial grounding-line retreat, the eastern Ross Sea followed a "warm" ocean scenario trajectory, potentially resulting from sub-surface ocean warming associated with Heinrich event 1 and/or MWP-1A, as indicated in the climate simulations (Menviel et al., 2011; Golledge et al., 2014; Lowry et al., 2019). In contrast, the western Ross Sea followed a "cool" ocean scenario trajectory, with a timing of retreat more consistent with MWP-1B. In the case of the eastern Ross Sea, the effect of the MWP-1A-related ocean warming was likely short-lived, however, as the grounding-line position remained relatively unchanged following the initial retreat until the early Holocene (Bart et al., 2018).

We note that the atmosphere forcings that yield the best fit to the geologic record are derived from climate model simulations rather than from paleoclimate proxy reconstructions. In particular, the relatively cooler SAT and higher back pressure forcings of TraCE-21ka and LOVECLIM-2 are important for delaying the timing of retreat by reducing both the surface flux and the sensitivity to elevated sub-shelf melt rates. In the TraCE-21ka and LOVECLIM simulations, the continental margins and coastal seas exhibit some of the greatest temperature anomalies due to changes in sea ice concentration. The SAT anomalies of these climate model simulations range from 2.3-3.3°C cooler at 18 ka than the more continentally located EDC and WDC ice cores. Few marine ice cores exist in the region to determine if the climatic effects of sea ice changes are more strongly experienced along the continental margin of the Ross embayment, however, the δ^{18}O records of EDC and Talos Dome display strong consistency, despite the more coastal location of the latter (Stenni et al., 2010).

Recent evidence from diatom oxygen isotopes, a proxy for ice discharge, and climate model simulations have implicated ocean thermal forcing as the main driver of Antarctic ice sheet retreat in the Holocene (Crosta et al., 2018).

We similarly show that changes in sub-shelf melt rates become increasingly important relative to the atmosphere forcings through the Holocene in terms of the grounding-line position in the Ross Embayment, particularly along the Siple Coast. This is notable given concerns for marine ice sheet instability and modern observations of dynamic thinning and grounding-line retreat of WAIS glaciers attributed to increased basal melt of ice shelves (Rignot et al., 2014). The Siple Coast has experienced such changes in recent years, as the grounding-line position of the Kamb Ice Stream has shown rapid retreat related to post-stagnation thinning (Horgan et al., 2017). The simulations here likewise suggest that the grounding line of the largest Antarctic ice shelf is potentially vulnerable to elevated sub-shelf melt rates from warm water incursions into the RIS cavity.

3.5 Conclusions

Past grounding-line retreat in the Ross Embayment has been substantial, however, the sensitivity of grounding-line dynamics to atmosphere and ocean forcing has remained poorly constrained in this area. To compensate for limitations in available paleoclimate proxy records and climate simulations, our regional ice sheet simulations use a wide range of climate forcings to highlight their effect on grounding-line migration. Differences between the ocean and atmosphere forcings are consequential for both the timing and spatial pattern of grounding-line retreat, particularly in the western and eastern Ross Sea, and therefore have implications for the sea level contribution from the Ross sector over the last deglaciation as well as the overall deglacial climate evolution of this region. The model results indicate that early deglacial atmospheric conditions can enhance or diminish ice sheet sensitivity to rising ocean temperatures, thereby controlling the initial timing and spatial pattern of grounding-line retreat. Simulations using warm ocean forcing better match the early onset of retreat in the eastern Ross Sea indicated by marine radiocarbon dates, but those using cool atmosphere and ocean forcings generally reproduce the best overall agreement with the geological constraints of the grounding-line retreat in the western Ross Sea and terrestrial ice thinning. These cool climate scenarios show retreat initiating from the central embayment and enhanced early Holocene ice thinning, synchronous with the timing of MWP-1B. High uncertainty with regard to the timing of grounding-line retreat exists, particularly in the western Ross Sea,

where the simulations exhibit considerable differences related to climate forcing selection. Establishment of age controls in this region should be prioritized. The ocean forcing is the main driver of grounding-line retreat following the formation of the RIS and the development of an ocean cavity. In the Holocene, the grounding line along Siple Coast shows strong sensitivity to small changes in sub-shelf melt rates, which has implications for future sea level rise.

3.6 Materials and Methods

3.6.1 Regional ice sheet model set up and initialization

Prior to the climate forcing experiments, we perform a full-continent spin-up run following the protocol of Martin et al. (2011). This first phase is a 100-yr smoothing run, in which the model evolves by internal deformation only in order to remove steep gradients and any inconsistencies in the input ice thickness data. This is followed by a 200-kyr thermal evolution run, in which the geometry remains fixed and the three-dimensional temperature field evolves to equilibrium according to the conservation of energy equation. Finally, we perform a 100-kyr evolutionary run with constant climate forcing. This length of spin-up is necessary because the thermal and dynamic evolution require at least a full glacial cycle due to the ice sheet thickness and slow velocities in the ice interior.

We then construct a regional drainage basin model of the Ross Embayment based on the ice sheet thickness and topography. The bathymetry used in the model is based on the Bedmap2 dataset (Fretwell et al., 2013). We employ the grounding-line scheme developed in Feldmann et al. (2014), which uses a sub-grid interpolation of basal driving stress to improve the accuracy of grounding-line movements. The regional model is tuned according to present-day (PD) conditions (i.e., grounding-line position, ice shelf extent, surface ice velocity, and ice thickness of the entire domain) by adjusting model parameters, namely, the calving thickness threshold and rate in the calving parameterization scheme, enhancement factors of the shallow ice and shallow shelf approximation equations, the effective pressure on the till, and the till friction angle.

The regional model is run at 10km resolution from 115 ka to 0 ka (total spin-up of 215 ka: 100 ka full continent, 115 ka regional). For the regional component of the model spin-up, we apply a paleoclimate forcing

using the EPICA Dome C (EDC) temperature record (Parrenin et al., 2007) with paleo-precipitation determined based on the Clausius-Clapeyron relationship to temperature as anomalies to a modern climatology (precipitation-temperature scaling of 7.0%/°C). For the first 100 ka of the regional simulation, the ice shelf extent is fixed, and for the remainder of the run (15-0 ka), the calving scheme is incorporated. We use the eigen calving parameterization developed in (Levermann et al., 2012), in which the calving rates are proportional to the product of the principle components of the strain rates, derived from the shallow shelf approximation velocities. The resulting 10km regional PD configuration serves as the initial condition for all experimental runs.

3.6.2 Sub-shelf melt rate/back pressure forcing sensitivity experiments

In the deglacial climate forcing experiments, we apply ocean forcing in the form of sub-shelf mass flux (melt rate) offsets. In PISM, the sub-shelf mass flux is used as a source in the mass continuity equation (Martin et al., 2011):

$$\delta_t H = M - S - \nabla \cdot Q \tag{3.1}$$

In the above equation, t is time, H is ice thickness, M is surface mass balance, S is basal mass balance (S > 0 is melting), and Q is the horizontal ice flux. The offset is a positive or negative flux applied to the basal mass balance of the ice shelf (ice loss or gain, respectively), and is measured in m yr^{-1}. The anomaly is applied uniformly, as in Golledge et al. (2014).

In addition, we apply back pressure (calving resistance) offsets, intended to mimic the resistive effects of iceberg mélange or dense sea ice that are not specifically modelled. Sea ice growth stiffens the mélange matrix, binding iceberg clasts together, thereby exerting a resistance against calving (Robel, 2017). Therefore, we assume here that thicker and more extensive sea ice associated with cooler climate states, such as the LGM, will result in reduced calving. Southern Ocean proxy records indicate more extensive and higher concentration at the LGM (Gersonde et al., 2005), and deglacial climate simulations exhibit strong negative correlations between sea ice concentration and thickness and SAT, with similar temporal evolution observed in the Ross Sea (Lowry et al., 2019).

The back pressure offset is applied as a scalar fraction () that is included in the stress boundary condition of the ice shelf (PISM, 2017). It is assumed that the back pressure (p_{seaice}) does not exceed the pressure of the ice column at the calving front ($p_{ice} - p_{ocean}$), thus the offset is in relation to the default value of 0 and is less than 1:

$$p_{seaice} = \lambda(p_{ice} - p_{ocean}) \tag{3.2}$$

$$\int_b^h (p_{ice} - (p_{ocean} + p_{seaice})) = (1 - \lambda) \int_b^h (p_{ice} - p_{ocean}) dz \tag{3.3}$$

In the above equations, λ represents the back pressure fraction (from 0 to 1), and b and h are the ice base and top surface elevations, respectively. With this forcing applied, the stress condition written in terms of the velocity components becomes modified as follows:

$$2\nu H(2u_x + u_y)n_x + 2\nu H(u_y + v_x)n_y = (1 - \lambda) \int_b^h (p_{ice} - p_{ocean}) dz n_x, \tag{3.4}$$

$$2\nu H(u_y + v_x)n_x + 2\nu H(2v_y + u_x)n_y = (1 - \lambda) \int_b^h (p_{ice} - p_{ocean}) dz n_y. \tag{3.5}$$

where ν is the vertically averaged ice viscosity, u and v are velocity components, and n represents the horizontal normal vector pointing oceanward from the ice boundary.

The basal melt rate forcing is applied based on the Southern Ocean δ^{18}O stack (SOT) (Elderfield et al., 2012), and the back pressure forcing is applied based on the EDC temperature reconstruction (Parrenin et al., 2007). To respectively convert the δ^{18}O and temperature reconstructions into basal melt rate and back pressure forcings, we use scaling relationships between two end-member states, i.e., LGM and PD, following the protocol of Golledge et al. (2014). The scaling relationships for each forcing are determined through a suite of sensitivity experiments (Table 3.2; Fig 3.9-3.10). These simulations initiate from the onset of the last interglaciation (131 ka) and are run to 0 ka, and are performed at 20 km resolution. In addition to the above forcings, we apply a paleoclimate forcing using the EDC temperature record with paleoprecipitation determined based on the Clausius-Clapeyron relationship to temperature as anomalies to a modern climatology (7%/°C), and sea level forcing based on statistical analysis of the sea level proxy record (Clark et al., 2009; Stanford et al., 2011; Deschamps et al., 2012). Although LGM constraints are limited, these experiments are assessed in comparison to LGM

grounding-line position and ice thickness estimations (Bentley et al., 2014; Anderson et al., 2014a) and PD conditions (i.e., grounding and calving line position, ice thickness, and ice surface velocity). The sub-shelf melt rate-back pressure forcing combination applied in simulations that best fit LGM and PD grounding-line position and ice thickness, and PD grounding and calving line position, ice thickness, and ice surface velocity, is selected for the deglacial experiments (Supplementary Information, Fig 3.9-3.10).

3.6.3 Climate forcing details

In our deglacial climate-forcing experiments, we use the temperature reconstructions of two Antarctic ice cores: the EDC and WDC ice cores (Parrenin et al., 2007; Cuffey et al., 2016). Temperature reconstructions of ice cores are commonly calculated as anomalies to modern temperatures based on deuterium (δD), deuterium excess (d) and oxygen isotope measurements (δ^{18}O) using site-specific temperature-dependence relationships that assume the modern-day calibration holds over the entire record (Parrenin et al., 2007). However, surface temperatures can also be more accurately determined with additional borehole temperature and nitrogen isotope data, as was the case for WDC (Cuffey et al., 2016). In addition to the Antarctic ice core records, we apply sub-shelf melt rates that are based on a global δ^{18}O stack (GOT) and a Southern Ocean δ^{18}O (SOT) record using the process described above (Lisiecki and Raymo, 2005; Elderfield et al., 2012). The GOT reconstruction is based on a compilation of 57 deep ocean records. The SOT is derived from a marine sediment core from offshore New Zealand.

The remaining climate forcings are derived from two transient climate simulations of the last deglaciation. TraCE-21ka is a transient climate simulation of the last 21,000 years using the Community Climate System Model version 3 (CCSM3), a coupled general circulation model (GCM) with atmosphere, ocean, land surface and sea ice components (Liu et al., 2009). The experiment included evolving orbital forcing according to Milankovich theory, greenhouse gas concentrations (CO_2, CH_4, N_2O), ice sheets and paleogeography, and imposed meltwater fluxes into the North Atlantic and Southern Ocean. The LOVECLIM deglacial experiment was performed with the intermediate complexity LOVECLIM model version 1.1, which includes atmosphere, ocean, sea ice-ocean, ocean carbon cycle and terrestrial vegetation components, for the period of 18ka to 3ka (Menviel et al., 2011). Similar

to TraCE 21ka, the transient experiment involved time-varying solar insolation, Northern Hemisphere ice sheet topography, and atmospheric CO_2 determined from the EDC ice core, with CH_4 and N_2O fixed at LGM levels. Freshwater pulses were applied to the North Atlantic and Southern Ocean based on $^{231}Pa/^{230}Th$ data of the North Atlantic. Since the climate model runs do not cover the entire time period of the deglacial ice sheet simulations (i.e., 35 ka to 0 ka), we use averages of the proxy records for the preceding years of the model runs.

As the climate forcings are applied uniformly as scalar anomalies to a modern climatology based on RACMO2.3 output (Lenaerts et al., 2012), we calculate regional average anomalies over the domain to obtain the atmosphere forcings of the climate model simulations. Since Antarctic ice sheet topography is not updated in the LOVECLIM deglacial experiment, the continental interior shows relatively lower LGM temperature anomalies than TraCE-21ka. Therefore, we consider two versions of the LOVECLIM atmosphere forcing: one covering the entire domain, which includes the likely biased continental interior (Lowry et al., 2019), and one constrained to the continental margin. The sub-shelf melt rates are based on regional averages of ocean temperatures at 450m depth in the Ross Sea (70—62, 168—160). We also consider a "cool" ocean case using the TraCE-21ka SST as the sub-shelf melt rate forcing. All sub-shelf melt rates are scaled to the same LGM anomaly of 5.0 m yr^{-1}, which is based on the sensitivity experiments described above.

3.6.4 Deglacial climate forcing experiments

Starting from the regional PD configuration described above, we perform an initial climate forcing simulation from 131 ka (last interglacial) to 35 ka (early glacial) at 10 km resolution. This simulation is forced by EDC-derived temperature, precipitation, and back pressure forcing, sub-shelf melt rate forcing derived from the SOT reconstruction, and sea level forcing based on statistical analysis of multiple sea level records (Clark et al., 2009; Stanford et al., 2011; Deschamps et al., 2012). From this 35 ka configuration, we then perform 36 climate forcing experiments using the atmosphere and ocean forcing combinations listed in Table 3.1. These experiments are run from 35 ka to 0 ka at 10 km resolution. All model parameter values applied in these experiments are listed in Table 3.2, and the ensemble average deglacial ice sheet evolution is shown in Fig 3.11 (Supplementary Information).

In addition to this main ensemble set, we perform a sensitivity experiment that is based on the scenario proposed in Kingslake et al. (2018). In this experiment, which is also run from 35 ka to 0 ka at 10 km resolution, we use all of the same model parameters in the main ensemble set, with one exception. The mantle viscosity term in this simulation is $5{\times}10^{20}$ Pa s, whereas in the main ensemble set the term is $1{\times}10^{19}$ Pa s. Additionally, we employ a sub-shelf melt rate forcing based on the WDC temperature record, which has a steeper increase in the early deglacial period. The higher mantle viscosity and more aggressive ocean forcing are applied to reproduce the early retreat and isostatic re-advance in the Holocene simulated in Kingslake et al. (2018), and we show similar timing of retreat and minimum grounding-line extent (Supplmentary Information, Fig 3.7), i.e., 9.8 ka in our simulation versus 9.7 ka in Kingslake et al. (2018).

3.7 Supplementary Information

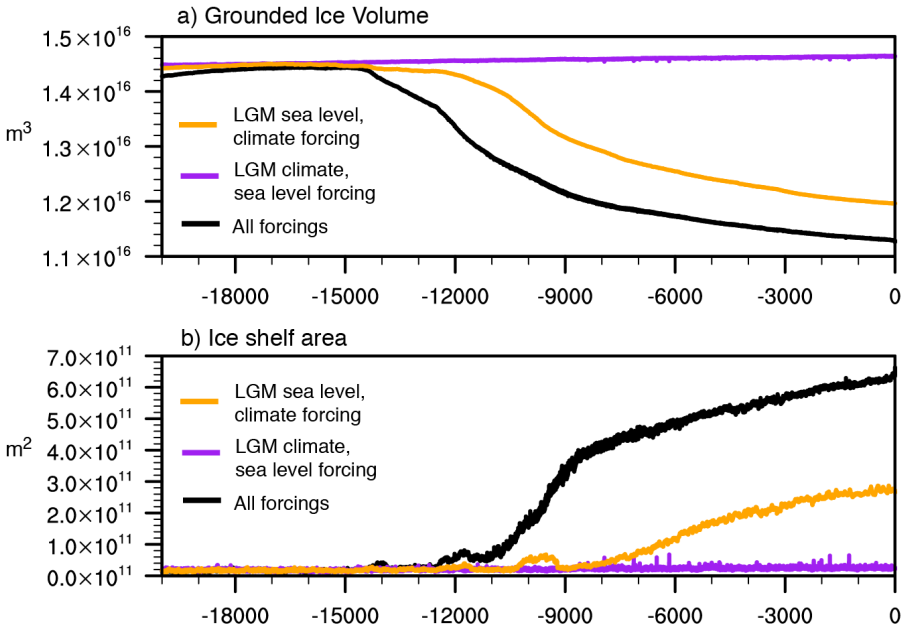

FIGURE 3.6: Sea level forcing effect on ice sheet-ice shelf evolution. Time-series of (a) grounded ice volume (m^3) and (b) ice shelf area (m^2) in three regional ice sheet simulations. The orange lines show a simulation forced by the model-proxy average (MPA) ocean and atmosphere forcings (see Fig 1a-c), with a constant LGM sea level (-125 m). The purple lines show a simulation forced by sea level, with constant LGM ocean and atmosphere. The black lines show the "moderate scenario," i.e., the simulation forced with MPA ocean and atmosphere forcing and sea level forcing.

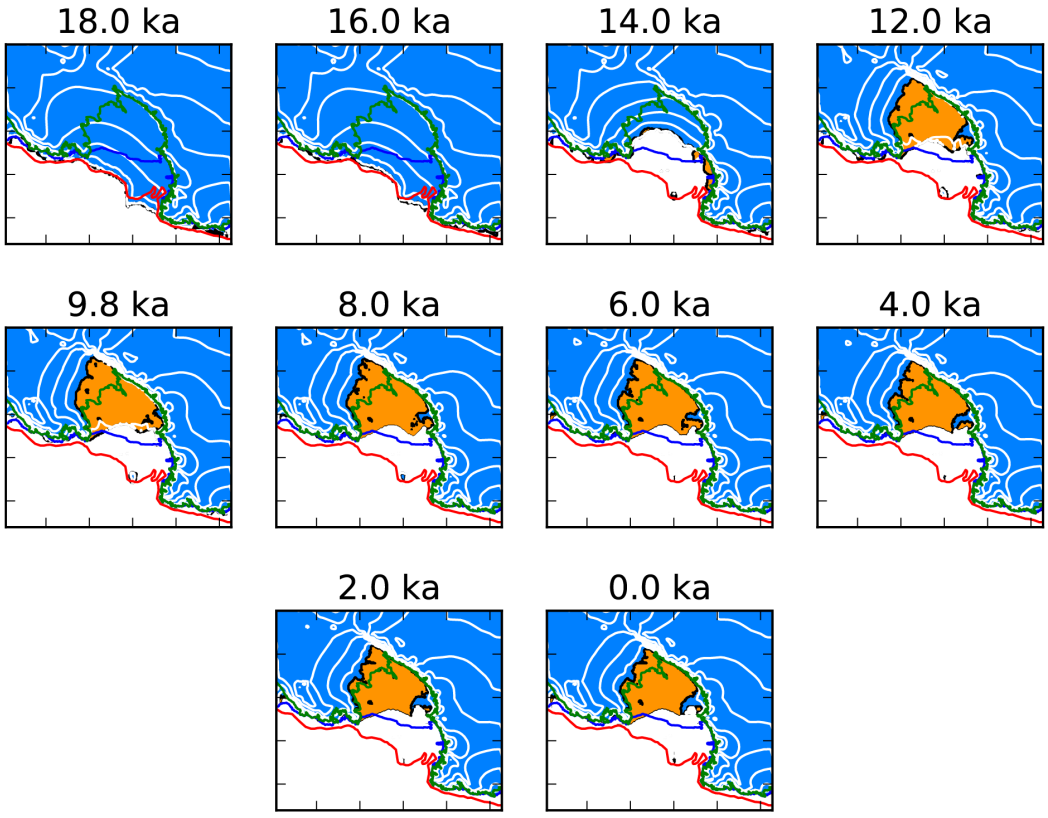

FIGURE 3.7: High mantle viscosity/ocean forcing simulation. Ice sheet-ice shelf evolution of the high mantle viscosity (5e20 Pa s) and strong ocean forcing simulation. Grounded ice is shown in blue and floating ice is shown in orange, with the modelled grounding line indicated by the black line. The green line shows the modern observed grounding line position, the red line shows the estimated LGM grounding line position, and the blue line shows the modern observed calving line position. The white lines are surface contours in 500 m intervals. Minimum grounding-line extent occurs at 9.8 ka.

	2.5 m yr^{-1} sub-shelf melt rate offset	*5.0 m yr^{-1} sub-shelf melt rate offset*	*7.5 m yr^{-1} sub-shelf melt rate offset*	*10.0 m yr^{-1} sub-shelf melt rate offset*
0.25 back pressure offset	2.5 ssmr 0.25 bp	5.0 ssmr 0.25 bp	7.5 ssmr 0.25 bp	10.0 ssmr 0.25 bp
0.5 back pressure offset	2.5 ssmr 0.5 bp	5.0 ssmr 0.5 bp	7.5 ssmr 0.5 bp	10.0 ssmr 0.5 bp
0.75 back pressure offset	2.5 ssmr 0.75 bp	5.0 ssmr 0.75 bp	7.5 ssmr 0.75 bp	10.0 ssmr 0.75 bp
1.0 back pressure offset	2.5 ssmr 1.0 bp	5.0 ssmr 1.0 bp	7.5 ssmr 1.0 bp	10.0 ssmr 1.0 bp

TABLE 3.2: Sub-shelf mass flux-sea ice back pressure sensitivity experimental setup. The combinations refer to individual simulations that we performed. Simulations were run at 20 km resolution from the last interglacial (131 ka) to present-day (PD; 0 ka). We find an intermediate range of the sub-shelf mass flux and back pressure offsets generally produces the best fit to observational data (i.e., 2.5 to 7.5 m yr^{-1} to 0.5 to 0.75, respectively), that is, the grounding line achieves an advance to near-LGM extent and a return to near-modern position. Since the main ensemble experiments are performed at 10 km resolution, we performed additional simulations at this resolution within the intermediate range of the sub-shelf mass flux/back pressure forcing combinations. Simulations within this range are able to achieve LGM grounding-line advance and present-day retreat, however, we achieve the best agreement with LGM thickness estimations of Anderson et al. (2014) using an LGM-PD melt rate offset of 5.0 m yr^{-1} and LGM-PD back pressure offset of 0.5. As a result, we applied these LGM-PD offsets in our deglacial climate forcing experiments.

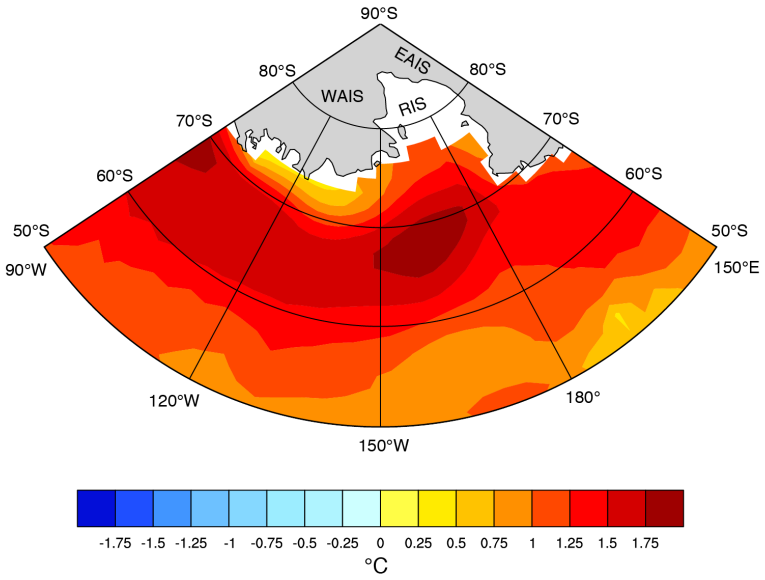

FIGURE 3.8: Southern Ocean freshwater forcing effect. Change in ocean temperature (°C) at 450m depth in TraCE-21ka simulation from 18-17.8 ka to 14.1-13.9 ka, corresponding to the onset of the last glacial termination and the timing of MWP-1A freshwater forcing, respectively.

Parameter	***Value***	***Units***
Domain Resolution (x,y)	10	km
Domain Resolution (z)	0.025	km
Run Length	131,000	yr
Spatial Output Interval	200	yr
Timeseries Output Interval	1	yr
Air Temperature Lapse Rate	0.008	$^{\circ}$ m^{-1}
Paleoprecipitation exponent	0.07	-
SIA Enhancement Factor	4.0	-
SSA Enhancement Factor	0.8	-
Till friction angle min (ϕ_{min}) for bed elevation below 200 m bsl	9	$^{\circ}$
Till friction angle max (ϕ_{max}) for bed elevation above 0 m bsl	30	$^{\circ}$
Flow law exponent (q)	0.25	-
Till effective overburden (N)	0.02	-
Eigen calving (K)	1.0e18	m s
Thickness calving threshold	160	m
Mantle viscosity (μ)	1.0e19	Pa s

TABLE 3.3: Ice sheet model parameters used in the deglacial climate-forcing experiments.

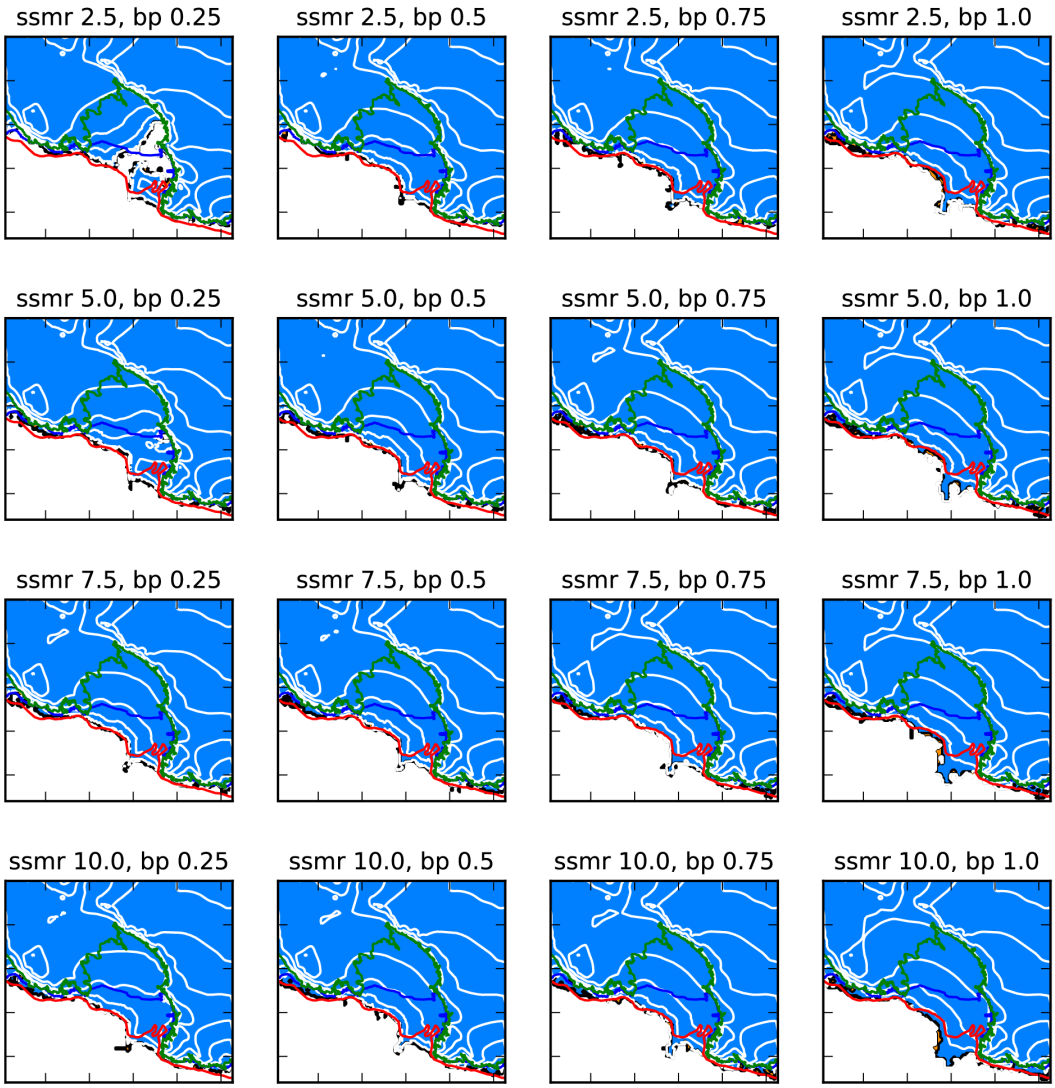

FIGURE 3.9: LGM (20 ka) results of the sub-shelf melt rate (ssmr)— back pressure (bp) experiments. The light blue colour represents grounded ice. The red line indicates the estimated LGM grounding line position based on Anderson et al. (2002); the green (blue) line denotes the modern day grounding (calving) line position. The white lines are surface contours of 500m.

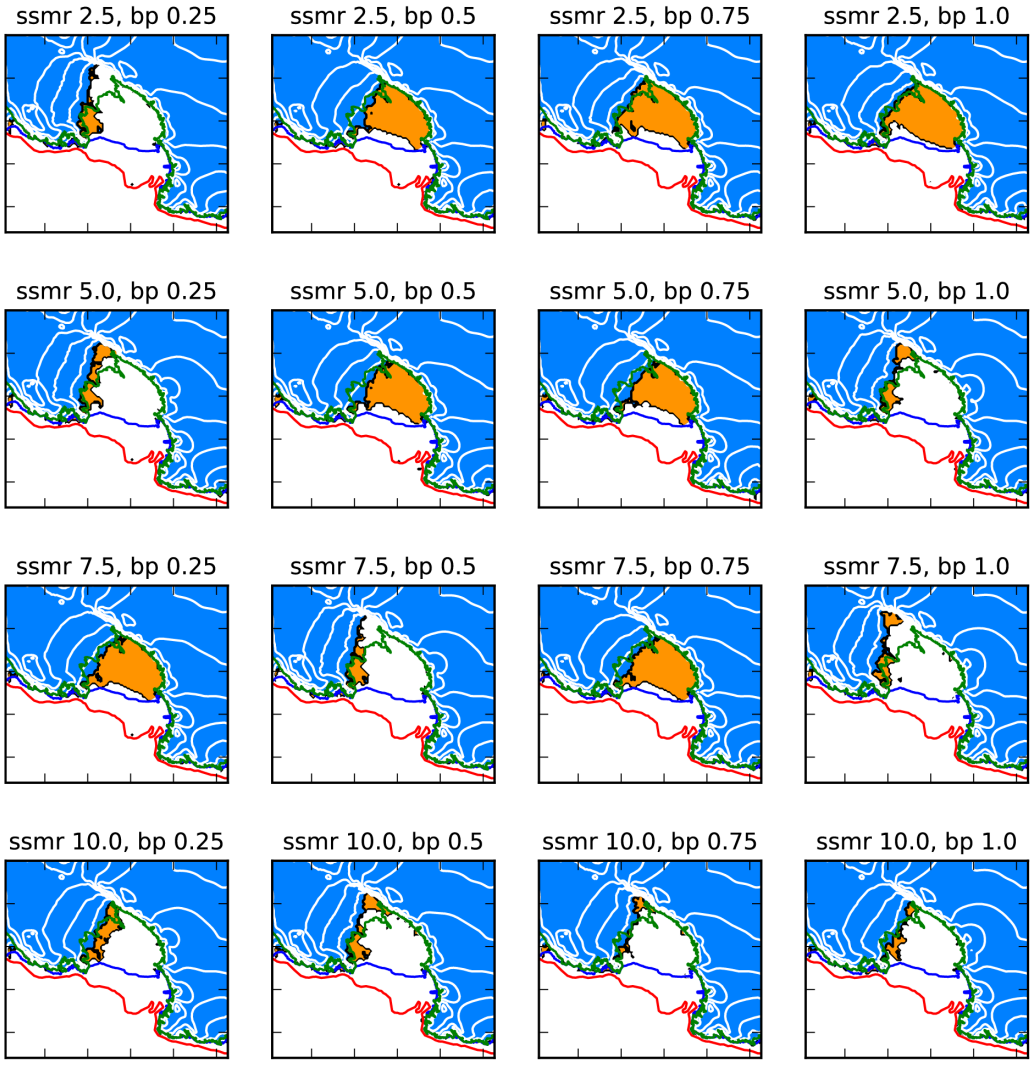

FIGURE 3.10: PD (0 ka) results of the sub-shelf melt rate (ssmr)-back pressure (bp) experiments. The light blue colour represents grounded ice, and the orange colour represents floating ice shelf. The red line indicates the estimated LGM grounding line position based on the geological record; the green (blue) line denotes the modern day grounding (calving) line position. The white lines are surface contours of 500m.

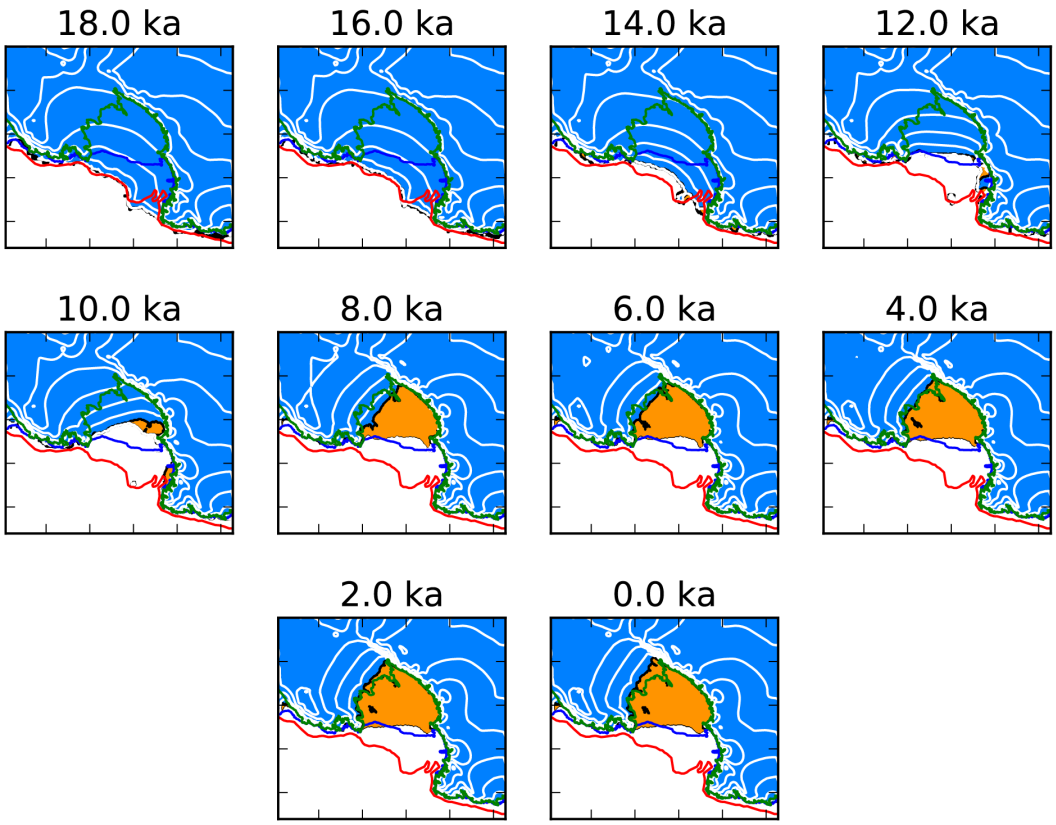

FIGURE 3.11: Moderate ocean/atmosphere simulation. Ice sheet-ice shelf evolution of the MPA ocean/atmosphere forced simulation (i.e. the "moderate scenario" in Fig 2b). Grounded ice is shown in blue and floating ice is shown in orange, with the modelled grounding line indicated by the black line. The green line shows the modern observed grounding line position, the red line shows the estimated LGM grounding line position, and the blue line shows the modern observed calving line position. The white lines are surface contours in 500 m intervals.

Chapter 4

Integration of climate and ice sheet model simulations with the Roosevelt Island Climate Evolution (RICE) ice core record for the last deglaciation

4.1 Abstract

Coastal ice cores are best suited to record the deglacial climate history of the peripheral ice sheet, where past ice sheet retreat has occurred. However, the isotopic signals of these ice cores are complicated by oceanic influences and ice sheet-related changes. Here, I apply climate and ice sheet model simulations to better interpret the stable isotope record of the Roosevelt Island Climate Evolution (RICE) ice core, obtained from a grounded ice dome in the eastern Ross Sea. The models show pronounced changes in sea ice and ice surface elevation that took place during the Antarctic Cold Reversal and subsequently through the Younger Dryas when the climate in the Southern Hemisphere warmed. These changes in sea ice extent and ice surface elevation may therefore have contributed to changes in the water stable isotopes (deuterium, δD) recorded in the ice core through this time interval. Using a RICE-specific climate forcing in regional ice sheet simulations yields a later, but more rapid retreat of the ice sheet grounding line in the Ross Embayment. In my experiments, precipitation forcing exerts the dominant control on the magnitude and rate of grounding line retreat along the Siple Coast of West Antarctica in the late Holocene, a mechanism that requires further consideration in future Antarctic ice sheet projections.

4.2 Introduction

A main concern for future sea level rise is the instability of the West Antarctic Ice Sheet (WAIS) given that the reverse slope bathymetry of the continental shelf creates an ice sheet configuration prone to runaway retreat (Mercer, 1978; Schoof, 2007; Joughin, Smith, and Medley, 2014). This process of marine ice sheet instability has been observed along parts of the WAIS grounding line, driven by warming oceanic conditions (Pritchard et al., 2012; Favier et al., 2014; Seroussi et al., 2017). However, large uncertainties remain in terms of the WAIS response to future climatic warming scenarios in numerical ice sheet models (Golledge et al., 2015; DeConto and Pollard, 2016; Golledge et al., 2019). Understanding periods of past grounding line retreat can help inform future predictions by constraining marine ice sheet sensitivities to changes in climatic conditions. The Ross Embayment is a useful candidate for this task as the grounding line has retreated by more than 1000 km since the Last Glacial Maximum (LGM; Bentley et al., 2010), but the influence of environmental forcings in this deglacial retreat are still unclear (Conway et al., 1999; Kingslake et al., 2018).

One of the main complications in understanding past WAIS sensitivity to climatic changes is that the sites of Antarctic ice cores used for paleoclimate reconstructions are often located at high altitudes on the East Antarctic Plateau, far from the fringes of the ice sheet (Veres et al., 2013). As a result, these continental ice cores may not provide an accurate representation of climate in the areas where grounding line retreat initiates. In this sense, marine ice cores, obtained from high accumulation and low elevation sites, are more useful, but they often have unique issues related to climate reconstructions that lead to higher uncertainties. In particular, sea ice variability can influence isotopic concentrations in precipitated snow over coastal areas through the increased contribution of enriched water vapour and higher moisture transport (Noone and Simmonds, 2004; Thomas and Bracegirdle, 2015; Küttel et al., 2012; Holloway et al., 2016). Isotopic signals can also be influenced by changes in moisture source regions (Uemura et al., 2012) and the seasonality of precipitation (Erb et al., 2018), both of which can change through time.

The application of numerical climate and ice sheet models can help address these uncertainties inherent in Antarctic ice core records and aid in the interpretation of paleoclimate reconstructions (e.g., Holloway et al., 2016). Models can also offer a more complete view of mechanisms of climatic and

glaciological change than proxy records, which are often limited to a single point in space. In turn, proxy records serve as an important test of model skill with assessment of a given model's ability to reproduce the data. With respect to marine ice cores, output from deglacial transient climate and ice sheet model simulations can be applied to investigate the relative impacts of changes in sea ice, precipitation and surface elevation on the isotopic signals observed in a given record.

For the Ross Embayment, the Roosevelt Island Climate Evolution (RICE) ice core is the best candidate to understanding both the regional climate history and WAIS evolution through the last deglaciation given its proximity to the Ross Sea. In this Chapter, I analyse the stable isotope record of the RICE ice core in the context of two deglacial climate simulations and an ensemble of regional ice sheet model simulations described in the previous chapters, with the addition of 6 new ice sheet model ensemble members. The goals of this integrative approach are to better understand the influence of sea ice, precipitation, and ice sheet extent and elevation changes on the RICE isotope record and improve the overall understanding of past ice sheet sensitivity to climate changes over the last deglaciation.

4.3 Geological Setting

4.3.1 Site glaciology

Roosevelt Island, West Antarctica, is a grounded ice dome located on a submarine plateau ($\sim$200 m bsl) in the eastern Ross Sea (Fig 4.1). It is the northernmost Antarctic ice core site on the western side of the Ross Embayment (Fig 4.1a). As noted in Bertler et al. (2018), ice accumulation on the ice rise is entirely local because the Ross Ice Shelf flows around, and not over, Roosevelt Island. The ice surrounding Roosevelt Island is WAIS-derived via the Bindschadler, MacAyeal and Echelmeyer ice streams (Fig 4.1b). The compilation of Bedmap2 data (Fretwell et al., 2013) indicate the thickness of the Ross Ice Shelf at this location is $\sim$500 m and that the western and eastern marine basins on either side of Roosevelt Island are 600m and 750m deep, respectively. At the RICE ice core drill site (79.364°S, 161.706°W, 550m asl), which is located near the summit of the ice dome, the ice is 764m thick and grounded 214m below sea level (Bertler et al., 2018).

Radar surveys across the Roosevelt Island ice divide exhibit well-developed "Raymond arches" (Raymond, 1983) of isochrones, which suggest a stable

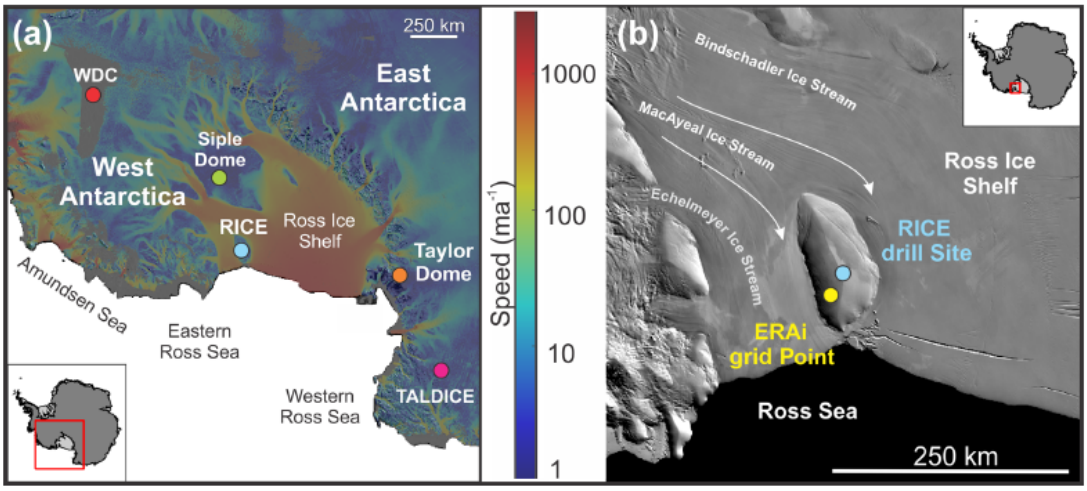

FIGURE 4.1: (a) Overview map from Bertler et al. (2018) of the Ross Sea region and eastern West Antarctica. Antarctic ice velocity derived from the Advanced Land Observing Satellite (ALOS) with the Phased Array type L-band Synthetic Aperture Radar (PALSAR), the European Space Agency (ESA) Envisat Advanced Synthetic Aperture Radar (ASAR), European Remote Sensing (ERS) satellites, ERS-1 and 2, and the the Canadian Space Agency (CSA) RADARSAT-1 and 2 satellite radar interferometry colour-coded on a logarithmic scale (Rignot et al., 2011). Coloured dots indicate the locations of ice core drilling sites used in this paper: RICE (blue), West Antarctic Ice Sheet Divide ice core (WDC; red), Siple Dome (green), TALDICE and Talos Dome TD96 (purple), Taylor Dome (orange). (b) Overview map of Roosevelt Island derived from the Moderate-resolution Imaging Spectroradiometer (MODIS) satellite images (Scambos et al., 2007). The maps were created using the Antarctic Mapping Tool (Greene et al., 2017). The coloured dots indicate the location of the RICE drill site (blue) and the nearest ERA-Interim (ERAi) grid point (yellow).

ice divide (Conway et al., 1999). The vertical velocity, constrained by phase-sensitive radio echo sounder (pRES) measurements, is approximately 20 cm/yr at the surface and 0 cm/yr at the bed (Kingslake et al., 2014). Over the past centuries, a small migration of the divide has occurred with the topographic divide offset to the south-west by approximately 500m (Bertler et al., 2018).

4.3.2 Site climatology

The modern climatology at the Roosevelt Island drill site is characterized by a local mean annual air temperature of -23.5°C, and annual snow accumulation is estimated to range from 0.18 m ice per year to 0.27 m ice per year, depending on the measurement method and time period analysed (Bertler et al., 2018; Herron and Langway, 1980; Conway et al., 1999; Kingslake et al., 2014). In terms of the source of precipitation, Tuohy et al. (2015) demonstrated that for the period of 2006–2012, 40–60% of precipitation arriving at Roosevelt Island originated from local sources in the southern Ross Sea. In addition, Emanuelsson et al. (2018) demonstrated the important role of blocking events, characterized by anticyclones that impede westerly circulation, which are associated with over 88% of large precipitation events at RICE.

Bertler et al. (2018) compared the deuterium (δD) record of a shallow ice core to the ERA-Interim reanalysis dataset (ERAi) of the European Centre for Medium-Range Weather Forecasts and automatic weather station data for the period of 1979-2012. Snow accumulation at RICE is negatively correlated with sea ice concentration (SIC) in the Ross Sea region and northern Amundsen Sea region (Fig 4.2a). The correlation between ERAi SIC and the optimised RICE δD record (Fig 4.2b) similarly shows a negative correlation of SIC in the Ross Sea (perhaps with the exception of the Ross and Terra Nova polynyas) and the northern Amundsen Sea, with more depleted values observed during years of increased SIC (Bertler et al., 2018).

In Fig 4.2c and 4.2d, the sea ice extent index (SIE_J) for the Ross–Amundsen Sea, developed by Jones et al. (2016), is correlated with ERAi SAT and precipitation data. Co-variance of sea ice extent (SIE) and SAT is observed, with increasing (decreasing) sea ice associated with cooler (warmer) SAT. This suggests an association of lower temperatures and less snow accumulation over the Ross Ice Shelf and western Marie Byrd Land during years of more extensive sea ice. The correlation between SIE_J and ERAi precipitation at RICE is r = -0.67, and the correlation between SIE_J and RICE snow accumulation is r = -0.56 (Bertler et al., 2018).

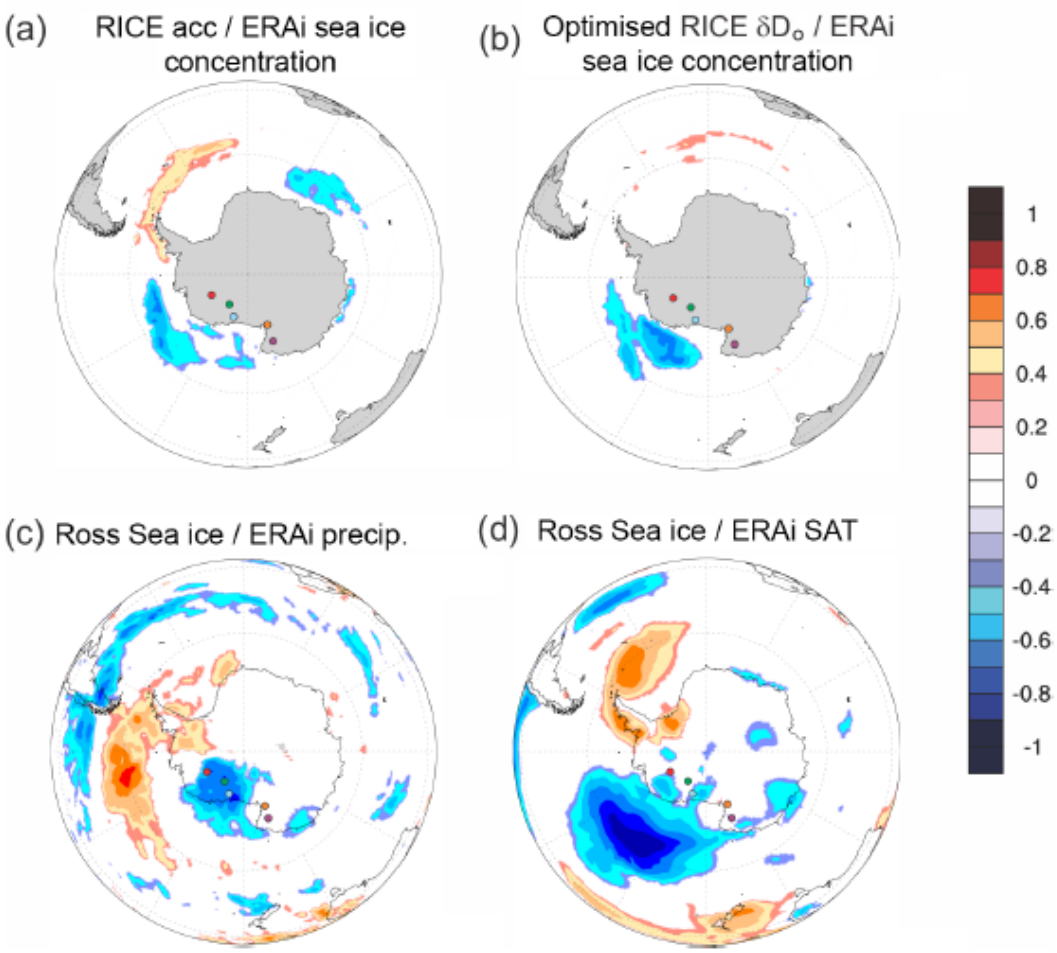

FIGURE 4.2: Spatial correlation plots from Bertler et al. (2018). (a-b) Spatial correlation of ERAi sea ice concentration (SIC) fields with the time series of (a) RICE snow accumulation and (b) RICE δD. (c-d) Spatial correlation of the Ross–Amundsen Sea SIE$_J$ time series (Jones et al., 2016) with (c) ERAi precipitation and (d) ERAi SAT fields. Only fields exceeding 95% significance are shown. The correlation has been performed using http://climatereanalyzer.org/, University of Maine, USA. Coloured dots indicate locations of WDC (red), Siple Dome (green), RICE (blue), TALDICE and Talos Dome (purple) and Taylor Dome (orange).

4.4 Materials and Methods

4.4.1 Ice core stable isotope record

Over the course of two field seasons, 2011–2012 and 2012–2013, a 764m long ice core was obtained from near the summit of Roosevelt Island. The drill system employed in the operation was based on the Danish Hans Tausen Drill with some design modification (Mandeno et al., 2013). The upper 60m of the borehole was cased with plastic pipe and the remainder of the drill hole filled with a mixture of Estisol-240 and Coasol to prevent closure. Description of the core quality and processing procedures for the RICE ice core are provided by Pyne et al. (2018).

In this study, I focus on the RICE δD record, which was measured using continuous-flow laser spectroscopy system with an off-axis integrated cavity output spectroscopy (OA-ICOS) analyser, manufactured by Los Gatos Research (LGR). A detailed description of the quality assessment of the continuous flow system is provided in Emanuelsson et al. (2014). Keller et al. (2018) provides the isotope calibration, cumulative uncertainties and assignment of depth. The age scale is based on synchronization of the RICE methane record with that of the high-resolution WAIS Divide ice core (WDC), and is described in detail in Lee et al. ("An 83,000 year old ice core from Roosevelt Island, Ross Sea, Antarctica"). I analyse the RICE δD record in the context of the δD records of other Antarctic ice cores, including WDC, Siple Dome (SD), Taylor Dome (TD), Talos Dome (TALDICE), and EPICA Dome C (EDC).

4.4.2 Climate Model Analysis

Here, I analyse model output of two transient deglacial climate simulations, namely, the TraCE-21ka and LOVECLIM DGns deglacial experiments. TraCE-21ka is a transient climate simulation of the last 22,000 years using the Community Climate System Model version 3 (CCSM3), a synchronously coupled GCM with atmosphere, ocean, land surface and sea ice components and a dynamic global vegetation module (Collins et al., 2006; Liu et al., 2009; He et al., 2013). The LOVECLIM DGns experiment was performed with the intermediate complexity LOVECLIM model version 1.1 (Driesschaert et

al., 2007; Goosse et al., 2007; Menviel et al., 2011), which includes a quasi-geostrophic atmosphere model, an ocean general circulation model, a dynamic/thermodynamic sea ice model as well as ocean carbon cycle and terrestrial vegetation components. Full model details are described in Chapter 2. Both simulations were performed with transient forcings and evolving boundary conditions to reproduce global climate through the deglaciation, including evolving solar insolation, greenhouse gas concentrations, ice sheet topography and prescribed freshwater fluxes. Of these forcings, the freshwater fluxes differ most between the simulations due to limited paleoconstraints, and this is consequential for the evolutions of Antarctic climate and Southern Ocean conditions (Lowry et al., 2019).

Within the climate models, I define specific regional areas representing the western Ross Embayment and the Ross Sea. Since individual model grid cells may have biases, particularly in coastal areas where the topography may be inadequately represented, these regional averages are preferred as they can offer a more complete view of the climate evolution. I use a latitude range of ∼75°S and a longitude range of ∼165°W for the western Ross Embayment, i.e., 4 land-based grid cells in LOVECLIM and 9 land-based grid cells in TraCE-21ka, given the higher resolution of the latter atmospheric model. The Ross Sea ranges from ∼75° to 60°S in latitude and ∼168°E to 160°W in longitude.

4.4.3 Ice sheet model simulations and analysis

To determine the effect of the regional climate and glaciological evolution on past ice sheet retreat in the Ross Embayment, I rely on an ensemble of regional ice sheet simulations described in the previous Chapter as well as additional sensitivity experiments. The regional ice sheet simulations are performed at 10km resolution using the Parallel Ice Sheet Model (PISM), a sophisticated ice sheet model which allows for realistic ice streams that exhibit the full range of observed ice stream velocities; it is one of the few ice sheet models capable of multi-millennia simulations of ice sheets containing freely-evolving ice streams (Bueler and Brown, 2009; Martin et al., 2011). The regional domain includes both the Ross ice shelf and its surrounding ice drainage basins of grounded ice, which are allowed to dynamically evolve. A larger area around the drainage basins is maintained at a constant thickness as a time-independent boundary condition. This smaller domain size is

preferred to full continental-scale simulations in order to improve the computational efficiency. Details of the regional model set up and spin-up procedure are described in the Materials and Methods section of the previous chapter.

The purpose of the model ensemble in Chapter 3 is to highlight the effects of ocean and atmosphere forcing on grounding line migration. The ocean forcing is in the form of basal ice shelf melt rate anomalies and is applied uniformly. The atmosphere forcings include surface temperature and precipitation anomalies and a back pressure forcing to heuristically represent the resistive effect of sea ice. The forcings are based on the two deglacial climate simulations described above as well as temperature reconstructions from two Antarctic ice cores, i.e., the EPICA Dome C (EDC) ice core from East Antarctica (75°S, 123°E) and the WAIS Divide (WDC) ice core from West Antarctica (∼79°S, 112°W), global and Southern Ocean benthic ocean temperature proxy reconstructions (GOT and SOT, respectively; Liesecki and Raymo, 2006; Elderfield et al., 2012), and model-proxy averages (MPA).

However, the climate forcings applied in the previous Chapter were limited in a number of ways, which I improve upon here. First, I perform simulations with atmospheric forcing derived from the RICE δD record. This record is more specific to the climatic changes experienced by the peripheral ice sheet in the Ross Embayment as compared to the more continentally located WDC and EDC ice cores. I use a simple linear scaling relationship between RICE δD that assumes an LGM temperature anomaly of 11.0 °C. While the true LGM temperature anomaly of Roosevelt Island is not currently known, the climate models demonstrate that this is a reasonable estimation. Secondly, the previous simulations used a simple linear temperature-precipitation scaling relationship for the precipitation forcing. Here, I further investigate the role of precipitation by performing simulations using the WDC accumulation record (Fudge et al., 2016), which has been shown to behave more independently of temperature. The RICE-forcing and WDC precipitation forcing experiments are respectively run with three ocean forcings, representing cooler, moderate, and warm scenarios, as in the previous Chapter.

4.5 Results

4.5.1 RICE δD record

The deglacial climate evolution indicated in the RICE δD record indicates key phases of change that are distinct from other ice core records of the Ross Embayment (Fig 4.3). In particular, the isotopic signatures of RICE δDiffer from those of other ice cores during periods of cool climate states or cooling (yellow bars in Fig 4.3). In the 2 ka preceding glacial termination ($\sim$18 ka; GL in Fig 4.3), RICE δD suggests a stable glacial climate, in contrast to the potential warming trend observed at WDC and cooling trend of TD, but similar to the isotopic trends of EDC, TALDICE, and the nearby Siple Dome ice cores. The ACR initiates $\sim$14.6 ka, relatively earlier than ice cores located further inland (i.e., WDC, EDC, and SD), and shows the most pronounced signal of the ice core records. The early-to-middle Holocene (EMH) is characterized by a slight cooling trend with high δD variability. Although the cooling trend is consistent with most of the ice core isotope records, with the only exception of WDC, the isotopic variability is highest at RICE, and the variability increases throughout this period.

In terms of the periods of warming indicated in the isotope records (white bars in Fig 4.3), the RICE δD record is unique in terms of the magnitude of increase during the Younger Dryas (YD). Additionally, RICE, along with the other coastal ice cores of TD and TALDICE, shows high variability through the late Holocene (LH). This behavior may be indicative of the sensitivity of this coastal region to changes in sea ice concentration, which affects both the temperature and moisture content of local air masses, thus influencing the isotopic signal. The YD signal may also reflect changing surface elevation related to the retreating ice sheet, which also affects surface temperature and precipitation. Previous ice sheet model simulations of the deglaciation have shown substantial surface elevation changes (>300 m) at Roosevelt Island during the period between 14 and 8 ka (Golledge et al., 2014), with the most rapid decrease between 11 and 10 ka. However, the relative contributions of surface elevation, sea ice concentration, and regional climate changes to the isotopic signals remain unclear.

4.5.2 Temporal climate evolution in climate simulations

In the early deglacial period (i.e., 18-14.6 ka), the climate model simulations show increasing surface temperature and precipitation in the western

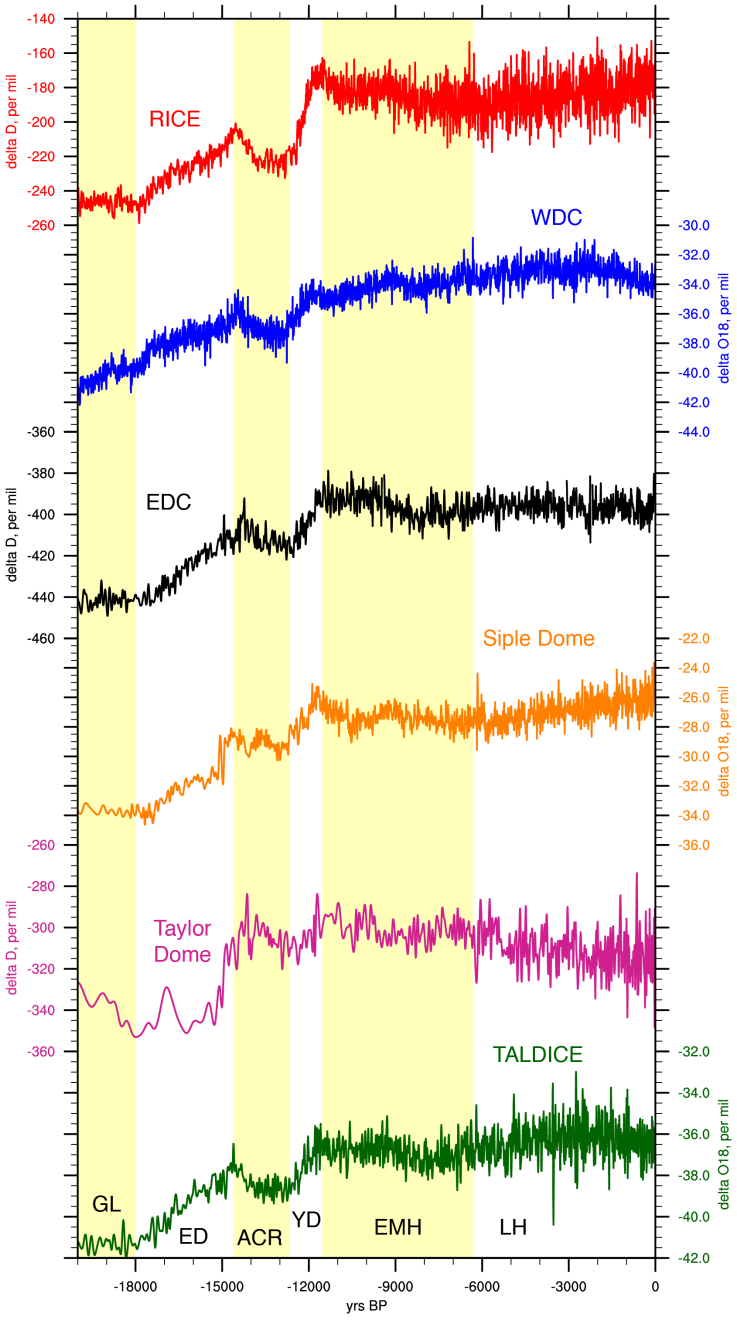

FIGURE 4.3: Decadally averaged stable isotope records of ice core sites in the Ross Sea region. Axes on the left (right) refer to δD (δ18O) records. Records were interpolated using spline interpolation. Yellow bars indicate cool climate states or periods of cooling in the RICE δD record, namely, the last glacial period (GL), Antarctic Cold Reversal (ACR), and early-to-middle Holocene (EMH). White bars indicate periods of warming in the RICE δD record, namely, the early deglacial period (ED), the Younger Dryas (YD), and the late Holocene (LH).

Ross Embayment, similar to the increase in δD content observed in the RICE record (Fig 4.4a-c). Over this time interval, the increase in average annual surface temperature is higher in DGns (Fig 4.4b), whereas the increase in annual average precipitation is higher in TraCE-21ka (Fig 4.4c). The seasonal variation in surface temperature and precipitation anomalies decreases in TraCE-21ka, but remains high in DGns. Surface temperature and precipitation decrease in response to freshwater pulses into the North Atlantic and Southern Ocean (see Menviel et al., 2011; He et al., 2011), however, the RICE ACR event has a longer duration than in the model simulations show for this region.

In a broader spatial context, both climate models show a pronounced cooling and drying over Antarctica and the Southern Ocean during the ACR relative to PI, with a few exceptions (Fig 4.5). In particular, the Antarctic plateau shows modest cooling and a slight increase in precipitation in DGns, with a coincident increase in precipitation observed along the East Antarctic coast (Fig 4.5a,c). The latter is likely due to model resolution limitations in LOVECLIM, which do not adequately reproduce the steep topographic gradient in the East Antarctic coastal region (Goosse et al., 2012; Lowry et al., 2019). TraCE-21ka shows slight increases in precipitation over the Antarctic Plateau and in northern Marie Byrd Land, in close proximity to Roosevelt Island (Fig 4.5d). TraCE-21ka also shows substantially cooler surface temperature anomalies than DGns over the continental interior (Fig 4.5b), primarily driven by differences in ice sheet topographic changes in the models (Lowry et al., 2019).

Some of the largest climatic changes associated with the ACR are observed in the coastal areas in close proximity to the ice sheet. The higher SICs associated with the ACR, shown in Fig 4.4d, lead to pronounced cooling and reduced precipitation over the Ross and Amundsen Seas in both simulations, however, the patterns of change show some differences. Surface temperature anomalies are more negative in the Ross Sea in TraCE-21ka ($< 7\,^{\circ}$C; Fig 4.5b), and the decrease in precipitation is more substantial over WAIS (< -15-20 cm yr^{-1}; Fig 4.5d). In contrast, DGns shows larger surface temperature and precipitation changes of similar magnitude further from the ice sheet in the Ross and Amundsen Sea sectors (i.e., latitudes of $\sim$60-75°S; Fig 4.5a,c).

Following the ACR, RICE δD displays a marked increase in the Younger Dryas (YD) period ($\sim$12.7 to 11.5 ka; Fig 4.4a). The climate models show increases in surface temperature and precipitation through this YD interval,

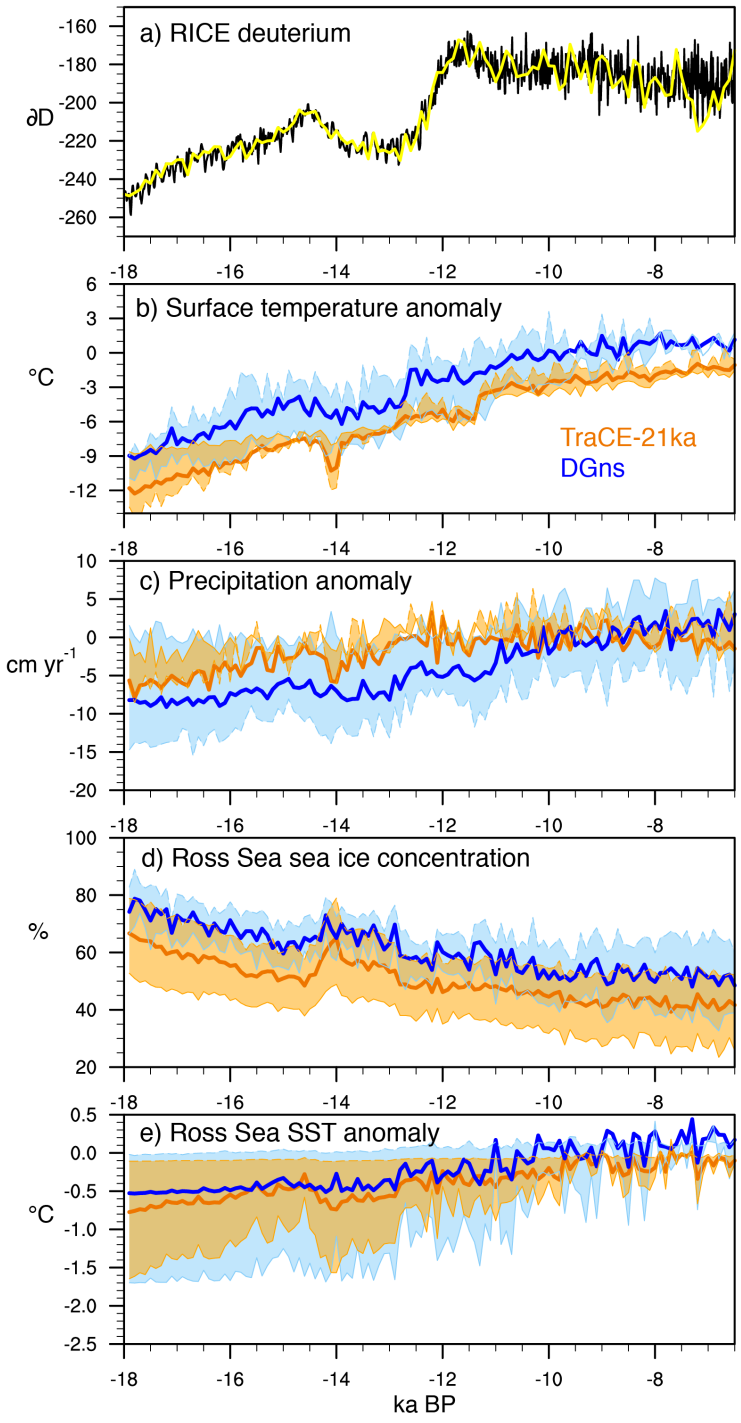

FIGURE 4.4: (a) Centennial and decadal δD at RICE (black and yellow, respectively). (b-e) Centenially averaged model output of anomalies relative to PI of the LOVECLIM DGns and TraCE-21ka simulations (blue and orange, respectively). The colored shading indicates the seasonal range calculated from the 100-yr average austral summer and winter temperature anomalies.

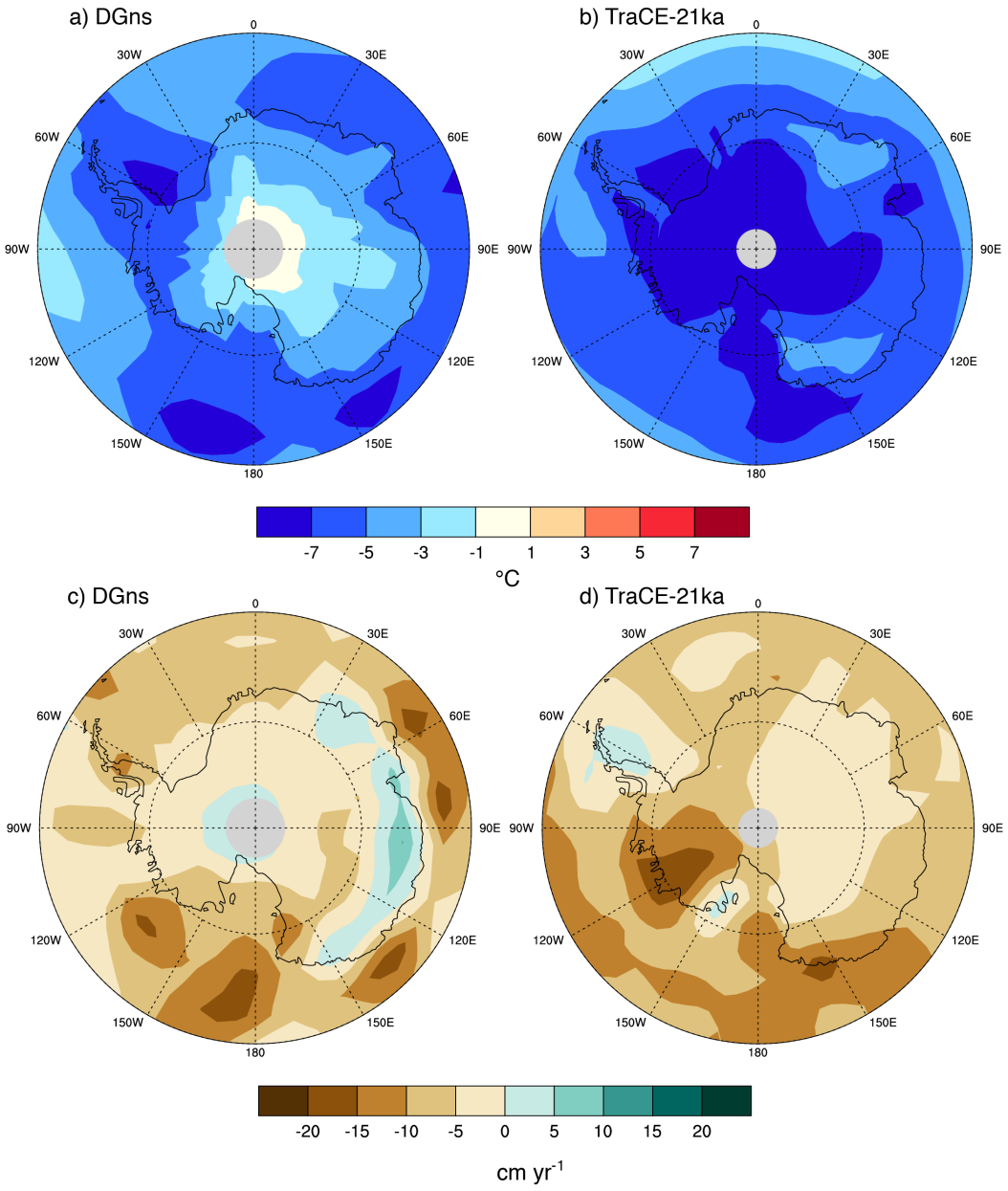

FIGURE 4.5: Modelled change at ACR relative to the Pre-industrial Era for (a,b) surface temperature (°C) and (c,d) precipitation (cm/yr) of the LOVE-CLIM DGns and TraCE-21ka simulations, respectively.

but at different times (Fig 4.4b,c). The increase in surface temperature occurs earlier in DGns than in TraCE-21ka, initiating at approximately 12.7 ka, closely matching the timing of the RICE δD increase. Preceding rapid surface warming, the average annual SIC in the Ross Sea declines considerably (Fig 4.4d). However, the duration of the 3°C increase in average annual surface temperature in DGns is short-lived, with surface temperature remaining fairly stable from 12.4 to 11.5 ka. TraCE-21ka likewise shows a short-lived increase of 2.4°C in average annual temperature at 11.3 ka, coinciding with a change in ice sheet topography in the model simulation. Precipitation trends through the YD are less clear, particularly in TraCE-21ka, however, average annual precipitation increases in DGns in two steps: $\sim$13 ka and $\sim$11.2 ka.

Average annual sea surface temperatures (SSTs) in the Ross Sea dramatically increase in the climate models during the YD and into the early Holocene (11.7 ka). This is primarily driven by increases in summer SSTs, which increase by >1.0°C in both models between 12.5 and 10 ka (Fig 4.4e). Winter SST anomalies remain near $\sim$0 °C through the deglacial period as the Ross sea surface remains near the freezing point in winter. In contrast to SST, SIC in the Ross Sea and its seasonal range show little change through the YD in both models (Fig 4.4d). DGns exhibits higher average annual SIC and SST variability than TraCE-21ka, and by the early Holocene (11.0 ka), Ross Sea SSTs exceed PI levels. This high SST variability with above-PI temperatures persists into the middle Holocene in DGns, and TraCE-21ka likewise exhibits higher SST variability (Fig 4.4e). The seasonal range of SIC increases in both models through this period.

A clear discrepancy exists between the RICE δD record and modelled surface temperature and precipitation in the western Ross Embayment in the early to middle Holocene (11.7 to 6.5 ka). As discussed previously, RICE, in contrast to other ice core records, displays a decreasing δD trend through this interval (Fig 4a). Both models show a slight increasing surface temperature trend through this period (Fig 4b), and DGns also displays a slight increasing precipitation trend (Fig 4.4c). TraCE-21ka does, however, show a slight decreasing precipitation in the middle Holocene ($\sim$9.0 to 6.5 ka), consistent with the RICE δD trend.

4.5.3 Factors influencing western Ross Embayment climate

Southern Ocean conditions have long been known exert a strong influence on Antarctic accumulation patterns and surface temperatures (Delaygue

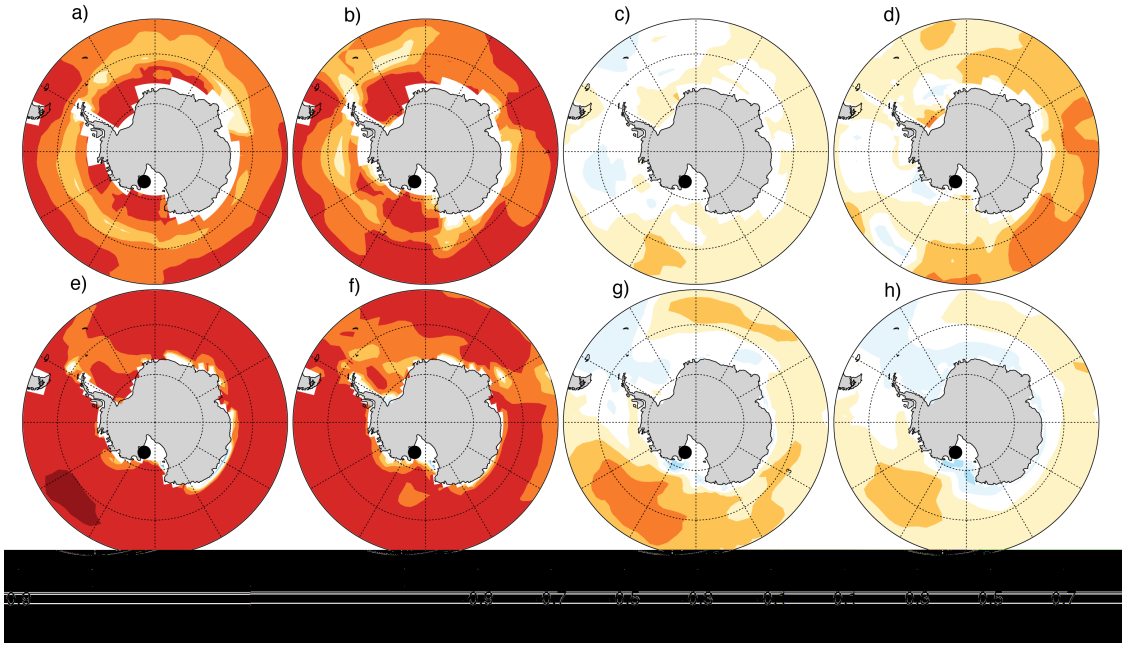

FIGURE 4.6: Spatial Pearson linear cross-correlation coefficients (r) between decadal SST and precipitation of the western Ross Embayment of the DGns simulation for (top row) and the TraCE-21ka simulation (bottom row) for 18-14.5 ka (a,e), 14.5-12.5 ka (b,f), 12.5-10 ka (c,g), and 10-6.5 ka (d,h).

et al., 2000; Stenni et al., 2010). As previously discussed, modern accumulation and surface temperature at the RICE Drill site display strong negative correlations with sea ice in the Ross and Amundsen Seas (Fig 4.2; Bertler et al., 2018). The spatial correlations between precipitation in the western Ross Embayment and Southern Ocean SSTs and sea ice concentrations shown here exhibit a consistent evolution through the deglacial period in two different climate models (Fig 4.6, 4.7). In particular, strong positive correlations are observed between precipitation in the western Ross Embayment and SSTs throughout the Southern Ocean in the early deglacial period (18-14.5 ka) and the ACR (14.5-12.5 ka). TraCE-21ka shows higher correlations ($r > 0.7$) than DGns, with the highest correlations in DGns constrained locally to the Ross Sea (Fig 4.6a,b). These high correlations are likely driven in part by the high millennial-scale variability that existed through these time intervals, resulting in precipitation and Southern Ocean SSTs synchronously responding to the same external forcings (e.g., changes in greenhouse gas concentrations, freshwater forcing, meridional heat transport, etc.).

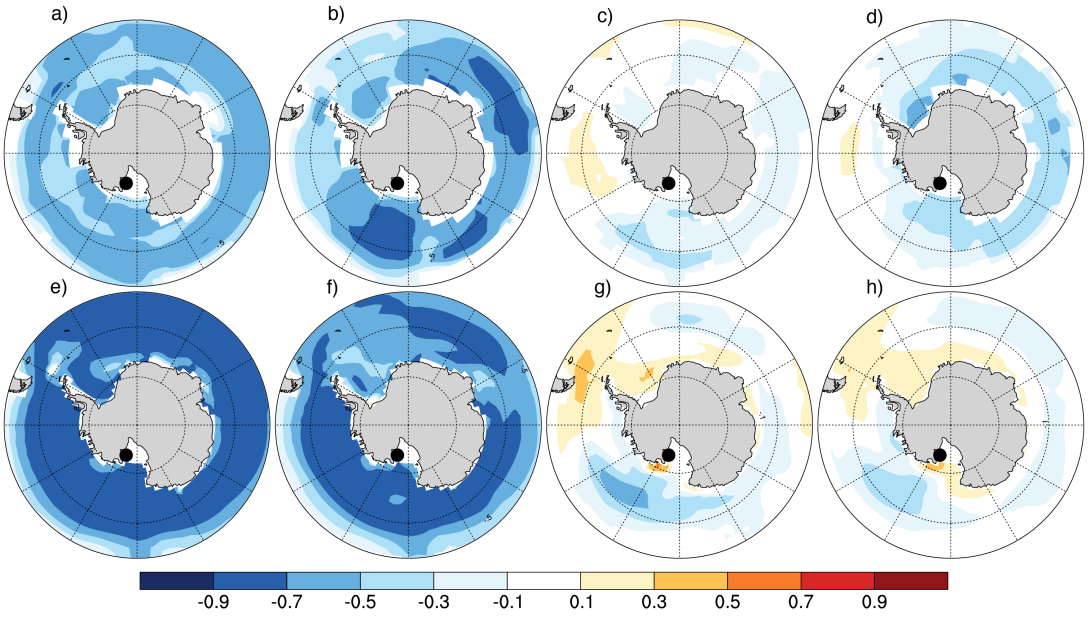

FIGURE 4.7: Spatial Pearson linear cross-correlation coefficients (r) between decadal sea ice concentration and precipitation of the western Ross Embayment of the DGns simulation for (top row) and the TraCE-21ka simulation (bottom row) for 18-14.5 ka (a,e), 14.5-12.5 ka (b,f), 12.5-10 ka (c,g), and 10-6.5 ka (d,h).

In the YD (12.5 to 10.0 ka) and middle Holocene (MH; 10.0 to 6.5 ka) periods, in which millennial-scale variability is lower, distinctly weaker correlations between Southern Ocean SST and precipitation in the western Ross Embayment are observed (Fig 4.6c,d,g,h). Relatively high positive correlations are still observed in TraCE-21ka in the Amundsen to eastern Ross Sea sector ($r > 0.5$ in YD, $r > 0.3$ in MH), indicating an association between warmer SSTs and higher precipitation in the western Ross Embayment. However, closer to the ice sheet, negative correlations are observed. DGns shows slightly weaker correlations in the Amundsen to eastern Ross Sea sector during the YD period ($r > 0.3$), and relatively strong positive correlations along the East Antarctic coast in the MH period ($r > 0.5$).

Spatial correlations between precipitation in the western Ross Embayment and Southern Ocean sea ice concentration show a similar evolution in both models (Fig 4.7). Strong negative correlations exist in both models in the early deglacial period ($r < -0.7$ in TraCE-21ka, $r < -0.5$ in DGns). DGns shows stronger local correlations with sea ice in the Amundsen Sea to eastern Ross Sea sector than with SST from the ACR to the MH (Fig 7b-d). TraCE-21ka also exhibits strong negative correlations in this area ($r < -0.5$ in YD, $r < -0.3$ in MH), with a pattern similar to that observed with SST. Closer to the ice

sheet, however, positive correlations are observed in TraCE-21ka in the YD and MH periods, particularly to the north of Marie Byrd Land (Fig 4.7g,h). The spatial correlations in TraCE-21ka in the YD and MH periods are similar to those observed with modern climatology, with strong negative correlations in the Amundsen Sea to eastern Ross Sea and positive correlations off the coast of the Antarctic Peninsula (Fig 4.2).

Despite the shift in correlation strength that occurs between the early deglacial period and the early Holocene, wind stress magnitude and direction remains similar in both models over the Ross Sea and the Ross Ice Shelf (Fig 4.8). However, further from the ice sheet, westerly winds show a clear weakening between the two periods, and the area of SIC of <50% expands to higher latitudes. Both models show northeasterly wind over the Ross Ice Shelf and Roosevelt Island, though the winds of TraCE-21ka are stronger in this region. In the early Holocene, SICs remain high (>95%) at latitudes higher than 70°S in DGns (Fig 4.8b). In contrast, the surface winds in TraCE-21ka deflect the sea ice to the Victoria Land and Marie Byrd Land coasts, with lower sea ice concentrations observed over the central Ross Sea (Fig 4.8d). Stronger winds associated with greater deflection of sea ice to the Marie Byrd Land coast allow for enhanced meridional transport of moisture, which may account for the positive correlations observed between sea ice concentration along the Marie Byrd Land coast and precipitation over the western Ross Embayment.

4.5.4 Effect of atmosphere forcing on ice sheet retreat

As previously discussed in Section 4.1, the RICE δD record exhibits a more pronounced ACR-associated decrease and YD-associated increase than the WDC and EDC records. It also shows higher variability throughout the Holocene and a decreasing trend from the early to middle Holocene that is not observed in the other ice cores. Applying these differences in the form of SAT, precipitation and back pressure anomalies relative to modern as climate forcings in regional ice sheet model simulations is consequential for the timing of ice sheet retreat in the Ross Embayment as well as the formation of the Ross Ice Shelf (Fig 4.9). The cooler ACR with higher back pressure delays the decline in grounded ice volume relative to simulations forced by EDC and WDC atmosphere forcings. However, the rapid increase in SAT and decrease in back pressure initiating at $\sim$12.8 ka result in a more rapid decrease in grounded ice volume $\sim$12.2 ka and an earlier ice shelf formation $\sim$11.7 ka.

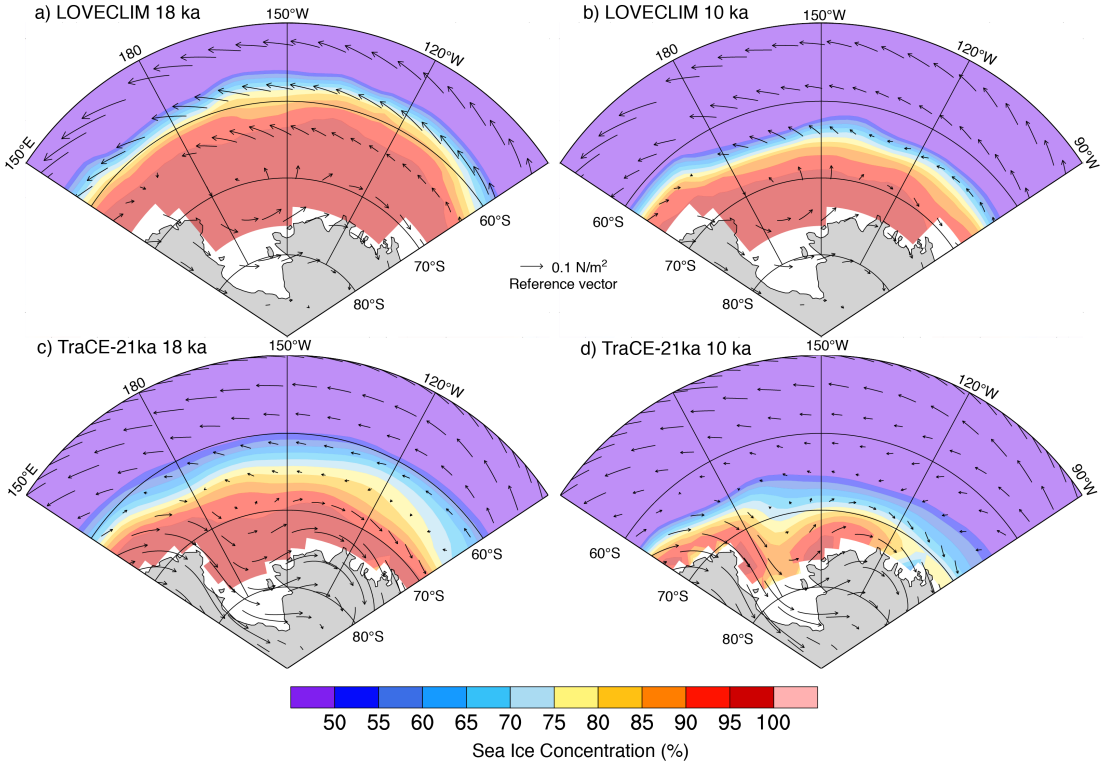

FIGURE 4.8: Modelled annual average wind stress (vectors) and sea ice concentration of the Ross Sea sector at 18 ka and 10 ka for LOVECLIM DGns (panel a and b, respectively) and TraCE-21ka (panel c and d, respectively).

Following the ice shelf formation, little difference is observed between the three simulations using different atmosphere forcings in terms of grounded ice volume and ice shelf area (Fig 4.9c,d).

The spatial pattern in grounding line retreat differs considerably among the simulations forced by RICE-, EDC- and WDC-derived atmosphere forcing, but the same ocean forcing (Fig 4.10). The main differences occur in the western and eastern Ross Sea, where the RICE-forced simulation has a delayed retreat relative to the EDC- and WDC-forced simulations; in contrast to the east and west, each simulation shows a similar initial timing and degree of early retreat in the central Ross Sea. This RICE-forced simulation is similar to the "saloon door" pattern of retreat suggested by McKay et al. (2016) and Lee et al. (2017). Following the ACR, the retreat in the RICE-forced simulation is rapid over the next 3 kyr, with the grounding line reaching Roosevelt Island by 10 ka (Fig 4.10a). In comparison, the WDC-forced simulation, shows the most rapid retreat prior to 13 ka, and shows relatively less extensive grounding line change through this post-ACR interval (Fig 4.10c). Seafloor bathymetry is the main driver in the spatial retreat pattern (Fig 4.10d), however, with each simulation showing ice remaining grounded on areas of topographic highs and a grounding line migration from the central embayment to the northern Transantarctic Mountains in the outer embayment (Fig 4.10a-c). In the inner embayment, steady grounding line progression occurs along the southern Transantarctic Mountains towards the Siple Coast and the grounding line remains connected to the Roosevelt Island ice dome for approximately 5 kyr. Through the last 9 kyr of the model runs, the grounding line progresses steadily toward the modern position at Siple Coast, with few differences between the simulations.

As the ocean cavity under the ice shelf expands, grounding line position becomes highly sensitive to the ocean forcing, which is in the form of sub-ice shelf melt rate anomalies (see Chapter 3). Through the middle to late Holocene (7 to 0 ka), simulations forced with the TraCE-21ka ocean output are distinct from those forced with other ocean forcings as the lower-than-PI sub-ice shelf melt rate anomalies result in higher grounded ice volume and lower ice shelf area as a consequence of delayed grounding line retreat along the Siple Coast (Fig 4.11). This is therefore relevant for the timing of grounding line retreat around Roosevelt Island, which is primarily dependent on the ocean forcing selection (Fig 4.11a-d). With the RICE atmosphere forcing, the grounding line reaches Roosevelt Island between 10.6 and 9.8 ka, and Roosevelt Island becomes fully separated from the Siple Coast grounding

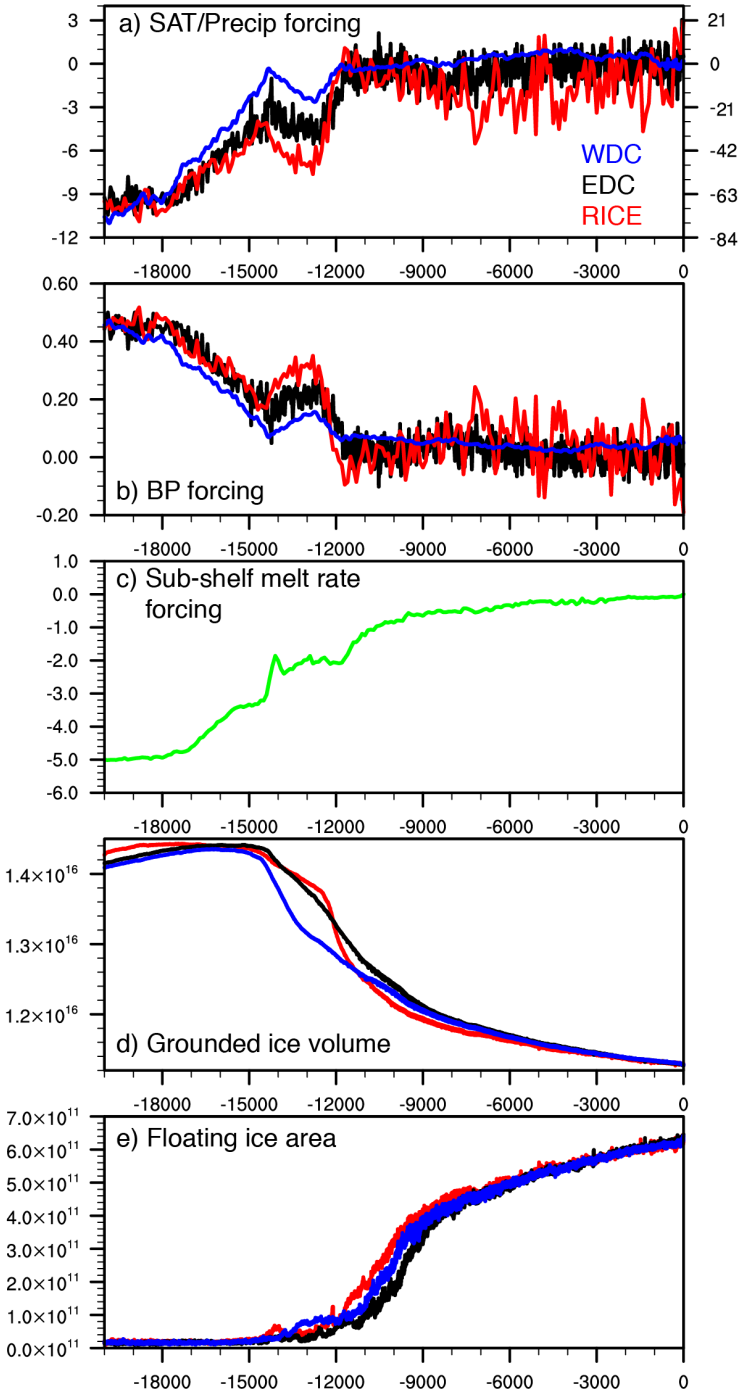

FIGURE 4.9: (a-b) Ice core-derived atmosphere forcings of the ice sheet model simulations. (c) MPA ocean forcing, in the form of sub-shelf melt rate anomalies, applied in the ice sheet model simulations. (d) Modelled grounded ice volume (m3) and (e) modelled floating ice shelf area (m2) for simulations forced with the same MPA ocean forcing, but with the different ice core-derived atmosphere forcings in panel a and b. The line colors correspond to those in panel a and b.

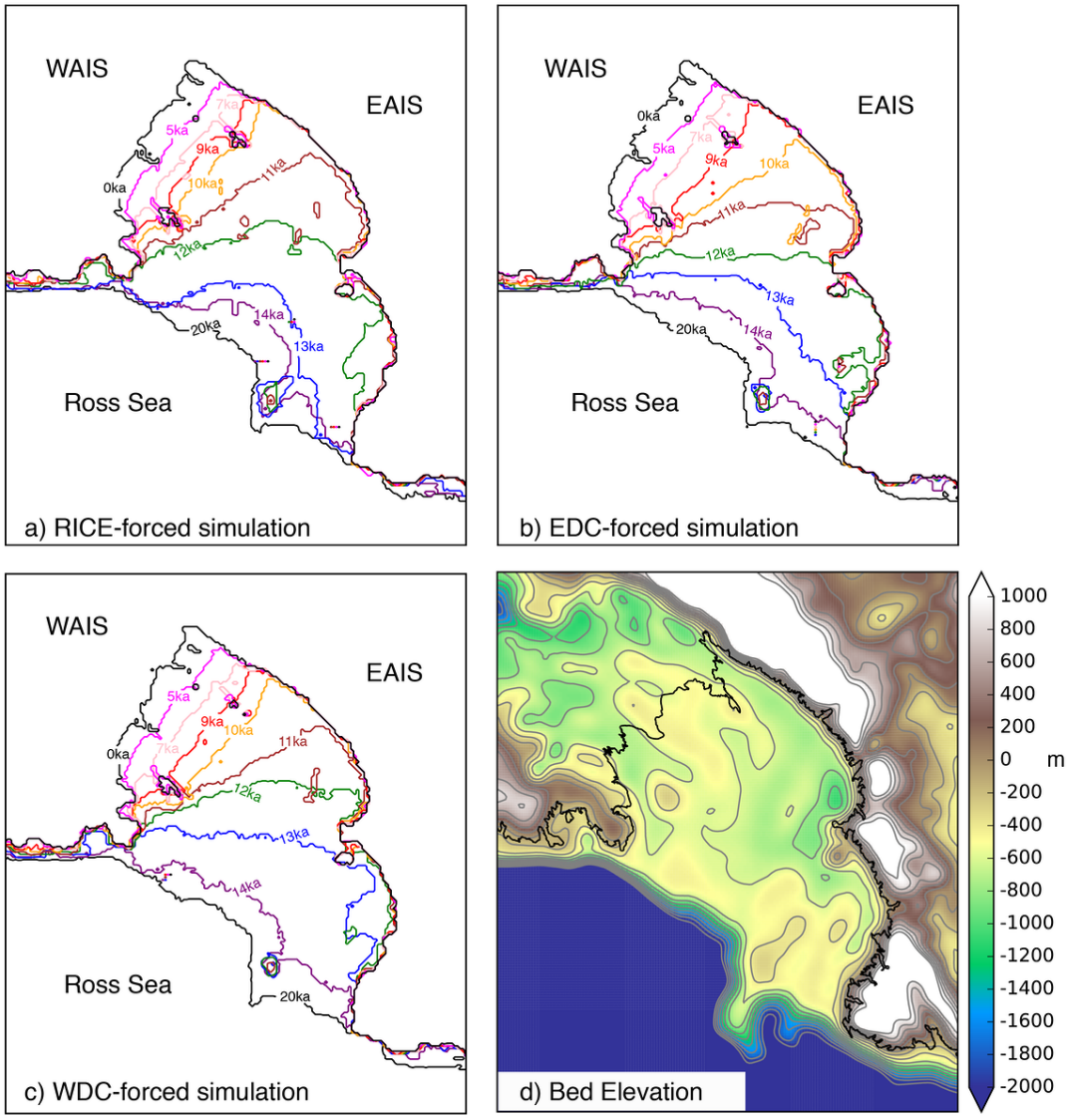

FIGURE 4.10: Grounding-line evolution of simulations forced with the same MPA ocean forcing and (a) RICE-derived atmosphere forcing, (b) EDC-derived atmosphere forcing, and (c) WDC-derived atmosphere forcing. (d) Smoothed bed elevation (m asl) used in the model simulations based on bedmap2. The gray lines show elevation contours of 200 m. The black line indicates the modern grounding line position.

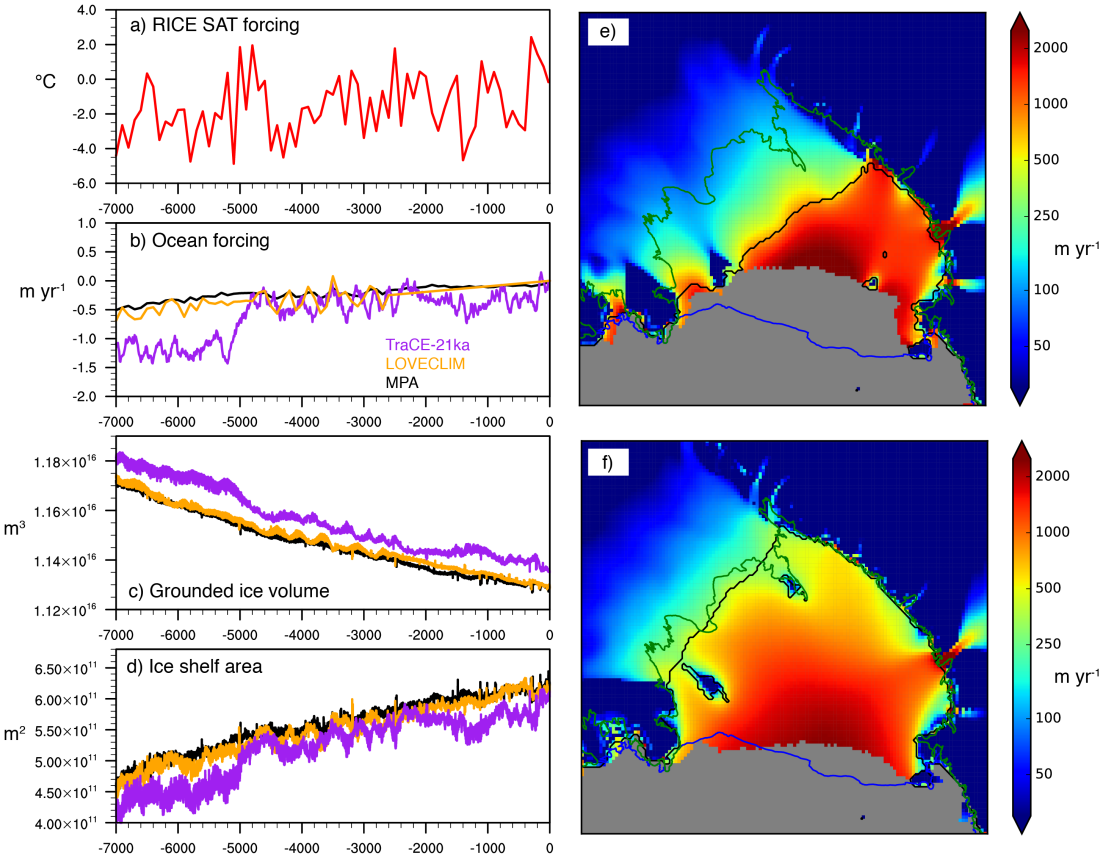

FIGURE 4.11: Time series of the RICE atmosphere forcing (a), three ocean forcings (b), and modelled (c) grounded ice volume (m^3) and (d) ice shelf area (m^2) of simulations forced with the RICE atmosphere forcings, but the different ocean forcings in panel b (with the corresponding color). (e-f) Modelled grounding line position (black line) and surface ice velocity before and after grounding line migration around Roosevelt Island. For comparison, modern grounding line position is indicated in green and modern calving line position is indicated in blue.

line between 6.4 and 5.6 ka. Through this period, the ice surface velocity increases as the ice becomes ungrounded over the marine basins to the east and west of Roosevelt Island (Fig 4.11e,f), with velocities >500 m yr^{-1} following the grounding line separation. However, the Bindschadler, MacAyeal and Echelmeyer ice streams from WAIS are less well defined than those from the East Antarctic Ice Sheet (EAIS), such as those from Byrd and Mulock Glaciers, which show the highest modelled surface ice velocity of the domain.

4.5.5 Effect of precipitation forcing on ice sheet retreat

Changes in Antarctic precipitation have generally been shown to scale with changes in temperature in accordance with the Clausius Clapeyron relation (Frieler et al., 2015). However, temperature and accumulation reconstructions at WDC have indicated a decoupling of this relationship over the last deglaciation (Fudge et al., 2016). Here, I explore the effect of this decoupling on ice sheet retreat by applying the relative changes in accumulation at WDC as a precipitation forcing over the full domain (referred to as WDC ACC). This is in contrast with the previously discussed ice sheet model simulations, in which the precipitation forcing is scaled with the temperature forcing with a relation of 7%/°C, including those forced by the RICE-derived surface temperature (referred to as RICE PTS). Both types of precipitation forcing are applied relative to a modern climatology based on RACMO2.3 (Lenaerts et al., 2012), but the key difference is that the PTS forcing is in the form of a relative percentage, whereas the WDC ACC forcing is a scalar offset in units of kg/m^2s. As a result, grid cells with lower modern precipitation than WDC have higher relative changes, and vice versa.

The WDC ACC- and RICE PTS-forced simulations are both run with warm, moderate and cool ocean forcing (Fig 4.12a), and are both shown as relative percentages of modern WDC precipitation in Fig 4.12b. WDC ACC forcing results in a lower glacial grounded ice volume ($\sim 4 \times 1015$ m^3) and higher sensitivity to the warm ocean forcing (cyan line in Fig 4.12c). Despite the lower glacial ice volume of the WDC ACC-forced simulations, the moderate and cool ocean forcing result in similar timing of the decline in grounded ice volume and increase in ice shelf area as the RICE PTS simulations (Fig 4.12c,d). However, a clear divergence between the two sets of simulations occurs in the late Holocene ($\sim$4.5 ka) as the WDC ACC forcing increases to above-PI levels, leading to a stabilization of grounded ice volume and ice shelf area to the end of the simulation. In comparison, the RICE PTS runs show a decreasing trend in grounded ice volume and an increasing trend in ice shelf area through this time interval (Fig 4.12 c,d).

Precipitation forcing has a relatively minor role in terms of the spatial pattern of grounding line migration (Fig 4.14). In the outer embayment, the use of WDC ACC forcing does exhibit higher sensitivity of the warm ocean forcing as compared to the RICE PTS case (Fig 4.14a,b), but strong agreement is observed between both types of precipitation forcing with the cool ocean forcing (Fig 4.14c,d). In all cases, the models show rapid grounding line retreat between 13 and 10 ka. The main difference in the retreat pattern occurs

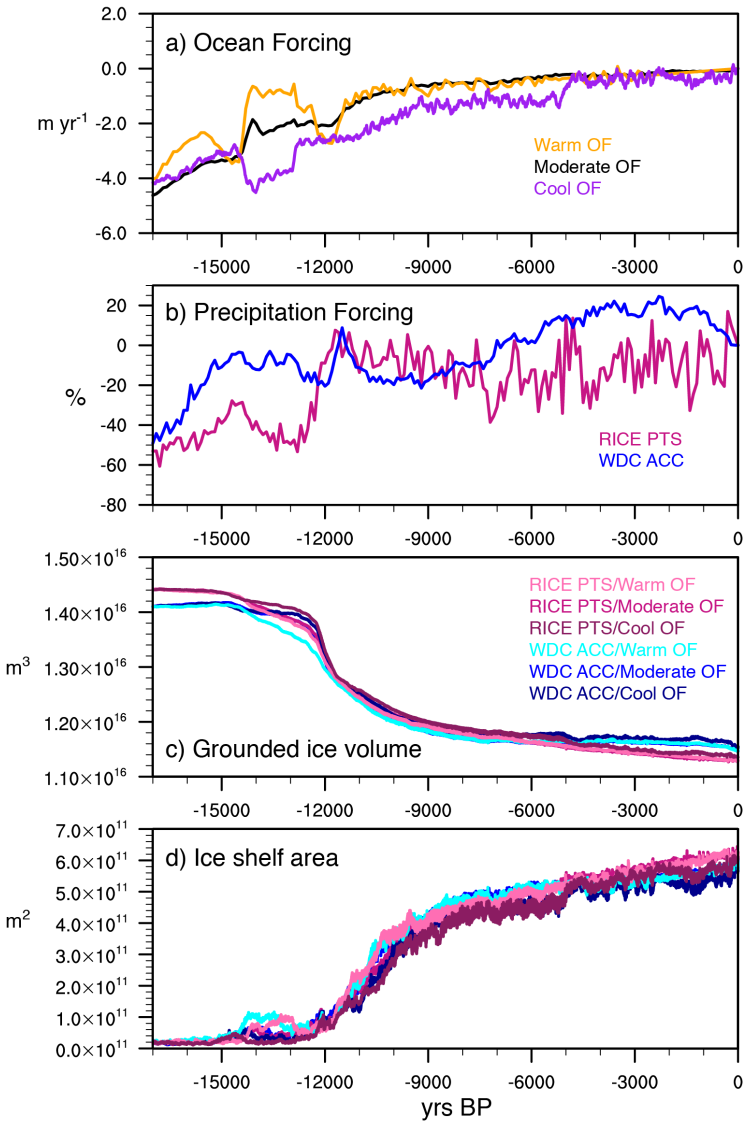

FIGURE 4.12: (a) Time series of warm, moderate and cool ocean forcings (OF) applied in the ice sheet model simulations. (b) RICE temperature-precipitation scaling (RICE PTS) and WDC-derived precipitation (WDC ACC) shown relative to modern WDC precipitation estimated from RACMO2.3. (c) Modelled grounded ice volume (m^3) and (d) ice shelf area (m^2) of simulations force with RICE PTS (pink) and WDC ACC (blue) with different OFs. Simulations forced with warm OF are lightly colored, whereas those forced with cool OF are dark.

in the Holocene (∼9-0 ka), when the WDC ACC precipitation forcing inhibits grounding line retreat along the Siple Coast.

We can compare the effect of precipitation forcing spatially at the start of the glacial termination (18 ka) and at the end of the simulation (Fig 4.14a,b). Considering a moderate ocean forcing, RICE PTS results in higher ice thickness over much of the domain (>50 m) relative to WDC ACC. The largest differences in ice thickness (>250 m) are observed over the modern central Ross Ice Shelf and the western Ross Sea, immediately south of the TD (pink square in Fig 4.14a). The difference in ice thickness is higher at WDC and SD than at RICE (green, yellow and orange squares, respectively). However, the WDC ACC simulation produces higher glacial ice thicknesses along the margin of the continental shelf. At 0 ka, RICE PTS shows relatively lower ice thickness than WDC ACC over the majority of the model domain, particularly over WAIS (Fig 4.14b). The relatively higher ice thickness in the WDC ACC simulation, driven by the higher late Holocene precipitation, reduces the southward grounding line progression at the Siple Coast.

The differences in ice thickness contribute to the different ice surface elevation evolutions observed at the ice core sites in the model domain. At WDC, for example, the WDC ACC forcing produces a lower glacial ice surface elevation, a higher precipitation-driven increase in ice surface elevation through the ACR and an earlier decline in the early Holocene (Fig 4.14c). Through the Holocene, the WDC ACC simulations are sensitive to the ocean forcing, with the cool ocean forcing showing stabilization at ∼1900 m. In comparison, the RICE PTS simulations show a decline in ice surface elevation through the Holocene, with better agreement with the modern WDC surface elevation. All model simulations show relatively modest changes in surface elevations at TD (Fig 4.14d), though the WDC ACC simulations produce an increase through the Holocene that is not observed in the PTS simulations.

At SD and RICE, the deglacial surface elevation changes are more significant than those at the higher elevation ice core locations of TD and WDC (Fig 4.14c-f). The RICE PTS forcing simulations are generally consistent with the model ensemble members of the previous chapter, but show a relatively rapid decrease in surface elevation in the early Holocene (Fig 4.14e,f). The WDC ACC forcing shows relatively lower LGM surface elevations at both sites, with an earlier decrease in the warm ocean forcing case. At SD, the WDC ACC forcing leads to an increase in surface elevation through the ACR, a more rapid decrease in the early to middle Holocene, and a stabilization,

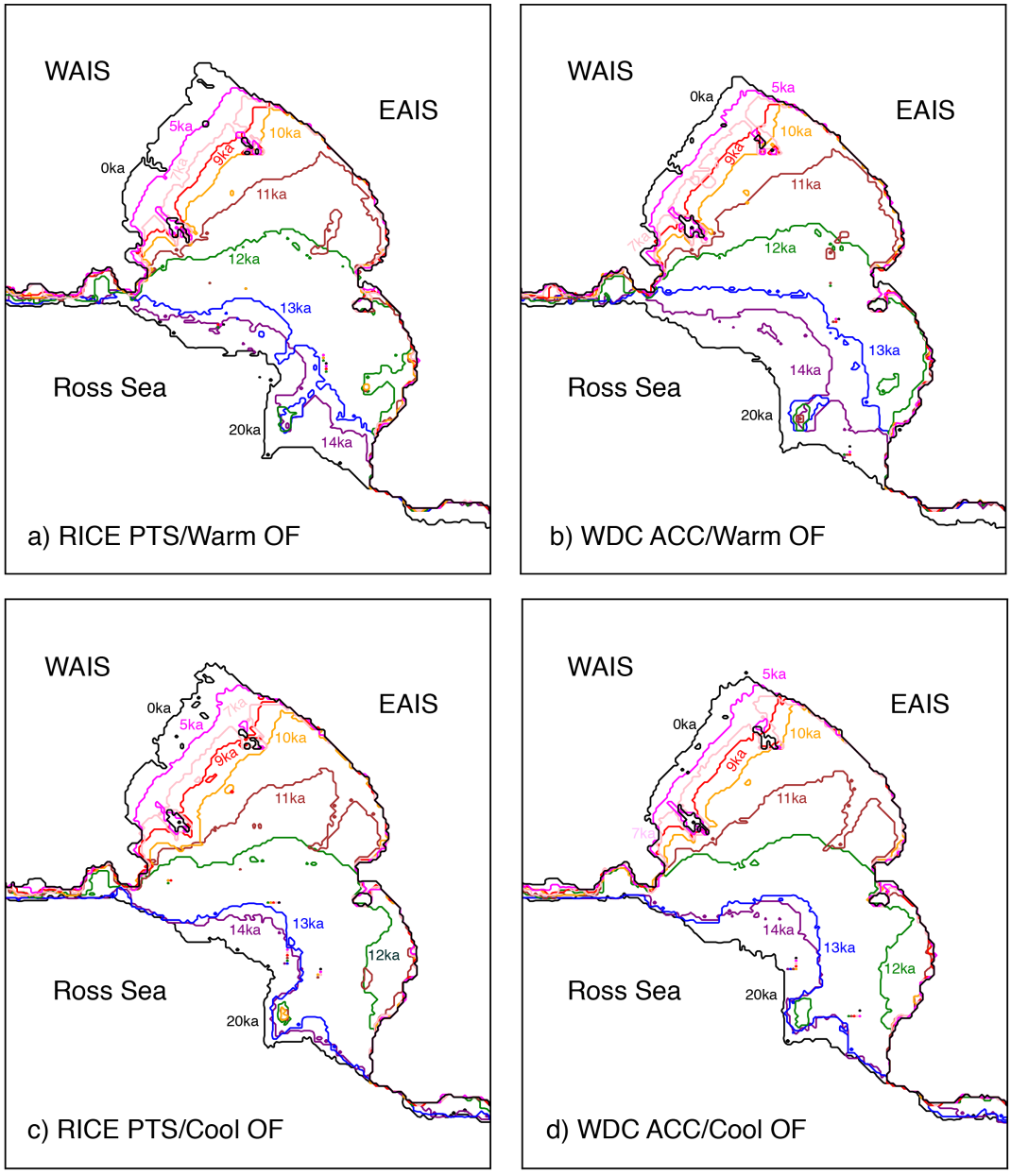

FIGURE 4.13: Grounding-line evolution of the simulation forced with (a) RICE temperature-precipitation scaling (RICE PTS) and warm ocean forcing, (b) WDC-derived precipitation (WDC ACC) and warm ocean forcing, (c) RICE PTS and cool ocean forcing, (d) WDC ACC and cool ocean forcing.

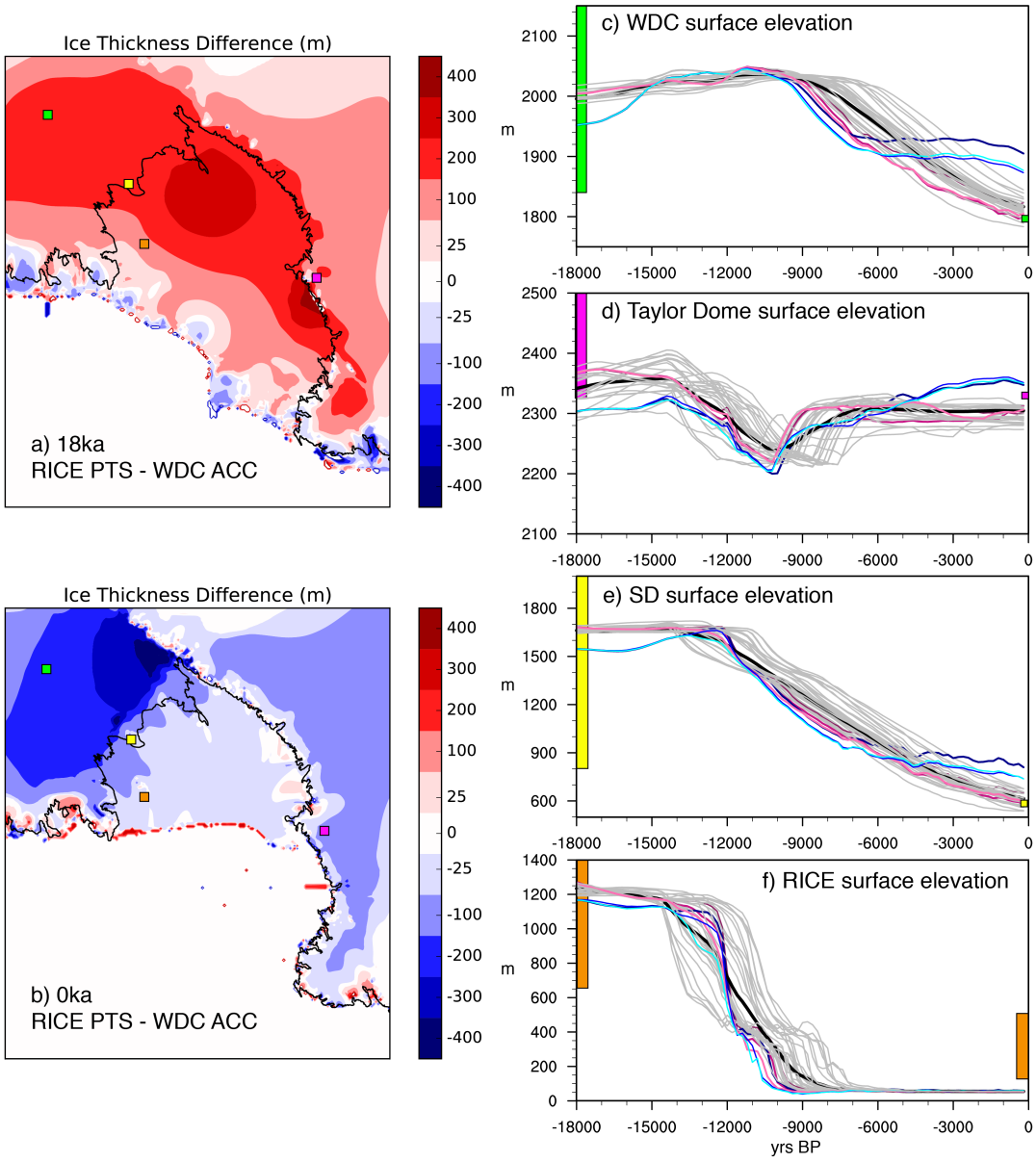

FIGURE 4.14: Difference in ice thickness (m) between the simulation forced with RICE precipitation-temperature scaling (RICE PTS) and moderate ocean forcing and the simulation forced with WDC-derived precipitation (WDC ACC) and moderate ocean forcing at (a) 18 ka and (b) 0 ka. Ice core locations of WDC, SD, RICE, and Taylor Dome are indicated by the colored boxes. (a-f) Modelled ice surface elevation changes at the ice core locations indicated in panels a and b. Gray lines indicate the model ensemble members of Lowry et al. (2019), the black line indicates the ensemble average and colored lines indicate the simulations shown in Fig 4.12. Modern ice surface elevations are indicated by the colored boxes on the right side of the panels and estimated LGM ice surface elevations are shown on the left. In the case of RICE, the modern ice surface elevation is shown as a larger range to represent the elevation range from the base to the top of the ice dome. The lower bound of the glacial ice surface elevation is based on the lowest elevation of the adjacent grid cells in the ICE-6G dataset (Argus et al., 2014); the ice dome of ICE-6G dataset is 946.3 m.

dependent on ocean forcing, in the late Holocene (Fig 4.14e). Surface elevation evolves differently at RICE, with most model ensemble members showing an initial rapid decrease that occurs over a large time span (∼14.5-10.0 ka), and a second smaller decrease in the early to middle Holocene (∼11.0 to 7.5 ka). All simulations forced with RICE temperature and back pressure forcing (i.e., RICE PTS and WDC ACC) exhibit the most rapid retreat (Fig 4.14f), coinciding with the YD warm period.

Estimations of LGM surface elevation at ice core sites generally have high uncertainties and can vary significantly (Cuffey et al. 2016), but the modelled LGM surface elevations at TD and WDC are reasonable and agreement is also observed with modern elevations at these sites (Fig 4.14c,d). Although the model ensemble average is consistent with the modern surface elevation at SD, all model simulations show substantially higher glacial surface elevations than the current estimation of ICE-6G, i.e., 521.3 m above present (Argus et al., 2014). However, the elevations are lower than the previous estimation of ICE-5G, i.e., 1819.5 m above present (Peltier, 2004). The application of WDC ACC forcing reduces the relative deglacial change from ∼850 m to ∼700 m, however, the modern surface elevation is overestimated, particularly in the cool ocean case (dark blue line in Fig 4.14e). Similarly, the models produce higher glacial surface elevation at RICE than ICE-6G (difference of ∼450-650 m), but are below the ICE-5G estimation of 1616 m above present. The overall deglacial surface elevation changes are even higher at RICE than at SD (Fig 4.14f). Model bias is observed in terms of the modern surface elevation. At 0 ka, modelled RICE elevation is ∼70-90 m asl, which is similar to the surrounding ice shelf (∼55 m). Prior to the secondary decrease in surface elevation in Fig 4.14f, however, the surface elevations at RICE are consistent with modern Roosevelt Island surface elevations (120-550 m; Le Brocq, Payne, and Vieli (2010)).

4.6 Discussion

4.6.1 Interpretation of the RICE δD reconstruction

The RICE record is unique among the ice core records of the Ross Embayment in terms of the high magnitude of isotopic change associated with the ACR and YD events, and the pronounced isotopic variability through the Holocene. The potential causes explored above in the climate and ice sheet

model simulations include (1) the strong relationship between surface temperature and precipitation over the western Ross Embayment and SIC, SIE and SST in the Ross and Amundsen Seas, and (2) changes in surface elevation and ice sheet extent during the deglaciation. Both factors need to be accounted for in the interpretation of the RICE δD reconstruction.

With regard to the first possibility, isotope-enabled climate modelling has demonstrated the strong influence of SIE on stable isotope concentrations at Antarctic ice core locations (Holloway et al., 2016). This is an important consideration for the ACR in particular, as Pedro et al. (2016) have argued that an important feedback of the bipolar see-saw effect driving Southern Hemisphere cooling was the expansion and thickening of sea ice in the Southern Ocean, which enhanced northward oceanic heat transport. Southern Ocean conditions may also have contributed to Southern Hemisphere warming during the YD due to enhanced wind-driven upwelling and ventilation of CO_2 (Anderson et al., 2009; Barker et al., 2009; Bova, Herbert, and Altabet, 2018). The climate models analysed here both exhibit an increase in SIC and SIE in the Ross Sea during the ACR, along with reduced surface temperature and precipitation along the peripheral ice sheet, followed by a decrease in SIC and SIE during the YD. However, it is difficult to assess the isotopic effect of sea ice and ocean temperature through this time interval at Roosevelt Island relative to the other ice core sites without an isotope-enabled regional climate model (RCM) with higher spatial resolution. The extent of the ice sheet is also a factor as the distance between Roosevelt Island and the open ocean changes as the ice sheet retreats, which would influence the moisture content and precipitation at the ice core site.

In addition to the influence of sea ice and ice sheet extent on ice core isotopic reconstructions, ice sheet surface elevation changes likely contribute to varying degrees at different ice core sites by changing the surface temperature via the atmospheric lapse rate. In the reconstruction of surface temperature of the WDC ice core, Cuffey et al. (2016) note the wide range of LGM surface elevations in ice sheet model simulation, ranging from a few hundred meters thinner to several hundred meters thicker, and suggest a reasonable range of uncertainty of 100-300 m, implying a lapse rate change effect of 0.7-3.0°C. The TraCE-21ka simulation, which uses the ICE-5G dataset for the change ice sheet topography (Peltier, 2004), has a notably larger change of 792.7 m change from 18 to 0 ka (lapse rate change effect of 5.6-7.9 °C). The ICE-5G elevation change is even more significant at both SD and RICE, however, the updated ICE-6G shows considerably lower elevation changes

(differences of 271.5 m, 1298.2, and 1072.3 m at WDC, SD, and RICE, respectively). Since TraCE-21ka uses the ICE-5G topography (Liu et al., 2009), it should be noted that the deglacial surface temperature change over WAIS is therefore likely to be overestimated.

The ice sheet model simulations exhibit higher LGM surface elevations at SD and RICE than estimated by the ICE-6G dataset (Argus et al., 2014). RICE also has additional model bias in that the simulations produce lower modern ice surface elevations than current observations. Despite these model-data discrepancies, the timing of ice surface lowering is still informative for the interpretation of the RICE δD record. The majority of simulations show little surface elevation change prior to the ACR, with the exception of the warm ocean/warm atmosphere scenarios discussed in the previous Chapter. None of the simulations show an increase in ice surface of elevation through the ACR, which suggests that surface elevation changes did not contribute to the ACR signal (δD depletion) in the RICE δD record. Following the ACR, the models rapidly decline in surface elevation, with a timing similar to previous deglacial thinning in ice sheet modelling studies (e.g., Golledge et al., 2014), as well as marine radiocarbon estimations of rapid grounding line retreat in the eastern Ross Sea (Bart et al., 2018). This especially true for the six simulations using RICE surface temperature and back pressure forcing, and the decrease coincides with the YD warming event in the RICE δD reconstruction. It is therefore conceivable that a significant change in surface elevation contributes to the YD signal (δD enrichment) in RICE.

The Siple Coast grounding line and calving line of the Ross Ice Shelf achieve near-modern positions in the ice sheet model simulations by the middle Holocene. No surface elevation changes are observed in the model simulations after $\sim$7 ka, hence it is unlikely that such changes contributed to the high isotopic variability observed increasing through the Holocene at RICE relative to the continental ice cores. The climate models show high variability in both Ross Sea SST and SIC initiating in the early Holocene. The increase in open ocean area and lowered surface elevation in the YD may have driven this increased isotopic variability in the Holocene by causing Roosevelt Island to be more susceptible to sea ice- and ocean temperature-related changes. It is also important to not discount the dynamic of local climate effects, such as the establishment of the Roosevelt Island polynya, with tropical and mid-latitude climate drivers, such as Southern Annular Mode and El Niño-Southern Oscillation, which together may influence the dipole relationship between the eastern and western Ross Sea (Bertler et al., 2018).

These climate drivers ultimately control the moisture source of precipitation at RICE, thereby influencing the isotopic signals (Uemura et al., 2012).

Additional chemistry data from the RICE ice core, such as methanesulphonic acid (MSA), can provide further insight into interpretation of the δD record. MSA, a product of biological productivity in surface ocean water, has cautiously been applied as a proxy for SIE (Curran et al., 2003; Abram et al., 2007; Abram et al., 2010; Thomas and Abram, 2016). Changes in MSA, which can be reflective of open ocean conditions, could inform how significantly the δD record is influenced by changes in sea ice conditions in the Ross Sea. The absence of MSA signals during key periods of isotopic change could indicate that the given δD change is unrelated to sea ice. However, it should be noted that MSA can be a recorder of atmospheric transport strength rather than sea ice conditions alone (Abram et al., 2010); therefore, it is necessary to interpret MSA only in the context of other ice core proxies, such as sea salt aerosols (Levine et al., 2014).

4.6.2 Climate sensitivity of ice sheet retreat

Atmospheric forcing is an important control on the timing and pathway of grounding line retreat, as described in the previous Chapter. Simulations forced with cooler LGM SAT anomalies have higher ice hardness, lower temperatures at the bed and slower ice flow, which makes the ice sheet more resistant to increases in ocean thermal forcing, thereby delaying retreat. The opposite is true for simulations forced with warmer LGM SAT anomalies, which are more responsive to ocean thermal forcing, and thus exhibit an earlier retreat. Similarly, steeper gradients of decreasing back pressure allow for higher ice flux, thereby inducing retreat. The differences between the EDC-, WDC-, and RICE-derived atmospheric forcings are therefore consequential to the ice sheet retreat history of the Ross Embayment. The cooler surface temperatures and higher back pressure during the ACR in the RICE-forced simulations lead to delayed retreat in the eastern and western Ross Sea, with early retreat only occurring in the central embayment. These simulations most resemble the saloon-door retreat pattern described in McKay et al. (2016) and Lee et al. (2017), based on marine radiocarbon ages and interpretations of seafloor bathymetry.

Although it can be assumed that the RICE ice core is a better representative of the deglacial climate history of the outer Ross Embayment considering its more proximal location than the EDC and WDC ice cores, the previous

section describes a number of factors that can influence the isotopic signals at RICE. The scaling between δD and surface temperature has inherent uncertainties that should be considered as different scaling relationships and could yield differences in ACR and YD surface temperature and back pressure changes. The utility of a large ensemble of simulations with a wide range of climate forcings is that these uncertainties are likely captured. It is also notable that with the expansion of the ocean cavity, the simulations are far more dependent on the ocean forcing, which has even higher uncertainties.

A novel aspect of this Chapter is that the effect of temperature-precipitation scaling, which is applied in many ice sheet modelling studies (e.g., Huybrechts, 1990; Deconto and Pollard, 2009; Golledge et al., 2014, among others), is explicitly investigated. Fudge et al. (2016) indicated decoupling through the deglaciation in this relationship with the reconstruction of accumulation and surface temperature at WDC, suggesting the importance of changing atmospheric dynamics and synoptic-scale processes in precipitation over WAIS. Although the climate models show temporal changes in the strength and location of the Amundsen Sea Low, this decoupling effect is not reproduced in the models over WAIS (Lowry et al., 2019), but it is consequential for the modelling of surface mass balance over the Ross Embayment. Application of the WDC ACC forcing results in reduced LGM ice thickness, higher sensitivity to warm ocean forcing, and reduced Holocene retreat along the Siple Coast. A major complexity of the climatology of the region is the previously described Ross Sea Dipole, which results in differences in snow accumulation over the eastern and western sides of the embayment (Bertler et al., 2018). This may account for some of the discrepancies between the rates of modelled ice sheet thinning and those estimated from Transantarctic surface exposure records (see previous Chapter), as precipitation over EAIS and the Transantarctic Mountains may be out of phase with the precipitation over WAIS. This remains a challenge to apply as a precipitation forcing without additional ice core accumulation records that offer a broader understanding of the evolution of this dipole.

Future Antarctic ice sheet projections need to consider the complexity and temporal evolution of both atmospheric dynamics and thermodynamics in the application of Antarctic surface mass balance forcing. Palerme et al. (2017) note that CMIP5 GCMs predict higher temperature-precipitation scaling due to the reduction in sea ice coverage, and models with the best agreement to current surface mass balance observations show the highest

scaling relationships (7.4 – 29.3%/°C), equivalent to 2.5 to 8.5 cm in global sea level compensation. Despite these predictions, the currently receding Thwaites Glacier on the Amundsen Coast of WAIS has not shown any increase accumulation over the past decades (Medley et al., 2013), and CMIP5 GCMs continue to have issues with the representation of the longitudinal position of the Amundsen Sea Low, one of the main controls on West Antarctic climate. Resolving these model-data discrepancies in climate models is a necessary task for accurate precipitation forcing in ice sheet model simulations. In the Ross Embayment specifically, the effect of high precipitation in delaying the retreat along the Siple Coast requires further exploration.

One of the main limitations of both the climate and ice sheet model simulations is that the models lack coupling between the ocean and ice sheet. In the case of the climate simulations, continental surface temperatures and precipitation over Antarctica are highly sensitive to prescribed freshwater forcings (Lowry et al., 2019). Clear biases are observed through the ACR and YD, suggesting that the Meltwater Pulse 1a and 1b events, of which there are few paleo-constraints for Antarctica (Weber et al., 2014), may not be adequately represented in these simulations. The ice sheet model simulations use a simple melt parameterization that is uniformly applied and does not account for circulation underneath the ice shelf. While not currently computationally feasible for deglacial time scales, coupling between the ocean and ice sheet/ice shelf may be required to accurately reproduce WAIS retreat through this time interval.

With regard to the ice sheet model bias observed at Roosevelt Island, it is noteworthy that none of the applied atmosphere/ocean forcing combinations can account for the lower-than-observed surface elevations in the simulations. This is true even for the simulations using the RICE-derived atmosphere forcing. Ice sheet model simulations are highly sensitive to the physical parameters of the bed as well as the evolution and deformation of the continental shelf, which can influence ice sheet sensitivity to climate forcing (Matsuoka et al., 2015; Kingslake et al., 2018; Colleoni et al., 2018; Whitehouse et al., 2019). In PISM, these parameters are applied uniformly over the entire domain, despite the known differences in geological conditions of the seafloor in the eastern and western Ross Sea (Halberstadt et al., 2016). The faster flowing ice streams of WAIS are especially sensitive to the underlying till (Alley et al., 1986; Hulbe et al., 2016), hence some of the model mismatch with observations may be related to inadequate representation of the subglacial till properties. The impact of model parameters related to the bed and

the solid earth are explored in more detail in the subsequent Chapter.

4.7 Summary and Conclusions

Given its proximity to the Ross Sea, the RICE ice core may offer the most accurate representation of the deglacial climate history of the peripheral ice sheet in the Ross Embayment. However, the isotopic signals of marine ice cores, such as RICE, are complicated by oceanic influences and ice sheet-related changes. The application of numerical models is therefore necessary to both interpret the ice core record and better understand the past climate sensitivity of this region. Transient climate simulations show pronounced sea ice changes corresponding to the ACR and YD, suggesting that changes in sea ice conditions may have contributed to the more significant δD signals observed in the ice core relative to other ice cores in the region through this time interval. Additionally, regional ice sheet model simulations also indicate substantial surface elevation changes corresponding to SH warming during the YD period, which also likely contributed to the YD signal in RICE. High variability in δD is observed through the Holocene, after the ice sheet models approach a near-modern configuration. An increase in open ocean area and changes in sea ice conditions may offer a better explanation for the δD variability through this time interval. Precipitation forcing is consequential for grounding line retreat along the Siple Coast. Future ice sheet model simulations need to consider the influence of atmospheric dynamics and the Ross Dipole on ice sheet surface mass balance in this region.

Chapter 5

Effects of basal properties, the solid Earth, and ice rheology on ice sheet sensitivity to deglacial climate forcing in the Ross Sector

5.1 Abstract

The role of external forcings in the deglacial ice sheet evolution of the Ross Embayment, Antarctica's largest catchment, continues to be a hot topic of debate. Although numerical ice sheet models indicate that ocean and atmosphere forcings were the main drivers of deglacial ice sheet retreat, these models have difficulty in accurately capturing both the timing and rate of retreat in every area of the embayment. Other factors, such as the physical properties of the bed, deformation of the continental shelf, and rheological properties of the ice influence the sensitivity of ice sheets to climate forcing. In this Chapter, I explore the extent to which specific model parameters impact the climate sensitivity of the ice sheet in the Ross Embayment over the last deglaciation. Mantle viscosity, the material properties of the till, and an enhancement factor of the shallow shelf approximation (E_{SSA}) component of the stress balance exhibit strong influences on the timing of ice sheet response to deglacial climate forcing, and may contribute to the asynchronous retreat behavior of the Eastern and Western Ross Sea. The Western Ross Sea is especially sensitive to both climate forcing and model parameter selection, with both cool climate forcing and low E_{SSA} producing better agreement with terrestrial ice thinning records. The evolution and extent of the Siple Coast grounding line is highly sensitive to the mantle viscosity and till properties in addition to ocean and precipitation forcing. Constraining

these physical model parameters is therefore paramount for accurate projections of the Antarctic ice sheet response to the predicted increase in ocean temperatures and precipitation.

5.2 Introduction

Fed by ice streams and outlet glaciers from both the West and East Antarctic Ice Sheets (WAIS and EAIS, respectively), the Ross Embayment is the largest drainage basin in Antarctica (Anderson et al., 2018). Estimates of the outflow of ice from the Siple Coast and the Transantarctic Mountains into the modern Ross Ice Shelf are 80+/-2 and 49+/-4 Gt yr^{-1}, respectively (Rignot et al., 2008). However, the response of these outflows from WAIS and EAIS to future climate warming scenarios in numerical ice sheet models remains uncertain, with large differences in ice sheet sensitivity to climate forcing related to model parameterizations (Golledge et al., 2015; DeConto and Pollard, 2016; Golledge et al., 2019; Edwards et al., 2019; Seroussi et al., 2019). As I explain in previous Chapters, constraining past grounding-line retreat in the Ross Embayment can help inform future predictions. In the Ross Embayment, the grounding line has retreated by more than 1000 km since the Last Glacial Maximum (LGM; Bentley et al., 2010), however, the influences of external and internal forcings of the ice sheet on both the timing and pattern of this retreat are still unclear (Conway et al., 1999; McKay et al., 2016; Kingslake et al., 2018; Goehring et al., 2019).

Previous studies have argued for a number of controls on the ice sheet retreat behavior in the Ross Embayment, as discussed in Chapter 3. The traditional "swinging gate" model, first proposed by Conway et al. (1999) and based on Transantarctic ice thinning records, suggested that Ross Sea grounding-line retreat was constrained to the late Holocene, in the absence of climate or sea level forcing. Interpretations have since evolved with radiocarbon dating of marine sediments and multibeam bathymetry data from the Ross Sea, and the current understanding is that a combination of marine forcing and physiographic controls resulted in an earlier retreat with a landward grounding-line migration from the central embayment (McKay et al., 2016; Halberstadt et al., 2016; Lee et al., 2017; Bart et al., 2018). However, the relative influences of specific external forcings are still hotly contested, with both sea level forcing (Goehring et al., 2019) and a combination of oceanic and atmospheric warming both proposed as the primary control of grounding-line migration in the Ross Embayment (Yokoyama et al., 2016; see Chapter 3).

Contributing to this ongoing debate, differences in the retreat behavior between the eastern and western Ross Sea (ERS and WRS, respectively) have been identified, suggesting an earlier retreat in the ERS relative to the WRS (Halberstadt et al., 2016; Bart et al., 2018). This has generally been attributed to differences in seafloor bathymetry, as the western Ross Sea has a greater abundance of ice rises that can stabilise the ice sheet (Halberstadt et al., 2016; Simkins, Anderson, and Greenwood, 2016; Greenwood et al., 2018; Anderson et al., 2019). Additionally, changes in ocean circulation related to the influx of meltwater into the Southern Ocean may have led to differences in sub-surface ocean temperatures that enhanced grounding-line retreat in the eastern basin relative to the western basin (Golledge et al., 2014). The isostatic response of the solid Earth to changes in deglacial Antarctic ice loss has also been suggested to have driven extensive deglacial retreat of WAIS, and may explain the presence of radiocarbon from beneath the Whillans, Kamb and Bindschadler ice streams (Kingslake et al., 2018). Although the extent to which these mechanisms enhanced or diminished grounding-line retreat in different regions of the embayment is poorly constrained, they likely contribute to the data-model mismatches described in Chapters 3 and 4.

Ice sheet models have been demonstrated to be highly sensitive to the physical representation of the bed as well as the evolution and deformation of the continental shelf, which can influence ice sheet sensitivity to climate forcing (Matsuoka et al., 2015; Kingslake et al., 2018; Colleoni et al., 2018). In addition, the faster flowing ice streams that flow into the Ross Embayment are especially sensitive to the conditions of the underlying till (Alley et al., 1986; Hulbe et al., 2016). In this Chapter, I explore the effect of physical model parameters that control basal properties, the solid Earth response to an evolving ice sheet, and ice flow and rheology on the response to deglacial climate forcing. Understanding the effect of each model parameter on ice sheet sensitivity to climate forcing is highly valuable, as it addresses the data-model mismatches discussed in the previous Chapters, and it can help prioritize the constraints required for accurate projections of the future Antarctic response to anthropogenic climate warming.

5.3 Materials and Methods

To determine the effect of model parameters on the climate sensitivity of ice sheet retreat in the Ross Embayment, I use the ensemble of regional ice sheet simulations of the previous Chapters as well as additional experiments.

All simulations are performed for a regional domain of the Ross Embayment at 10km resolution using the Parallel Ice Sheet Model (PISM; Bueler et al., 2009; Martin et al., 2011), as described in the previous Chapters. Full descriptions of the regional model set up and spin-up procedure are described in Chapters 1 and 3 of this thesis. The purpose of the model ensemble discussed in Chapter 3 and 4 is to highlight the effects of ocean and atmosphere forcing on grounding line migration. The ocean forcing is in the form of basal ice shelf melt rate anomalies and is applied uniformly. The atmosphere forcings include surface temperature and precipitation anomalies and a back pressure forcing to heuristically represent the resistive effect of sea ice. The overall climate forcing ensemble consists of 42 simulations, each with a different ocean/atmosphere forcing combination.

In addition to the climate forcing model ensemble, I perform simulations that use the same climate forcing (moderate ocean/atmosphere forcing discussed in Chapter 3), but with an individual model parameter adjusted to assess the influence of each parameter on deglacial ice sheet retreat. In total, 17 additional simulations are performed to explore the effect of parameters related to ice rheology and subglacial conditions on the response to deglacial climate forcing. Specifically, I perform three simulations with different enhancement factors of the shallow ice approximation (SIA) and shallow shelf approximation (SSA) components of the stress balance, respectively, three simulations with higher sliding exponent parameters (q), three simulations with lower minimum till friction angles (ϕ_{min}), three simulations with different mantle viscosity values, one simulation with no bed deformation, and one simulation with reduced bed smoothing. Descriptions of each parameter are described in the subsequent section in relation to their effect on ice sheet retreat. These simulations are compared to the moderate climate forcing simulation of Chapter 3, and in the context of the larger climate forcing model ensemble (total of 59 simulations).

5.4 Results

5.4.1 Effect of external forcing on ice sheet retreat

As the previous Chapters discuss in detail, the combination of atmosphere and ocean forcing controls both the timing and spatial pattern of grounding-line retreat in the regional ice sheet model simulations. The atmosphere forcings, in the form of surface temperature and back pressure anomalies, exert a strong influence on the timing of the initial ice sheet retreat from the continental shelf edge. In particular, the simulation forced with the highest surface temperature and lower back pressure in the early deglacial period (i.e. the warm scenario) displays earlier retreat that is relatively synchronous across the outer embayment (Fig 5.1a). The simulation forced with relatively cooler early deglacial surface temperature anomalies, high back pressure and cooler ocean forcing (i.e. the cool scenario) shows delayed retreat in the WRS and ERS as compared to the central embayment (Fig 5.1b), resembling the marine-based models of McKay et al. (2016), Halberstadt et al. (2016) and Lee et al. (2017). In this cool scenario, grounding line retreat is most rapid in the early Holocene ($\sim$12-10 ka).

Although ice sheet retreat cannot initiate in the absence of climate forcing (see Chapter 3), sea level forcing is an important contributor to the modelled ice sheet retreat in the Ross Embayment. Figures 5.1c and 5.1d show two simulations, each forced by moderate ocean/atmosphere forcing; the difference is that in the second simulation, the sea level forcing is maintained at the LGM level of -125m. The initial retreat between 18 and 14 ka is similar, however, in the absence of a rising sea level, the grounding-line retreat becomes delayed for the remainder of the simulation. The delay increases through time, with a delay of $\sim$2ka in the outer embayment, but $\sim$3-5 ka in the inner embayment (Fig 5.1c vs. 5.1d). The position at 0 ka is advanced along the Siple Coast relative to modern observations and the simulations with both climate and sea level forcing. As a result, WAIS remains thicker through the Holocene, resulting in higher ice loading and isostatic subsidence, and thus lower basal topography in this region.

With development of the ice shelf and ocean cavity, the sub-shelf melt rate forcing is the dominant control on grounding-line position (see Chapter 3). However, higher Holocene precipitation forcing can modulate this effect on the grounding-line position along the southern Siple Coast by the Kamb, Whillans and Mercer ice streams (see Chapter 4). Sea level forcing also enhances the effect of ocean thermal forcing. With a constant LGM sea level, as

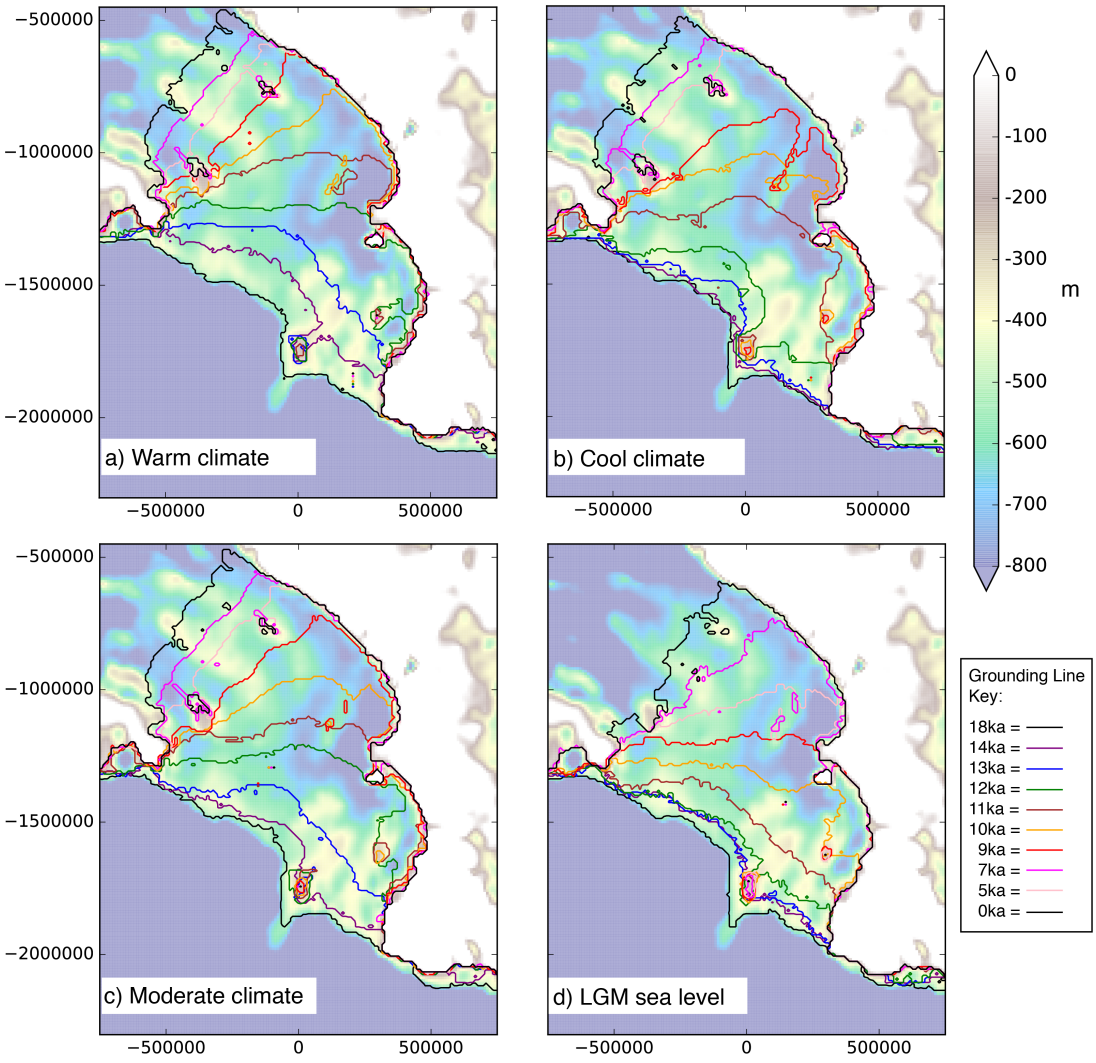

FIGURE 5.1: Grounding line evolution (colored lines) with warm (LOVECLIM ocean/atmosphere forcing) cool (TraCE-21ka ocean/atmosphere forcing), and moderate (model-proxy average ocean/atmosphere forcing) climate forcing, respectively. (d) Grounding line evolution with moderate climate forcing, but constant LGM sea level forcing. The grounding line positions are overlain on the basal topography at the end of the simulation (0 ka).

the grounding line retreats to the Siple Coast, Roosevelt Island acts as a pinning point over the last 7 ka of the simulation (Fig 5.1d), hence ocean forcing alone is insufficient for achieving an accurate grounding line position along the northern Siple Coast. With the addition of sea level forcing, the pinning effect only lasts for approximately 4.2 ka before the grounding line retreats beyond Roosevelt Island (see Chapter 3). By the end of the simulation with combined ocean and sea level forcing, the grounding-line position is consistent with observations in this region (Fig 5.1c).

5.4.2 Influence of the stress balance on ice sheet retreat

All of the ice sheet model simulations performed in this thesis employ a hybrid approximation of the Stokes stress balance, which was developed to model the large range of ice flow velocities observed in ice sheets (Bueler and Brown, 2009). In this hybrid stress balance scheme, velocities are calculated by the superposition of the SIA, which dominates in grounded regions, and the SSA, which dominates in ice shelves and ice streams and serves as a basal sliding velocity of grounded regions (Winkelmann et al., 2011). By using the SSA as a sliding law for grounded regions, this scheme avoids discontinuities at the onset of sliding, and is thus advantageous for modeling marine ice sheets with transitions between grounded and floating ice. To account for anisotropy and other uncertainties related to variations in viscosity and basal resistance, enhancement factors of the SIA and SSA can be applied (E_{SIA} and E_{SSA}, respectively); in general, E_{SIA} is greater than 1, and E_{SSA} is less than 1 (Martin et al., 2011). Larger E_{SSA} values produce faster ice streams and thinner ice shelves, and smaller E_{SIA} values produce thicker grounded ice (Kingslake et al., 2018).

In the previous Chapters, I use an E_{SIA} = 4.0 and E_{SSA} = 0.8 for the climate forcing experiments. Here, I perform six additional experiments with E_{SIA} values of 2.0, 3.0, and 5.0, and E_{SSA} values of 0.4, 0.6, and 1.0. The E_{SIA} parameter influences the grounded ice volume at LGM (Fig 5.2), with E_{SIA} = 2.0 showing the highest and E_{SIA} = 3.0 showing the lowest (difference of $\sim$6 x 1014 m^3). In the case of E_{SIA} = 3.0, parts of the western Ross Sea, north of Ross Island, remain as open ocean or ice shelf at 18 ka, contributing to this difference in grounded ice volume. No substantial difference in the LGM ice sheet configuration is observed at higher E_{SIA} values of 4.0 and 5.0, but the timing in the decline of grounded ice volume and increase in ice shelf area occurs later with E_{SIA} = 4.0. The ice sheet evolution through the Holocene

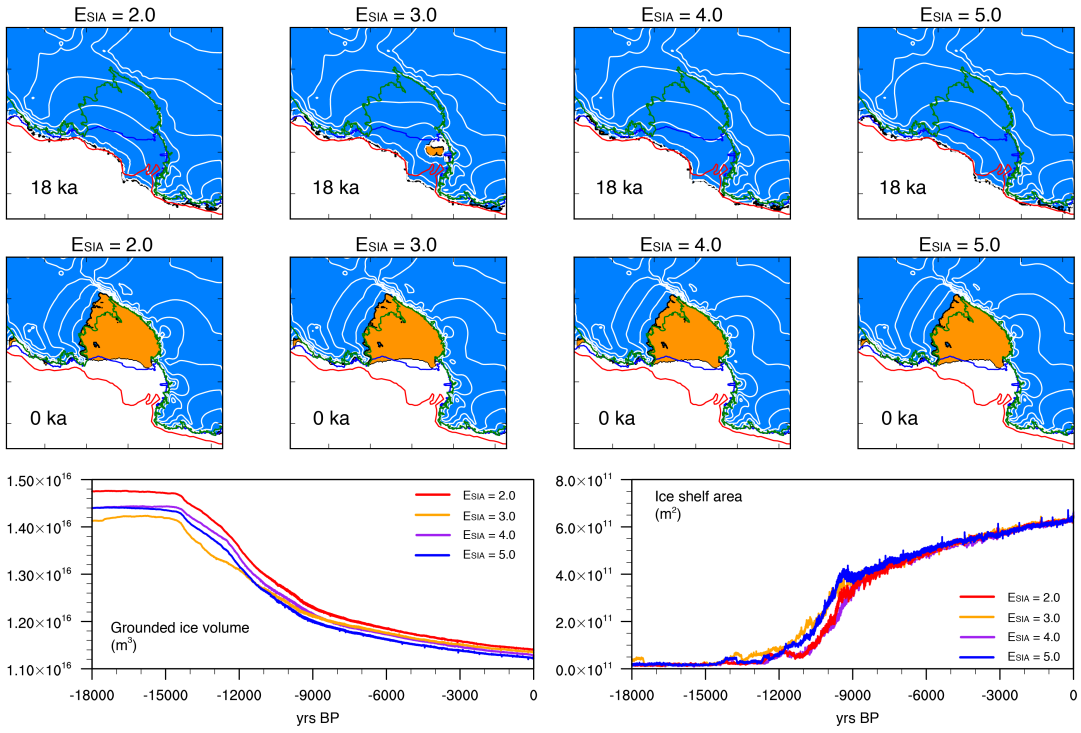

FIGURE 5.2: Experiments varying the enhancement factor of the shallow ice approximation. The top row shows modelled ice configuration at 18 ka and the middle row shows the ice configuration at 0 ka, where blue indicates grounded ice, orange indicates floating ice, and the black line shows the modelled grounding line position. White lines denote surface elevation contours of 500 m. Observed grounding and calving line positions are shown in green and blue, respectively, and the estimated LGM ice sheet extent is shown in red. The bottom row shows time series of grounded ice volume (m^3) and ice shelf area (m^2) evolution of the full model domain from 18 to 0 ka.

is relatively consistent among the experiments, resulting in similar PD configurations. The main difference is in the extent of the southern Siple Coast grounding line, which retreats further with lower E_{SIA} values. As a result, decreasing E_{SIA} reduces the total grounded ice volume by the end of the simulation.

The E_{SSA} parameter experiments are consistent in terms of the LGM configuration with the exception of the simulation with E_{SSA} = 1.0 (Fig 5.3), in which parts of the western Ross Sea, north of Ross Island, remain as open ocean or ice shelf, similar to the experiment with E_{SIA} = 3.0. Increasing E_{SSA} also yields an earlier ice sheet retreat, with the decline in grounded ice occurring at ~15 ka with E_{SSA} = 1.0 versus ~11 ka with E_{SSA} = 0.4. The ice shelf also begins to form more gradually with lower E_{SSA} values of 0.4 and 0.6 in comparison to that with E_{SSA} of 0.8. The PD configuration differs

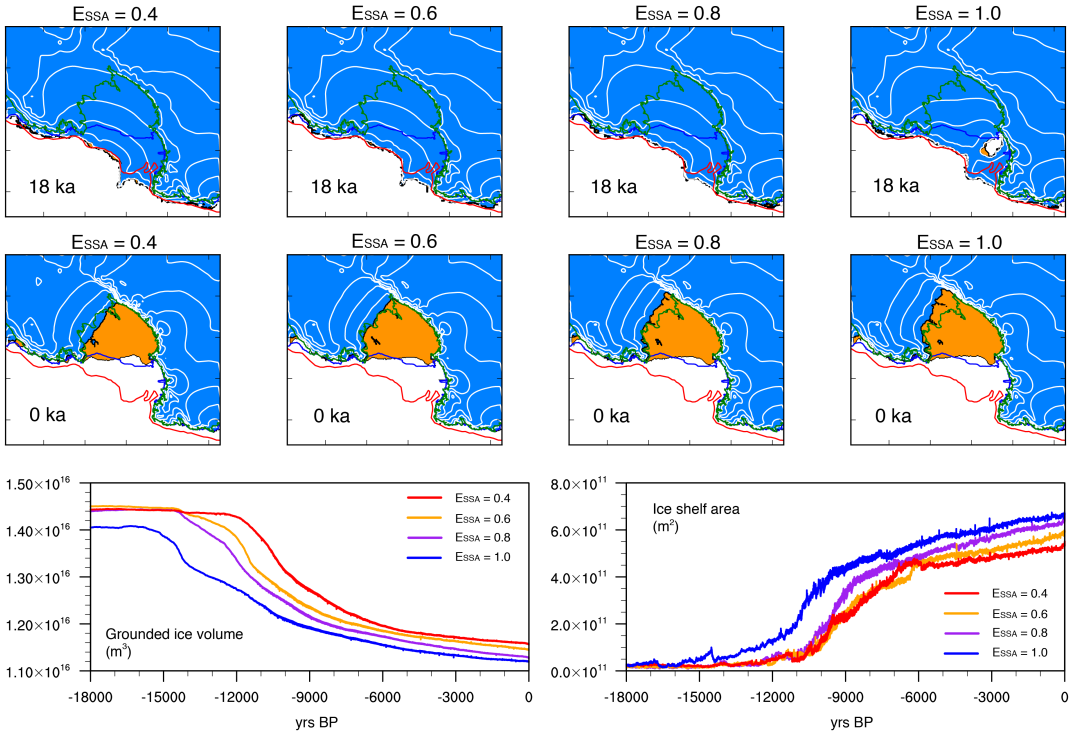

FIGURE 5.3: Experiments varying the enhancement factor of the shallow shelf approximation. The top row shows modelled ice configuration at 18 ka and the middle row shows the ice configuration at 0 ka, where blue indicates grounded ice, orange indicates floating ice, and the black line shows the modelled grounding line position. White lines denote surface elevation contours of 500 m. Observed grounding and calving line positions are shown in green and blue, respectively, and the estimated LGM ice sheet extent is shown in red. The bottom row shows time series of grounded ice volume (m^3) and ice shelf area (m^2) evolution of the full model domain from 18 to 0 ka.

considerably among the experiments, with higher E_{SSA} values resulting in greater ice shelf area and lower grounded ice volume. Similar to the E_{SIA} experiments, the differences are observed along the Siple Coast, however, the range of grounding line positions is larger. The best match with to modern observation is found with E_{SSA} = 0.6, with lower (higher) E_{SSA} values underestimating (overestimating) the Siple Coast grounding line extent. The exceptions are the MacAyeal and Bindschadler ice streams along the northern Siple Coast, where E_{SSA} of 0.8 better produces the observed grounding line extent.

5.4.3 Influence of basal resistance on ice sheet retreat

The sliding parameterization in PISM is in the form of a power law that ranges from plastic Coloumb sliding to sliding in which the sliding velocity is linearly related to the till strength (PISM, 2017; Kingslake et al., 2018):

$$\tau_b = -\tau_c \frac{u}{u_{threshold}^q |u|^{q-1}} \tag{5.1}$$

In the above power law, τ_b is the basal shear stress, τ_c is the yield stress, u is velocity, where $u_{threshold}$ is a threshold velocity, and q is the sliding exponent parameter, where q = 0 is purely plastic sliding, and q = 1 is sliding linearly related to the sliding velocity. The default value for this parameter is q = 0.25, which is the value used in the climate forcing model ensemble of the previous Chapters. Here, I consider higher values of q = 0.5, q = 0.75 and q = 1.0, as in Kingslake et al. (2018).

Another important sliding-related parameter is the till friction angle, which is related to the material properties of the till and influences:

$$\tau_c = c_0 + (tan\phi) N_{till} \tag{5.2}$$

where is the till cohesion (set to 0 in PISM by default), is the effective pressure of the till, and is the till friction angle parameter (PISM, 2017). In PISM, can be a spatially variable rather than uniform by adjusting (Kingslake et al., 2018). Previous ice sheet modelling work has heuristically determined as a piecewise linear function of the bed elevation (Winkelmann et al., 2011; Martin et al., 2011; Aschwanden, Aðalgeirsdóttir, and Khroulev, 2013; Kingslake et al., 2018), which is a method I apply here:

$$\phi(x,y) = \begin{cases} \phi_{min}, b(x,y) \leq b_{min}, \\ \phi_{min} + (b(x,y) - b_{min})M, b_{min} < b(x,y) < b_{max}, \\ \phi_{max}, b_{max} \leq b(x,y) \end{cases} \tag{5.3}$$

where b is the bed elevation, M is defined as (ϕ_{max} - ϕ_{min})/($b_{max} - b_{min}$), and (x,y) refers to a given point in space (PISM authors). While the default value in PISM is 30°, the model ensemble in the previous Chapters sets the minimum till friction angle (ϕ_{min}) to 9° for topography less than 200 m below sea level and the maximum till friction angle (ϕ_{max}) to 30° for topography at sea level. Here, I also experiment with lower values of ϕ_{min}, i.e., 3°, 4°, and 6° at 200 m below sea level.

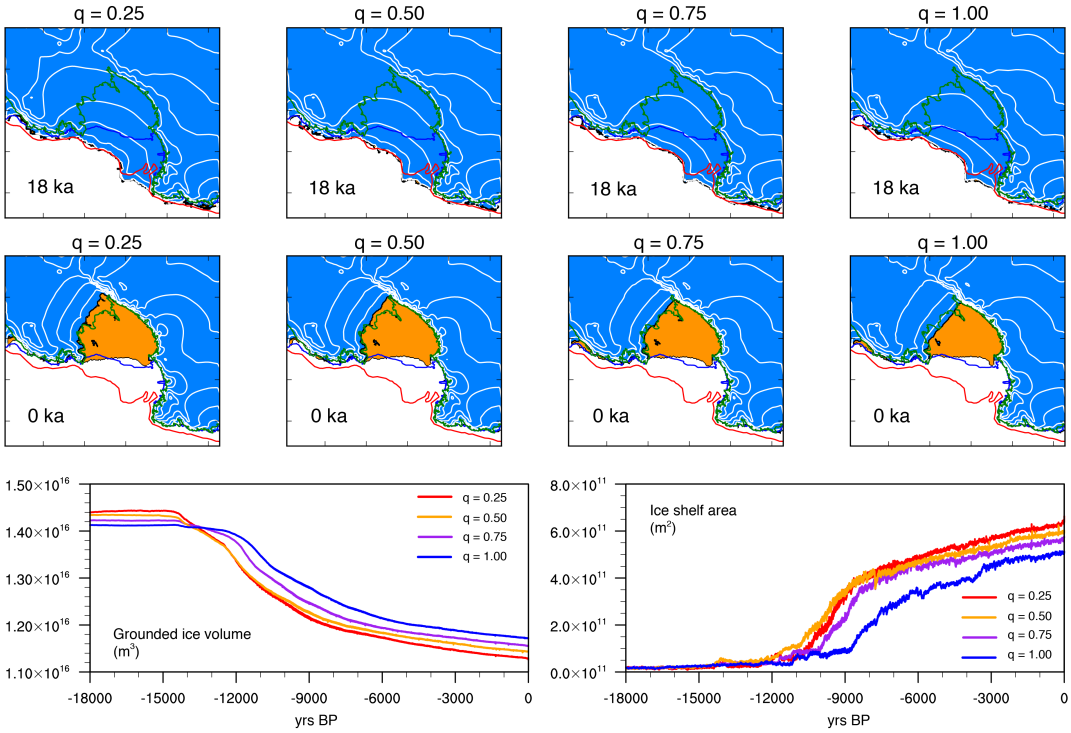

FIGURE 5.4: Experiments varying the basal resistance parameter, q. The top row shows modelled ice configuration at 18 ka and the middle row shows the ice configuration at 0 ka, where blue indicates grounded ice, orange indicates floating ice, and the black line shows the modelled grounding line position. White lines denote surface elevation contours of 500 m. Observed grounding and calving line positions are shown in green and blue, respectively, and the estimated LGM ice sheet extent is shown in red. The bottom row shows time series of grounded ice volume (m^3) and ice shelf area (m^2) evolution of the full model domain from 18 to 0 ka.

In the experiments with different q values, the ice sheet advances to the continental shelf edge in every case at LGM (Fig 5.4). The main difference at LGM is that q of 0.25 yields thicker ice over WAIS, contributing to the higher grounded ice volume. The response to climate forcing is delayed as q increases, despite the lower total grounded ice volume of the domain. For q of 1.0, grounded ice volume declines at approximately 12ka, and the ice shelf area does not show a substantial increase until 8.7 ka. The PD configurations of the q experiments are consistent in terms of the positions of the calving line and the grounding line along the Transantarctic Mountains, however, higher q leads to reduced grounding line extent along the Siple Coast. The experiment with q of 0.25 best matches the observed grounding line extent with the MacAyeal and Bindschadler ice streams along the northern Siple Coast, the experiments with q of 0.5 and 0.75 show better agreement with observations along the grounding line to the south of Siple Dome.

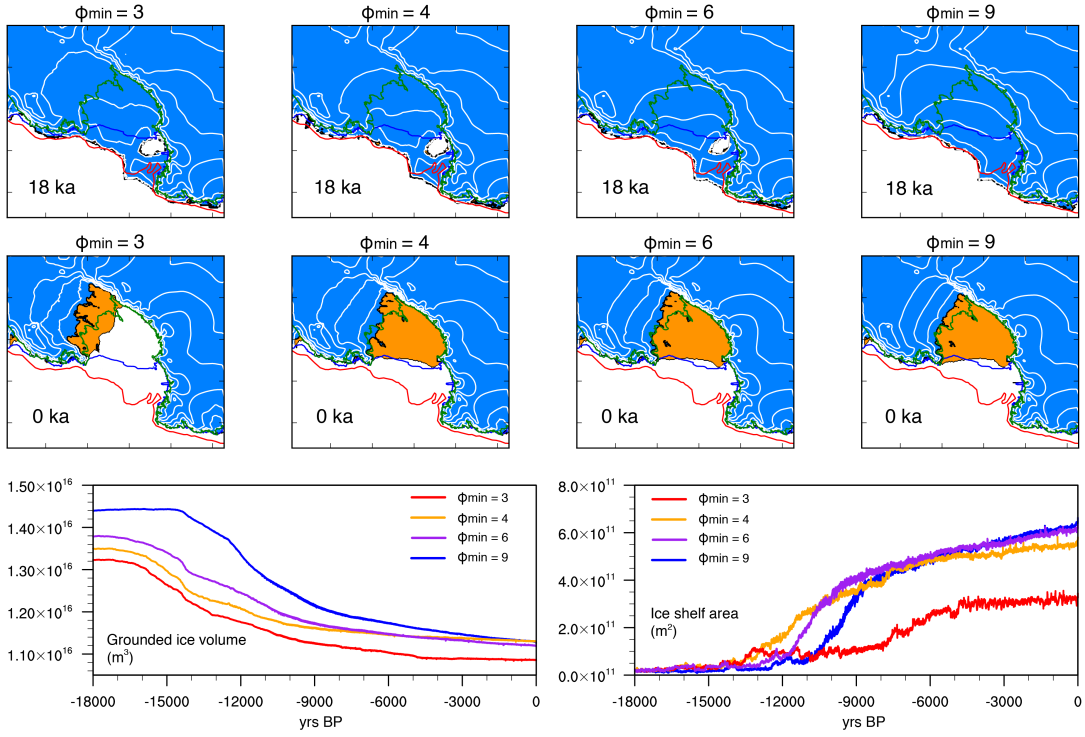

FIGURE 5.5: Experiments varying the minimum till friction angle, ϕ_{min}. The top row shows modelled ice configuration at 18 ka and the middle row shows the ice configuration at 0 ka, where blue indicates grounded ice, orange indicates floating ice, and the black line shows the modelled grounding line position. White lines denote surface elevation contours of 500 m. Observed grounding and calving line positions are shown in green and blue, respectively, and the estimated LGM ice sheet extent is shown in red. The bottom row shows time series of grounded ice volume (m^3) and ice shelf area (m^2) evolution of the full model domain from 18 to 0 ka.

The selection of ϕ_{min} is also consequential for both the LGM and PD ice sheet configurations. The best agreement in terms of both LGM and modern grounding line position is observed using the higher value of ϕ_{min} (9°; Fig 5.5). The lower values result in open ocean in the western Ross Sea (north of Ross Island) at LGM, and reduced ice surface elevation over WAIS, particularly at Siple Dome (see white surface elevation contours in Fig 5.5). The decline in grounded ice volume and increase in ice shelf area occurs more gradually with decreasing ϕ_{min}. At the lowest value of 3°, reduced buttressing due to ice shelf collapse leads to grounding line retreat beyond the modern day position in the PD configuration. At intermediate values (4° and 6°), minimum grounding line is overestimated along the southern Siple Coast and overestimated along the northern Siple Coast in the PD configuration.

5.4.4 Influence of the solid Earth on ice sheet retreat

The isostatic response of the solid Earth to the growth and decay of the Antarctic ice sheet has been argued to be the fundamental control of the grounding-line dynamics of West Antarctica (Kingslake et al., 2018; Whitehouse et al., 2019). In Chapter 3, the application of a higher mantle viscosity (5e20) led to a rapid response to deglacial climate forcing, with a retreat beyond the modern grounding-line position of Siple Coast, and readvancement through the Holocene, consistent with the findings of Kingslake et al., (2018). In contrast, the main model ensemble, in which a mantle viscosity value of 1e19 Pa s is applied, exhibited no such readvance behavior. At 100 km depth, the mantle viscosity of the Ross Embayment is spatially variable, with values ranging from 1e18 to 1e22 Pa s (Whitehouse et al., 2019). In general, the highest mantle viscosity values are observed over EAIS, with the lowest observed over the western Ross Sea and parts of WAIS. To better capture the full mantle viscosity range of the Ross Embayment, I consider three additional mantle viscosity values of 1e18, 1e20, and 1e21 Pa s.

The modelled ice sheet configuration at 18 ka is similar among the mantle viscosity experiments, however, the total grounded ice volume is considerably lower using a mantle viscosity of 1e21 Pa s (Fig 5.6). All of the simulations show similar timing in the decline of grounded ice volume, initiating around $\sim$14 ka. Little difference is observed in the ice sheet evolution between the 1e18 and 1e19 simulations. However, the response to climate forcing is more pronounced in the high mantle viscosity simulations (i.e., 1e20 and 1e21 Pa s), with the ice shelf forming earlier, particularly in the 1e21 experiment. These simulations maintain higher ice shelf area through the Holocene, but only the experiment with a mantle viscosity of 1e21 Pa s displays ice sheet readvance ($\sim$6 ka). This readvance is later and less extensive than the 5e20 mantle viscosity experiment discussed in Chapter 3. The PD configuration of the 1e21 simulation overestimates grounding line extent along Siple Coast and a portion of the ice shelf north of Ross Island becomes grounded. In comparison, the lower mantle viscosity experiments show better agreement with the PD grounding-line position along the Transantarctic Mountains.

The bed deformation scheme employed by PISM is based on the viscoelastic deformable Earth model of Bueler, Lingle, and Brown (2007). If this scheme is not applied during the deglaciation, ice sheet retreat occurs rapidly between 14 and 11 ka (Fig 5.7). In the outer continental shelf, grounding-line retreat initiates in the ERS and WRS, rather than in the central basin. Ice

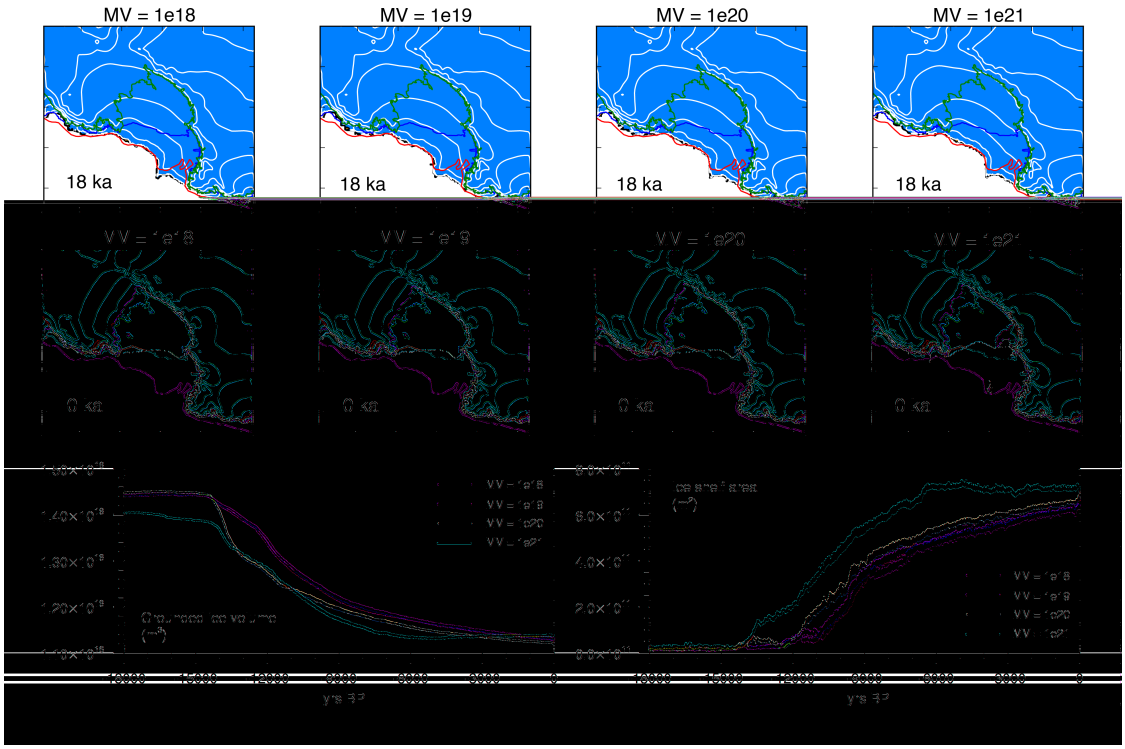

FIGURE 5.6: Experiments varying the mantle viscosity term. The top row shows modelled ice configuration at 18 ka and the middle row shows the ice configuration at 0 ka, where blue indicates grounded ice, orange indicates floating ice, and the black line shows the modelled grounding line position. White lines denote surface elevation contours of 500 m. Observed grounding and calving line positions are shown in green and blue, respectively, and the estimated LGM ice sheet extent is shown in red. The bottom row shows time series of grounded ice volume (m^3) and ice shelf area (m^2) evolution of the full model domain from 18 to 0 ka.

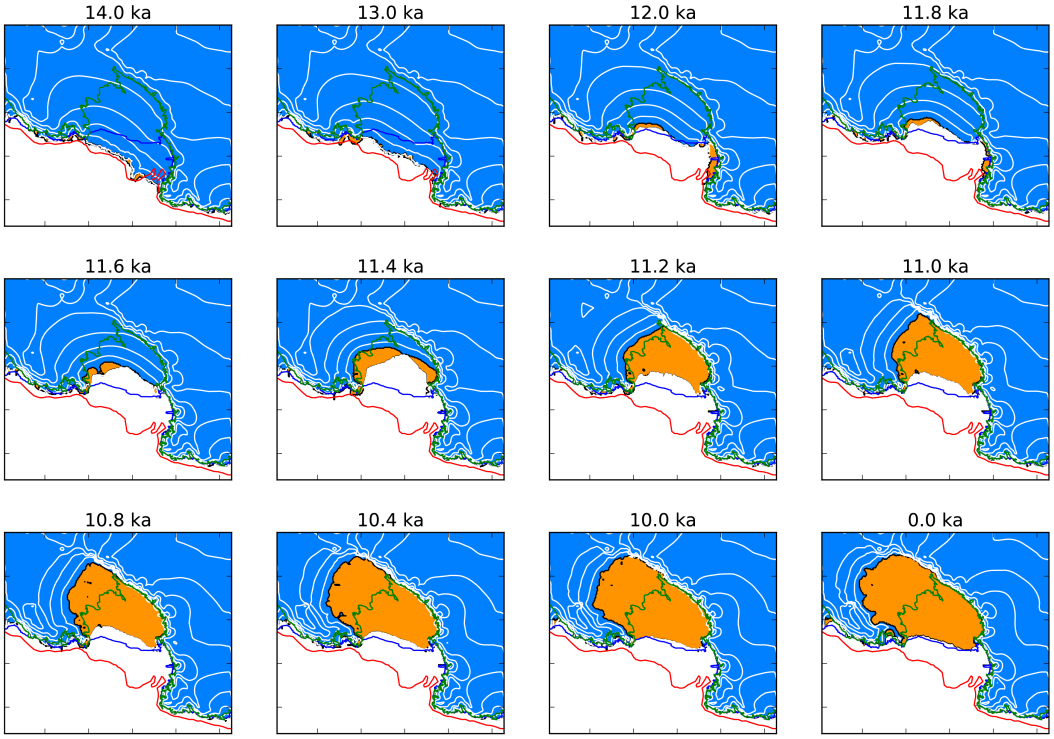

FIGURE 5.7: Time slices of ice sheet evolution in the simulation with no bed deformation. As in the previous figures, blue indicates grounded ice, orange indicates floating ice, and the black line shows the modelled grounding line position. White lines denote surface elevation contours of 500 m. Observed grounding and calving line positions are shown in green and blue, respectively, and the estimated LGM ice sheet extent is shown in red.

from both WAIS and EAIS becomes ungrounded in the early Holocene (by 11.4 ka). Propagation of retreat to the Transantarctic Mountains and the modern Siple Coast is completed by 11.2 ka, with the merging of ice shelf from the east and west into the main Ross Ice Shelf at this time. The grounding line continues to rapidly retreat on the WAIS side of the embayment over the next 1.2 ka, but the position remains fixed along the Transantarctic Mountains. Roosevelt Island becomes ungrounded ∼10.4 ka. Over the last 10 ka of the simulation, the ice sheet shows relatively little change. The 0 ka configuration is consistent with the observed grounding line position along the Transantarctic Mountains and the modern calving line position. However, this simulation highlights the importance of bed deformation in the representation of ice sheet for the low-lying WAIS.

5.4.5 Spatiotemporal uncertainty

Selection of model parameters and parameterizations of physical processes in ice sheet models have previously been shown to govern the ice sheet sensitivity to climate forcing (Ritz et al., 2015; DeConto and Pollard, 2016; Kingslake et al., 2018; Edwards et al., 2019). Here, I demonstrate the effect of individual parameters on deglacial ice sheet retreat in the Ross Embayment from a spatiotemporal perspective. Among the four simulations of each parameter described in Sections 3.2 to 3.4, the selection of ϕ_{min} has the most significant impact on ice thickness through the deglacial period (Fig 5.8a-e), followed by mantle viscosity and E_{SSA}. In comparison, the E_{SIA} simulations show relatively strong agreement in terms of ice thickness over this time interval. With the exception of q, each parameter shows relatively high ice thickness standard deviations (> 400 m) in the western Ross Sea region. For q, the highest standard deviations (> 200 m) are observed along the southern Siple Coast. The ϕ_{min} simulations also exhibit high standard deviations over much of the modern Ross Ice Shelf and wider WAIS region (> 400 m).

For the compilation of ice sheet parameter simulations (16 simulations; the simulation with no bed deformation is not included), it is clear that the areas that are most sensitive to model parameter selection are the western Ross Sea, both to the north and south of Ross Island, and the southern Siple Coast (Fig 5.8f). This is similar to the climate forcing model ensemble discussed in previous simulations (42 simulations; Fig 5.8g), which also shows the highest standard deviation of ice thickness in the western Ross Sea. However, it is notable that the standard deviations are relatively higher in Fig 5.8f than in Fig 5.8g, suggesting that the selection of model parameters tested in this Chapter is more important in terms of the timing and pattern of ice sheet retreat than the selection of climate forcings described in Chapter 3 and 4 of this thesis. One reason for this is that there is a larger range of LGM and PD ice volumes in the model parameter ensemble versus the climate forcing ensemble. In contrast to the model parameter ensemble members, the end-member states of the climate forcing ensemble members are relatively consistent, hence the differences primarily result from differences in the timing of grounding line retreat.

The total standard deviation of ice thickness through the deglacial period among the 58 simulations shows the key area of uncertainty is the western Ross Sea, with standard deviation > 400 m to the north and south of Ross Island (Fig 5.8h). Relatively high standard deviations also observed in the southern Siple Coast region and along the modern calving line. The

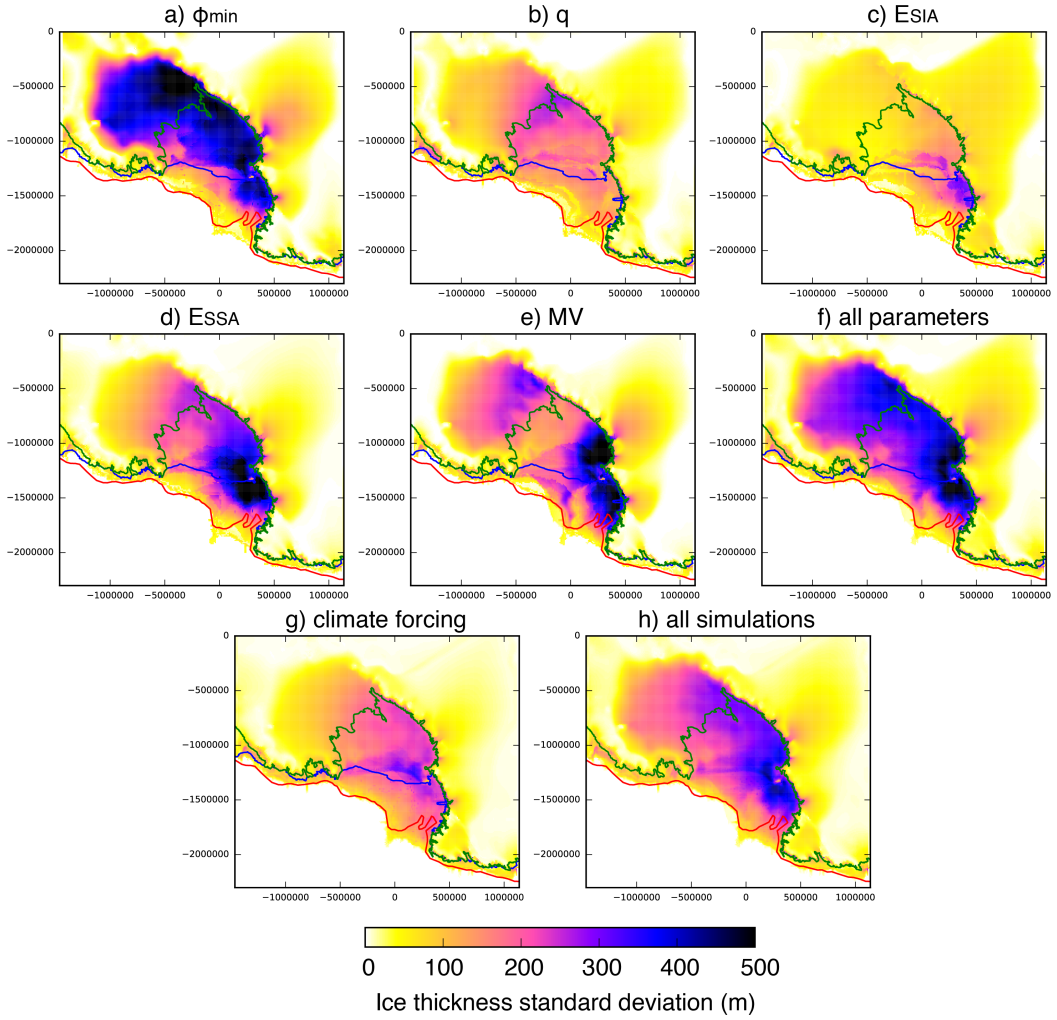

FIGURE 5.8: (a-e) Time-averaged standard deviation of ice thickness (m) for the period of 18-4 ka in experiments varying a single model parameter, i.e., till friction angle (ϕ_{min}), basal resistance (q), enhancement factors of SIA and SSA (E_{SIA} and E_{SSA}, respectively) and mantle viscosity (MV). (f) Time-averaged standard deviation of ice thickness of all experiments from panels a-e (16 simulations total). (g) Time-averaged standard deviation of ice thickness of all experiments from Chapter 3 and 4 (42 simulations total). (h) Time-averaged standard deviation of ice thickness of all experiments in panels a-e and g (58 simulations total).

WAIS catchment shows higher standard deviation than the EAIS catchment, though the ice streams of the Transantarctic Mountains show relatively high standard deviations. The model parameter ensemble contributes to the high standard deviations over the WAIS catchment, considering that the climate forcing ensemble shows relatively higher agreement in this region. Geological constraints of the bed may therefore be more valuable for understanding WAIS retreat, whereas in the western Ross Sea, both climatic and geological constraints are required.

5.4.6 Comparison to EAIS and WRS proxy records

Cosmogenic nuclide surface-exposure records of ice thinning at marginal sites in the Transantarctic Mountains generally show enhanced thinning rates in the early-to-mid Holocene, although the precise timing differs among individual glaciers over a large time range of ∼14-6 ka (Todd et al., 2010; Jones et al., 2015; Anderson et al., 2017; Spector et al., 2017; Goehring et al., 2019). As explained in Chapter 3, comparisons between ice sheet model simulations and surface-exposure records are difficult due to limitations in model resolution, which may not be sufficient for resolving smaller-scale features. However, the parameter model experiments in this Chapter allow for analysis of which model parameters may contribute to the model-proxy discrepancies observed between regional ice thinning in the climate forcing model ensemble of Chapter 3 and individual glaciers. Here, I compare ice thickness changes of the model ensemble in three regions from which cosmogenic nuclide surface-exposure records exist: the Northern Transantarctic Mountain (NTAM) region, the McMurdo region, and the Southern Transantarctic region (STAM; Fig 5.9).

One of the main model-proxy mismatches shown in Chapter 3 is the difference in the rate of ice thinning in the early Holocene, which is more rapid in the model simulations than indicated in the surface-exposure records, particularly in the NTAM and McMurdo regions (Fig 5.9a,b). It was argued in Chapter 3 that the bed smoothing parameterization contributed to this difference, as a rough bed would have more potential pinning points. Considering the abundance of ice rises in the western Ross Sea in particular (Simkins, Anderson, and Greenwood, 2016), this is an important consideration. The red lines in Fig 5.9 show the effect of reduced bed smoothing (bed smoothing parameter decreased from 25e3 to 10e3); although this higher bed roughness

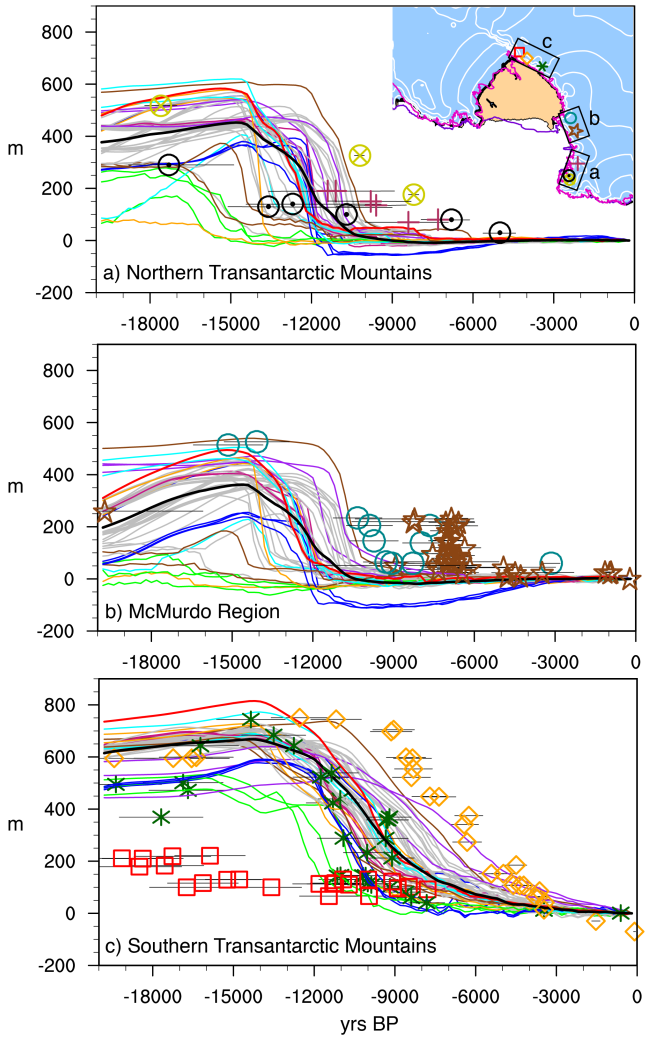

FIGURE 5.9: Regional ice thickness anomalies relative to PD of the model simulations for the (a) NTAM, (b) McMurdo, and (c) STAM regions vs. ice thickness anomalies of cosmogenic nuclide surface-exposure records of glaciers within each region. Climate forcing simulations from Chapter 3 are shown in gray, with the exception of the moderate climate forcing scenario from Fig 5.1 shown in black. The magenta and blue lines show the RICE TPS and WDC ACC experiments in Chapter 4, respectively. The cyan and brown lines show the E_{SIA} and E_{SSA} experiments, respectively. The purple, green and red lines show the q, ϕ_{min}, and bed roughness experiments, respectively. The orange lines show the mantle viscosity experiments. The NTAM glacier data were obtained from Goehring et al., (2019). Data for Mt Discovery and Mackay Glacier were obtained from Anderson et al., (2017) and Jones et al., (2015), respectively. The STAM glacier data were obtained from Spector et al., (2017) and Todd et al., (2010). All exposure ages were recalculated following recent improvements to global production rate (Borchers et al., 2016). Age uncertainties of the records are indicated by the horizontal bars. The inset in panel (a) shows the region locations (black box outline) and the glacier locations overlaid on the ensemble average of the final modeled RIS configuration (yellow shows floating ice, blue shows grounded ice, thick black line shows modeled grounding-line position, white contours show surface elevation in 500m intervals, pink line shows observed modern grounding-line position, and purple line shows observed modern calving line position).

leads to increased glacial ice thickness, the rate of early Holocene ice thinning increases (Fig 5.9a-c), in contrast to the previously proposed hypothesis. However, it should be noted that the bed in these simulations, which is based on the bedmap2 dataset, is considerably smoother than reality even in the higher roughness simulation, hence uncertainty on its effect on ice sheet retreat remains.

Among the other model parameters tested, E_{SSA} shows the widest range in ice thinning in the NTAM and McMurdo regions (brown lines in Fig 5.9a,b). Using lower values of E_{SSA}, which reduces the velocity of ice streams and ice shelves, leads to higher glacial ice thickness and later ice thinning in these regions, whereas the reverse is true for the simulations that use higher E_{SSA} values. Although q does not show high standard deviation of ice thickness in this region (Fig 5.8), higher q also yields a relatively later ice thinning, more consistent with Mt Discovery (Fig 5.9b), with an effect similar to cooler climate forcing. No model simulation captures the mid-Holocene readvance observed at Mt Discovery and Mackay Glacier, indicating that this is a local signal that the model is incapable of resolving, or that the climate forcing (i.e., precipitation and ocean forcing) is inadequate for this region, as discussed in Chapter 3. In the NTAM region, low E_{SSA} (0.4) and high q (1.0) yield delayed retreat, more consistent with Scott Glacier (Fig 5.9c). Reducing ϕ_{min} (green lines), increasing q, and application of the WDC ACC precipitation forcing (blue lines) produce lower glacial ice thickness in NTAM, but still result in higher glacial ice thickness than estimated at Reedy Glacier.

The applications of cooler climate forcing, lower E_{SSA} values, and higher q delay the timing of grounding-line retreat in the western Ross Sea (Fig 5.10). Some commonalities exist among the pattern of retreat, regardless of model parameter selection and climate forcing, highlighting the importance of seafloor bathymetry in driving the pattern of grounding line retreat, as discussed in Chapter 3 and argued in Halberstadt et al. (2016), McKay et al., (2016) and Lee et al. (2017). For example, each grounding line retreat evolution in Fig 5.10 shows instances of grounding line stabilization from Pennel Bank, Crary Bank and Ross Island, with relatively rapid retreat occurring between these pinning points. However, differences are observed, with the simulation with q = 1.0 (i.e., linear sliding law) displaying a more constant rate of retreat and no ice remaining grounded on Pennel and Crary Banks following ice sheet retreat. The other simulations (i.e., moderate climate, cool climate, and low E_{SSA}) are more consistent with the sequence of retreat suggested in the marine-based model of Halberstadt et al. (2016) based on interpretation

of the geomorphic features of the seafloor.

5.4.7 Comparison to WAIS deglacial reconstructions

Reconstruction of WAIS is more difficult than in the Transantarctic Mountains considering the lack of surface-exposure records. Those that do exist are from marginal sites of Marie Byrd Land, are temporally constrained to the early Holocene and show a wide range of surface elevation changes. For example, surface-exposure ages from Mt Waesche, a volcanic nunatak in Marie Byrd Land, indicate an ice surface elevation ∼45 m above present at 10 ka (Ackert et al., 1999). In contrast, glacial deposits in the Ford Ranges of Marie Byrd Land suggest ∼700 m of continuous ice thinning since 10 ka (Stone et al., 2003). Attempts have also been made to estimate changes in surface elevation in the WAIS interior through the deglacial period from a modelling perspective. Continental-scale climate-forced ice sheet model simulations have produced LGM ice thickness changes ranging from <50 m to 360 m at WAIS Divide (Pollard and DeConto, 2009; Golledge et al., 2014; Pollard, DeConto, and Alley, 2015). The ICE-5G and ICE-6G glacial isostatic adjustment model scenarios, generally used in climate model simulations, suggest larger ice thickness changes of WAIS through the deglacial period (Peltier, 2004; Argus et al., 2014). Given the wide range of estimates and evolving nature of interpretations, high uncertainties of WAIS ice thickness changes remain.

At WAIS Divide, the climate forcing model ensemble shows LGM surface elevation changes of ∼200 m, within the range of the above-mentioned continental-scale ice sheet model simulations, but below the ICE-5G and ICE-6G estimations (Fig 5.11a). The climate forcing model ensemble members are also generally consistent with the modern WAIS Divide surface elevation of 1797 m. Increasing q and decreasing ϕ_{min} reduces the LGM ice surface elevation (purple and green lines in Fig 5.11a, respectively), and in the simulations with lower ϕ_{min}, the modern surface elevation is underestimated. Other outliers from the model parameter ensemble members include the simulation with E_{SSA} of 0.4, in which the total deglacial change is ∼80 m and the modern surface elevation is overestimated by 140 m, and the simulation with mantle viscosity of 1e21 Pa s (orange line in Fig 5.11a), which is the only showing decreasing surface elevation in the early Holocene (∼11.8 ka) and isostatic rebound-driven increase in surface elevation in the late Holocene. The relative change of this simulation with high mantle viscosity is similar

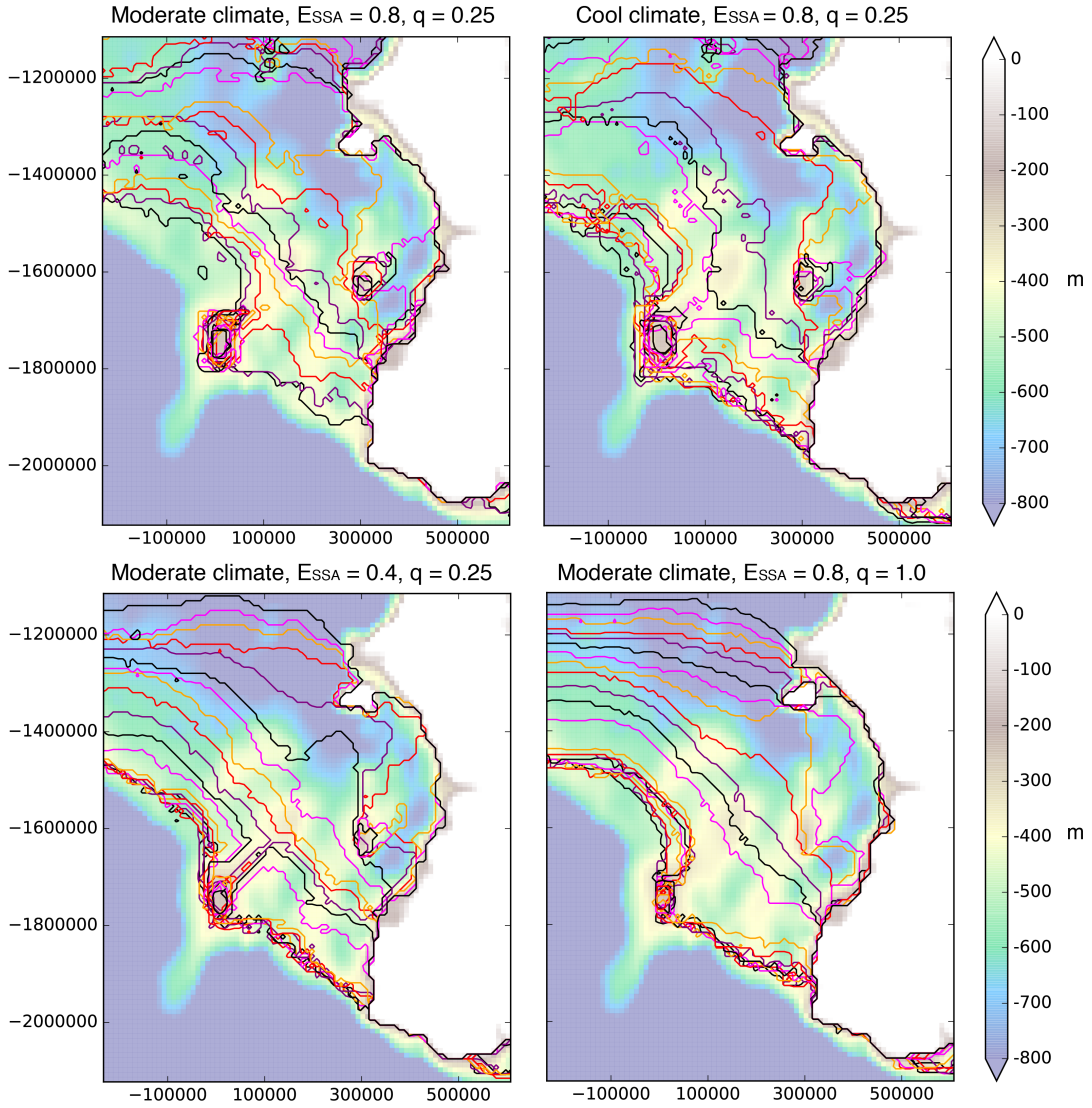

FIGURE 5.10: Changes in grounding-line position in the Western Ross Sea for the period of 14 to 10 ka. Black lines indicate grounding-line position for periods of 1000 years, whereas colored lines indicate 200-yr grounding-line changes with the sequential order of purple, red, orange, pink. The grounding lines overlay modelled basal topography at 10 ka.

to the ICE-5G and ICE-6G estimations, but the modelled surface elevation is lower through this interval and the modern surface elevation is slightly underestimated (<100 m).

Closer to the Ross Sea, the difference between the ICE-5G and ICE-6G estimations is more significant in terms of the LGM WAIS surface elevation, with the model simulations generally producing higher LGM surface elevations than ICE-6G and lower LGM surface elevations than ICE-5G at Siple Dome and Roosevelt Island (Fig 5.11b,c). Similar to WAIS Divide, the outliers of the model parameter ensemble include the ϕ_{min}, q, E_{SSA} and high mantle viscosity experiments (green, purple, brown, and orange lines, respectively). Decreasing ϕ_{min} improves the model fit to ICE-6G estimations at Siple Dome, whereas increasing q leads to higher-than-observed modern ice surface elevation at this site (Fig 5.11b). At Roosevelt Island, decreasing ϕ_{min} also yields an LGM surface elevation that is more consistent with ICE-6G, but the high q, low E_{SSA} and cool climate forcing simulations, which produce a delayed ice sheet retreat, are more consistent with the timing of the ICE-6G decrease (Fig 5.11c). The high mantle viscosity simulation shows a rapid decrease in ice surface elevation at both sites in response to ocean thermal forcing at $\sim$14 ka.

In terms of the grounding-line evolution along the Siple Coast, the moderate climate forcing simulation discussed in Chapters 3 and 4 shows a southwestward propagation of the grounding line from Roosevelt Island and Crary Ice Rise through the mid-to-late Holocene (Fig 5.12a). The grounding-line position at 0 ka is consistent with modern observations along the northern Siple Coast (i.e., MacAyeal and Bindschadler ice streams), but retreat is overestimated to the south. Application of cool ocean forcing and WDC-derived precipitation forcing, which is higher through the Holocene, improves the fit to modern observations of grounding-line position (Fig 5.12b). Although decreasing ϕ_{min} yields an ice surface elevation evolution at Siple Dome that is more consistent with ICE-6G, the simulation with ϕ_{min} of 4 shows overestimated grounding-line retreat of the southern Siple Coast by 7 ka, and underestimated grounding-line retreat of the northern Siple Coast by 0 ka (Fig 5.12c). Mantle viscosities above 1e20 Pa s are required for the ice sheet retreat-readvance scenario proposed by Kingslake et al. (2018). With mantle viscosity of 1e21 Pa s, the readvance initiates by 6 ka, later than the 5e20 simulation discussed in Chapter 3, but the grounding-line extent at 0 ka still overestimates modern observations (Fig 5.12d).

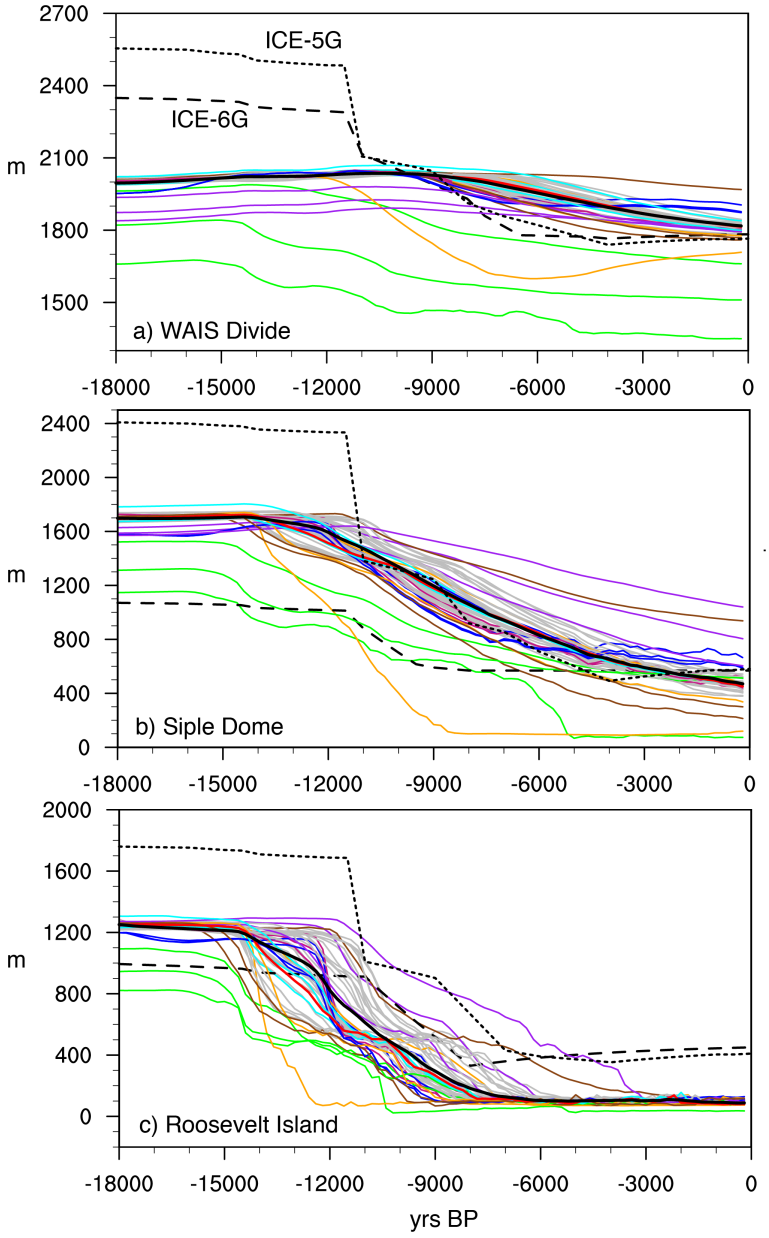

FIGURE 5.11: Modelled ice surface elevation at (a) WAIS Divide, (b) Siple Dome, and (c) Roosevelt Island compared to ICE-5G and ICE-6G reconstructions (Peltier et al., 2004; Argus et al., 2014). Climate forcing simulations from Chapter 3 are shown in gray, with the exception of the moderate climate forcing scenario from Fig 5.1 shown in black. The magenta and blue lines show the RICE TPS and WDC ACC experiments in Chapter 4, respectively. The cyan and brown lines show the E_{SIA} and E_{SSA} experiments, respectively. The purple, green and red lines show the q, ϕ_{min}, and bed roughness experiments, respectively. ICE-5G and ICE-6G are indicated by the small and large dashes, respectively.

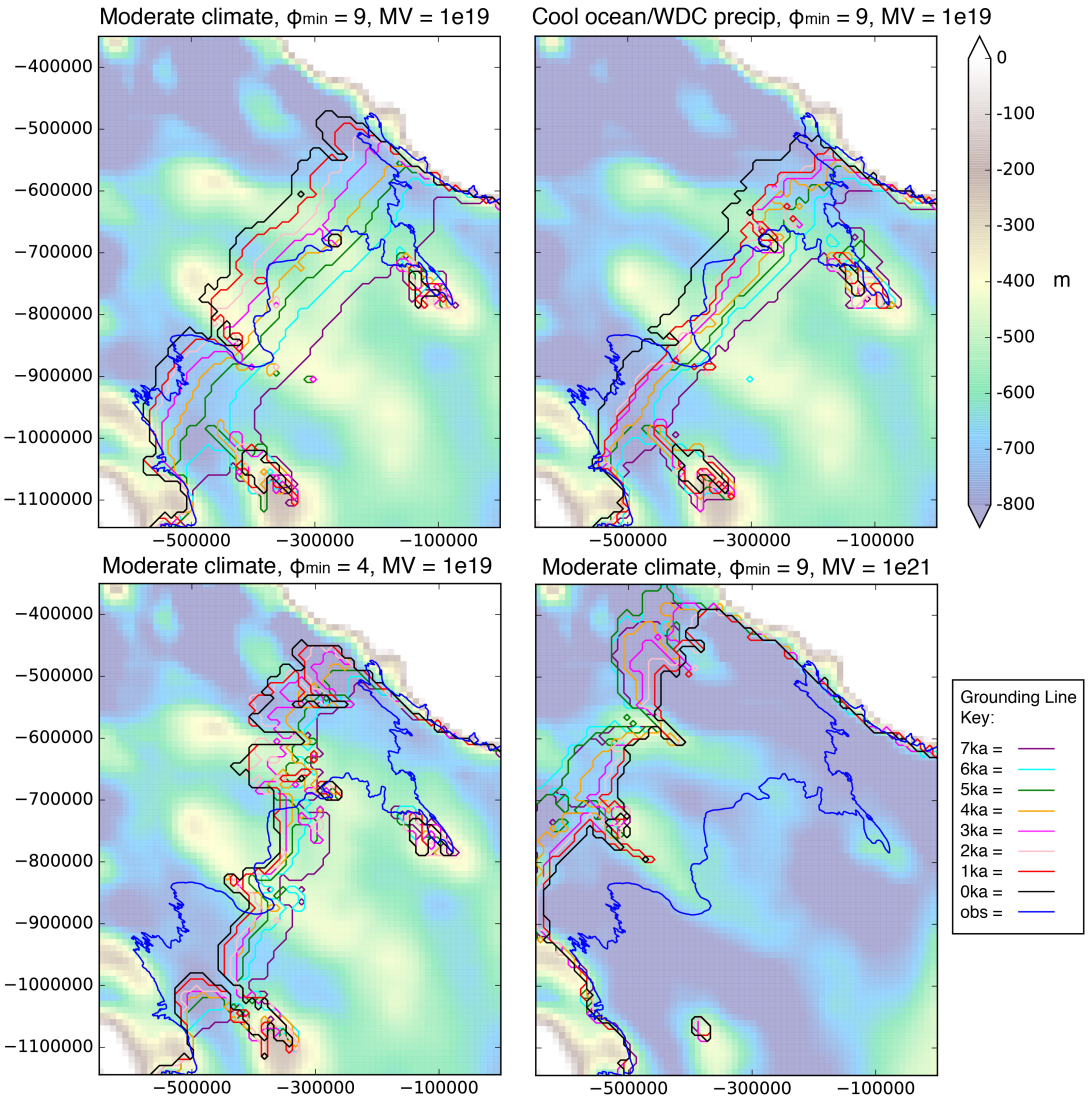

FIGURE 5.12: Modelled changes in grounding-line position along the Siple Coast for the period of 7 to 0 ka. The blue line indicates the observed grounding line position. The grounding lines overlay modelled basal topography at 0 ka.

5.5 Discussion

Of the model parameters examined in this Chapter, ϕ_{min}, mantle viscosity, and E_{SSA} show the greatest influence on the broader-scale ice sheet sensitivity to climate forcing. As the ϕ_{min} parameter increases, the LGM ice thickness increases, and the ice sheet becomes less sensitive to deglacial climate forcing. In comparison, the E_{SSA} experiments show less variation in terms of the LGM configuration, but increasing E_{SSA}, which enhances ice shelf and ice stream velocity and basal sliding, yields higher sensitivity to climate forcing. Increasing mantle viscosity causes the ice sheet to respond more rapidly to climate forcing, but the retreat-readvance scenario described in Kingslake et al. (2018) is only reproduced with mantle viscosity >1e20 Pa s, which is consistent with their findings. Although the E_{SIA} and q parameters show relatively less influence on ice sheet retreat behavior, E_{SIA} does impact the LGM ice thickness, and increasing q, which increases basal resistance, delays the ice sheet response to climate forcing, as expected.

Within the model domain, these model parameters may contribute to the differences in the local grounding-line retreat and ice thinning behavior observed in proxy records and reconstructions of different locations. For example, Halberstadt et al. (2016) proposes an asynchronous pattern of grounding-line retreat between the ERS and WRS. This is generally confirmed in comparing available WAIS radiocarbon ages (Bart et al., 2018; Kingslake et al., 2018) with surface-exposure records of the Transantarctic Mountains (Jones et al., 2015; Anderson et al., 2017), which suggest a later WRS retreat and delayed ice thinning of EAIS outlet glaciers. While it is difficult to determine how differences in climate forcing and ocean circulation influenced this pattern of retreat, we show here that geological and glaciological factors cannot be discounted as controls. In particular, the relatively low mantle viscosity of the WRS likely reduced the ice sheet response to climate forcing as compared to the ERS, which has a higher mantle viscosity (Whitehouse et al., 2019). The spatial heterogeneity of this parameter therefore poses a significant challenge in modeling the embayment-scale retreat pattern and requires consideration in comparing individual model simulations to proxy records.

Although the climate forcing ensemble of Chapters 3 and 4 use a low mantle viscosity (1e19 Pa s), consistent with the WRS, the majority of model simulations show earlier ice thinning than surface-exposure records from Mackay glacier and Mt Discovery (Jones et al., 2015; Anderson et al., 2017). Simulations that use of cool atmosphere and ocean forcings, which show delayed

WRS grounding-line retreat, are more consistent with these records, as explained in Chapter 3. Here, I also show that reducing E_{SSA} and increasing q also delay ice thinning in the Southern Victoria Land region. Using an E_{SSA} of 0.4 reduces the ice shelf velocity and allows the temporary ice shelf that fringes the EAIS outlet glaciers in the early Holocene to last for a longer duration. Although a q of 1.0 also delays WRS grounding-line retreat, the retreat pattern is inconsistent with the sequence of retreat described in Halberstadt et al., (2016), as no ice remains grounded on Pennel and Crary Banks following ice sheet retreat. These models therefore suggest that the rheological properties and flow velocities of EAIS-derived ice, as they relate to E_{SSA}, and climate forcing are the relevant controls to focus on in improving the model-data fit in this region.

However, one of the outstanding issues in Southern Victoria Land is the middle Holocene ($\sim$8.5 ka) ice sheet readvance indicated in Greenwood et al. (2018), and observed in the Mackay glacier and Mt Discovery records (Jones et al., 2015; Anderson et al., 2017). The readvance was significant enough to increase ice thickness by $\sim$200 m at both sites, with the grounding-line reaching as far as Joides Trough, but none of the model simulations reproduce this behavior. Greenwood et al. (2018) attribute the readvance to flow-switching and enhanced flow velocity associated with the unzipping of ice sheet sub-sectors as the grounding line retreated toward the South Victoria Land outlet glaciers, and also suggest that an increase in precipitation, related to the increased available moisture from the open ocean, may have occurred. The model simulations may fail to reproduce this advance due to the limitations in model resolution, which may inadequately represent the local-scale ice dynamics involved in this flow-switching behavior, and in the precipitation forcing, which does not increase substantially through this interval (see Chapter 3). Ocean circulation may also be an important element to this readvance as the ocean cavity beneath the Ross Ice Shelf begins to form. Enhanced basal melting from the local ice shelf and the forming Ross Ice Shelf in the mid-Holocene may have increased marine ice formation, similar to the modern process of sea ice stabilization from the ice shelf cavity freshwater flux observed in the WRS (Hellmer, 2004). Since the ocean thermal forcing applied in these simulations neglects circulation, such ice-ocean interactions and feedbacks are lacking, which may also account for the model-data mismatch.

In Northern Victoria Land, the Tucker and Aviator glacier records exhibit a similar timing in the initial ice thinning, but show a more gradual decrease

than the model simulations. Although Goehring et al. (2019) note the similarity between the ice thinning chronologies of the glaciers and global sea level, sea level forcing alone cannot account for ice sheet retreat in these ice sheet model simulations (see Chapter 3). Ocean and atmosphere forcing are the primary controls on ice sheet retreat, though sea level forcing does enhance their effect. The discrepancy in rate can partially be accounted for by the E_{SSA} term, which can be adjusted to show better agreement to both glaciers, and increasing bed roughness, which stabilizes the ice thickness in this region following the initial decrease. In addition, the back pressure forcing, which is intended to mimic the resistance effect of dense sea ice, may decrease too dramatically in the early Holocene. The back pressure forcing is derived from a scaling relationship of ice core surface temperature records and modelled surface temperature of deglacial climate simulations (see Chapter 3). As a result, the forcing may be impacted by a decrease in ice surface elevation that may partially account for the temperature increase in the early Holocene in the ice core records (see Chapter 4), and in one of the climate models (see Chapter 2). A back pressure forcing scaled to modelled or reconstructed sea ice concentration or thickness may decrease more gradually through the early Holocene and improve the model fit to the surface-exposure data of North Victoria Land.

For WAIS, the most influential parameter discussed in this Chapter is ϕ_{min}. Decreasing ϕ_{min} reduces the LGM surface elevation and causes earlier ice sheet retreat and ice shelf formation. At the specific sites of Siple Dome and Roosevelt Island, the simulations with lower ϕ_{min} show better agreement with the ICE-6G estimations of Argus et al. (2014), however, these simulations are least consistent at WAIS Divide. ϕ_{min} is related to the material properties of the till, and although this term becomes spatially variable through its relationship to bed elevation (Equation 3), it is difficult to determine a ϕ_{min} value that improves model fit in each part of the model domain. Till deformation has been shown to be an important control on WAIS-derived ice stream flow (Alley et al., 1986; Hulbe et al., 2016). Considering the proximity of Roosevelt Island and Siple Dome to these ice streams, accurate reconstruction of their surface elevation may depend on adequate representation of the till properties in ice sheet models. In this Chapter, I focus on ϕ_{min}, but the bed elevation terms and ϕ_{max} are also important components in τ_c. Future work should explore the influences of each component as it relates to the WAIS-derived ice streams.

The other parameter likely driving differences between WAIS and EAIS

evolution and grounding-line retreat in the ERS and WRS is the previously discussed mantle viscosity term, which is higher in the ERS (Whitehouse et al., 2019). This may in part explain the early retreat indicated in marine radiocarbon ages in the Whales Deep Basin (Bart et al., 2018), as the high mantle viscosity (>1e20 Pa s) could have made the ice sheet more sensitive to sub-surface ocean warming resulting from melting of the Antarctic Peninsula and the mid-to-outer Weddell Sea (Golledge et al., 2014). The simulations with higher increases in Meltwater Pulse 1a-associated sub-shelf melt rates in Chapter 3 are consistent with the early retreat timing of Bart et al., (2018), as are those with mantle viscosity 5e20. However, the scenario of Bart et al., (2018) also indicates a grounding-line stabilization on the outer-continental shelf following the initial retreat until the early Holocene ($\sim$11.5 ka). This stabilization is not reproduced in the high mantle viscosity experiments.

The ERS grounding-line stabilization is also difficult to reconcile with the retreat-readvance scenario of Kingslake et al., (2018) based on the presence of finite radiocarbon ages measured in the organic carbon from subglacial sediments underneath WAIS ice streams. In this scenario, the grounding line retreated beyond the modern-day position along Siple Coast in the early Holocene and readvanced to its current position due to isostatic rebound. In model simulations also using PISM, they simulate the furthest retreat in the Ross sector at 9.7 ka. Considering the radiocarbon ages from the outer continental shelf, this would indicate rapid and extensive grounding-line retreat occurring between 11.5 and 9.7 ka. With mantle viscosity of 1e21 Pa s, the maximum grounding-line retreat occurs $\sim$6ka, but the grounding-line does not readvance to the modern Siple Coast position. As previously mentioned, the main challenge in addressing the role of mantle viscosity is its uniform application in ice sheet models. Spatial heterogeneity of this term, which would allow for parts of the ice sheet to be more sensitive to climate forcing than others, may cause a more reasonable retreat in ice sheet models, in which the retreat occurs at a later date, but the grounding-line still achieves an accurate modern-day position following the readvance.

Other controls on Siple Coast grounding-line position in the mid-to-late Holocene are ocean and precipitation forcing. Application of the WDC ACC precipitation forcing (see Chapter 4), which has higher precipitation through the Holocene than using a constant precipitation-temperature scaling relationship, produces a thicker WAIS that is more resistant to late Holocene grounding-line retreat. Cooler ocean forcing (i.e. lower sub-shelf melt rate

anomalies) also yields less extensive grounding-line retreat. and in combination with the WDC ACC precipitation forcing, the most accurate grounding-line position is produced for the southern Siple Coast. The effect of these external forcings on modulating or driving the retreat-readvance scenario proposed in Kingslake et al. (2018) requires consideration and further exploration. The influence of the interaction of these forcings on grounding-line retreat behavior also has implications for future WAIS grounding-line changes as basal melting has been eroding the ice shelves fringing the Amundsen sector of WAIS (Pritchard et al., 2012; Favier et al., 2014; Seroussi et al., 2017), and Antarctic precipitation is predicted to increase (Palerme et al., 2017).

5.6 Conclusions

The response of ice sheet models to climate forcing has previously been shown to be highly sensitive to specific model parameters, parameterizations of physical processes, and representation of the bed (Matsuoka et al., 2015; Kingslake et al., 2018; Colleoni et al., 2018; Edwards et al., 2019; Seroussi et al., 2019). In this Chapter, I explore the effect of physical model parameters that control basal properties, the solid Earth, and ice flow and rheology on the ice sheet response to deglacial climate forcing in the Ross Embayment. The main conclusions of this Chapter are as follows:

Of the parameters explored in this Chapter, ϕ_{min}, mantle viscosity, and E_{SSA} show the greatest influence on the broader-scale ice sheet sensitivity to climate forcing. Increasing ϕ_{min} leads to increased LGM ice thickness and reduced sensitivity to deglacial climate forcing. Increasing E_{SSA}, which enhances ice shelf and ice stream velocity and basal sliding, yields higher sensitivity to climate forcing. Increasing mantle viscosity causes the ice sheet to respond rapidly to climate forcing, and with mantle viscosity >1e20, the retreat-readvance scenario of WAIS proposed by Kingslake et al. (2018) is reproduced. In comparison to the climate forcing model ensemble of Chapters 3 and 4, the parameter model ensemble shows larger deviation in the deglacial ice sheet evolution.

The WRS is a key area of uncertainty from both a climate forcing and model parameter selection perspective. Application of cooler climate forcing delays WRS grounding-line retreat and ice thinning in North and South Victoria Land, producing an ice sheet evolution that is more consistent with surface-exposure and marine radiocarbon records. Reducing E_{SSA}, which allows for the temporary ice shelf that fringes the EAIS outlet glaciers in the

early Holocene to last for a longer duration, also delays retreat and improves consistency with surface-exposure records of individual glaciers.

The Siple Coast grounding-line evolution and extent is sensitive to mantle viscosity and ϕ_{min}. A cooler ocean forcing paired with higher precipitation over WAIS during the Holocene improves the accuracy of the modern grounding-line configuration. The interaction between these model parameters and external forcings requires more exploration in order to understand grounding-line evolution in this region.

A key challenge in paleo-ice sheet modelling is the selection of model parameters and climate forcings that are representative of the given region. However, no perfect combination of model parameters or climate forcing exists, as local properties of the bed, solid Earth evolution, ice rheology and climate evolution can have large effects. These effects require consideration in model-proxy comparisons.

Chapter 6

Research Chapter Synthesis and Discussion

6.1 Research Chapter Synthesis

6.1.1 Deglacial evolution of Antarctic climate and the Southern Ocean

Since the Last Glacial Maximum (LGM), global climate has experienced a number of abrupt millennial-scale climate changes, including the glacial termination, Heinrich event 1, the Bølling Warm Period/Antarctic Cold Reversal (ACR), the Younger Dryas (YD), and the mid-Holocene optimum (Dansgaard et al., 1984; Alley and Clark, 1999; Menviel et al., 2011; He et al., 2013). Antarctic ice core records indicate continental warming associated with the glacial termination initiated at approximately 20 ka in West Antarctica, and ∼18 ka in East Antarctica (Buizert et al., 2015). This difference in timing has been suggested to be due to the closer proximity of West Antarctic ice core sites to circum-Antarctic sea ice (Fudge et al., 2013). The ACR cooling event interrupted deglacial surface warming in the Southern Hemisphere, lasting from ∼14.7 ka to ∼13.0 ka (Pedro et al., 2016), and was followed by pronounced warming into the early Holocene (Cuffey et al., 2016). During this time interval, rapid changes in global sea level occurred, including the Meltwater Pulse 1a event (Deschamps et al., 2012), and the potential Meltwater Pulse 1b event (Bard, Hamelin, and Delanghe-Sabatier, 2010). As discussed in Chapters 2 and 4, the precise timing and magnitudes of the isotopic changes associated with these millennial-scale climate changes differ among the Antarctic ice core records.

Notably, the timing of these events also differed between the Northern and Southern Hemispheres (Buizert et al., 2015), and it has been argued that freshwater forcing from glacial runoff of the melting ice sheets triggers a

"bipolar seesaw" pattern of climate change, in which cool (warm) climate events in the Northern Hemisphere are associated with warming (cooling) in Antarctica (Broecker, 1998; Pedro et al., 2011). Proxy records and climate models support the mechanism of freshwater-induced perturbations of Atlantic Meridional Overturning Circulation (AMOC) driving these interhemispheric climate changes during Dansgaard-Oeschger events (McManus et al., 2004; Liu et al., 2009; Menviel et al., 2011; Gottschalk et al., 2015). Changes in AMOC strength alter the meridional heat transport of both the ocean and the atmosphere (Markle et al., 2016). Climate feedbacks in the form of sea ice expansion and wind-driven upwelling and ventilation of CO_2 in the Southern Ocean have also been suggested to amplify the surface cooling during the ACR and the surface warming in the early Holocene, respectively (Anderson et al., 2009; Menviel, Spence, and England, 2015; Pedro et al., 2016).

In terms of the ocean and atmosphere forcing of the Antarctic Ice Sheet through the deglaciation, it is important to note that atmospheric and surface ocean temperatures evolve differently than ocean temperatures at intermediate depths and in the deep ocean (Elderfield et al., 2012). Meltwater fluxes into both the North Atlantic and Southern Ocean increase sea ice concentrations, but reduce the formation of North Atlantic Deep Water and Antarctic Bottom Water, respectively (Menviel et al., 2010; Menviel et al., 2011; He et al., 2013). In the transient climate model simulations examined in this thesis, freshwater forcing results in surface cooling over Antarctica, but subsurface ocean warming along the Antarctic coasts. Although the timing and durations of the temperature changes in the atmosphere and ocean differ between LOVECLIM DGns and TraCE-21ka in relation to differences in the prescribed freshwater forcings, both simulations capture the centennial-scale rates of change in Antarctic surface temperature recorded in ice core records. This suggests that the climate models may reasonably represent the relevant processes, and that improved paleo-constraints of deglacial meltwater fluxes are key to capturing the precise timing of abrupt climate changes in models.

The evolution of snow accumulation has generally scaled linearly with surface temperature over East Antarctica (Frieler et al., 2015), but more complex behaviour is indicated in the WAIS Divide (WDC) ice core record in West Antarctica following the ACR (Fudge et al., 2016). In particular, reconstructed snow accumulation decreases while surface temperature increases

during the early Holocene, in contrast to the expected thermodynamic scaling relationship. However, in the mid-to-late Holocene (8-0 ka), the accumulation-temperature scaling relationship is strongly positive (i.e., 17% °C^{-}1), and is much higher than the average of the East Antarctic ice cores (i.e., ∼5.9% °C^{-}1). As explained in Chapter 2, LOVECLIM DGns and TraCE-21ka are unable to capture this behaviour, which is likely driven by changes in atmospheric dynamics. Precipitation in West Antarctica is highly dependent on the strength and position of the Amundsen Sea Low (ASL), of which climate models are known to have biases (Hosking et al., 2013). Over the last deglaciation, changes in atmospheric teleconnections from the Northern Hemisphere and tropics have been suggested to influence West Antarctic climate by influencing ASL strength (Timmermann et al., 2010; Jones et al., 2018), but these mechanisms require further exploration (Lowry et al., 2019).

In the Ross Sea, the Roosevelt Island Climate Evolution (RICE) ice core exhibits Holocene isotopic signatures that are distinct from other ice core records located further inland, as discussed in Chapter 4. Specifically, the deuterium (δD) record of RICE is characterized by high Holocene variability with contrasting trends to the WDC record. While surface elevation changes may contribute to isotope changes in ice core records (Cuffey et al., 2016), the ice sheet model simulations show stabilization in the surface elevation of Roosevelt Island by the mid-Holocene (i.e. 7 ka). As a result, the simulations indicate that the isotopic variability and trends at RICE in the mid-to-late Holocene are climate-driven, and I also show that coastal regions of Antarctica are highly sensitive to changes in sea ice concentration and extent in the climate models (see Chapters 2 and 4). With the retreat of the ice sheet, precipitation and temperature at coastal ice core sites may therefore become more heavily influenced by local and regional sea ice variability.

6.1.2 Role of climate forcing on ice sheet retreat in the Ross Embayment

One of the main motivations of this thesis is the sparse paleoclimate record in Antarctica, which offers a limited number of potential deglacial climate forcings for ice sheet model simulations. Although the transient climate model simulations can provide a more complete interpretation of the regional climate evolution, they have their own biases with regard to uncertainties in boundary conditions and forcings, such as the prescribed freshwater forcings described above, as well as limitations in resolution, which may

be inadequate for some coastal regions (Lowry et al., 2019). In recognizing that each climate forcing has advantages and disadvantages, I apply a wide range of climate forcings in the ice sheet model ensemble. This is useful for identifying the competing influences of ocean and atmosphere forcings considering the differences in evolution in ocean and atmosphere temperatures, sea ice concentration and thickness, and precipitation through the millennial-scale events of the last deglaciation. In particular, I explore the interaction of the MWP-1A and ACR events, in which surface air temperatures decrease, sea ice thickens, and sub-surface ocean temperatures warm. In the Holocene, precipitation and surface temperature may or may not scale linearly, which has implications for ice sheet surface mass balance. Although each climate forcing is simplistic, the application of the various combinations of climate trajectories demonstrate the ice sheet sensitivity to each aspect.

The ice sheet model simulations discussed in Chapters 3 to 5 indicate that ocean and atmosphere forcing, in combination, are the primary controls on the timing of ice sheet retreat in the Ross Embayment, and secondarily influence the spatial pattern of grounding-line migration. Surface air temperatures in the early deglacial can enhance or diminish ice sheet responses to changes in sub-shelf melt rates and back pressure forcing in the eastern and western parts of the embayment. As a result, the grounding-line retreat resembles the "saloon-door" model of retreat discussed in McKay et al. (2016) and Lee et al. (2017) using a relatively cool ocean-atmosphere forcing combination, whereas relatively warm forcings yield a retreat pattern more similar to the "swinging-gate" model of Conway et al., (1999). The exception is in the western Ross Sea, adjacent to South Victoria Land (SVL), where the grounding-line migration is guided by the seafloor bathymetry, as shown in Chapter 5. As the main Ross Ice Shelf forms, the development of an ocean cavity underneath the ice shelf causes the sub-shelf melt rates to be the dominant control in grounding-line retreat along the Transantarctic Mountains and toward the Siple Coast. In the late Holocene, however, higher precipitation forcing, which increases WAIS ice thickness, can counteract grounding-line retreat of the Siple Coast.

Radiocarbon ages of marine sediments from the Ross Sea (McKay et al., 2016; Bart et al., 2018) and identification of subglacial landforms from multibeam bathymetry data (Halberstadt et al., 2016; Lee et al., 2017; Greenwood et al., 2018) suggest an asynchronous pattern of grounding-line retreat, in which earlier retreat occurred in the eastern embayment relative to the west. The ice sheet model simulations indicate that ocean forcing with elevated

sub-shelf melt rates during Heinrich event 1 or MWP-1A could prompt the early retreat suggested by Bart et al. (2018) in the eastern Ross Sea (ERS). Both transient climate simulations show that the addition of freshwater forcing into the Southern Ocean increases ocean temperatures at the depths of ice sheet grounding lines (Lowry et al., 2019), and full continent-scale deglacial simulations show early deglacial melting from the Antarctic Peninsula and outer Weddell Sea (Golledge et al., 2014). Following this initial ERS retreat, the grounding line was stabilized until the early Holocene (Bart et al., 2018), which could be explained by cooling surface air temperatures and reduced calving during the ACR.

Grounding-line retreat is thought to have occurred later in the western Ross Sea (WRS) relative to the ERS, driven in part by the abundance of ice rises that can stabilize the ice sheet (Simkins, Anderson, and Greenwood, 2016; Halberstadt et al., 2016). This is consistent with terrestrial ice thinning records from EAIS outlet glaciers that indicate an early-to-mid Holocene decline in ice thickness (Jones et al., 2015; Anderson et al., 2017; Goehring et al., 2019). Best agreement with the surface-exposure chronologies is observed with simulations forced with cool atmosphere and ocean forcing. The cool ocean forcing, derived from TraCE-21ka at a near-surface depth, has a decrease in sub-shelf melt rate anomalies following MWP-1A, in contrast to all other ocean forcings used in the simulations. It is important to reiterate that the ocean forcings are simplistic in that the basal melt rate anomalies are applied uniformly to all floating ice, and oceanic circulation is not taken into account. However, in the modern ocean circulation of the Ross Sea, enhanced freshwater flux from the ice shelf cavity leads to increased marine ice formation and sea ice stabilization in the WRS. Following MWP-1A, meltwater from the eastern and central embayment may have stabilized the ice sheet in the WRS through reduced sub-shelf melting and increased back pressure forcing.

It has recently been proposed that sea level forcing is the primary control of ice sheet retreat in the WRS, as the surface-exposure chronologies of glaciers in North Victoria Land (NVL) exhibit linear ice thinning, similar to global sea level records (Goehring et al., 2019). The ice sheet simulations in this thesis show that sea level forcing enhances the combined effects of ocean and atmosphere forcing, but alone cannot account for deglacial grounding line retreat in this region. The WRS is particularly sensitive to climate forcing, with a wide range in timing of modelled ice thinning in both NVL and SVL. Application of cool ocean and atmosphere forcing delays ice thinning, with

timing more consistent with Mackay Glacier and Mt Discovery ice thinning (Jones et al., 2015; Anderson et al., 2017), but the rate of ice thinning is more rapid than indicated by Tucker and Aviator Glaciers in SVL (Goehring et al., 2019). While this model-data discrepancy may be due to local geological conditions of individual glaciers that are not replicated in the model, ocean circulation may also be a contributing factor, as a more gradual decrease in back pressure or increase in sub-shelf melting would yield a regional ice sheet evolution that is more consistent with the records.

The simplicity of the precipitation forcing, which does not account for atmospheric circulation, is also likely to contribute to model-data discrepancies of both EAIS and WAIS. Modern climatology and shallow ice core analysis of RICE suggests that the late Holocene can be characterised by a dipole pattern of snow accumulation on the eastern and western sides of the embayment, potentially related to local sea ice conditions (Bertler et al., 2018). In addition to surface temperature, sea ice conditions in the Ross Sea depend on both the ocean circulation (Hellmer, 2004) as well as the local wind stress (Holland and Kwok, 2012). As a result, precipitation forcing derived from a scaling relationship to temperature or from a single ice core may fail to capture inter-basin differences in snow accumulation. In the late Holocene, the application of the WDC ACC precipitation forcing, which has higher precipitation through the Holocene than using a constant precipitation-temperature scaling relationship (see Chapter 5), produces a thicker WAIS that is more resistant to late Holocene grounding-line retreat. Therefore, precipitation forcing is an important component in the ice sheet grounding-line retreat history and these limitations require further consideration in comparisons between the model output and surface-exposure chronologies.

6.1.3 Modulators of ice sheet sensitivity to climate forcing

The physiography of the WRS has been suggested to be an important element in controlling the timing and pattern of grounding-line retreat, with a number of geological features on the seafloor indicating periods of ice sheet stability (Simkins, Anderson, and Greenwood, 2016; Anderson et al., 2019). In particular, large and small-scale grounding zone wedges (> 50 m and < 50 m, respectively), which are depositional features that form while the grounding line is stabilized, occur on the seafloor of this region (Halberstadt et al., 2016), in addition to isolated volcanic seamounts, which can act as ice sheet pinning points (Simkins, Anderson, and Greenwood, 2016). The direction

of past ice flow is indicated by mega-scale glacial lineations, which are interpreted as forming from till deformations underneath ice streams (Halberstadt et al., 2016). Reconstructions of post-LGM ice flow direction in the WRS form these mega-scale glacial lineations indicate ice flow from SVL glaciers, toward the central embayment (Lee et al., 2017), in contrast to the ice flow direction expected by the "swinging gate" scenario proposed by Conway et al. (1999). As a result, grounding-line retreat was likely more complex and dynamic in this region than previously thought.

The ice sheet model simulations discussed in this thesis are able to capture some of the complex retreat behaviour of the WRS. Although a grounding-line retreat pattern resembling the "swinging gate" model can be reproduced with warm ocean and atmosphere forcing for most of the embayment, the WRS by SVL is the exception, as the retreat always occurs from the central embayment and toward the EAIS outlet glaciers in this region. The simulated ice sheet remains grounded on Pennel Bank and Crary Bank into the Holocene, consistent with the sequence of retreat proposed by Halberstadt et al. (2016). However, some smaller-scale features are not reproduced, and the models generally show a more rapid and earlier retreat than expected by the EAIS outlet glaciers. While this may be due to issues with the ocean and back pressure forcings, as explained above, limitations in the seafloor bathymetry, which may fail to capture all ice pinning points, may also contribute. Although reducing the bed smoothing factor did not slow retreat in this area, it should be noted that the bedmap2 dataset, from which the bathymetry in the model is based, also has large data gaps and high uncertainties (Fretwell et al., 2013).

A model parameter that can decrease the sensitivity of the ice sheet response to climate forcing in the WRS is the E_{SSA} parameter. As stated in Chapter 5, E_{SSA} is an enhancement factor of the shallow shelf approximation component of the stress balance, which dominates in ice shelves and ice streams. Lower E_{SSA} values lead to reduced ice shelf and ice stream velocities and delayed retreat in the WRS, with a timing of ice thinning more consistent with the SVL surface-exposure chronologies. The ice in this region is derived from EAIS (Anderson et al., 2014a), which is characterized by a cooler and drier climate than WAIS (Lenaerts et al., 2012). Therefore, it can be expected that EAIS-derived ice has different rheological properties than WAIS-derived ice and a single value for the E_{SSA} parameter may be insufficient for representing both sides of the embayment. In addition to differences in climate forcing and seafloor bathymetry, E_{SSA} may also account for some

of the asynchronous retreat behaviour observed in the ERS and WRS. Additional constraints in the WRS, including estimations of atmosphere and ocean forcing, glaciological properties, and age controls of grounding-line retreat, are required, particularly because the model simulations are highly sensitive to model parameter and climate forcing selection in this region.

Another potential driver of the asynchronous retreat pattern between the ERS and WRS is the isostatic response of the solid Earth to an evolving ice sheet. Increasing the mantle viscosity term in the ice sheet models to >1e19 yields higher sensitivity to climate forcing, with a stronger, but later glacial isostatic adjustment. This may contribute to the differences between WAIS and EAIS grounding-line migration because the modern mantle viscosity is higher in the ERS than in the WRS (Whitehouse et al., 2019). Bart et al. (2018) suggest an early initial ice sheet retreat in the Whales Deep Basin based on marine radiocarbon ages. As suggested in Chapter 5, high mantle viscosity may have made the ice sheet more sensitive to sub-surface ocean warming resulting from melting of the Antarctic Peninsula and the mid-to-outer Weddell Sea (Golledge et al., 2014). The simulations with mantle viscosity 5e20 Pa s are consistent with the early retreat timing of Bart et al. (2018), as the ice sheet responds rapidly to early deglacial oceanic and atmospheric warming. However, these high mantle viscosity simulations do not reproduce the subsequent grounding-line stabilization on the outer-continental shelf, which marine radiocarbon ages indicate lasted until the early Holocene ($\sim$11.5 ka).

Based on finite radiocarbon ages measured from subglacial sediments underneath the ice streams of WAIS, Kingslake et al. (2018) proposed the earliest retreat scenario of any study thus far, in which the grounding-line retreated beyond the modern-day position along the Siple Coast by the early Holocene ($\sim$9.7 ka) and subsequently readvanced to its current position. The mechanism of this retreat-readvance scenario is the same as in the high mantle viscosity simulations, i.e., the ice sheet responds rapidly to deglacial climate forcing and isostatic rebound results in the Holocene readvance. As discussed in Chapter 3 and 5, the timing of this scenario is difficult to reconcile with marine radiocarbon ages and surface-exposure records from the Ross Embayment. In this thesis, I offer alternative mechanisms to the grounding-line retreat and readvance, as the Siple Coast grounding line becomes highly sensitive to both ocean and precipitation forcing in the mid-to-late Holocene. In combination with a high mantle viscosity, these climate forcings could account for this grounding-line behavior.

One of the main challenges in these ice sheet model simulations is that

there are a number of model parameters that influence ice sheet sensitivity to climate forcing that are applied uniformly to the entire embayment. The ice sheet model simulations clearly demonstrate that no combination of model parameter values and climate forcings can result in agreement of each individual proxy record. In this sense, the ice sheet model ensemble, with a total of 60 ice sheet simulations, is valuable because it highlights the effect of particular climate forcings and model parameters of different regions. While the external forcings are the drivers of ice sheet retreat, selection of individual model parameters can have a more significant impact than selection among the wide range of forcings by enhancing or diminishing ice sheet sensitivity to the forcings. For EAIS and WRS, ice rheological properties need consideration in addition to the climate forcings in the context of the deglacial ice sheet retreat. In contrast, for WAIS and ERS, the spatial heterogeneity of mantle viscosity and its effect on the solid Earth response to ice sheet retreat needs to be further explored, particularly as it relates to ocean and precipitation forcing in the mid-to-late Holocene.

6.2 Discussion

6.2.1 Future of the Ross Embayment

Projections for the sea level contribution of the Antarctic ice sheet vary significantly for the coming centuries, depending on both the emissions scenario and ice shelf parameterizations used in the ice sheet model (Edwards et al., 2019). The higher range estimates are from the ice sheet simulations of DeConto and Pollard (2016), which employ a parameterization for marine ice cliff instability (MICI). This scheme is based on observations of the rapid retreat of the Jakobshavn and Crane glaciers of Greenland and Antarctica, respectively, and calibrated to mid-Pliocene sea level estimations. Under the high emissions scenario of RCP 8.5, the Antarctic sea level contribution is 77 cm by 2100, with WAIS collapsing within 250 years (DeConto and Pollard, 2016). In this model, the Ross Ice Shelf collapses at approximately 2100, which is followed by rapid retreat of the Siple Coast grounding line over the subsequent decades. However, Edwards et al. (2019) note that the MICI mechanism is not necessary to simulate mid-Pliocene sea levels, and projections without the mechanism show lower Antarctic sea level contributions of <43 cm by 2100 (95th percentile). Even without the MICI mechanism, ice sheet models indicate the Ross Ice Shelf and Siple Coast grounding line are

vulnerable over centennial and millennial timescales for lower emissions scenarios of RCP 4.5 and RCP 6.0 (Golledge et al., 2015).

Previous ice sheet model projections have relied on ocean and atmosphere forcings derived from an individual climate model projection (e.g., DeConto and Pollard, 2016), or an ensemble mean of multiple climate model projections (e.g., Golledge et al., 2015; Golledge et al., 2019). However, individual CMIP5 models show large deviations in ocean temperature, precipitation, and atmosphere temperature evolution for different RCP scenarios. For example, the CMIP5 models of CCSM4 (Gent et al., 2011), MRI-CGCM3 (Yukimoto et al., 2012), and HadGEM2-ES (Jones et al., 2011) show divergent trajectories in annual ocean temperature changes in the Ross Sea at the depth of the ice shelf cavity (Fig 6.1). Differences are more significant between individual models rather than between the same model under different RCP scenarios (i.e., 4.5 and 8.5), with HadGEM2-ES showing substantial ocean warming of 0.8 to 1.6°C, CCSM4 showing relatively little change in ocean temperature, and MRI-CGCM3 showing ocean cooling of 0.5 to 0.7°C. Considering the sensitivity of the Siple Coast grounding line to small changes in sub-shelf melt rates in the late Holocene in the deglacial ice sheet simulations, forward projections using these ocean temperature trajectories would likely result in a high standard deviation of the Ross Embayment sea level contribution.

Atmosphere forcing in the form of surface air temperature and precipitation also show large differences between the three CMIP5 models (Fig 6.2 and 6.3), though the RCP scenario is a more important factor than in the case of ocean temperature. These climate variables are also noisier than ocean temperature, with especially high interannual variability in precipitation over the Ross sector of Antarctica. MRI-CGCM3, which shows ocean cooling at the depth of the ocean cavity, displays the greatest temperature and precipitation increases for the period between 2080-2100 for RCP 8.5. Palerme et al. (2017) demonstrate that CMIP5 models generally show increasing Antarctic precipitation, with a sea level compensation in surface mass balance of 2.5 to 8.5 cm. However, these three CMIP5 models show relatively modest increasing trends in precipitation for the Ross Sea sector, with significant surface warming of 4 to 7.5°C in the RCP 8.5 scenario. Although models indicate that sub-shelf melting was likely a primary driver of grounding-line retreat in the Holocene (see Chapter 3), these higher surface air temperatures may also increase surface melting of ice shelves, contributing to ice shelf disintegration, as has been suggested for the Larsen B ice shelf (Broeke, 2005).

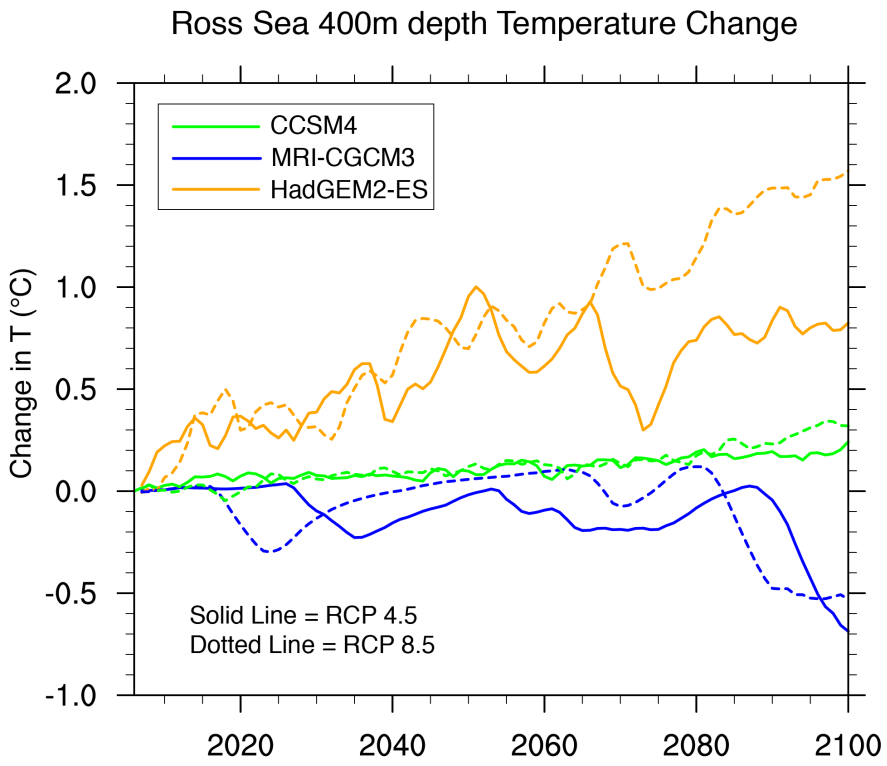

FIGURE 6.1: Projected ocean temperature anomalies at 400 m depth of the Ross Sea of three CMIP5 models for the RCP4.5 and RCP8.5 scenarios.

In addition to ocean temperature, precipitation, and surface air temperature, Antarctic sea ice concentration and extent are projected to decline in CMIP5 models (Palerme et al., 2017), although the models fail to capture the observed increase in Antarctic sea ice extent from the 1970s until recent years (Turner et al., 2013; Bracegirdle et al., 2015). The ice core records and climate models discussed in this thesis indicate that sea ice concentrations are related to Antarctic precipitation and temperature (Bertler et al., 2018; Lowry et al., 2019). Sea ice has also been discussed in terms of its effect on ocean temperatures and basal melting of ice shelves (Golledge et al., 2014; Stewart et al., 2019), as well as its stabilizing effect and relationship to calving (Robel, 2017), which is heuristically incorporated into the ice sheet model simulations of this thesis (see Chapter 3). As a result, changes in sea ice will likely influence the future ice sheet evolution in the Ross Embayment in a number of ways. Reductions in sea ice concentration and thickness in the Ross Sea may lead to increases in continental precipitation, basal and surface melting of ice shelves, and calving, but to attain accurate predictions the biases in CMIP5 models need to be addressed and a better understanding of the above processes is required.

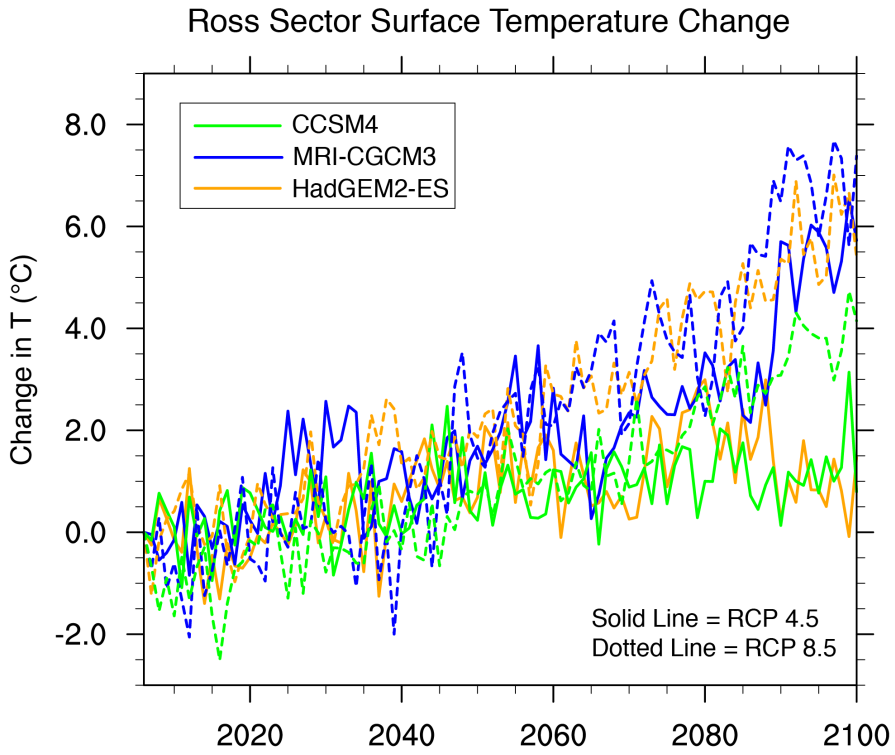

FIGURE 6.2: Projected continental surface temperature anomalies of three CMIP5 models for the RCP4.5 and RCP8.5 scenarios for the Ross sector of Antarctica.

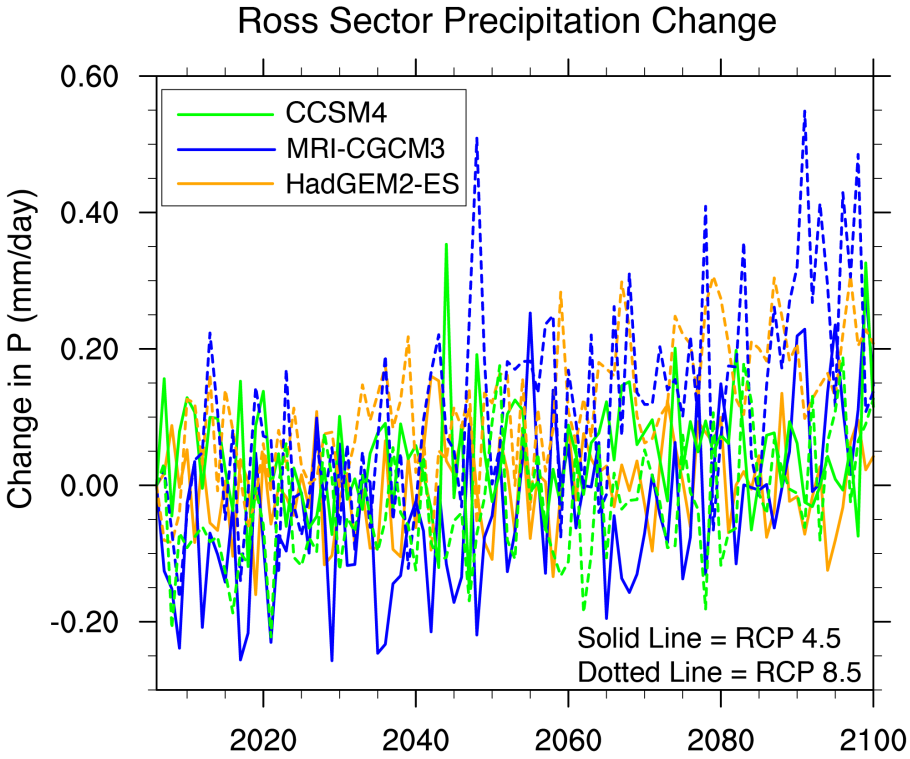

FIGURE 6.3: Projected continental precipitation anomalies of three CMIP5 models for the RCP4.5 and RCP8.5 scenarios for the Ross sector of Antarctica.

An important consideration in projecting ice sheet responses to these future climate forcings is the past climate forcing, which is another motivation for the paleo-ice sheet model simulations described in this thesis. In modelling experiments, Robel, Roe, and Haseloff (2018) demonstrate that the response rates of marine terminating glaciers to external forcings occur on both a fast timescale of decades to centuries and a slow timescale of millennia, and conclude that the future glacier changes will therefore depend on past climate changes. Bed slope is also a controlling factor, hence individual glaciers will respond in different ways to short- and long-term climate forcings. The ice sheet response to the millennial- and centennial-scale climate forcings in the deglacial simulations also show delays in different areas of the embayment, related to the ocean and atmosphere forcing combination and the physical model parameters. Projecting the response of the Ross Ice Shelf and the Siple Coast grounding line to future climate changes will therefore require both paleoclimate and geological constraints.

6.2.2 Intermodel comparisons and priorities for Antarctic Ice Sheet modelling

Considering differences in ice sheet model projections for the Greenland and Antarctic ice sheets, the community has prioritized intermodel comparisons to assess the causes of model spread and identify best practices (Bindschadler et al., 2013; Goelzer et al., 2018). For Antarctica, a recent intercomparison effort has been conducted to identify the effect of model initialization procedures on the ice sheet response to external forcings (Seroussi et al., 2019). This project is the first phase of the Ice Sheet Model Intercomparison Project 6 (ISMIP6), conducted in close coordination with the Coupled Model Intercomparison Project 6 (CMIP6), and is referred to as initMIP Antarctica. A total of 16 ice sheet modelling centers from around the world contributed 25 sets of ice sheet model simulations using different ice sheet models, initialization methods, and grounding line parameterizations. From these initial states, three 100 yr forward projections were performed using a simple surface mass balance anomaly forcing (asmb), a simple basal mass balance anomaly forcing (abmb), and no external forcing (ctrl). Details of the external forcings are described in Seroussi et al. (2019). These experiments highlight the key areas of disagreement between the models in terms of ice sheet responses to external forcings.

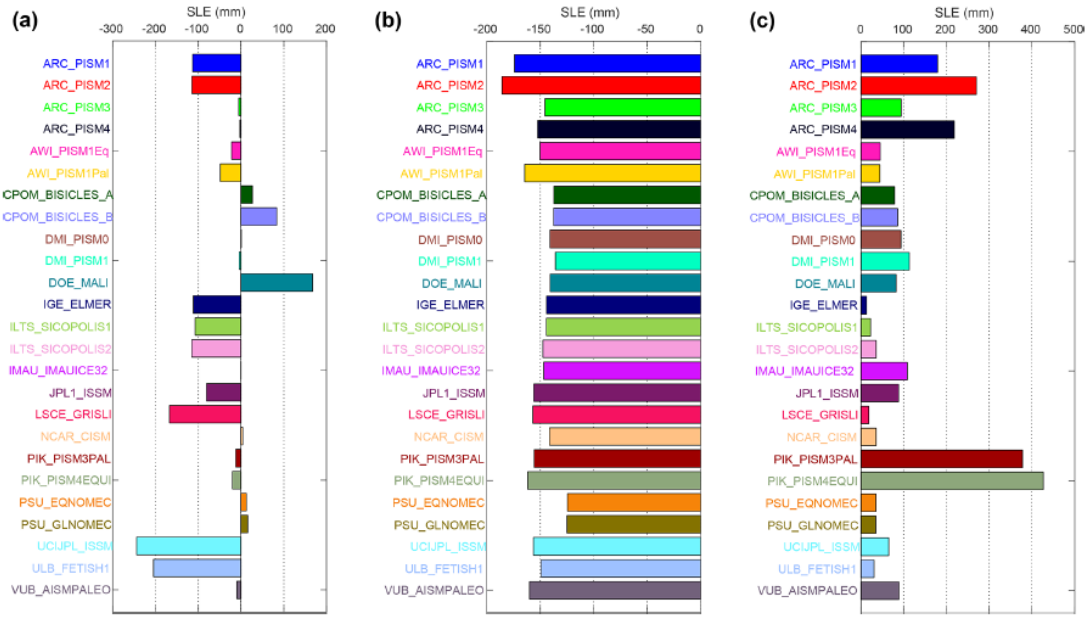

FIGURE 6.4: Sea level equivalent (SLE) mass changes of initMIP-Antarctica models for the (a) control experiment, (b) surface mass balance anomaly experiment, and (c) basal mass balance anomaly experiment (Fig 4 in Seroussi et al., 2019). Negative values indicate an increases in ice sheet mass.

In the ctrl experiment (i.e., no external forcing), the models vary between 243 mm of ice gain (sea level equivalent) and 167 mm of ice loss (Fig 6.4a). Of the 25 simulations, 14 show modest changes in ice sheet mass (<50 mm). Of the ice sheet models for which multiple simulations are performed, all simulations using PISM and SICOPOLIS show ice gain, whereas all simulations using the PSU and BISICLES show ice loss, regardless of the initialization procedure. The models show a consistent response in the asmb experiment, with a range of ice gain of 125-186 mm (Fig 6.4b). In contrast, the abmb experiment exhibits a much larger range of ice sheet change, with ice loss ranging from 13-486 mm (Fig 6.4c). For simulations using the same model and initialization procedure, the grounding line parameterization influences the ice sheet response to the external forcings. In Fig 6.4b and 6.4c, ARC-PISM-2 and ARC-PISM-4 are duplicate experiments of ARC-PISM-1 and ARC-PISM-3 in terms of the ice sheet spin-up procedure, but use a sub-grid-scale parameterization at the junction of grounded and floating ice that smoothes the basal shear stress field and tracks and interpolated grounding-line position through time. The application of this grounding-line scheme, which is also used in this thesis, yields a larger response to external forcing (red vs. blue bars and black vs green bars in Fig 6.4).

In terms of the spatial pattern of ice sheet changes due to external forcings, Fig 6.5 and 6.6 show the mean and standard deviations of ice thickness and horizontal velocity for the asmb and abmb experiments relative to the ctrl experiments, respectively. In the asmb experiments, much of the increase in ice thickness is concentrated along the Antarctic coasts (Fig 6.5a). Changes in horizontal velocity are mainly constrained to the ice shelves, with the Ross Ice Shelf increasing, but the Ronne Ice Shelf velocity decreasing (Fig 6.5b). The standard deviations of both parameters are low, with the exception of ice shelf velocity in some locations (Fig 6.5c,d). In comparison, the abmb experiments show substantial mean changes in both ice thickness and horizontal velocity of ice shelves (Fig 6.6a,b), but also high standard deviations (Fig 6.6c,d). The largest changes are associated with the Amundsen Sea coastline, however, the Ross Ice Shelf also shows high standard deviation of velocity (Fig 6.6d). Changes in the ice shelf area are also not consistent among the models in the abmb experiments (Fig 6.7), with approximately half of the simulations showing considerable decreases in ice shelf area, and others showing slight increases.

The experiments of initMIP Antarctica, which are not meant to be predictive, demonstrate that the key area of model disagreement is the ice shelf response to changes in basal melt. This is relevant to the findings of this thesis, as changes in sub-ice shelf melt rates are the primary control of grounding-line retreat in the Ross Embayment following ice shelf formation in the Holocene, but many different factors can influence ice sheet sensitivity to this forcing. In PISM, for example, I demonstrate that bed topography, mantle viscosity, till properties, and SIA and SSA enhancement factors strongly modulate the ice sheet response to deglacial ocean and atmosphere forcings. At present, large data gaps exist for the bed topography under Antarctica, as mentioned above (Fretwell et al., 2013), but the bed topography is one of the main controls on grounding-line and ice stream dynamics (Schoof, 2007; Jamieson et al., 2012). The other parameters are represented uniformly in PISM, but the spatial heterogeneity of these terms in reality is an important consideration for the development of future ice sheet models. The model simulations in this thesis and Kingslake et al. (2018) are highly sensitive to the mantle viscosity term, and recent observations of bedrock uplift suggest that the solid Earth response to WAIS mass changes is occurring on timescales relevant for ice sheet model projections (Barletta et al., 2018). Ice sheet models that lack bed deformation schemes or spatial heterogeneity in mantle viscosity may fail to capture this response.

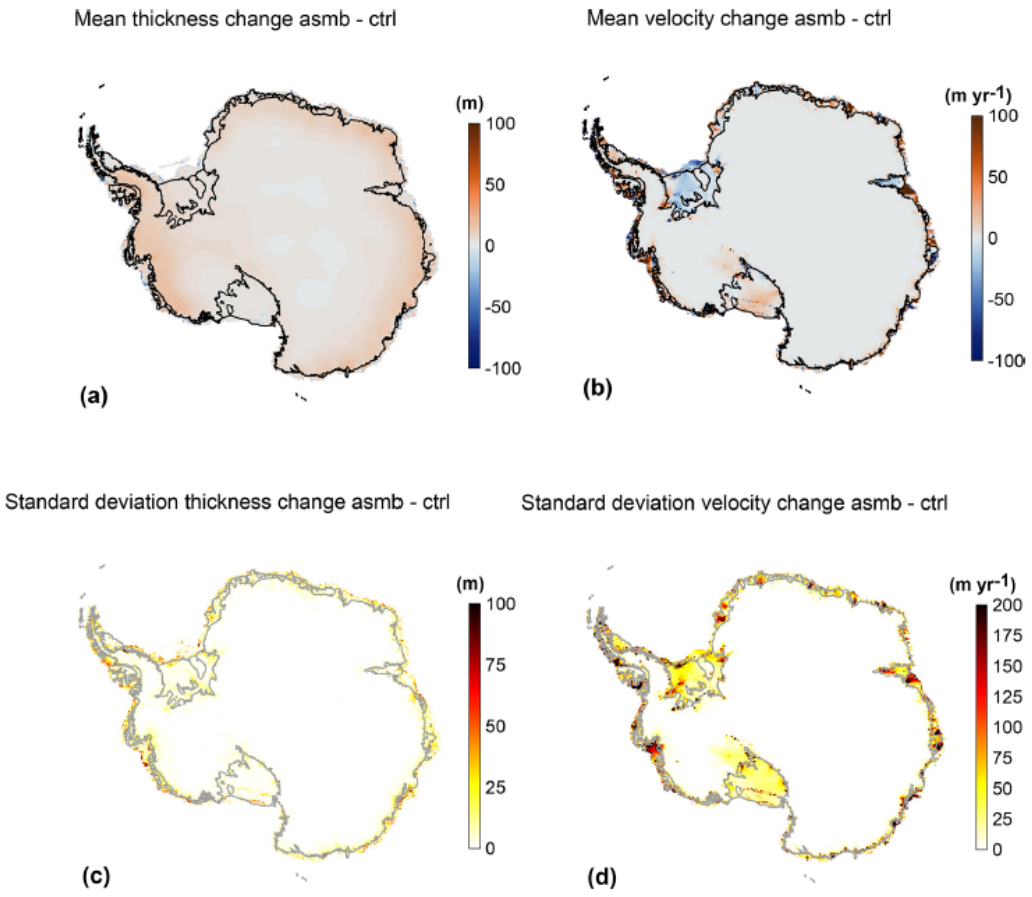

FIGURE 6.5: (a,b) Mean and (c,d) standard deviation of modelled ice thickness (m) and velocity (m yr^{-1}) change of the asmb experiment relative to the ctrl experiment of initMIP Antarctica (Fig 8 in Seroussi et al., 2019).

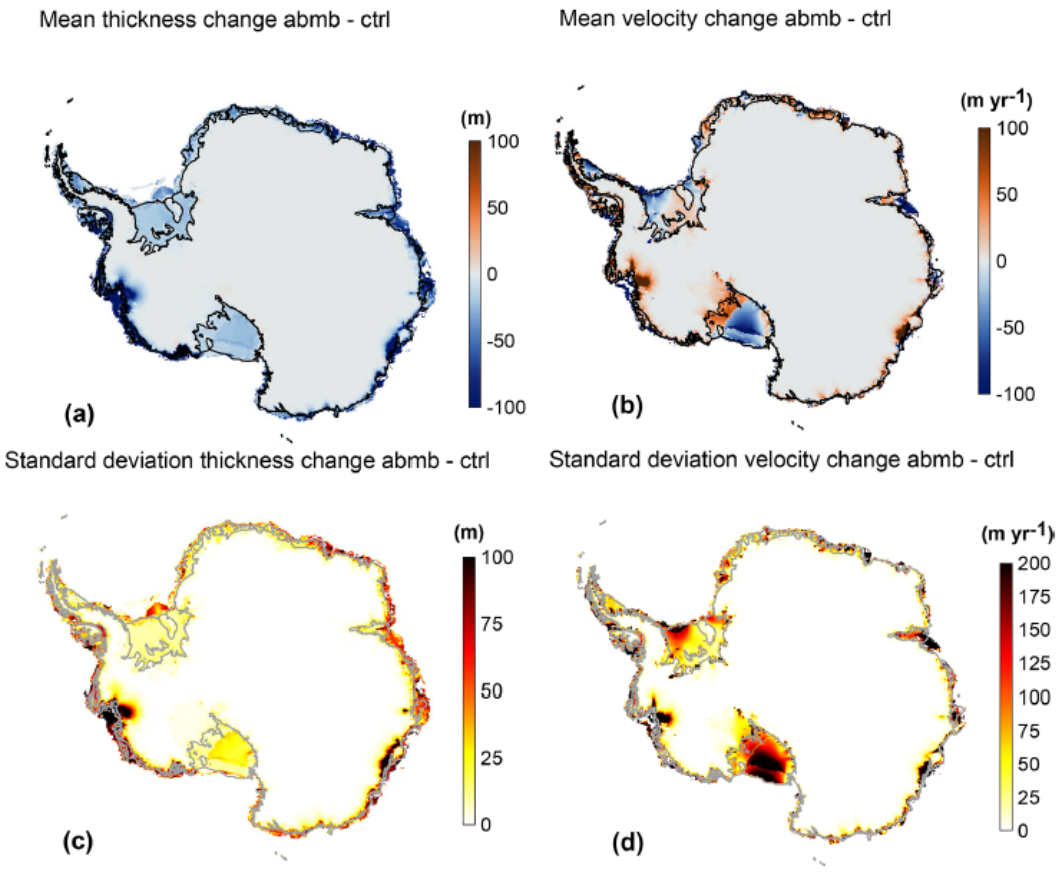

FIGURE 6.6: (a,b) Mean and (c,d) standard deviation of modelled ice thickness (m) and velocity (m yr^{-1}) change of the abmb experiment relative to the ctrl experiment of initMIP Antarctica (Fig 8 in Seroussi et al., 2019).

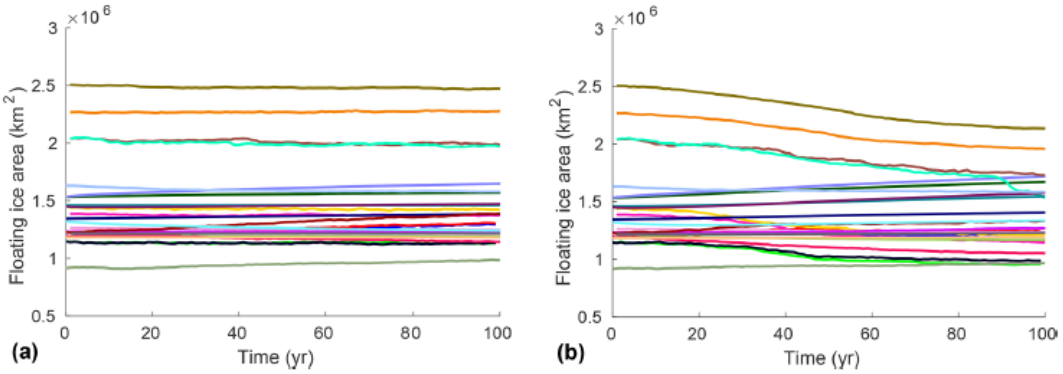

FIGURE 6.7: Evolution of ice shelf area (km^2) of the (a) ctrl and (b) abmb experiments of initMIP Antarctica (Fig 11 in Seroussi et al., 2019).

Best practices for sub-shelf melt, MICI and hydro-fracturing, and ice shelf calving parameterizations remain unclear (Pattyn et al., 2017; Edwards et al., 2019). While I use a simplified sub-shelf melt rate anomaly forcing scaled to reconstructed and modelled ocean temperature, more accuracy can be achieved with coupling to ocean circulation models (Seroussi et al., 2017). This coupling may be necessary for capturing important ice-ocean interactions and feedbacks as meltwater input from Antarctica into the Southern Ocean has been shown to create a positive feedback in ocean warming at the depths of modern grounding lines in climate models (Golledge et al., 2019). However, coupling of dynamic ice sheet models with Earth System Models is computationally expensive and will therefore limit the temporal and spatial scales of model simulations until computational capacity improves. In terms of the other parameterizations that influence calving, more observational data are required to better constrain MICI, hydro-fracturing and the buttressing effects of ice mélange and sea ice. In particular, the combination of MICI and hydro-fracturing parameterizations can have large impacts on Antarctic ice sheet projections (DeConto and Pollard, 2016), and inclusion of MICI strongly skews model distributions to higher values of projected sea level change (Edwards et al., 2019). Improving representation of these ice shelf processes in ice sheet models is therefore a primary concern in the community.

It is also important to note that previous intermodel comparisons of ice sheet models have focused on the responses to single surface mass balance and basal melt forcings (Bindschadler et al., 2013; Seroussi et al., 2019). However, climate models differ substantially in projections of ocean temperature, surface air temperature, precipitation, and sea ice concentration (see Figs 6.1-6.3), and deglacial paleoclimate reconstructions show large differences and have high uncertainties (see Chapter 2). A challenge in coordinating international intermodel comparison efforts is the time-intensive nature of performing the simulations, hence the number of simulations required to participate has generally been low. This thesis demonstrates the value in ice sheet model ensembles that use many combinations of ocean and atmosphere forcings to better explore ice sheet sensitivities to individual external forcings and quantify uncertainties from a spatial and temporal perspective. The ice sheet modelling community should prioritize these types of analysis, with emphasis on the climate sensitivity of specific ice sheet models and parameterizations of physical processes.

Chapter 7

Summary and Conclusions

The Ross Embayment, Antarctica's largest catchment, has experienced extensive grounding-line retreat since the Last Glacial Maximum. Understanding past grounding-line migration can help inform future sea level projections by constraining marine ice sheet sensitivities to changes in climatic conditions. However, a limited number of paleoclimate and geological constraints exist in this region, providing only an incomplete picture of the deglacial climate and ice sheet evolution in this region. In this thesis, I address this issue with analysis of the output of two deglacial climate model simulations and an ensemble of regional ice sheet model simulations, the specific conclusions of which are offered below.

In Chapter 2, I examine two transient climate model simulations of the last deglaciation in the context of the broader-scale Antarctic and Southern Ocean paleoclimate and paleoceanographic records. The analysis highlights the main strengths and limitations of the models in terms of climate variables that impact ice sheet mass balance and addresses the spatial and temporal gaps in the observational record. The models are able to capture centennial-scale rates of temperature and accumulation change as recorded in Antarctic ice core records. However, clear model-proxy differences are observed with regard to the timing and duration of the Antarctic Cold Reversal (ACR) and early Holocene warming. These discrepancies may be related to the representation of the timing, magnitude and locations deglacial meltwater forcings, which are applied in different ways due to limited paleo-constraints. This is consequential for the evolution of circum-Antarctic coastal ocean temperatures at grounding line depths, which is highly sensitive to the meltwater forcings.

In Chapter 3, I perform an ensemble of regional ice sheet model simulations for the last deglaciation using different combinations of ocean and

atmosphere forcings derived from the climate models and proxy records discussed in Chapter 2. This model ensemble addresses the conflicting interpretations of past grounding-line retreat in the Ross Embayment, which imply either extremely high or very low sensitivity of the ice sheet to external forcings. The simulations show earliest retreat in the central embayment and rapid terrestrial ice sheet thinning during the early Holocene. Early deglacial atmospheric conditions can enhance or diminish ice sheet sensitivity to rising ocean temperatures, thereby controlling the initial timing and spatial pattern of grounding-line retreat. Simulations using warm ocean forcing are more consistent with the early onset of retreat in the eastern Ross Sea indicated by marine radiocarbon ages, but those using cool atmosphere and ocean forcings generally reproduce the best overall agreement with the geological constraints of the grounding-line retreat in the western Ross Sea and terrestrial ice thinning. As the ocean cavity below the ice shelf expands through the Holocene, grounding-line position becomes highly sensitive to sub-shelf melt rates.

In Chapter 4, I analyze the climate model simulations discussed in Chapter 2 and the model ensemble of Chapter 3 to better constrain the stable isotope record of the Roosevelt Island Climate Evolution (RICE) ice core. Additional ice sheet model simulations using a RICE-specific climate forcing and WAIS-specific precipitation forcing are also performed. The models indicate that pronounced changes in sea ice and ice surface elevation occurred the Antarctic Cold Reversal and subsequently through the Younger Dryas when the climate in the Southern Hemisphere warmed. These changes in sea ice extent and ice surface elevation may therefore have contributed to changes in deuterium (δD) recorded in the ice core through this time interval. Using a RICE-specific climate forcing in regional ice sheet simulations yields a later, but more rapid retreat of the ice sheet grounding line in the Ross Embayment. Precipitation forcing is a key control on the magnitude and rate of grounding line retreat along the Siple Coast of West Antarctica in the late Holocene, a mechanism that requires further consideration in future Antarctic ice sheet projections.

In Chapter 5, I consider the influence of specific model parameters on the climate sensitivity of the ice sheet. I expand the regional ice sheet model ensemble with additional experiments that isolate parameters related to basal properties, glacial isostatic adjustment and ice rheology. The model ensemble shows that mantle viscosity, the material properties of the till, and an enhancement factor of the shallow shelf approximation (E_{SSA}) component of

the stress balance exhibit strong influences on the timing of ice sheet response to deglacial climate forcing, and may contribute to the asynchronous retreat behavior of the Eastern and Western Ross Sea. In particular, the Western Ross Sea is highly sensitive to both model parameter and climate forcing selection, and should therefore be prioritized as a location for paleo-constraints. Based on the differences between the simulations, it is clear that no perfect combination of model parameters or climate forcing exists, as local properties of the bed, solid Earth evolution, ice rheology and climate evolution can have outsized effects. These effects require consideration in ice sheet model-proxy comparisons.

The future of the Ross Embayment and the Antarctic Ice Sheet as a whole remains uncertain, depending on the extent to which regional atmospheric and oceanic temperatures increase. The model simulations discussed in this thesis indicate that ocean and atmosphere forcings were the primary controls on past ice sheet retreat in this region. This thesis also demonstrates that there is significant value in performing ice sheet model ensembles that use many combinations of ocean and atmosphere forcings to better explore ice sheet sensitivities to individual external forcings and quantify uncertainties from a spatial and temporal perspective. Geological constraints of the bed are paramount as basal properties strongly influence the sensitivity of the ice sheet to climate forcing, and the ice sheet model community should consider the spatial heterogeneity of mantle viscosity and other model parameters that are uniformly applied in models. Although it is computationally challenging, coupling of dynamic ice sheet models with Earth System Models should also be prioritized to more accurately represent ice-ocean interactions that are important for the global and regional climate evolution as well as ice sheet dynamics.

Bibliography

Abram, N.J. et al. (2007). "Ice core records as sea ice proxies: An evaluation from the Weddell Sea region of Antarctica". In: *Journal of Geophysical Research: Atmospheres* 112.D15.

Abram, N.J. et al. (2010). "Ice core evidence for a 20th century decline of sea ice in the Bellingshausen Sea, Antarctica". In: *Journal of Geophysical Research: Atmospheres* 115.D23.

Ackert, R.P. et al. (1999). "Measurements of past ice sheet elevations in interior West Antarctica". In: *Science* 286.5438, pp. 276–280.

Albrecht, T. et al. (2011). "Parameterization for subgrid-scale motion of ice-shelf calving fronts". In: *The Cryosphere* 5, pp. 35–44.

Alley, R.B. (2000). "The Younger Dryas cold interval as viewed from central Greenland". In: *Quaternary science reviews* 19.1-5, pp. 213–226.

Alley, R.B. and P.U. Clark (1999). "The deglaciation of the northern hemisphere: a global perspective". In: *Annual Review of Earth and Planetary Sciences* 27.1, pp. 149–182.

Alley, R.B. et al. (1986). "Deformation of till beneath ice stream B, West Antarctica". In: *Nature* 322.6074, p. 57.

Anderson, J.B. et al. (2014a). "Ross Sea paleo-ice sheet drainage and deglacial history during and since the LGM". In: *Quaternary Science Reviews* 100, pp. 31–54.

Anderson, J.B. et al. (2019). "Seismic and geomorphic records of Antarctic Ice Sheet evolution in the Ross Sea and controlling factors in its behaviour". In: *Geological Society, London, Special Publications* 475.1, pp. 223–240.

Anderson, J.T.H. et al. (2017). "Reconciling marine and terrestrial evidence for post LGM ice sheet retreat in southern McMurdo Sound, Antarctica". In: *Quaternary Science Reviews* 157, pp. 1–13.

Anderson, R.F. et al. (2009). "Wind-driven upwelling in the Southern Ocean and the deglacial rise in atmospheric CO2". In: *Science* 323.5920, pp. 1443–1448.

Anderson, R.F. et al. (2014b). "Biological response to millennial variability of dust and nutrient supply in the Subantarctic South Atlantic Ocean". In: *Phil. Trans. R. Soc. A* 372.2019, p. 20130054.

Andrews, J.T. et al. (1999). "Problems and possible solutions concerning radiocarbon dating of surface marine sediments, Ross Sea, Antarctica". In: *Quaternary Research* 52.2, pp. 206–216.

Argus, D.F. and W.R. Peltier (2010). "Constraining models of postglacial rebound using space geodesy: a detailed assessment of model ICE-5G (VM2) and its relatives". In: *Geophysical Journal International* 181.2, pp. 697–723.

Argus, D.F. et al. (2014). "The Antarctica component of postglacial rebound model ICE-6G_C (VM5a) based on GPS positioning, exposure age dating of ice thicknesses, and relative sea level histories". In: *Geophysical Journal International* 198.1, pp. 537–563.

Aschwanden, A., G Aðalgeirsdóttir, and C Khroulev (2013). "Hindcasting to measure ice sheet model sensitivity to initial states." In: *Cryosphere* 7.4.

Baggenstos, Daniel et al. (2018). "A horizontal ice core from Taylor Glacier, its implications for Antarctic climate history, and an improved Taylor Dome ice core time scale". In: *Paleoceanography and Paleoclimatology* 33.7, pp. 778–794.

Bakker, P. et al. (2017). "Centennial-scale Holocene climate variations amplified by Antarctic Ice Sheet discharge". In: *Nature* 541.7635, p. 72.

Bard, E., Bruno Hamelin, and Doriane Delanghe-Sabatier (2010). "Deglacial meltwater pulse 1B and Younger Dryas sea levels revisited with boreholes at Tahiti". In: *Science* 327.5970, pp. 1235–1237.

Barker, S. et al. (2009). "Interhemispheric Atlantic seesaw response during the last deglaciation". In: *Nature* 457.7233, p. 1097.

Barletta, V.R. et al. (2018). "Observed rapid bedrock uplift in Amundsen Sea Embayment promotes ice-sheet stability". In: *Science* 360.6395, pp. 1335–1339.

Bart, P.J. et al. (2018). "A centuries-long delay between a paleo-ice-shelf collapse and grounding-line retreat in the Whales Deep Basin, eastern Ross Sea, Antarctica". In: *Scientific reports* 8.1, p. 12392.

Beckmann, A. and H. Goosse (2003). "A parameterization of ice shelf–ocean interaction for climate models". In: *Ocean modelling* 5.2, pp. 157–170.

Bentley, M.J. et al. (2014). "A community-based geological reconstruction of Antarctic Ice Sheet deglaciation since the Last Glacial Maximum". In: *Quaternary Science Reviews* 100, pp. 1–9.

Bereiter, B. et al. (2018). "Mean global ocean temperatures during the last glacial transition". In: *Nature* 553.7686, p. 39.

Berger, A.L. (1978). "Long-Term Variations of Caloric Insolation Resulting from the Earth's Orbital Elements 1". In: *Quaternary research* 9.2, pp. 139–167.

Bertler, N.A.N. et al. (2018). "The Ross Sea Dipole-temperature, snow accumulation and sea ice variability in the Ross Sea region, Antarctica, over the past 2700 years". In: *Climate of the Past* 14.2, pp. 193–214.

Bindschadler, R.A. et al. (2013). "Ice-sheet model sensitivities to environmental forcing and their use in projecting future sea level (the SeaRISE project)". In: *Journal of Glaciology* 59.214, p. 195.

Bopp, L. et al. (2013). "Multiple stressors of ocean ecosystems in the 21st century: projections with CMIP5 models". In: *Biogeosciences* 10, pp. 6225–6245.

Borchers, B. et al. (2016). "Geological calibration of spallation production rates in the CRONUS-Earth project". In: *Quaternary Geochronology* 31, pp. 188–198.

Bova, S.C., T.D. Herbert, and M.A. Altabet (2018). "Ventilation of Northern and Southern Sources of Aged Carbon in the Eastern Equatorial Pacific During the Younger Dryas Rise in Atmospheric CO2". In: *Paleoceanography and Paleoclimatology* 33.11, pp. 1151–1168.

Bracegirdle, T.J. et al. (2015). "The importance of sea ice area biases in 21st century multimodel projections of Antarctic temperature and precipitation". In: *Geophysical Research Letters* 42.24, pp. 10–832.

Braconnot, P. et al. (2012). "Evaluation of climate models using palaeoclimatic data". In: *Nature Climate Change* 2.6, p. 417.

Brady, E.C. et al. (2013). "Sensitivity to glacial forcing in the CCSM4". In: *Journal of Climate* 26.6, pp. 1901–1925.

Briegleb, P. et al. (2004). "Scientific description of the sea ice component in the Community Climate System Model, Version 3". In:

Broecker, W.S. (1998). "Paleocean circulation during the last deglaciation: a bipolar seesaw?" In: *Paleoceanography* 13.2, pp. 119–121.

Broeke, M. van den (2005). "Strong surface melting preceded collapse of Antarctic Peninsula ice shelf". In: *Geophysical Research Letters* 32.12.

Brook, E.J. et al. (2005). "Timing of millennial-scale climate change at Siple Dome, West Antarctica, during the last glacial period". In: *Quaternary Science Reviews* 24.12-13, pp. 1333–1343.

Bueler, E. and J. Brown (2009). "Shallow shelf approximation as a "sliding law" in a thermomechanically coupled ice sheet model". In: *Journal of Geophysical Research: Earth Surface* 114.F3.

Bueler, E.D., Craig S Lingle, and Jed Brown (2007). "Fast computation of a viscoelastic deformable Earth model for ice-sheet simulations". In: *Annals of Glaciology* 46, pp. 97–105.

Buizert, C. et al. (2015). "Precise interpolar phasing of abrupt climate change during the last ice age". In: *Nature* 520.7549, p. 661.

Calov, R. et al. (2018). "Simulation of the future sea level contribution of Greenland with a new glacial system model". In: *The Cryosphere* 12, pp. 3097–3121.

Calvo, E. et al. (2007). "Antarctic deglacial pattern in a 30 kyr record of sea surface temperature offshore South Australia". In: *Geophysical Research Letters* 34.13.

Caniupán, M. et al. (2011). "Millennial-scale sea surface temperature and Patagonian Ice Sheet changes off southernmost Chile (53 S) over the past 60 kyr". In: *Paleoceanography* 26.3.

Cavitte, M.G.P. et al. (2018). "Accumulation patterns around Dome C, East Antarctica, in the last 73 kyr". In: *The Cryosphere* 12.4, pp. 1401–1414.

Church, J.A. et al. (2013). "Climate change 2013: the physical science basis. Contribution of Working Group I to the Fifth Assessment Report of the Intergovernmental Panel on Climate Change". In: *Sea level change*, pp. 1137–1216.

Clark, P.U. et al. (2009). "The last glacial maximum". In: *science* 325.5941, pp. 710–714.

Colleoni, F. et al. (2018). "Past continental shelf evolution increased Antarctic ice sheet sensitivity to climatic conditions". In: *Scientific reports* 8.1, p. 11323.

Collins, W.D. et al. (2006). "The community climate system model version 3 (CCSM3)". In: *Journal of Climate* 19.11, pp. 2122–2143.

Conway, H. et al. (1999). "Past and future grounding-line retreat of the West Antarctic Ice Sheet". In: *Science* 286.5438, pp. 280–283.

Crosta, X. et al. (2018). "Ocean as the main driver of Antarctic ice sheet retreat during the Holocene". In: *Global and Planetary Change* 166, pp. 62–74.

Cuffey, K.M. et al. (2016). "Deglacial temperature history of West Antarctica". In: *Proceedings of the National Academy of Sciences* 113.50, pp. 14249–14254.

Curran, M. AJ et al. (2003). "Ice core evidence for Antarctic sea ice decline since the 1950s". In: *Science* 302.5648, pp. 1203–1206.

Danabasoglu, G. et al. (2012). "The CCSM4 ocean component". In: *Journal of Climate* 25.5, pp. 1361–1389.

Dansgaard, W. et al. (1984). "North Atlantic climatic oscillations revealed by deep Greenland ice cores". In: *Climate processes and climate sensitivity* 29, pp. 288–298.

DeConto, R.M. and D. Pollard (2016). "Contribution of Antarctica to past and future sea-level rise". In: *Nature* 531.7596, p. 591.

Delaygue, G. et al. (2000). "The origin of Antarctic precipitation: a modelling approach". In: *Tellus B* 52.1, pp. 19–36.

Denton, G.H. et al. (2010). "The last glacial termination". In: *science* 328.5986, pp. 1652–1656.

Depoorter, M.A. et al. (2013). "Calving fluxes and basal melt rates of Antarctic ice shelves". In: *Nature* 502.7469, p. 89.

Deschamps, P. et al. (2012). "Ice-sheet collapse and sea-level rise at the Bølling warming 14,600 years ago". In: *Nature* 483.7391, p. 559.

Downes, S.M. and Andrew McC Hogg (2013). "Southern Ocean circulation and eddy compensation in CMIP5 models". In: *Journal of Climate* 26.18, pp. 7198–7220.

Driesschaert, E. et al. (2007). "Modeling the influence of Greenland ice sheet melting on the Atlantic meridional overturning circulation during the next millennia". In: *Geophysical Research Letters* 34.10.

Edwards, T.L. et al. (2019). "Revisiting Antarctic ice loss due to marine ice-cliff instability". In: *Nature* 566.7742, p. 58.

Elderfield, H. et al. (2012). "Evolution of ocean temperature and ice volume through the mid-Pleistocene climate transition". In: *Science* 337.6095, pp. 704–709.

Emanuelsson, B.D. et al. (2014). "High-resolution continuous-flow analysis setup for water isotopic measurement from ice cores using laser spectroscopy". In: *Atmospheric Measurement Techniques* 8.7, pp. 2869–2883.

Emanuelsson, B.D. et al. (2018). "The role of Amundsen–Bellingshausen Sea anticyclonic circulation in forcing marine air intrusions into West Antarctica". In: *Climate dynamics* 51.9-10, pp. 3579–3596.

Erb, M.P. et al. (2018). "Model evidence for a seasonal bias in Antarctic ice cores". In: *Nature communications* 9.1, p. 1361.

Farneti, R. and T.L. Delworth (2010). "The role of mesoscale eddies in the remote oceanic response to altered Southern Hemisphere winds". In: *Journal of Physical Oceanography* 40.10, pp. 2348–2354.

Favier, L. et al. (2014). "Retreat of Pine Island Glacier controlled by marine ice-sheet instability". In: *Nature Climate Change* 4.2, p. 117.

Feldmann, J. et al. (2014). "Resolution-dependent performance of grounding line motion in a shallow model compared with a full-Stokes model according to the MISMIP3d intercomparison". In: *Journal of Glaciology* 60.220, pp. 353–360.

Fretwell, P. et al. (2013). "Bedmap2: improved ice bed, surface and thickness datasets for Antarctica". In: *The Cryosphere* 7.1, pp. 375–393.

Frieler, K. et al. (2015). "Consistent evidence of increasing Antarctic accumulation with warming". In: *Nature Climate Change* 5.4, p. 348.

Fudge, T.J. et al. (2013). "Onset of deglacial warming in West Antarctica driven by local orbital forcing". In: *Nature* 500.7463, p. 440.

Fudge, T.J. et al. (2016). "Variable relationship between accumulation and temperature in West Antarctica for the past 31,000 years". In: *Geophysical Research Letters* 43.8, pp. 3795–3803.

Gent, P.R. and James C Mcwilliams (1990). "Isopycnal mixing in ocean circulation models". In: *Journal of Physical Oceanography* 20.1, pp. 150–155.

Gent, P.R. et al. (1995). "Parameterizing eddy-induced tracer transports in ocean circulation models". In: *Journal of Physical Oceanography* 25.4, pp. 463–474.

Gent, P.R. et al. (2011). "The community climate system model version 4". In: *Journal of Climate* 24.19, pp. 4973–4991.

Genthon, G. et al. (1987). "Vostok ice core: climatic response to CO2 and orbital forcing changes over the last climatic cycle". In: *Nature* 329.6138, p. 414.

Gersonde, R. et al. (2005). "Sea-surface temperature and sea ice distribution of the Southern Ocean at the EPILOG Last Glacial Maximum—a circum-Antarctic view based on siliceous microfossil records". In: *Quaternary Science Reviews* 24.7, pp. 869–896.

Goehring, B.M. et al. (2019). "Late-glacial grounding line retreat in the northern Ross Sea, Antarctica". In: *Geology* 47.4, pp. 291–294.

Goelzer, H. et al. (2018). "Design and results of the ice sheet model initialisation initMIP-Greenland: an ISMIP6 intercomparison". In: *The Cryosphere* 12.4, pp. 1433–1460.

Golledge, N.R. et al. (2012). "Dynamics of the last glacial maximum Antarctic ice-sheet and its response to ocean forcing". In: *Proceedings of the National Academy of Sciences* 109.40, pp. 16052–16056.

Golledge, N.R. et al. (2013). "Glaciology and geological signature of the Last Glacial Maximum Antarctic ice sheet". In: *Quaternary Science Reviews* 78, pp. 225–247.

Golledge, N.R. et al. (2014). "Antarctic contribution to meltwater pulse 1A from reduced Southern Ocean overturning". In: *Nature communications* 5, p. 5107.

Golledge, N.R. et al. (2015). "The multi-millennial Antarctic commitment to future sea-level rise". In: *Nature* 526.7573, p. 421.

Golledge, N.R. et al. (2017). "East Antarctic ice sheet most vulnerable to Weddell Sea warming". In: *Geophysical Research Letters* 44.5, pp. 2343–2351.

Golledge, N.R. et al. (2019). "Global environmental consequences of twenty-first-century ice-sheet melt". In: *Nature* 566.7742, p. 65.

Goosse, H. et al. (2007). "Information on the early Holocene climate constrains the summer sea ice projections for the 21st century". In: *Climate of the Past* 3.4, pp. 683–692.

Goosse, H. et al. (2010). "Description of the Earth system model of intermediate complexity LOVECLIM version 1.2". In: *Geoscientific Model Development* 3, pp. 603–633.

Goosse, H. et al. (2012). "Antarctic temperature changes during the last millennium: evaluation of simulations and reconstructions". In: *Quaternary Science Reviews* 55, pp. 75–90.

Gottschalk, J. et al. (2015). "Abrupt changes in the southern extent of North Atlantic Deep Water during Dansgaard–Oeschger events". In: *Nature geoscience* 8.12, p. 950.

Greenwood, S.L. et al. (2018). "Holocene reconfiguration and readvance of the East Antarctic Ice Sheet". In: *Nature communications* 9.

Gregoire, L.J. et al. (2016). "Abrupt Bølling warming and ice saddle collapse contributions to the Meltwater Pulse 1a rapid sea level rise". In: *Geophysical research letters* 43.17, pp. 9130–9137.

Halberstadt, A.R.W. et al. (2016). "Past ice-sheet behaviour: retreat scenarios and changing controls in the Ross Sea, Antarctica". In: *The Cryosphere* 10.3, p. 1003.

Hargreaves, J.C. et al. (2013). "Skill and reliability of climate model ensembles at the Last Glacial Maximum and mid-Holocene". In: *Climate of the Past* 9.2, pp. 811–823.

He, F. (2011). *Simulating transient climate evolution of the last deglaciation with CCSM 3*. Vol. 72. 10.

He, F. et al. (2013). "Northern Hemisphere forcing of Southern Hemisphere climate during the last deglaciation". In: *Nature* 494.7435, p. 81.

Hellmer, H.H. (2004). "Impact of Antarctic ice shelf basal melting on sea ice and deep ocean properties". In: *Geophysical Research Letters* 31.10.

Herron, M.M. and Chester C Langway (1980). "Firn densification: an empirical model". In: *Journal of Glaciology* 25.93, pp. 373–385.

Holland, P.R. and R. Kwok (2012). "Wind-driven trends in Antarctic sea-ice drift". In: *Nature Geoscience* 5.12, p. 872.

Holloway, M.D. et al. (2016). "Antarctic last interglacial isotope peak in response to sea ice retreat not ice-sheet collapse". In: *Nature communications* 7, p. 12293.

Horgan, H.J. et al. (2017). "Poststagnation Retreat of Kamb Ice Stream's Grounding Zone". In: *Geophysical Research Letters* 44.19, pp. 9815–9822.

Horton, B.P. et al. (2014). "Expert assessment of sea-level rise by AD 2100 and AD 2300". In: *Quaternary Science Reviews* 84, pp. 1–6.

Hosking, J.S. et al. (2013). "The influence of the Amundsen–Bellingshausen Seas low on the climate of West Antarctica and its representation in coupled climate model simulations". In: *Journal of Climate* 26.17, pp. 6633–6648.

Hulbe, C.L. et al. (2016). "Flow variability and ongoing margin shifts on Bindschadler and MacAyeal Ice Streams, West Antarctica". In: *Journal of Geophysical Research: Earth Surface* 121.2, pp. 283–293.

Huybrechts, P. (1990). "A 3-D model for the Antarctic ice sheet: a sensitivity study on the glacial-interglacial contrast". In: *Climate Dynamics* 5.2, pp. 79–92.

Jamieson, S. SR et al. (2012). "Ice-stream stability on a reverse bed slope". In: *Nature Geoscience* 5.11, p. 799.

Jones, C.D. et al. (2011). "The HadGEM2-ES implementation of CMIP5 centennial simulations". In: *Geoscientific Model Development* 4.3, pp. 543–570.

Jones, J.M. et al. (2016). "Assessing recent trends in high-latitude Southern Hemisphere surface climate". In: *Nature Climate Change* 6.10, p. 917.

Jones, R.S. et al. (2015). "Rapid Holocene thinning of an East Antarctic outlet glacier driven by marine ice sheet instability". In: *Nature communications* 6, p. 8910.

Jones, R.S. et al. (2019). "Impact of glacial isostatic adjustment on cosmogenic surface-exposure dating". In: *Quaternary Science Reviews*.

Jones, T.R. et al. (2018). "Southern Hemisphere climate variability forced by Northern Hemisphere ice-sheet topography". In: *Nature* 554.7692, p. 351.

Joos, F. and R. Spahni (2008). "Rates of change in natural and anthropogenic radiative forcing over the past 20,000 years". In: *Proceedings of the National Academy of Sciences* 105.5, pp. 1425–1430.

Joughin, I., R.B. Alley, and D.M. Holland (2012). "Ice-sheet response to oceanic forcing". In: *Science* 338.6111, pp. 1172–1176.

Joughin, I., B.E. Smith, and B. Medley (2014). "Marine ice sheet collapse potentially under way for the Thwaites Glacier Basin, West Antarctica". In: *Science* 344.6185, pp. 735–738.

Jouzel, J. et al. (1997). "Validity of the temperature reconstruction from water isotopes in ice cores". In: *Journal of Geophysical Research: Oceans* 102.C12, pp. 26471–26487.

Jouzel, J. et al. (2003). "Magnitude of isotope/temperature scaling for interpretation of central Antarctic ice cores". In: *Journal of Geophysical Research: Atmospheres* 108.D12.

Jouzel, J. et al. (2007). "Orbital and millennial Antarctic climate variability over the past 800,000 years". In: *science* 317.5839, pp. 793–796.

Kaiser, J., F. Lamy, and D. Hebbeln (2005). "A 70-kyr sea surface temperature record off southern Chile (Ocean Drilling Program Site 1233)". In: *Paleoceanography* 20.4.

Keller, E.D. et al. (2018). "Calculating uncertainty for the RICE ice core continuous flow analysis water isotope record". In: *Atmospheric Measurement Techniques* 11.8, pp. 4725–4736.

Kingslake, J. et al. (2014). "Full-depth englacial vertical ice sheet velocities measured using phase-sensitive radar". In: *Journal of Geophysical Research: Earth Surface* 119.12, pp. 2604–2618.

Kingslake, J. et al. (2018). "Extensive retreat and re-advance of the West Antarctic ice sheet during the Holocene". In: *Nature* 558.7710, p. 430.

Kohfeld, K.E. et al. (2013). "Southern Hemisphere westerly wind changes during the Last Glacial Maximum: paleo-data synthesis". In: *Quaternary Science Reviews* 68, pp. 76–95.

Kopp, R.E. et al. (2014). "Probabilistic 21st and 22nd century sea-level projections at a global network of tide-gauge sites". In: *Earth's future* 2.8, pp. 383–406.

Küttel, M. et al. (2012). "Seasonal climate information preserved in West Antarctic ice core water isotopes: relationships to temperature, large-scale circulation, and sea ice". In: *Climate Dynamics* 39.7-8, pp. 1841–1857.

Lambeck, K. et al. (2014). "Sea level and global ice volumes from the Last Glacial Maximum to the Holocene". In: *Proceedings of the National Academy of Sciences* 111.43, pp. 15296–15303.

Le Brocq, A.M., A.J. Payne, and A. Vieli (2010). "An improved Antarctic dataset for high resolution numerical ice sheet models (ALBMAP v1)." In: *Earth system science data.* 2.2, pp. 247–260.

Leduc, G. et al. (2010). "Holocene and Eemian sea surface temperature trends as revealed by alkenone and Mg/Ca paleothermometry". In: *Quaternary Science Reviews* 29.7, pp. 989–1004.

Lee, J.E. et al. "An 83,000 year old ice core from Roosevelt Island, Ross Sea, Antarctica". In:

Lee, J.I. et al. (2017). "Widespread persistence of expanded East Antarctic glaciers in the southwest Ross Sea during the last deglaciation". In: *Geology* 45.5, pp. 403–406.

Lenaerts, J.T.M. et al. (2012). "A new, high-resolution surface mass balance map of Antarctica (1979–2010) based on regional atmospheric climate modeling". In: *Geophysical Research Letters* 39.4.

Levermann, A. et al. (2012). "Kinematic first-order calving law implies potential for abrupt ice-shelf retreat". In: *The Cryosphere* 6, pp. 273–286.

Levine, J.G. et al. (2014). "Sea salt as an ice core proxy for past sea ice extent: A process-based model study". In: *Journal of Geophysical Research: Atmospheres* 119.9, pp. 5737–5756.

Lisiecki, L.E. and M.E. Raymo (2005). "A Pliocene-Pleistocene stack of 57 globally distributed benthic δ18O records". In: *Paleoceanography* 20.1.

Liu, Z. et al. (2009). "Transient simulation of last deglaciation with a new mechanism for Bølling-Allerød warming". In: *Science* 325.5938, pp. 310–314.

Liu, Z. et al. (2014). "The Holocene temperature conundrum". In: *Proceedings of the National Academy of Sciences* 111.34, E3501–E3505.

Lorius, C. et al. (1985). "A 150,000-year climatic record from Antarctic ice". In: *Nature* 316.6029, p. 591.

Lowry, D.P. et al. (2019). "Deglacial evolution of regional Antarctic climate and Southern Ocean conditions in transient climate simulations". In: *Climate of the Past* 15.1, pp. 189–215.

Mackintosh, A. et al. (2011). "Retreat of the East Antarctic ice sheet during the last glacial termination". In: *Nature Geoscience* 4.3, p. 195.

Mandeno, D. et al. (2013). "Ice coring at Roosevelt Island: Drill design, performance and refrigeration solutions at a low altitude'warm coastal'Antarctic location". In: *7th International Workshop on Ice Core Drilling Technology, Pyle Centre, University of Wisconsin, Madison, USA*.

Markle, B.R. et al. (2016). *Global atmospheric teleconnections during Dansgaard-Oeschger events, Nat. Geosci., 10, 36–40*.

Martin, M.A. et al. (2011). "The Potsdam Parallel Ice Sheet Model (PISM-PIK)–Part 2: Dynamic equilibrium simulation of the Antarctic ice sheet". In: *The Cryosphere* 5.3, pp. 727–740.

Matsuoka, K. et al. (2015). "Antarctic ice rises and rumples: Their properties and significance for ice-sheet dynamics and evolution". In: *Earth-science reviews* 150, pp. 724–745.

McKay, R. et al. (2016). "Antarctic marine ice-sheet retreat in the Ross Sea during the early Holocene". In: *Geology* 44.1, pp. 7–10.

McManus, J.F. et al. (2004). "Collapse and rapid resumption of Atlantic meridional circulation linked to deglacial climate changes". In: *Nature* 428.6985, p. 834.

Medley, B. et al. (2013). "Airborne-radar and ice-core observations of annual snow accumulation over Thwaites Glacier, West Antarctica confirm the spatiotemporal variability of global and regional atmospheric models". In: *Geophysical Research Letters* 40.14, pp. 3649–3654.

Menviel, L., P Spence, and MH England (2015). "Contribution of enhanced Antarctic Bottom Water formation to Antarctic warm events and millennial-scale atmospheric CO2 increase". In: *Earth and Planetary Science Letters* 413, pp. 37–50.

Menviel, L. et al. (2010). "Climate and biogeochemical response to a rapid melting of the West Antarctic Ice Sheet during interglacials and implications for future climate". In: *Paleoceanography and Paleoclimatology* 25.4.

Menviel, L. et al. (2011). "Deconstructing the Last Glacial termination: the role of millennial and orbital-scale forcings". In: *Quaternary Science Reviews* 30.9-10, pp. 1155–1172.

Menviel, L. et al. (2014). "Hindcasting the continuum of Dansgaard–Oeschger variability: mechanisms, patterns and timing". In: *Climate of the Past* 10.1, pp. 63–77.

Menviel, L. et al. (2018). "Southern Hemisphere westerlies as a driver of the early deglacial atmospheric CO 2 rise". In: *Nature communications* 9.1, p. 2503.

Mercer, J.H. (1978). "West Antarctic ice sheet and CO2 greenhouse effect: a threat of disaster". In: *Nature* 271.5643, p. 321.

Monnin, E. et al. (2001). "Atmospheric CO2 concentrations over the last glacial termination". In: *Science* 291.5501, pp. 112–114.

Mulvaney, R. et al. (2012). "Recent Antarctic Peninsula warming relative to Holocene climate and ice-shelf history". In: *Nature* 489.7414, p. 141.

Noone, D. and I. Simmonds (2004). "Sea ice control of water isotope transport to Antarctica and implications for ice core interpretation". In: *Journal of Geophysical Research: Atmospheres* 109.D7.

Pahnke, K. et al. (2003). "340,000-year centennial-scale marine record of Southern Hemisphere climatic oscillation". In: *Science* 301.5635, pp. 948–952.

Palerme, C. et al. (2017). "Evaluation of current and projected Antarctic precipitation in CMIP5 models". In: *Climate dynamics* 48.1-2, pp. 225–239.

Palm, S.P. et al. (2017). "Blowing snow sublimation and transport over Antarctica from 11 years of CALIPSO observations". In: *The Cryosphere* 11.6, pp. 2555–2569.

Parrenin, F. et al. (2007). "The EDC3 chronology for the EPICA Dome C ice core". In: *Climate of the Past* 3, pp. 485–497.

Pattyn, F. et al. (2017). "Progress in numerical modeling of Antarctic ice-sheet dynamics". In: *Current Climate Change Reports* 3.3, pp. 174–184.

Pedro, J.B. et al. (2011). "The last deglaciation: timing the bipolar seesaw". In: *Climate of the Past* 7.2, pp. 671–683.

Pedro, J.B. et al. (2016). "The spatial extent and dynamics of the Antarctic Cold Reversal". In: *Nature Geoscience* 9.1, p. 51.

Peltier, W.R. (1994). "Ice age paleotopography". In: *Science* 265.5169, pp. 195–201.

— (2004). "Global glacial isostasy and the surface of the ice-age Earth: the ICE-5G (VM2) model and GRACE". In: *Annu. Rev. Earth Planet. Sci.* 32, pp. 111–149.

Petit, J.-R. et al. (1999). "Climate and atmospheric history of the past 420,000 years from the Vostok ice core, Antarctica". In: *Nature* 399.6735, p. 429.

PISM (2017). In: *The Parallel Ice Sheet Model: User's Manual*. URL: `http://pism-docs.org/sphinx/manual/`.

Pollard, D., R.M. DeConto, and R.B. Alley (2015). "Potential Antarctic Ice Sheet retreat driven by hydrofracturing and ice cliff failure". In: *Earth and Planetary Science Letters* 412, pp. 112–121.

Pollard, D. and Robert M DeConto (2009). "Modelling West Antarctic ice sheet growth and collapse through the past five million years". In: *Nature* 458.7236, p. 329.

Pollard, D., Robert M DeConto, and Richard B Alley (2019). "A continuum model of ice mélange and its role during retreat of the Antarctic Ice Sheet". In: *Geoscientific Model Development*.

Prahl, F.G. et al. (2010). "Systematic pattern in U37K–temperature residuals for surface sediments from high latitude and other oceanographic settings". In: *Geochimica et Cosmochimica Acta* 74.1, pp. 131–143.

Pritchard, H.D. et al. (2012). "Antarctic ice-sheet loss driven by basal melting of ice shelves". In: *Nature* 484.7395, p. 502.

Pyne, R.L. et al. (2018). "A novel approach to process brittle ice for continuous flow analysis of stable water isotopes". In: *Journal of Glaciology* 64.244, pp. 289–299.

Rae, J.W.B. et al. (2018). "CO 2 storage and release in the deep Southern Ocean on millennial to centennial timescales". In: *Nature* 562.7728, p. 569.

Raftery, A.E. et al. (2017). "Less than 2 C warming by 2100 unlikely". In: *Nature Climate Change* 7.9, p. 637.

Raphael, M.N. et al. (2016). "The Amundsen sea low: variability, change, and impact on Antarctic climate". In: *Bulletin of the American Meteorological Society* 97.1, pp. 111–121.

Raymond, C.F. (1983). "Deformation in the vicinity of ice divides". In: *Journal of Glaciology* 29.103, pp. 357–373.

Rignot, E. et al. (2008). "Recent Antarctic ice mass loss from radar interferometry and regional climate modelling". In: *Nature geoscience* 1.2, p. 106.

Rignot, E. et al. (2014). "Widespread, rapid grounding line retreat of Pine Island, Thwaites, Smith, and Kohler glaciers, West Antarctica, from 1992 to 2011". In: *Geophysical Research Letters* 41.10, pp. 3502–3509.

Rintoul, S.R. (2018). "The global influence of localized dynamics in the Southern Ocean." In: *Nature* 558.7709, pp. 209–218.

Ritz, C., V. Rommelaere, and C. Dumas (2001). "Modeling the evolution of Antarctic ice sheet over the last 420,000 years: Implications for altitude changes in the Vostok region". In: *Journal of Geophysical Research: Atmospheres* 106.D23, pp. 31943–31964.

Ritz, C. et al. (2015). "Potential sea-level rise from Antarctic ice-sheet instability constrained by observations". In: *Nature* 528.7580, p. 115.

Robel, A.A. (2017). "Thinning sea ice weakens buttressing force of iceberg mélange and promotes calving". In: *Nature Communications* 8, p. 14596.

Robel, A.A., G.H. Roe, and M. Haseloff (2018). "Response of Marine-Terminating Glaciers to Forcing: Time Scales, Sensitivities, Instabilities, and Stochastic Dynamics". In: *Journal of Geophysical Research: Earth Surface* 123.9, pp. 2205–2227.

Rogelj, J., M. Meinshausen, and R. Knutti (2012). "Global warming under old and new scenarios using IPCC climate sensitivity range estimates". In: *Nature climate change* 2.4, p. 248.

Rojas, M. et al. (2009). "The Southern Westerlies during the last glacial maximum in PMIP2 simulations". In: *Climate Dynamics* 32.4, pp. 525–548.

Schmidt, G.A. et al. (2012). "Climate forcing reconstructions for use in PMIP simulations of the Last Millennium (v1. 1)". In: *Geoscientific Model Development* 5, pp. 185–191.

Schoof, C. (2003). "The effect of basal topography on ice sheet dynamics". In: *Continuum Mechanics and Thermodynamics* 15.3, pp. 295–307.

— (2007). "Ice sheet grounding line dynamics: Steady states, stability, and hysteresis". In: *Journal of Geophysical Research: Earth Surface* 112.F3.

Seroussi, H. et al. (2017). "Continued retreat of Thwaites Glacier, West Antarctica, controlled by bed topography and ocean circulation". In: *Geophysical Research Letters* 44.12, pp. 6191–6199.

Seroussi, H. et al. (2019). "initMIP-Antarctica: an ice sheet model initialization experiment of ISMIP6". In: *The Cryosphere* 13.5, pp. 1441–1471.

Simkins, L.M., JB Anderson, and SL Greenwood (2016). "Glacial landform assemblage reveals complex retreat of grounded ice in the Ross Sea, Antarctica". In: *Geological Society, London, Memoirs* 46.1, pp. 353–356.

Simms, A.R. et al. (2019). "Balancing the last glacial maximum (LGM) sea-level budget". In: *Quaternary Science Reviews* 205, pp. 143–153.

Slangen, A.B.A. et al. (2014). "Projecting twenty-first century regional sea-level changes". In: *Climatic Change* 124.1-2, pp. 317–332.

Spector, P. et al. (2017). "Rapid early-Holocene deglaciation in the Ross Sea, Antarctica". In: *Geophysical Research Letters* 44.15, pp. 7817–7825.

Stanford, J.D. et al. (2011). "Sea-level probability for the last deglaciation: A statistical analysis of far-field records". In: *Global and Planetary Change* 79.3-4, pp. 193–203.

Steig, E.J. et al. (2000). "Wisconsinan and Holocene climate history from an ice core at Taylor Dome, western Ross Embayment, Antarctica". In: *Geografiska Annaler: Series A, Physical Geography* 82.2-3, pp. 213–235.

Stenni, B. et al. (2010). "The deuterium excess records of EPICA Dome C and Dronning Maud Land ice cores (East Antarctica)". In: *Quaternary Science Reviews* 29.1-2, pp. 146–159.

Stewart, C.L. et al. (2019). "Basal melting of Ross Ice Shelf from solar heat absorption in an ice-front polynya". In: *Nature Geoscience*, p. 1.

Stone, J.O. et al. (2003). "Holocene deglaciation of Marie Byrd land, west Antarctica". In: *Science* 299.5603, pp. 99–102.

Stuhne, G.R. and W.R. Peltier (2015). "Reconciling the ICE-6G_C reconstruction of glacial chronology with ice sheet dynamics: The cases of Greenland and Antarctica". In: *Journal of Geophysical Research: Earth Surface* 120.9, pp. 1841–1865.

Sueyoshi, T. et al. (2013). "Set-up of the PMIP3 paleoclimate experiments conducted using an Earth system model, MIROC-ESM". In: *Geoscientific Model Development* 6.3, pp. 819–836.

Thomas, E.R. and N.J. Abram (2016). "Ice core reconstruction of sea ice change in the Amundsen-Ross Seas since 1702 AD". In: *Geophysical Research Letters* 43.10, pp. 5309–5317.

Thomas, E.R. and Thomas J. Bracegirdle (2015). "Precipitation pathways for five new ice core sites in Ellsworth Land, West Antarctica". In: *Climate dynamics* 44.7-8, pp. 2067–2078.

Thomas, E.R. and T.J. Bracegirdle (2009). "Improving ice core interpretation using in situ and reanalysis data". In: *Journal of Geophysical Research: Atmospheres* 114.D20.

Tierney, J.E. and M.P. Tingley (2018). "BAYSPLINE: a new calibration for the alkenone paleothermometer". In: *Paleoceanography and Paleoclimatology* 33.3, pp. 281–301.

Timmermann, A. et al. (2010). "Towards a quantitative understanding of millennial-scale Antarctic warming events". In: *Quaternary Science Reviews* 29.1-2, pp. 74–85.

Todd, C. et al. (2010). "Late Quaternary evolution of Reedy Glacier, Antarctica". In: *Quaternary Science Reviews* 29.11, pp. 1328–1341.

Trusel, L.D. et al. (2015). "Divergent trajectories of Antarctic surface melt under two twenty-first-century climate scenarios". In: *Nature Geoscience* 8.12, p. 927.

Tuohy, A. et al. (2015). "Transport and deposition of heavy metals in the Ross Sea Region, Antarctica". In: *Journal of Geophysical Research: Atmospheres* 120.20, pp. 10–996.

Turner, J. et al. (2013). "An initial assessment of Antarctic sea ice extent in the CMIP5 models". In: *Journal of Climate* 26.5, pp. 1473–1484.

Uemura, R. et al. (2012). "Ranges of moisture-source temperature estimated from Antarctic ice cores stable isotope records over glacial–interglacial cycles". In: *Climate of the Past* 8.3, pp. 1109–1125.

Veres, D. et al. (2013). "The Antarctic ice core chronology (AICC2012): an optimized multi-parameter and multi-site dating approach for the last 120 thousand years". In: *Climate of the Past* 9.4, pp. 1733–1748.

Vizcaíno, M. et al. (2014). "Greenland surface mass balance as simulated by the community earth system model. Part II: twenty-first-century changes". In: *Journal of climate* 27.1, pp. 215–226.

Weber, M.E. et al. (2014). "Millennial-scale variability in Antarctic ice-sheet discharge during the last deglaciation". In: *Nature* 510.7503, p. 134.

Whitehouse, P.L. et al. (2012). "A new glacial isostatic adjustment model for Antarctica: calibrated and tested using observations of relative sea-level change and present-day uplift rates". In: *Geophysical Journal International* 190.3, pp. 1464–1482.

Whitehouse, P.L. et al. (2019). "Solid Earth change and the evolution of the Antarctic Ice Sheet". In: *Nature communications* 10.1, p. 503.

Winkelmann, R. et al. (2011). "The Potsdam parallel ice sheet model (PISM-PIK)–Part 1: Model description". In: *The Cryosphere* 5.3, pp. 715–726.

Yeager, S.G. et al. (2006). "The low-resolution CCSM3". In: *Journal of Climate* 19.11, pp. 2545–2566.

Yokoyama, Y. et al. (2016). "Widespread collapse of the Ross Ice Shelf during the late Holocene". In: *Proceedings of the National Academy of Sciences* 113.9, pp. 2354–2359.

Yukimoto, S. et al. (2012). "A new global climate model of the Meteorological Research Institute: MRI-CGCM3—model description and basic performance". In: *Journal of the Meteorological Society of Japan. Ser. II* 90, pp. 23–64.